

BIOHYBRID AND BIOMIMETIC PLATFORMS FOR PROGRAMMABLE
THERAPEUTIC DELIVERY

Except where reference is made to the work of others, the work described in this dissertation is my own or was done in collaboration with my advisory committee. This dissertation does include proprietary or classified information.

Siddarth Venkatesh

Certificate of Approval:

Robert Chambers
Professor
Chemical Engineering

Mark E. Byrne, Chair
Assistant Professor
Chemical Engineering

Douglas Goodwin
Associate Professor
Chemistry and Biochemistry

Christopher Roberts
Professor
Chemical Engineering

Jacek Wower
Professor
Animal Sciences

George T. Flowers
Interim Dean
Graduate School

BIOHYBRID AND BIOMIMETIC PLATFORMS FOR PROGRAMMABLE
THERAPEUTIC DELIVERY

Siddarth Venkatesh

A Dissertation

Submitted to

the Graduate Faculty of

Auburn University

in Partial Fulfillment of the

Requirements for the

Degree of

Doctor of Philosophy

Auburn, Alabama

August 9, 2008

BIOHYBRID AND BIOMIMETIC PLATFORMS FOR PROGRAMMABLE
THERAPEUTIC DELIVERY

Siddarth Venkatesh

Permission is granted to Auburn University to make copies of this dissertation at its discretion, upon request of individuals or institutions and at their expense. The author reserves all publication rights.

Signature of Author

Date of Graduation

DISSERTATION ABSTRACT

BIOHYBRID AND BIOMIMETIC PLATFORMS FOR PROGRAMMABLE
THERAPEUTIC DELIVERY

Siddarth Venkatesh

Doctor of Philosophy, August 9, 2008
(B.S., University of Madras, India, 2003)

304 Typed Pages

Directed by Mark E. Byrne

Drug and gene delivery carriers such as hydrogels and metallic nanoparticles have shown remarkable promise as programmable platforms in the targeted delivery of their payload. In this work, the fundamental principles of biomimesis have been applied for the synthesis of recognitive hydrogels from monomers of diverse chemical functionalities. We exploit the configurational biomimetic imprinting process, which creates macromolecular memory for the drug within the network and delays the transport of drug from the matrix *via* interactions with the functional groups organized within the structure. The most biomimetic network, which was synthesized from four functional monomers, demonstrated 6 times enhanced loading over the non-imprinted network and 3 times enhanced loading over the networks containing two or three functional monomers.

Delayed release kinetics of therapeutically relevant concentrations of drug was observed over 5 days. All imprinted networks had significantly lower diffusion coefficients than non-imprinted networks, in spite of comparable mesh sizes (21-31 Å) and equilibrium polymer volume fractions in the swollen state (0.634 ± 0.025). Furthermore, the most biomimetic network had a diffusion coefficient which was lesser by factors of 15, 76, 49, and 113 from the networks synthesized from two or three functional monomers.

In this work, we show the controlled release of nucleic acid therapeutics loaded into hydrogels, *via* enzymatic and physical triggers such as specific and non-specific endonucleases and temperature. The physiological relevance of the platform was demonstrated by the in-vitro down regulation of a HIV Tat/Rev gene by the specific release of an anti-HIV deoxyribozyme from the hydrogel. Furthermore, the crosslinking densities of the hydrogels were varied in order to obtain tunable release profiles of DNA.

Substrate non-specific (DNase I) enzymes were used to trigger the release of fluorescent neomycin immobilized onto gold nanoparticles. Surface coverage densities of the DNA were quantified and optimized by varying buffer ionic strengths, reaction times and sonication. Such novel schemes could be used for the intracellular delivery of multiple drugs from the same platform, as injectable systems targeted to specific cells using functionalized ligands such as folic acid. We anticipate that our study will spur further inquiry into nucleic acid based programmable on-demand switches and modulatory mechanisms, with exquisite control and sensitivity.

ACKNOWLEDGEMENTS

At the outset, I acknowledge the following organizations for research support- National Science Foundation, Auburn University Biogrant, Sigma Xi. My doctoral investigations have been conducted under the auspices of many individuals. I find myself indebted to Dr. Mark Byrne for sterling mentorship, insights in polymer chemistry, and for instilling rigor in research and integrity in personal relationships. Dr. Jacek Wower is credited with magical inspiration, for shaping my raw thinking and teaching me technique and theory. I feel deeply obliged to Dr. Christopher Roberts for his steadfast support during critical circumstances, and wish to recognize Dr. Douglas Goodwin and Dr. Robert Chambers for thoughtful criticisms and approachability. In intimate conversations, Santhosh Palani and Naveed Ansari, through painstaking analysis and a deep understanding of human nature, have prevented me from making far too many blunders in my personal and academic life. Stephen Sizemore and Jishnu Saha are thanked profusely for experimental collaboration. Rosa Jackson, Sue Ellen Abner, Karen Cochran and Sherry Ray have provided sound administrative counsel. I appreciate the concern that Dr. Anthony DeRoss and Dr. Christine Dykstra have shown in furthering my career. Finally, I express gratitude to my dear friends at Auburn, for enriching my life with indelible memories and camaraderie, and to my parents, for understanding my desire to pursue a second doctorate at Rockefeller University, New York City.

Style manual or journal used: Nature Biotechnology.

Computer software used: DeLanoScientific PyMol, Mfold, Bio-Rad Laboratories ChemWindow, Microsoft Visio, Microsoft Office, Adobe Photoshop, Microcal Origin, MathType, and Endnote.

TABLE OF CONTENTS

LIST OF TABLES	xiii
LIST OF FIGURES	xv
1.0. INTRODUCTION	1
2.0. MOLECULAR RECOGNITION AND THERAPEUTIC DELIVERY	4
2.1. Biological Molecular Recognition.....	6
2.2. Recognition in Biology.....	8
2.3. Biomimesis and Biomimetic Systems	11
2.4. Current Trends in the Design of Biomimetic Systems	14
2.4.1. Nucleic Acid Biology	14
2.4.1.1. Ribozymes	15
2.4.1.2. Artificial and Natural Aptamers	17
2.4.1.3. RNA Interference	19
2.4.1.4. DNA-Based Nanoconstruction.....	22
2.4.2. Virology.....	25
2.4.3. Immunology and Vaccine Design	27
2.4.4. Nanotechnology.....	30
2.4.5. Polymer Science and Engineering.....	33
2.5. Conclusions.....	34

2.6. List of References	34
3.0. MOLECULAR IMPRINTED POLYMERS IN DRUG DELIVERY	57
3.1. Introduction to Recognitive Polymers	58
3.2. Macromolecular Memory: A Host-Guest Templating Phenomenon.....	59
3.3. Molecular Recognition <i>via</i> Non-Covalent Interactions	62
3.4. Thermodynamic Evaluation of the Imprinting Process	63
3.5. Analogies between Natural and Synthetic Polymers	67
3.6. Design or Operational Parameters of Molecularly Imprinted Networks	68
3.6.1. Pressure.....	69
3.6.2. Temperature.....	71
3.6.3. Solvent Weight Percentage.....	73
3.6.4. Monomer-Template Ratio	76
3.6.5. Crosslinking Monomer Length and Density.....	78
3.6.6. Initiator Weight Percentages and the Use of Controlled/Living Polymerization	85
3.7. List of References	87
4.0. ENHANCED LOADING AND REACTION ANALYSIS ON BIOMIMETIC RECOGNITIVE CONTACT LENSES.....	108
4.1. Scientific Rationale.....	109
4.2. Historical Background and Current Trends in Ocular Drug Delivery	110
4.3. The Mammalian Inflammation Pathway	115
4.4. Materials and Methods: Synthesis of a Therapeutic Contact Lens <i>via</i> Imprinting	116

4.4.1. Materials	116
4.4.2. Methods: Synthesis of a Typical Imprinted Network.....	117
4.4.3. Methods: Equilibrium Rebinding Studies	119
4.4.4. Methods: Polymerization Reaction Analysis.....	120
4.5. Results and Discussion	121
4.5.1. Enhanced Loading of Networks formed from Pre-polymerization Mixtures of Diverse Functionalities.....	122
4.5.2. Imprinting Effects on Polymerization Kinetics	124
4.6. List of References	125
5.0. TRANSPORT AND STRUCTURAL ANALYSIS OF MOLECULAR IMPRINTED HYDROGELS FOR CONTROLLED DELIVERY OF OCULAR THERAPEUTICS.....	138
5.1. Scientific Rationale.....	139
5.2. Analysis of Diffusion and Controlled Release in Hydrogels.....	140
5.3. Diffusion Models	144
5.4. Materials and Methods.....	147
5.4.1. Methods: Kinetic Release Profiles of Ketotifen Fumarate from Loaded Networks	148
5.4.2. Methods: Diffusion Analysis of Ketotifen from Kinetic Release Profiles.....	148
5.4.3. Methods: One Dimensional Diffusion Analysis.....	150
5.4.4. Methods: Determination of Structural Parameters	152
5.4.5. Methods: Mechanical Analysis of Imprinted Networks	155

6.3.6. Methods: <i>In-vitro</i> Kinetic Release of DNA Strands on Deoxynuclease I Trigger.....	193
6.3.7. Methods: Physiological validation of the platform: Down regulation of HIV-1 Tat/Rev mRNA	194
6.3.8. Methods: Generation of the Neomycin Aptamer Spectrum	195
6.3.9. Methods: Functionalization and characterization of gold nanoparticles	197
6.4. Results and Discussions.....	198
6.5. List of References	205
7.0 CONCLUSIONS	231
APPENDIX A: Data sets collected from experiments	236
APPENDIX B: Buffer compositions	273
APPENDIX C: Oligonucleotide sequences used in experiments.....	276
APPENDIX D: Error analysis	283

LIST OF TABLES

5.1. Transport Coefficients and Swelling Data of poly(n-co-HEMA-co-PEG200DMA) networks.....	178
A.1. Dry Volumes of Non-imprinted Poly(n-co-HEMA-co- PEG200DMA) Networks.....	247
A.2. Dry Volumes of imprinted Poly(n-co-HEMA-co- PEG200DMA) Networks.....	248
A.3. Swollen Volumes of Non-imprinted Poly(n-co-HEMA-co- PEG200DMA) Networks.....	249
A.4. Swollen Volumes of imprinted Poly(n-co-HEMA-co- PEG200DMA) Networks.....	250
A.5. Slopes of the tensile curves of the non-imprinted poly(n-co-HEMA-co-PEG200DMA) networks.....	267
A.6. Slopes of the tensile curves of the imprinted poly(n-co-HEMA-co-PEG200DMA) networks.....	268
A.7. Average molecular weight between crosslinks of the non-imprinted poly(n-co-HEMA-co-PEG200DMA) networks.....	269
A.8. Average molecular weight between crosslinks of the imprinted poly(n-co-HEMA-co-PEG200DMA) networks	270

A.9. Average mesh size calculations of the non-imprinted	
poly(n-co-HEMA-co-PEG200DMA) networks.....	271
A.10. Average mesh size calculations of the non-imprinted	
poly(n-co-HEMA-co-PEG200DMA) networks.....	272

LIST OF FIGURES

2.1. Classification of Biomimetic Systems.....	54
2.2. Molecular Interactions in the Hedgehog Signaling Pathway.....	55
2.3. T cell Differentiation and Memory T Cell Formation	56
3.1. General Schematic of a Polymer Network.....	103
3.2. General Schematic of the Configurational Biomimetic Imprinting Synthesis Scheme.....	104
3.3. Design Parameters of a Hydrogel	105
3.4. Porosity Within Imprinted Hydrogels.....	106
3.5. General Schematic of Mesh Size	107
4.1. Mammalian Allergy Pathway and Biomimetic Synthesis of Recognitive Contact Lenses.....	131
4.2. Representation of the Crystal Structure of the H1 Receptor.....	132
4.3. One-To-One Correspondence of Amino Acids and Functional Monomers in Memory Sites.....	133
4.4. Ketotifen Equilibrium Binding Isotherm in Water for Poly(AM-co-AA-co-HEMA-co- PEG200DMA) Networks.....	134
4.5. Comparison of Enhanced Loading of Ketotifen in Functionally Diverse Poly(n-co-HEMA-co-PEG200DMA) Networks	135
4.6. Polymerization Reaction Rate versus Conversion for	

Poly(AM-co-HEMA-co-PEG200DMA) Networks	136
4.7. Polymerization Reaction Rate versus Conversion for Varying Comonomer	
Percentages in Poly(n-HEMA-co-PEG200DMA) Networks	137
5.1. Controlled Release Strategies in Hydrogels	167
5.2. Schematic Representation of One-dimensional Planar Diffusive Transport	
from a Polymer Network	168
5.3. Dynamic Extended Release in Biomimetic Networks.....	169
5.4. Cumulative Mass of Ketotifen Released in Artificial Lachrymal Fluid for	
Poly(AA-co-AM-co-NVP-co-HEMA-co-PEG200DMA) Networks	170
5.5. Comparison between Ketotifen Delivery by Therapeutic Contact	
Lenses and Topical Eye Drops	171
5.6. Effect of Protein on Dynamic Release of Ketotifen	172
5.7. Equilibrium Weight Swelling Ratios for	
Poly(AM-co-AA-co-HEMA-co-PEG(200)DMA) Networks	173
5.8. Partition Coefficients for Poly(n-co-HEMA-co-PEG200DMA) Networks	174
5.9. Equilibrium Polymer Volume Fractions in the Swollen State for	
Poly(n-co-HEMA-co-PEG200DMA) Networks	175
5.10. Diffusion Coefficients for Poly(n-co-HEMA-co-PEG200DMA) Networks.....	176
5.11. The Tumbling Model of Drug Diffusion in Imprinted Networks.....	177
6.1. First Generation “Intelligent” Networks.....	215
6.2. Second Generation “Intelligent” Networks	216
6.3. Third Generation “Intelligent” Networks	217
6.4. Controlled Release of Nucleic Acids from Synthetic Polymers	

<i>via</i> Enzymatic Triggers	218
6.5. Optimization of DNA hybridization conditions	219
6.6. <i>In-vitro</i> restriction enzyme digestion	220
6.7. Covalent immobilization of acrylated annealed duplex.....	221
6.8. Tailored release of DNA by enzymatic trigger.....	222
6.9. Tailored release of DNA by temperature ramp.....	223
6.10. Clinical viability of platform triggered by enzymes	224
6.11. Interaction of HIV-1 TAT/Rev mRNA with the deoxyribozyme.....	225
6.12. Catalytic down regulation of HIV-1 TAT/Rev mRNA by deoxyribozyme released by enzymatic trigger	226
6.13. Tunable Release Profiles via Structural Control.....	227
6.14. Programmable, Multiple Drug Delivery Platform Via Aptamer-Gold Nanoparticle Conjugates	228
6.15. Binding efficacy of the wild type neomycin binding aptamer.....	229
6.16. Differences in Binding efficacy of two neomycin binding mutant aptamers	230
A.1. Ketotifen dynamic binding isotherm in water for poly(AM-co- HEMA-co-poly(ethylene glycol)200 dimethacrylate) networks with a crosslinking percentage of 5%.....	238
A.2. Ketotifen dynamic binding isotherm in water for poly(AA-co- HEMA-co-poly(ethylene glycol)200 dimethacrylate) networks with a crosslinking percentage of 5%	239
A.3. Ketotifen equilibrium binding isotherm in water for poly(AA-co- HEMA-co-poly(ethylene glycol)200 dimethacrylate) networks with a	

crosslinking percentage of 5%	241
A.4. Ketotifen equilibrium binding isotherm in water for poly(AM-co- HEMA-co-poly(ethylene glycol)200 dimethacrylate) networks with a crosslinking percentage of 5%	242
A.5. Ketotifen equilibrium binding isotherm in water for poly(NVP-co- HEMA-co-poly(ethylene glycol)200 dimethacrylate) networks with a crosslinking percentage of 5%	243
A.6. Ketotifen equilibrium binding isotherm in water for poly(AA-co-AM-co- HEMA-co-poly(ethylene glycol)200 dimethacrylate) networks with a crosslinking percentage of 5%	244
A.7. Ketotifen equilibrium binding isotherm in water for poly(AA-co-AM-co- NVP-co-HEMA-co-poly(ethylene glycol)200 dimethacrylate) networks with a crosslinking percentage of 5%	245
A.8. Equilibrium weight swelling ratio for Poly(AA-co-HEMA-co- poly(ethylene glycol)200 dimethacrylate) networks in water with a crosslinking percentage of 5%	251
A.9. Equilibrium weight swelling ratio for poly(AA-co-HEMA-co-poly (ethylene glycol)200 dimethacrylate) networks in 0.5 mg/ml ketotifen solution in water with a crosslinking percentage of 5%	252
A.10. Equilibrium weight swelling ratio for Poly(AM-co-HEMA-co- poly(ethylene glycol)200 dimethacrylate) networks in water with a crosslinking percentage of 5%	253
A.11. Equilibrium weight swelling ratio for poly(AM-co-HEMA-co-poly	

(ethylene glycol)200 dimethacrylate) networks in 0.5 mg/ml ketotifen solution in water with a crosslinking percentage of 5%	254
A.12. Equilibrium weight swelling ratio for Poly(AA-co-AM-co-HEMA-co- poly(ethylene glycol)200 dimethacrylate) networks in water with a crosslinking percentage of 5%	255
A.13. Equilibrium weight swelling ratio for poly(AA-co-AM-co-HEMAco-poly (ethylene glycol)200 dimethacrylate) networks in 0.5 mg/ml ketotifen solution in water with a crosslinking percentage of 5%	256
A.14. Polymerization reaction signature for the poly(AM-co-HEMA-co- PEG200DMA) network	258
A.15. Polymerization reaction signature for the poly(AA-co-HEMA-co- PEG200DMA) network	259
A.16. Polymerization reaction signature for the poly(NVP-co-HEMA-co- PEG200DMA) network	260
A.17. Polymerization reaction signature for the poly(AA-co-AM-co-HEMA-co- PEG200DMA) network	261
A.18. Polymerization reaction signature for the poly(AA-co-AM-co-NVP-co- HEMA-co-PEG200DMA) network	262
A.19. Double bond conversion versus time for the poly(n-co-HEMA-co- PEG200DMA) network	263
A.20. Tensile behavior of the non-imprinted poly(AA-co-AM-co-HEMA- co-PEG200DMA) network	265
A.21. Tensile behavior of the imprinted poly(AA-co-AM-co-HEMA-	

co-PEG200DMA) network	266
-----------------------------	-----

1.0 INTRODUCTION

The field of targeted drug delivery is very nascent, and yet its potential in revolutionizing clinical therapy cannot be underestimated, as highlighted by the fact that it is currently a multi-billion dollar industry. Over the last thirty years, researchers have placed major emphasis on developing a sound technical background for drug delivery systems with the end purpose of utilizing them for the targeted delivery of pharmaceuticals in the clinical arena. It is highly desirable to control the rate of pharmaceutical release at the targeted site over extended periods of time, as an effective pharmacological action is achieved with lower side effects, lesser off-targets, and non-toxic drug concentrations. The explosion in the number of research articles in recent years reflect the growing need to develop more efficacious translational delivery systems, which can dramatically improve contemporary patient diagnostic and care procedures and enhance the quality of life. In conjunction with the rapid discovery of newer and more potent small molecules as drugs, such delivery systems hold immense promise in the control and treatment of complex multifactorial diseases such as type-1 diabetes and various cancers. Such efforts also usher in the age of personalized treatment regimes, by which individualized therapy can be planned based on the patient's genetic predisposition towards various diseases and negative reactions of the patient's individual cell types towards pharmaceutical compounds and treatments such as chemotherapy. Understanding the molecular mechanisms by which

such systems interact with the human body will enable us to tune them for accommodating patient needs.

The field of targeted drug delivery has a vast and comprehensive body of literature, but there are significant challenges which lie ahead. For example, drug delivery systems trigger strong inflammatory reactions with the innate and adaptive arms of the immune system due to their artificial surface epitopes. The extracellular matrix and lamina are tight barriers to drug and gene transport, and sharply decrease access to the target cell. Once the therapeutic has reached its target, receptor-mediated endocytosis is immediately followed by degradation in lysosomes, which prevents the availability of the drug or the gene in the cytoplasm and nucleus.

It becomes immediately clear that the field of drug delivery is built upon the concepts and principles of molecular recognition- specifically how biomolecules and artificial materials recognize and interact with each other. In particular, this process of design by mimicry, termed biomimesis, has spurred the development of more versatile and efficacious biomimetic systems. Chapter 2 details the current advances being made in the design and applicability of biomimetic systems.

This dissertation is focused on developing new technologies for the controlled delivery of therapeutics using hydrogels as carriers. There has been an exponential increase in interest in these delivery platforms due to their attractive properties such as biocompatibility (hydrogels) and efficient cellular uptake (gold nanoparticles). Previous work on hydrogels has dealt with controlling release rates by tuning either the macromolecular architecture or the thermodynamic nature of the solvent, but there is a pressing need to control the loading and release characteristics of drug. The objective of this work is to investigate and develop methods to synthesize and optimize hydrogels *via* a novel bottom-up approach known as the configurational

biomimetic imprinting process (CBIP), enhance partitioning of the drug into these networks, and delay release kinetics without causing any significant network rearrangements such as swelling of the macromolecular structure. The methods of synthesis of biomimetic hydrogels and the mechanical and kinetic analysis of such therapeutic hydrogels are depicted in chapter 3, while the transport and structural characteristics are presented in chapter 4.

Much of the present research efforts of chemists and engineers are directed towards the development of new materials with exquisite sensitivity to changes in physical and chemical stimuli. Previous work in the field has involved the synthesis of hydrogels which are responsive to physical and biochemical environments. In chapter 6, we describe the methods of synthesis and characterization of novel hydrogels that are versatile, programmable platforms for the systemic and local controlled delivery of drugs and nucleic acid therapeutics *via* a variety of enzymatic and physical triggers such as specific and non-specific endonucleases and temperature. Furthermore, we also describe the functionalization of gold nanoparticles with aptamers specific for neomycin, which has the potential to be taken up by cells by receptor-based endocytosis and delivered to the cytoplasm without being degraded by endosomal agents such as lysosomes.

The results presented in this dissertation conclusively demonstrate the value of creative and novel synthetic strategies for the development of highly intelligent and tailorable drug carriers.

2.0 MOLECULAR RECOGNITION AND THERAPEUTIC DELIVERY

In the following chapter, we describe the concepts of biomimesis and biomimetic systems, i.e. the extraction of fundamental biological principles of molecular recognition followed by the rational design of materials and devices based on such rules. Intense scientific scrutiny at the cellular level has led to a deeper understanding of biological mechanisms such as signal cascades, binding mechanisms, and innate and adaptive immunity. This has led to the development of “biomimetic systems”, and examples are provided which demonstrate that these systems are attractive solutions to contemporary biomedical and cellular problems. We present the spectrum of length scales beginning from the level of the gene to the microscale, first concentrating on biological recognition and mechanisms and then transitioning into current biomimetic strategies. The concepts presented in the following chapter have been published as two overviews^{1, 2}, which emphasize the need for a synergy between the basic and applied sciences for the identification of novel therapeutic strategies. In a similar vein to these research efforts, we have applied the concepts of biomimesis to develop novel platforms for drug delivery, which are described in chapters 3 to 6. Therapeutic contact lenses have been synthesized from diverse functional monomers based on principles garnered from structural biology. Such a synthetic scheme has enabled us to tailor the loading and release characteristics of these drug delivery carriers. Novel synthetic polymers loaded with nucleic acid strands

have been shown to undergo programmable, on-demand release on the application of physical and biological triggers. These materials have been designed along the rules of molecular biology, gene cloning and analysis. Gold nanoparticles have been functionalized with short nucleic acid strands capable of binding the antibiotic neomycin with high affinity. The biomimetic approach is thus being used to great advantage for the creation of intelligent, programmable drug delivery vehicles.

2.1 Biological Molecular Recognition

Molecular recognition is a fundamental phenomenon with sweeping biological implications, since molecular interactions underlie all biological processes. It can formally be defined as the summation of non-covalent interactions which take place between two biomolecular species, such as antigens and antibodies, nucleic acids and proteins, enzymes and their substrates, and sugars and glycoproteins. Unraveling the basic rules of molecular recognition is thus vital for a deeper understanding of biological processes, and presents a tempting intellectual challenge to molecular biologists, medical engineers and chemists.

The scientific community has adopted a multi-pronged strategy to understand molecular recognition. In the structural approach³, specific emphasis is laid on the three-dimensional topology of the recognition site, i.e. of the conformations of docking sites of these molecules. This helps us to detail the non-covalent interactions experienced by molecules as they approach the recognition site, as well as the conformational changes which take place when the molecule binds with the target site. In the kinetic and thermodynamic approaches, information is garnered based on the rate and equilibrium constants. Cognition of the activities of the biomolecules and their affinities to the binding sites helps us to build the stepwise mechanism of the recognition process. Understanding the thermodynamic considerations allows us to predict which reactions in a pathway are energetically allowed and which need to be coupled with others. Thermodynamics also informs us about which energetic constraints need to be satisfied

by proteins and nucleic acids in order to assume their functional quaternary structures for catalysis and binding.

These investigations are essential for both understanding disease pathology, as well as to devise strategies for the delivery of therapeutics to the diseased tissue or cell. As an illustration of how these approaches are tied together, the elucidation of the signaling and trafficking processes occurring between first messengers and membrane proteins in an in-vivo normal cell allows us to diagnose deviant processes in pathological cells⁴⁻⁶. Competitive inhibitors or allosteric modulators can then be designed as therapeutic intervention schemes.

The confluence of nanotechnology with other sciences has provided new avenues for the bottom-up engineering of materials and devices with nanoscale precision and control that promises to revolutionize the way health care is administered. Significant strides have been made in the targeted delivery of molecules, especially of drugs⁷⁻⁹ and peptides^{10, 11}, by understanding their molecular interactions with their carriers, their targeted proteins and nucleic acids, and the immune system. These efforts also include the design of novel drug delivery platforms, which have already made significant contributions to medicine, especially in the areas of cardiothoracic and bone surgery, respiratory and reproductive problems and genetic disorders. Parallel advances by molecular biologists and pathologists in understanding the cell cycle¹²⁻¹⁵, the molecular mechanisms of differentiation¹⁶⁻¹⁸, and gene regulation¹⁹⁻²¹, are also providing a physiological landscape for devising novel molecular therapies.

In a recent perspective on nanotechnology, Whitesides²² emphasizes the value of the microscale in the current enthusiasm of nanoscale science and technology. The length

scales encountered in biology, medicine, and biotechnology range from the micro- to nanometer and developments will continue to progress and expand on both levels. This chapter is presented in much the same manner of thought, with an analysis of exciting and novel technologies that are equally as relevant in the realm of nanotechnology, but are not strictly classified as nanoscale.

2.2 Recognition in biology

Biology is replete with marvelous instances of molecular recognition serving to maintain the delicate balance between life and death. Every interaction process between molecules is a careful interplay of events such as recognition, binding and change in conformation, an illustration of which can be obtained from the crystal structure of the voltage-gated potassium ion channel, where a helix-turn-helix structure moves from inside the membrane to the periphery and hence opens the pore, leading to downstream nerve impulses in axons^{23, 24}. Enzymes, metal ions, nucleic acids, steroids, and carbohydrates interact with each other in exquisite mechanisms which are only now coming to light using structural, biochemical, electrophysiological and genetic approaches.

To illustrate the sheer efficacy and precision of recognition at the molecular level, one needs to look no further than the versatile proteins. Proteins build, repair, and turnover cellular structures and genetic material. They control the permeability of their plasma membranes as ion channels. They catalyze an incredible number of biochemical reactions, with high specificity, as enzymes. As hormones, they regulate the signal

transduction pathways. They transport respiratory gases and other metabolites, and are responsible for muscular contraction. They fashion the innate and adaptive arms of the immune system by serving as antibodies, MHC molecules, and receptors in T and B lymphocytes, offering protection against antigens of varying pathology. They form integrins and adherins, which help in cell adhesion and signaling. Such varied functions are a consequence of chaperone-mediated folding and post-translational modifications²⁵.

Ion and protein channels are a classic example of biomolecular cognitive splendor^{26, 27}. In 1998, a landmark article described the X-ray crystal structure of the potassium ion channel in the cell membrane²⁸, and solved the dilemma of how the channel recognizes potassium ions and not sodium ions, even though the latter is much smaller. Their elegant studies showed that the potassium ion, which is always hydrated in extra-cellular environments, sheds its water shell before entering the selectivity filter of the channel- a tetramer protein consisting of four subunits²⁹. The spatial conformation of the protein supports only a dehydrated potassium ion and not a sodium ion. The amino acids in the selectivity filter of the potassium channel are oriented to make sites which mimic the hydration shells. The channel adopts a K⁺-water-K⁺-water (1, 3 configuration) or a water-K⁺-water-K⁺ (2, 4 configuration), and conducts the ions at a staggering rate of hundred million ions per second. Furthermore, scorpion venom, which is specific to the potassium ion, binds tightly to mammalian, bacterial, and fly Shaker ion channels, thus proving that the structure is evolutionarily conserved³⁰. The channel maintains its structure only in the presence of high potassium ion concentration, and collapses when sodium ion concentration.

The subtle variations in the potassium channel structures could be exploited to target specific T cells such as effector memory cells, which play a central role in the pathogenesis of type-1 diabetes, rheumatoid arthritis, multiple sclerosis etc³¹⁻³³. Potassium channels play an especially critical role in the activation of naïve T cells, and their expression patterns vary sharply in all T cell subsets, i.e. naïve, effector, central memory and effector memory cells. Kv1.3 channels are up regulated in effector memory cells, whereas IKCa1 and CRAC channels are up regulated during the activation from naïve to effector cells. Thus, the Kv1.3 channel is an attractive target for pharmacological intervention during autoimmune diseases and graft rejections during organ transplantation, wherein it is necessary to suppress the effector memory cell response.

The signal hypothesis^{34, 35}, which proved pivotal in spurring scientific inquiry into cellular translocation, is another exemplification of molecular recognition directing critical life processes. Protein translocation across the endoplasmic reticulum membrane is a critical early step in the synthesis of many secreted proteins. Intracellular traffic is tightly regulated and each protein is delivered to the membrane, to which it is transported by certain trafficking agents^{36, 37}. The original hypothesis proposed the existence of protein channels, which would form an exit route for nascent peptides, and structural confirmation was recently obtained³⁸. These channels help in the translocation of newly formulated proteins to outside the cell. A sequence of amino acids at the amino terminal, the signal sequence, helps in directing the newly formed proteins towards the endoplasmic reticulum^{39, 40}. The channel shows great conformational and sieving skills in only allowing the protein across, and not allowing other smaller molecules with better mobilities through. While the transport takes place, the signal peptide is generally

removed from the protein. The proteins are routed outside, where they assume their familiar three dimensional conformation by folding and coiling with the help of chaperone proteins⁴¹.

These ideas have shed light on diseases such as hypercholesterolemia, lysosomal storage disorders, and hyperoxaluria, which causes kidney stones in children⁴²⁻⁴⁴. Protein signal sequences have also become a tool for researchers who genetically modify proteins to tag them for secretion. Furthermore, the targeting of proteins to organelles *via* signal sequences could also be exploited for the development of drugs that target specific diseased sections of the cell. Such efforts fall under the paradigm of biomimesis.

2.3 Biomimesis and Biomimetic Systems

Biomimesis is the application of the fundamental laws of molecular recognition to design novel systems in order to address pressing problems in biology and medicine. Central to it is the need of a firm command of the internal machinery of the cell. How cells grow and divide; how they regulate metabolic fluxes; how they communicate with each another; how hormones affect signal transduction pathways and how the cell responds to the extracellular milieu; which genes are expressed during various stages of development and the hyperfine control processes which regulate these temporal events- answering such questions is vital in the pursuit of novel biomimetic systems for medical intervention.

To clarify the context and definition of biomimetic systems, we offer a putative classification as (i) biological, (ii) biohybrid, and (iii) synthetic structures (Figure 2.1).

Biological structures denote materials consisting of natural biological molecules such as proteins, DNA, RNA, and recombinant proteins prepared *via* cloning. The biohybrid structures comprise materials that combine synthetic structures (e.g., polymeric chains, metal particles, etc.) and natural biological molecules. Lastly, synthetic structures represent materials based on man-made building blocks, such as synthetic polymers, gold nanoparticles, carbon nanotubes, and unnatural amino acids, prepared by in-vitro solid phase synthesis.

Biomimetic systems can be put to many uses: to investigate diseased cells and tissues; to target such locations with therapeutic formulations; or just to study the internal machinery of the cell. Such systems can be utilized in two approaches. One attempts mimicry for the processes where the recognitive principles are understood, for the aforementioned purposes. Most current biomimetic designs are based on well understood recognitive principles. The future of biomimesis falls under the umbrella of basic science investigations, wherein one endeavors to elucidate the molecular mechanisms of biochemical pathways, so that they can be regulated in future treatment regimes.

Through evolution, living organisms have developed a powerful immune response to the non-self. Hence, introducing biomimetic systems into living organisms without invoking strong immune responses, zeroing in on the tissue or cell of interest, and finally the controlled release of the therapeutic, are strong concerns^{45, 46}. Certain polymers have been especially useful in drug and gene delivery systems as they provide solutions to some of these problems and are inherently biocompatible^{47, 48}. Also, the past has seen the use of biomimetic poly(ethylene) glycol (PEG) for its stealth characteristics, but the future may hold novel passivation strategies using epitopes that are recognized as self by

the immune system effector cells. Biomimetic systems thus have the potential to rapidly transform the field of controlled release and greatly enhance the performance of existing pharmaceutical compounds.

Signal transduction pathways are responsible for sustaining life by integrating myriads of signaling molecules, metabolic pathways, and cytotrafficking agents. Cellular function is largely a response to many extracellular signaling molecules like growth factors, cytokines, hormones etc. These molecules bind transmembrane receptors, and initiate the relevant signal pathway. Many drugs have been devised on biomimetic binding strategies, i.e. competitively binding with the receptor protein, or by repressing the regulator molecule.

The pharmacokinetic properties of such receptor agonists depend not only on receptor binding affinity but also on intracellular signaling cascades and endocytic trafficking of the ligand-receptor complexes⁴⁹. Endocytic trafficking often serves to attenuate the generated signals, resulting in ligand depletion and receptor down-regulation. Contemporary attempts to solve this problem have involved the design of drugs with increased affinity for the targeted cell-surface receptor. However, the strength of the ligand-receptor binding decides the fate of the ligand. A strong interaction results in trafficking the ligand to the lysosomes, leading to a time-dependant depletion of ligand. On the other hand, a weak interaction results in the dissociation of the complex and recycling of the receptor back to the plasma membrane. *In-silico* studies and site-directed mutagenesis of critical histidine residues on the surface of Granulocyte Colony-Stimulating Factor (GCSF), one of the most influential cytokines in the body, were used to weaken binding to the Granulocyte Colony-Stimulating Factor Receptor at endosomal

pH. At the cell surface, where the pH is 7, His is largely neutral. But it gets protonated in the endosomes, where the pH is 5-6⁵⁰. The positive charge repels the positively charged GCSF Receptor, resulting in enhanced intracellular residence time of the ligand and recycling of the receptor back to the cell surface. Such efforts epitomize a biomimetic system, where one probes the cell by shrewd manipulation of the cognitive principles.

2.4 Current Trends in the Design of Biomimetic Systems

Biomimetic systems can be designed by extraction of the biological principles that govern them. To emphasize the sweeping effects of biomimetic systems, we analyze various exciting and novel investigations that are at the forefront of mainstream scientific inquiry. In this section, we focus on fields such as nucleic acid biology, virology, immunology, bionanotechnology, and micro-scale polymer science. We present both current biomimetic schemes as well as biological mechanisms of recognition, which could be harnessed in future biomimetic strategies.

2.4.1 Nucleic Acid Biology

Recent discoveries in the fields of gene expression and regulation, such as RNAi, microRNAs, ribozymes, aptamers, and riboswitches have revolutionized medicine and genetics, and researchers are finding ways to harness these technologies to treat disorders such as AIDS, hepatitis, and influenza. Initial results have been very promising and a number of pharmaceutical companies are already focusing on commercialization of

various disease-specific strategies or technological platforms⁵¹. However, recent research has made it clear that important safety issues need to be addressed before RNAi-based drugs are ready for clinical use.

2.4.1.1 Ribozymes

The first major breakthrough in RNA biology occurred with the discovery that RNA has a strong catalytic role⁵²⁻⁵⁵. These “ribozymes” are as catalytically competent as proteins, and in fact are responsible for some of the more critical life processes in the cell such as protein synthesis, intron splicing, RNA editing etc. The first crystal structure of a ribozyme⁵⁶ revealed complex loops, furrows and grooves, rendering it ideal for recognition and catalysis. Capable of specific cleaving of nucleic acid sequences, ribozymes hold excellent therapeutic promise in targeting mutant genes.

Unlike synthetic systems, ribozymes hold the distinct advantage of amenability to delivery using recombinant methods. Recombinant adenoviruses have been used with great success in ribozyme delivery. Epstein-Barr virus (EBV), a γ -herpesvirus which causes lymphoproliferation of B-cells, is an excellent model of study, as understanding how the immune system combats it, could be used to control other persistent infections. The infection is characterized by the presence of EBV Nuclear Antigen 1 (EBNV-1), a phosphoprotein found in the nuclei of latently infected cells, which is critical for the replication cycle of the virus and hence its persistence in infection⁵⁷. When Epstein-Barr virus infects a B-cell, the viral genome circularizes, and replicates along with the host chromosomes during S phase of the cell cycle. This is followed by equidistribution of

replicated genomes into the daughter cells- a process mediated by EBV-1. Adenoviruses were used to deliver three hammerhead ribozymes targeted against EBV-1, to transformed B-cells⁵⁸. Using flow cytometry, the authors found that αv integrins, the adenovirus internalization receptors were up-regulated in the infected cell lines. The susceptibility to adenovirus-mediated transformation was confirmed by using green fluorescent protein (GFP) as a marker. Two B cell lines, Ramos and RPMI 8226, were compared, of which only RPMI 8226 can express αv integrins, and it was conclusively shown that these cells support adenoviral delivery.

Ribozymes can repair defective mRNA with high fidelity and specificity^{59, 60}. Modified trans-splicing ribozymes were targeted against the Tn9 chloramphenicol acetyl transferase, cucumber mosaic virus coat protein and human immunodeficiency virus (HIV) TAT mRNAs for repair *in vivo*⁶¹. This is strong evidence of the specificity of these ribozymes, which suggests that the technique should allow distinction between transcripts bearing point mutations. Trans-splicing group I ribozymes were used to repair a number of defective p53 mutants and restored transactivation of a p53 responsive promoter⁶². Trans-splicing ribozyme from the Tetrahymena group I intron have also been transfected into erythrocyte precursor cells to repair β -globin mRNAs into transcripts encoding the γ -globin protein, which prevents sickling of nuclei^{63, 64}. The authors rationally designed the ribozymes by analyzing the secondary structure, antisense complementarity, and different promoters. This maximized the efficiency and targeting specificity of the trans-splicing ribozyme, with minimal off-target effects.

2.4.1.2 Artificial and natural aptamers

In the early 1990's, pioneering work was published^{65, 66}, which demonstrated that large libraries of synthetic RNA molecules (pools of 10^{15} molecules) could be screened *in vitro* to identify and bind ligands with high binding selectivities and affinities for a specific target. These short RNA sequences were termed aptamers, and the selection process, was called SELEX (systematic evolution of ligands by exponential enrichment). These groundbreaking developments opened the door to the widespread application of the unique recognition capabilities of aptamers.

RNA carries out its exotic functions *via* its ability to recognize a vast repertoire of molecules⁶⁷. Using SELEX, one can now capture short aptamers that bind a wide assortment of molecules such vitamins^{68, 69} (Vitamin B₁₂ and Vitamin H), citrulline, antibiotics⁷⁰⁻⁷⁴ (neomycin and tobramycin), second messengers (cyclic AMP⁷⁵), and dyes⁷⁶ (Malachite Green, Cibaron blue). In particular, aptamers have proven to be valuable therapeutic agents with comparable and some enhanced properties relative to antibodies⁷⁷. Such structures can be easily tagged with proteins, fluorophores and antibiotics, and can be chemically ligated with cytotoxic agents and radionucleides for therapy and diagnosis of aberrant cells⁷⁸.

Aptamers can also be used in gene regulation and ribozyme function where such aptamer domains deactivate or trigger function by the binding of certain small molecules like ATP and theophylline, and the natural aptamer domain can be mutated for regulating protein expression. Such aptamers when tagged by fluorophores, are exquisitely sensitive

biosensors for proteins and other molecules^{79, 80}, as they undergo conformational switches when they bind to their ligands.

Perhaps the greatest implication from SELEX has been the wealth of information that has come from X-ray and NMR structures of aptamer-ligand complexes. Very little is still known about how RNA recognizes its ligands in nature and performs its repertoire of functions. As an example, aminoglycoside antibiotics such as tobramycin interfere with intron splicing, and it was only when aptamers were selected against tobramycin *via* SELEX, that the rules governing the recognition processes began to be understood^{71, 73, 74}.

One major conundrum was that if Darwinian evolution could be used to select aptamers from large pools, wouldn't Nature also have harnessed the exotic functions which RNA is capable of? This would provide a satisfying solution to the problem of gene regulation in the "RNA World" when proteins (repressors, activators and enhancers) had not yet evolved. The discovery of riboswitches by Breaker showed that natural aptamers do exist, and they exert genetic control *via* surprisingly elegant mechanisms^{81, 82}.

The chief mechanisms by which riboswitches act are transcriptional termination, translation inhibition and autocleavage. As an example, the crystal structure of the guanine riboswitch shows that hypoxanthine serves as a stabilizing agent which initiates transcriptional termination when critical concentrations of guanine are reached⁸³. Metabolite-sensing riboswitches have been implicated in the regulated biosynthesis and transport of co-enzymes⁸⁴⁻⁸⁶, and amino acids⁸⁷⁻⁹⁰. These genetic regulations take place in the complete absence of enzymes. Entire metabolic pathways could be turned off by delivering artificial ligands, which could bind competitively to riboswitches instead of

their natural ligands, and hence these high-specific metabolite-binding RNA molecules are attractive targets for therapy.

2.4.1.3 RNA Interference

RNA interference, one of the most important discoveries in biology for the last twenty years, holds stunning potential in gene annotation and drug development⁹¹⁻⁹⁷. Highly specific, it can potentially be used to silence the transcripts of aberrant genes differing by their wild type counterparts by just a point mutation before translation occurs in the cytosol⁹⁸. RNAi is utilized as a functional genomic tool, by the post-transcriptional silencing of the messenger and observation the metabolic and cellular effects on the phenotype. RNAi is especially important in determining the function of those genes which are critical for basal-level metabolism, and which cannot be knocked out using classical genetics. RNAi silencing knocks out around 75% of the mRNA transcripts, so that the rest can be coded into protein for those critical processes. Moreover, unlike classical genetics studies, the genome of the organisms remains untouched during RNAi studies. And as long as the RNA duplexes are up to 30 nucleotides long, they do not activate interferon-mediated cytotoxicity.

What makes RNAi such an important discovery is that RNAi is not a man-made manipulation of biological systems, but instead is a natural novel form of gene regulation. The basic pathway is universally conserved across the phyla. RNAi evolved as an ancient defense mechanism in plants and invertebrates, which lacked proteinacious immunity, and developed nucleic acid based immunity against viruses and transposons. Thus, RNAi

is physio-compatible, and we can expect therapeutic strategies to be immune compatible and effective, once we develop delivery strategies. The readers are directed towards authoritative reviews by experts in the field^{19, 20, 99, 100}. In certain cases, nucleic acid specificity is not as critical as targeting. Using just a single siRNA may be ineffective against viruses which rapidly mutate in vivo to escape immune action, such as HIV. In such a case, a randomized pool of siRNA designed to cover the spectrum of mutations would serve well to keep viral titers low enough. The potential caveat of this is obvious-off-side effects, wherein genes critical in certain metabolic activities may be silenced.

While RNAi is an excellent technology to treat disorders, it can also be used as an effective probe for gene annotation. Fundamental details of each cell type's developmental pathway will help us in elucidating the mechanisms determining cell fate, and will feed us key information to control runaway processes such as cancer. SiRNA-based screens were used to find key genes involved in Hedgehog signaling in *Drosophila*, a pathway which is responsible for cellular differentiation during early embryonic development. Unrestrained Hedgehog signaling leads to cancer¹⁰¹. Figure 2.2 is a schematic of the Hedgehog pathway, which is a series of repressive steps wherein the Hedgehog protein (*Hh*) binds to the Patched protein (*Ptc*) and inactivates it. Thus, *Ptc* can no longer suppress Smoothed protein (*Smo*), which has a suppressing action on the Cytoplasmic Complex (*CC*). The *CC* is now incapable of suppressing the transcription factor Cubitus Interruptus (*CI*). In the study, luciferase luminescence assays were used to create a genetic map which included known genes and four new genes- Dally-like protein (*Dlp*), *CK1 α* , caupolican and *CG9211*. *Dlp* was shown to be required for reception of the *Hh* signal. *CK1 α* and caupolican were shown to be regulators. Some of the genes bore

homology with murine and human genes which have developmental defects when their Hedgehog signaling goes awry. The homologue of CK1 α is implicated in colon cancer, basal cell carcinoma, and medulloblastoma. Furthermore, the authors used cyclopamine, a drug which targets *Smo*, to control reckless Hedgehog signaling responsible for the maintenance of metastasis in prostate cancer cell lines¹⁰². This is logical as active *CC* can then suppress *CI*. Even more interestingly, normal prostate tissue does not contain any *Smo* mRNA, but cancerous tissue has increased levels with increasing activity, leading to the conclusion that *Smo* expression is the trigger for Hedgehog signaling. This opens the door to cyclopamine-based therapeutics for prostate cancer. Such studies are excellent examples of RNAi based systematic identification and annotation of key genes leading to clinical strategies.

Elegant proof-of-concept experiments were conducted showing the viability of using siRNA against lentiviruses such as HIV¹⁰³. The authors used MAGI cell lines, which express human CD4, and a fused gene encoding the HIV-1 long terminal repeat (LTR) and a β -galactosidase (β -gal) reporter gene. Cells can be counted by flow cytometry by staining for β -gal, which is transactivated by the Tat protein, through the LTR promoter. siRNA targeted against CD4 downregulated its expression to about one-fourth, while mRNA expression was reduced to one-eighth as shown by Northern blots. The cells were challenged with M and T-tropic strains of HIV and it was shown that viral entry was reduced to about one-fourth. In the next stage, the authors used HeLa cells, which are immortalized cell lines growing by contact inhibition. Loss of contact inhibition is a classic sign of oncogenic behavior, leading to multilayer formation. HeLa cells expressing CD4 were targeted by p24-siRNA, which led to a four fold decrease in

viral protein expression, as shown by Northern blots. Also, *nef* is a negative regulator of transcription in the HIV genome, and it is found near the 3' end. Expression of the *gag* gene, leading to p24 expression, would definitely also lead to *nef* expression, as *gag* is upstream to *nef*. *nef* expression was also downregulated, which proved that siRNA had silenced viral genes essential for the replication cycle, and hold therapeutic potential. Thus, HIV therapy in the future might target the receptors and coreceptors on the cell membrane, and viral RNA before and after the replication cycle of the virus.

2.4.1.4 DNA-Based Nanoconstruction

Biomimesis is highlighted by the familiar example of DNA-mediated nanoconstruction¹⁰⁴, where the property of complementary pairing of the genetic alphabet is exploited. Sticky ends, formed when there are overhangs of deoxyribonucleotides, are the most robust form of molecular recognition, and are being utilized for the non-covalent assembly of complex molecular architecture. Seeman and coworkers have pioneered the field of DNA-based nanoconstruction^{105, 106}. In early studies, the authors made a cube¹⁰⁷ with double helical edges, and with ligases joining the open ends to make the faces of the cube. Complex topologies like Borromean rings¹⁰⁸, knots¹⁰⁹, and octahedrons¹¹⁰ were synthesized using Watson-Crick pairing. They then made a stiffer motif for nanoarray assemblies¹¹¹- the DNA crossover molecules, known as DX and DX+J molecules, which consisted of two double helices, coupled by short strands. Such novel chemistry has the potential to shed light on the recombination events occurring at tetra-armed DNA intermediates formed during genetic recombination known as Holliday Junctions. These

short-lived junctions are always mobile, thus making them hard to characterize, and such branched DNA could prove useful in understanding them.

The self-replication of nanomachines made of nucleic acids remains a huge challenge. The reason is that DNA polymerase requires a DNA or RNA primer with a free hydroxyl group at the 3' end and also requires single stranded DNA as template. A possible strategy is to make such constructs, unwind them so that they can be amplified, and then wind them back. An octahedron of 1669 nucleotides on the size scale of viruses was constructed, the edges of which were DX molecules¹¹², which was then unwound and replicated by PCR. Such spontaneously rigid frameworks could also be used for crystallizing RNA-protein complexes, when they prove recalcitrant to conventional methods of crystallization. Recently, the genetic alphabet has been expanded by the assembly of non-natural bases into chains and their replication *via* artificial ligases¹¹³. The design strategy involves modifying DNA polymerase^{114, 115}, so that it recognizes and pairs a non-natural base¹¹⁶ with its complement.

Nucleotides can be used as crosslinking agents for the construction of nano-assemblies. Figure 2.6 typifies the directed assembly of nanoparticles using DNA oligonucleotides¹¹⁷. By attaching different complementary sequences of DNA strands on the nanoparticles, the inter-particle distances, stability, and spatial arrangement of the assembly can be controlled¹¹⁸. Such assemblies have sharp optical¹¹⁹, electrical¹²⁰, and melting¹²¹ transitions, which make them highly programmable platforms. DNA allows ease of operation with analytical techniques like PCR, gel electrophoresis and digestion with nucleases. Recently, it has been discovered that gold nanoparticles bearing antisense

strands can down regulate genes with almost no toxicity to the cells, thus rendering them as attractive gene carriers¹²².

DNA has been used as a sequestering agent for carbon nanotubes. When carbon nanotubes are synthesized, they tend to aggregate, and it is impossible to select a nanotube of desired specification from the mixture. Solubilizing these nanotubes is impractical due to the solvent phobic characteristics of carbon nanotubes. However, single stranded DNA can be used to prevent aggregation^{123, 124}. The interactions between the nanotubes and the DNA strands are similar to the π -stacking by which the nitrogenous bases keep the helix stable¹²⁵, while the sugar domains of the DNA strands are responsible for binding the hydrophobic nanotube surfaces.

Watson-Crick pairing is being used to direct the organic synthesis of libraries of non-natural compounds^{126, 127}. When reagents are tethered to complementary strands, hybridization between the strands increases the effective molarity of reactants due to proximity. Successful synthetic scheme have included thioether formation from maleimide-thiol interaction and S_N2 substitutions¹²⁸, alkyne-azide cycloadditions; and heterocyclic compounds like monocyclic and bicyclic oxazolidines¹²⁹, and the traditionally tricky macrocyclization¹³⁰.

DNA sequences have been grafted onto magnetic nanoparticles to develop novel sensors for viruses such as adenovirus and herpes virus¹³¹. The nanosensor, on detecting the virus, forms a virus-nanoparticle complex, which changes the magnetic resonance signal^{132, 133}. When a serotonin-nanoparticle conjugate was incubated with myeloperoxidase, an enzyme concerned with coronary problems, there were significant changes in the T2 relaxation times of the solution. These nanoparticle conjugates have

also been shown to serve as *in-vivo* sirens for peroxidase-induced diseases¹³⁴, and telomerase activity¹³⁵.

Scaffoldings of titanium oxide nanocrystals and DNA have been designed, which are sensitive to X-ray detection. These nanostructures have been used to target mutant genes¹³⁶. The tethered DNA strand is designed to be complementary to that of the malfunctioning gene, so that spontaneous hybridization would occur when the scaffold is introduced into the cell.

2.4.2 Virology

There is a tremendous need to devise new antiviral strategies as newer and more novel mechanisms of viral replication and infection are being uncovered. Understanding the nature of viral pathogenesis will undoubtedly aid us in developing more effective therapies to combat diseases and will also spur the design of biomimetic systems with stealth properties. Such systems can mimic the mechanisms used by viruses to subvert the immune system.

Cutting edge research into the biology of Human Immunodeficiency Virus (HIV) entry, fusion, replication and persistence in recent years has brought therapeutic hope for AIDS patients. HIV is hard to combat since it tends to mutate very rapidly, so that adaptive immunity, which produces a clone of effectors, proves ineffective. HIV and Simian Immunodeficiency Virus (SIV) utilize CD4 as the primary receptor to gain entry into immune effectors¹³⁷. Entry is also mediated by the chemokine receptors CCR5 and CXCR4, which are fusion coreceptors for M and T-trophic HIV-1 respectively¹³⁸⁻¹⁴⁰.

Interestingly, the macrophage inflammatory protein 1 α (MIP-1 α) and MIP-1 β , which have a high affinity for CCR5, can inhibit M-trophic HIV-1 infection. So, one of the stages of AIDS therapy could include a MIP-1 α antagonistic model.

The long terminal repeat (LTR) is a nucleotide sequence required for viral integration into host genome, using the integrase protein. Upstream LTRs are promoters and enhancers, while downstream LTRs are polyadenylation sites. Transactivation of transcription (Tat) is a nuclear protein which is essential for HIV-1 infectivity. It stimulates the production of key structural proteins for the virion using the LTR and induces apoptosis in uninfected CD4⁺ T helper cells¹⁴¹. Tat has a dramatic influence on macrophages and monocytes, the innate immune cells central to the HIV invasion scheme. Tat greatly up-regulated coreceptor chemokine expression in peripheral blood mononuclear cells (PBMCs) using immunofluorescence staining and flow cytometry. Specifically, the percentage of cells expressing CCR5, CXCR4 and CCR3 increased from 19.4 to 81.7, 16.1 to 89.4 and 49.9 to 86.3 respectively¹⁴². This up-regulation tends to become very important for viral entry. The reason is that HIV also produces proteins like Nef and Vpu which downregulate CD4 expression, in order to debilitate the immunity. Up-regulating the coreceptors, makes up for the decreased receptor expression, and enhances infectivity of the virus. These investigations highlight the import of Tat and point towards an anti-Tat therapy program.

In a dramatic study, it has also been discovered that Tat also subverts the RNAi-based antiviral machinery in the cell. The HIV genome has short viral siRNA (vsiRNA), which are up regulated as HIV-1 infection progresses¹⁴³. Short hairpin RNA (shRNA) designed to target the HIV TAR sequence silence the gene, but in the presence of Tat, the

silencing potency is lowered in a dose-dependant manner. The virus has a double stranded duplex which is conserved across all lentiviruses and hence should be protected from the RNAi machinery in the cell. In order to combat this problem, the virus represses the central enzyme Dicer and subdues the RNAi mechanism. These surprising schemes of viral invasion reveal key information about potential drug targets inhibiting the replication and pathogenesis of viruses.

Viruses could also be used as novel carriers. Raman spectroscopy has found use in mapping the cell and detailing the shapes and relative sizes of the organelles. However, due to the minute length scales involved, the Raman signals are weak and gold nanoparticles are used as spectroscopic enhancers. However, these are ejected immediately by the cellular immune system. In an imaginative leap, the Brome Mosaic Virus (BMV) has been used to smuggle the gold nanoparticles into the cell, using the stealth properties which viruses demonstrate while infecting a host cell¹⁴⁴. The gold is incorporated into the capsid of the virus by a novel scheme involving capsid disassembly in alkaline medium, gold nanoparticle addition, and reassembly of the gold-rich capsid by acidification.

2.4.3 Immunology and Vaccine Design

The established goal of a vaccination is to inoculate a healthy individual with an attenuated strain of a pathogen in order to provide immunity against pathology^{145, 146}. In principle, a vaccine speeds up adaptive response and creates immunological memory. This proves critical in controlling infection, as primary adaptive response is delayed by

almost a week due to the clonal selection and proliferation of B and T lymphocytes. Thus, vaccines provide a baseline number of resting T and B cells, which on secondary antigen exposure, show rapid kinetics and cytolytic properties. Future strategies in antiviral and antibacterial vaccination rely heavily on a piecewise dissection of T cell differentiation¹⁴⁷, and a cognition of innate and adaptive strategies, to maintain low pathogen titers and clearing out infection. Some of these concepts are detailed in a commanding review on the subject¹⁴⁸.

T and B cells are positively selected in the thymus and bone marrow respectively. The thymus screens the immature thymocytes by expressing promiscuous genes, and induces apoptosis in the thymocytes which interact weakly with antigen or too strongly with self-antigen. Naïve T cell precursor cells remain inactive until they are activated by antigen presenting cells in the secondary lymph nodes. Langerhans cells, immature dendritic cells, with high macropinocytic propensity circulate in the peripheral tissues. When pathogen is encountered and taken up, dendritic cells migrate to the secondary lymph nodes, with an increase in their antigen presentation ability. This is marked by the expression of MHC molecules and costimulatory molecules like CD80 and CD86, which activate T cells by binding to CD28. Antigen presentation by the peptide-MHC complex is restricted by self-MHC molecules^{149, 150}. The adaptive immunity consists of B and T cells, generated through somatic recombination. On activation, T cells begin a proliferative program by entering the cell cycle and secreting IL-2 which acts in an autocrine fashion. T cells are either CD8⁺ Cytotoxic T cell lymphocytes (CTLs) or CD4⁺ T helper lymphocytes. T helper cells are themselves composed of T_H1 and T_H2 cells, which carry out critical immune functions. The T_H1/T_H2 dichotomy is decided by unique

transcription factors and cytokines. T_H1 cells are found in environments characterized by T-bet based transcription, STAT-4 signaling and secretion of IL-12 and IFN- γ . T_H2 cells are found in environments characterized by GATA-3 based transcription, STAT-6 signaling and secretion of granulocyte macrophage colony stimulating factor (GM-SCF), IL-3, IL-4, IL-5, IL-6, IL-9 and IL-13 secretion¹⁵¹⁻¹⁵³. Each set of conditions reciprocally inhibits the other and skews the pathways in its favor. Future biomimetic strategies could involve the generation of a specific population of immune cells by controlling transcription factor and cytokine expressions and driving immune cell fate decisions.

After the infection is dealt with, primarily by the lytic action of CD8⁺ CTLs, most of the cells undergo apoptosis to prevent scavenging, while the rest form a baseline number of memory T cells which show anamnesis. A future vaccine could be designed to lower this apoptotic loss of antigen-specific clones, so that memory T cell numbers are increased. Memory CD8⁺ and CD4⁺ T cells that reside in the peripheral tissues are termed “effector” memory T cells (T_{EM}), while the CD8⁺ and CD4⁺ T cells that remain in the lymphoid organs are called “central memory T cells” (T_{CM}). Figure 2.3 is a schematic of the memory T cell pathways in mammals. The swift kinetics, lytic competence and *in vivo* cytotoxicity¹⁵⁴ of memory T cells are crucial for the success of the vaccine. It is crucial to determine which subsets of effectors are compromised during various diseases, so that vaccines could be devised for replenishment of these effector cells.

2.4.4 Nanotechnology

Technological advances have revolutionized clinical medicine and dramatically improved patient care and quality of life. These technologies include X-rays, the electron microscope, radioactive tracers, ultrasound and ultrasonic imaging, computer-aided topography, magnetic resonance imaging, endoscopy, pacemakers, the ventricular defibrillator, the blood-heat exchanger, contact lenses, heart valves, artificial kidney, etc. At the transition into the 21st century, technology is becoming progressively controlled at the molecular level, and is driving the next generation of commercial diagnostic and therapeutic devices¹⁵⁵. The application of nanodevices for biological and medical applications is leading to fundamental insights about intra- and inter-cellular communication^{156, 157}, forces and flows and the effects on individual cells¹⁵⁸, the structure and function of proteins, nucleic acids, and other biological molecules¹⁵⁹, and pharmacogenetics and genetic predisposition toward disease. In this section, we present a few examples of biomimetic sensors which have potential in future therapeutic platforms.

A sensor is characterized by two key components, a sensing element, which has a specific interaction with an analyte or environmental condition, and a transducing element, which converts this interaction into a measurable effect. For biomedical applications, the sensing element is designed to interact specifically with target molecules. Molecular recognition between biomolecules are the most common sensing strategies in biosensors, due to their high affinity and specificity¹⁶⁰. Biomimetic sensing elements are advantageous over their biological counterparts because they can be designed to mimic biological recognition pathways and at the same time exhibit other

favorable abiotic properties, such as greater stability in harsh environments and custom synthesis¹⁶¹. Common transducing elements, such as optical, electrochemical, gravimetric, and micromechanical, have been highlighted in recent reviews¹⁶²⁻¹⁶⁵.

Microarrays, dubbed DNA arrays, DNA chips, and Gene chips, have been established as the preferred method for carrying out genetic profiling and diagnosis on a massive scale¹⁶⁶. However, care must be taken that gene expression profiles obtained from such platforms should not be over interpreted. As an example, increased up regulation and down regulation of particular genes due to a particular stimulus might not be connected to the stimulus, as the gene expression pattern could be a response to any kind of stress.

Microfluidic systems are extremely attractive platforms for gene profiling and annotation for several reasons- accurate analysis of nanoscale volumes, low well-characterized manufacturing schemes, and capability of probing single cell gene expression. Microfluidic compact discs with spherical beads have been used for cell lysis of *E. coli* and *S. cerevisiae*¹⁶⁷. Such a technology has the potential to improve bacterial transformation techniques, which involve chemical or enzymatic treatments for cell lysis, and require further purification steps. An exciting advance which could revolutionize contemporary cloning schemes involves the parallel isolation and purification of *E. coli* DNA¹⁶⁸. Such efforts can spur the development of chips for the determination of regulatory RNA expression profiles and epigenetic differences that decide cell fates. Furthermore, continuous-flow microfluidic PCR techniques have been used recently for multigene analysis from hundreds of individual bacterial in parallel¹⁶⁹. In general, the

future of such technologies lies in their application to discriminate between single nucleotide polymorphisms, and detection of alternate splicing and rare mutations.

Novel sensing technologies such as nanopore sequencing, have demonstrated the possibility to make sequencing analysis faster and cheaper¹⁷⁰. These investigations began with the observation that there is a drop in current when an oligonucleotide enters a nanopore compared to any electrolyte, and this principle has been used to design biosensors. A translocating molecule alters the ionic current through the pore relative to its open state, and this current change is monitored versus time and then correlated to the specific characteristics of the target macromolecule. Nanopores made of α -hemolysin, a toxin that forms a transmembrane channel in a lipid layer, have been designed, to characterize polynucleotides by single-channel recording¹⁷¹. The authors attached a probe to the mouth of the pore, which can give different current intensities when a complementary strand enters the pore, compared to a random sequence¹⁷². Such a pore has been shown to distinguish between different oligonucleotides in solution. Recently, nanofabrication methods have been applied to reproducibly create more robust, synthetic nanopores that can be tailored to have desired dimensions¹⁷³⁻¹⁷⁵.

Optical nanosensors have been shown to highly efficacious in making quantitative measurements of ions in the intracellular environment¹⁷⁶. Probes encapsulated by biologically localized embedding (PEBBLEs), with diameters on order of 40 nanometers, have been utilized to measure intracellular values of pH, calcium, magnesium, potassium, and oxygen^{177, 178}. In another sensing application, optical nanofibers, with a tip diameter of approximately 50 nanometers, were fabricated and then functionalized with antibodies, allowing for nanometer resolved spatial measurements of a target analyte¹⁵⁷.

2.4.5 Polymer science and engineering

Today, polymer scientists and engineers can synthesize a wide variety of macromolecules with precise control of their molecular structure and physiochemical properties. By designing the molecular functionality and structure of a synthetic polymer network to mimic biological systems, three-dimensional network structures exhibiting structural similarities can be created with tailorable drug delivery properties.

Synthetic networks that recognize and bind bio molecules can be prepared using template-mediated polymerization techniques (e.g. molecular imprinting). There have been many excellent reviews on the field of molecular imprinting^{179, 180}, and we direct the reader to the following chapter for an overview on the field. Recent reviews^{181, 182} highlight the advantages that such drug delivery systems provide such as sustained release, enhanced loading capacity, and enantioselective loading or release. These reviews also discuss the problems to be solved in the design of synthetic recognition-based networks, and recent efforts toward integrating imprinted polymers in controlled drug delivery systems and sensing devices.

Biologically active molecules can be incorporated into polymer networks to produce conjugated biomaterials, which has been highlighted in a recent review¹⁸³. In many situations, localized delivery is critical for a therapeutic molecule to have an optimized effect. Biologically active entities conjugated to polymer networks have applicability in targeted delivery of therapeutic compounds¹⁸⁴. An example of biomimetic

targeting is *via* glycoprotein mimics. Researchers have synthesized glycopolymers that function as an artificial multivalent ligand able to facilitate site-specific drug delivery¹⁸⁵.

2.5 Conclusions

In view of the above discussions, it is clear that the convergence of many streams of science will lead to a new era of medicine, wherein rationally designed biomimetic systems will aid in the diagnosis and treatment of disease. Although the application of biomimesis is in its infancy, the unlimited potential is clear, especially in medical science and technology. Advances in the fields of gene regulation, signal transduction, immunology, and structural biology will serve to expedite the design and introduction of biomimetic systems into mainstream medicine.

2.6 List of References

1. Venkatesh, S., Byrne, M.E., Peppas, N.A. & Hilt, J.Z. Applications of biomimetic systems in drug delivery. *Exp. Opin. Drug Del.* **2**, 1085-1096 (2005).
2. Byrne, M.E. & Venkatesh, S. Biomimetic systems: a synergy of scientific and engineering approaches. (*Horizon Bioscience*, 2007).
3. Fersht, A. Enzymes: Structures and Reaction Mechanisms. (*W.H. Freeman & Company*, 1983).
4. Sutherland, E.W. Mechanism of hormone action. *Prix Nobel*, 240-257 (1972).

5. Rodbell, M. Signal transduction: evolution of an idea (Nobel Lecture). *Angew. Chem. Int. Ed.* **34**, 1420-1428 (1995).
6. Gilman, A.G. G proteins and regulation of adenylate cyclase (Nobel Lecture). *Angew. Chem. Int. Ed.* **34**, 1406-1419 (1995).
7. Peppas, N.A. Intelligent therapeutics: biomimetic systems and nanotechnology in drug delivery. *Adv. Drug Del. Rev.* **56**, 1529-1531 (2004).
8. Langer, R. Drug delivery and targeting. *Nature* **392**, 5-10 (1998).
9. Langer, R. Drug delivery. Drugs on target. *Science* **293**, 58-59 (2001).
10. Noguchi, H. et al. A new cell-permeable peptide allows successful allogeneic islet transplantation in mice. *Nat. Med.* **10**, 305-309 (2004).
11. Kondo, E., Seto, M., Yoshikawa, K. & Yoshino, T. Highly efficient delivery of p16 antitumor peptide into aggressive leukemia/lymphoma cells using a novel transporter system. *Mol. Cancer Ther.* **3**, 1623-1630 (2004).
12. Hartwell, L.H. & Weinert, T.A. Checkpoints: controls that ensure the order of cell cycle events. *Science* **246**, 629-634 (1989).
13. Nurse, P., Masui, Y. & Hartwell, L. Understanding the cell cycle. *Nat. Med.* **4**, 1103-1106 (1998).
14. Hunt, T. & Kirschner, M. Cell multiplication. *Curr. Opin. Cell Biol.* **5**, 163-165 (1993).
15. Dinarina, A. et al. Characterization of a new family of cyclin-dependent kinase activators. *Biochem. J* **386**, 349-355 (2005).
16. Hartwell, L.H. & Kastan, M.B. Cell cycle control and cancer. *Science* **266**, 1821-1828 (1994).

17. Hartwell, L.H., Szankasi, P., Roberts, C.J., Murray, A.W. & Friend, S.H. Integrating genetic approaches into the discovery of anticancer drugs. *Science* **278**, 1064-1068 (1997).
18. Paulovich, A.G., Toczyski, D.P. & Hartwell, L.H. When checkpoints fail. *Cell* **88**, 315-321. (1997).
19. Hannon, G.J. RNA interference. *Nature* **418**, 244-251 (2002).
20. Novina, C.D. & Sharp, P.A. The RNAi revolution. *Nature* **430**, 161-164 (2004).
21. Kim, D.H. & Rossi, J.J. Strategies for silencing human disease using RNA interference. *Nat. Rev. Genet.* **8**, 173-184 (2007).
22. Whitesides, G.M. The 'right' size in nanobiotechnology. *Nat. Biotechnol.* **21**, 1161-1165 (2003).
23. Jiang, Y. et al. X-ray structure of a voltage-dependent K⁺ channel. *Nature* **423**, 33-41 (2003).
24. Jiang, Y., Ruta, V., Chen, J., Lee, A. & MacKinnon, R. The principle of gating charge movement in a voltage-dependent K⁺ channel. *Nature* **423**, 42-48 (2003).
25. Branden, C. & Tooze, J. Introduction to Protein Structure. (*Routledge*, 1992).
26. MacKinnon, R. Ion channels: Potassium channels and the atomic basis of selective ion conduction (Nobel Lecture). *Angew. Chem. Int. Ed.* **43**, 4265-4277 (2004).
27. Hille, B., Armstrong, C.M. & MacKinnon, R. Ion channels: from idea to reality. *Nat. Med.* **5**, 1105-1109 (1999).
28. Doyle, D.A. et al. The structure of the potassium channel: molecular basis of K⁺ conduction and selectivity. *Science* **280**, 69-77 (1998).

29. Zhou, Y., Morais-Cabral, J.H., Kaufman, A. & MacKinnon, R. Chemistry of ion coordination and hydration revealed by a K⁺ channel-Fab complex at 2.0 Å resolution. *Nature* **414**, 43-48 (2001).
30. MacKinnon, R., Cohen, S.L., Kuo, A., Lee, A. & Chait, B.T. Structural conservation in prokaryotic and eukaryotic potassium channels. *Science* **280**, 106-109 (1998).
31. Wulff, H. & Pennington, M. Targeting effector memory T-cells with Kv1.3 blockers. *Curr. Opin. Drug Discov. Dev.* **10**, 438-445 (2007).
32. Chandy, K.G. et al. K⁺ channels as targets for specific immunomodulation. *Trends Pharmacol. Sci.* **25**, 280-289 (2004).
33. Wulff, H., Beeton, C. & Chandy, K.G. Potassium channels as therapeutic targets for autoimmune disorders. *Curr. Opin. Drug Discov. Dev.* **6**, 640-647 (2003).
34. Blobel, G. & Dobberstein, B. Transfer to proteins across membranes. II. Reconstitution of functional rough microsomes from heterologous components. *J. Cell Biol.* **67**, 852-862. (1975).
35. Blobel, G. & Dobberstein, B. Transfer of proteins across membranes. I. Presence of proteolytically processed and unprocessed nascent immunoglobulin light chains on membrane-bound ribosomes of murine myeloma. *J. Cell Biol.* **67**, 835-851. (1975).
36. Gilmore, R., Blobel, G. & Walter, P. Protein translocation across the endoplasmic reticulum. I. Detection in the microsomal membrane of a receptor for the signal recognition particle. *J. Cell Biol.* **95**, 463-469. (1982).

37. Gilmore, R., Walter, P. & Blobel, G. Protein translocation across the endoplasmic reticulum. II. Isolation and characterization of the signal recognition particle receptor. *J. Cell Biol.* **95**, 470-477. (1982).
38. van den Berg, B. et al. X-ray structure of a protein-conducting channel. *Nature* **427**, 36-44 (2004).
39. Simon, S.M. & Blobel, G. Signal peptides open protein-conducting channels in *E. coli*. *Cell* **69**, 677-684 (1992).
40. Simon, S.M. & Blobel, G. Mechanisms of translocation of proteins across membranes. *Subcell. Biochem.* **21**, 1-15 (1993).
41. Hartl, F.U. & Hayer-Hart, M. Molecular chaperones in the cytosol: from nascent chain to folded protein. *Science* **295**, 1852-1858 (2002).
42. Leslie, M. Lost in translation: the signal hypothesis. *J. Cell Biol.* **170**, 338 (2005).
43. Birmingham, K. A nobel for blobel. *Nat. Med.* **5**, 1230 (1999).
44. Matlin, K.S. When cell biology grew up. *Traffic* **1**, 291-292 (2000).
45. Peppas, N.A. & Langer, R. New challenges in biomaterials. *Science* **263**, 1715-1720 (1994).
46. Langer, R. & Tirrell, D.A. Designing materials for biology and medicine. *Nature* **428**, 487-492 (2004).
47. Pack, D.W., Hoffman, A.S., Pun, S. & Stayton, P.S. Design and development of polymers for gene delivery. *Nat. Rev. Drug Discov.* **4**, 581-593 (2005).
48. Duncan, R. Polymer conjugates as anticancer nanomedicines. *Nat. Rev. Cancer* **6**, 688-701 (2006).

49. Sarkar, C.A. & Lauffenburger, D.A. Cell-level pharmacokinetic model of granulocyte colony-stimulating factor: implications for ligand lifetime and potency in vivo. *Mol. Pharmacol.* **63**, 147-158 (2003).
50. Sarkar, C.A. et al. Rational cytokine design for increased lifetime and enhanced potency using pH-activated histidine switching. *Nat. Biotechnol.* **20**, 908-913 (2002).
51. Bumcrot, D., Manoharan, M., Koteliansky, V. & Sah, D.W.Y. RNAi therapeutics: a potential new class of pharmaceutical drugs. *Nat. Chem. Biol.* **2**, 711-719 (2006).
52. Doudna, J.A. & Cech, T.R. The chemical repertoire of natural ribozymes. *Nature* **418**, 222-228 (2002).
53. Kruger, K. et al. Self-splicing RNA: autoexcision and autocyclization of the ribosomal RNA intervening sequence of Tetrahymena. *Cell* **31**, 147-157 (1982).
54. Stark, B.C., Kole, R., Bowman, E.J. & Altman, S. Ribonuclease P: An enzyme with an essential RNA component. *PNAS* **75**, 3717-3721 (1978).
55. Guerrier-Takada, C., Gardiner, K., Marsh, T., Pace, N. & Altman, S. The RNA moiety of ribonuclease P is the catalytic subunit of the enzyme. *Cell* **35**, 849-857 (1983).
56. Cate, J.H. et al. Crystal structure of a group I ribozyme domain: Principles of RNA packing. *Science* **273**, 1678-1685 (1996).
57. Munz, C. Epstein-barr virus nuclear antigen 1: from immunologically invisible to a promising T cell target. *J. Exp. Med.* **199**, 1301-1304 (2004).

58. Huang, S., Stupack, D., Mathias, p., Wang, Y. & Nemerow, G. Growth arrest of Epstein-Barr virus immortalized B lymphocytes by adenovirus-delivered ribozymes. *PNAS* **94**, 8156-8161 (1997).
59. Sullenger, B.A. & Gilboa, E. Emerging clinical applications of RNA. *Nature* **418**, 252-258 (2002).
60. Lan, N. et al. Enhancing RNA repair efficiency by combining trans-splicing ribozymes that recognize different accessible sites on a target RNA. *Mol. Ther.* **2**, 245-255 (2000).
61. Kohler, U., Ayre, B.G., Goodman, H.M. & Haseloff, J. Trans-splicing Ribozymes for Targeted Gene Delivery. *J. Mol. Biol.* **285**, 1935-1950 (1999).
62. Watanabe, T. & Sullenger, B.A. Induction of wild-type p53 activity in human cancer cells by ribozymes that repair mutant p53 transcripts. *PNAS* **97**, 8490-8494 (2000).
63. Lan, N., Howery, R.P., Lee, S.-W., Smith, C.A. & Sullenger, B.A. Ribozyme-mediated repair of sickle beta-globin mRNAs in erythrocyte precursors. *Science* **280**, 1593-1596 (1998).
64. Byun, J., Lan, N., Long, M. & Sullenger, B.A. Efficient and specific repair of sickle b-globin RNA by trans-splicing ribozymes. *RNA* **9**, 1254-1263 (2003).
65. Ellington, A.D. & Szostak, J.W. In vitro selection of RNA molecules that bind specific ligands. *Nature* **346**, 818-822 (1990).
66. Tuerk, C. & Gold, L. Systematic evolution of ligands by exponential enrichment: RNA ligands to bacteriophage T4 DNA polymerase. *Science* **249**, 505-510 (1990).

67. James, W. Aptamers in the virologists' toolkit. *J. Gen. Virol.* **88**, 351-364 (2007).
68. Lorsch, J.R. & Szostak, J.W. In vitro selection of RNA aptamers specific for cyanocobalamin. *Biochemistry* **33**, 973-982 (1994).
69. Wilson, C., Nix, J. & Szostak, J. Functional requirements for specific ligand recognition by a biotin-binding RNA pseudoknot. *Biochemistry* **37**, 14410-14419 (1998).
70. Wang, Y., Killian, J., Hamasaki, K. & Rando, R.R. RNA molecules that specifically and stoichiometrically bind aminoglycoside antibiotics with high affinities. *Biochemistry* **35**, 12338-12346 (1996).
71. Patel, D.J. et al. Structure, recognition and adaptive binding in RNA aptamer complexes. *J. Mol. Biol.* **272**, 645-664 (1997).
72. Jiang, L., Suri, A.K., Fiala, R. & Patel, D.J. Saccharide-RNA recognition in an aminoglycoside antibiotic-RNA aptamer complex. *Chem. Biol.* **4**, 35-50 (1997).
73. Jiang, L. & Patel, D.J. Solution structure of the tobramycin-RNA aptamer complex. *Nat. Struct. Biol.* **5**, 769-774 (1998).
74. Jiang, L. et al. Saccharide-RNA recognition in a complex formed between neomycin B and an RNA aptamer. *Structure* **7**, 817-827 (1999).
75. Koizumi, M. & Breaker, R.R. Molecular Recognition of cAMP by an RNA Aptamer. *Biochemistry* **39**, 8983-8992 (2000).
76. Flinders, J. et al. Recognition of planar and nonplanar ligands in the malachite green - RNA aptamer complex. *ChemBioChem* **5**, 62-72 (2004).
77. Nimjee, S.M., Rusconi, C.P. & Sullenger, B.A. Aptamers: an emerging class of therapeutics. *Annu. Rev. Med.* **56**, 555-583 (2005).

78. Hermann, T. & Patel, D.J. Adaptive recognition by nucleic acid aptamers. *Science* **287**, 820-825 (2000).
79. Hamaguchi, N., Ellington, A. & Stanton, M. Aptamer beacons for the direct detection of proteins. *Anal. Biochem.* **294**, 126-131 (2001).
80. Jhaveri, S., Rajendran, M. & Ellington, A.D. In vitro selection of signaling aptamers. *Nat. Biotechnol.* **18**, 1293-1297 (2000).
81. Mandal, M., Boese, B., Barrick, J.E., Winkler, W.C. & Breaker, R.R. Riboswitches control fundamental biochemical pathways in *Bacillus subtilis* and other bacteria. *Cell* **113**, 577-586 (2003).
82. Mandal, M. & Breaker, R.R. Gene regulation by riboswitches. *Nat. Rev. Mol. Cell Biol.* **5**, 451-463 (2004).
83. Batey, R.T., Gilbert, S.D. & Montagne, R.K. Structure of a natural guanine-responsive riboswitch complexed with the metabolite hypoxanthine. *Nature* **432**, 411-415 (2004).
84. Nahvi, A. et al. Genetic Control by a Metabolite Binding mRNA. *Chem. Biol.* **9**, 1043-1049 (2002).
85. Winkler, W.C., Cohen-Chalamish, S. & Breaker, R.R. An mRNA structure that controls gene expression by binding FMN. *PNAS* **99**, 15908-15913 (2002).
86. Fuchs, R.T., Grundy, F.J. & Henkin, T.M. The SMK box is a new SAM-binding RNA for translational regulation of SAM synthetase. *Nat. Struct. Mol. Biol.* **13**, 226-233 (2006).
87. Lipfert, J. et al. Structural transitions and thermodynamics of a glycine-dependent riboswitch from *Vibrio cholerae*. *J. Mol. Biol.* **365**, 1393-1406 (2007).

88. Mandal, M. et al. A Glycine-Dependent Riboswitch That Uses Cooperative Binding to Control Gene Expression. *Science* **306**, 275-279 (2004).
89. Rodionov, D.A., Vitreschak, A.G., Mironov, A.A. & Gelfand, M.S. Regulation of lysine biosynthesis and transport genes in bacteria: yet another RNA riboswitch? *Nucleic Acids Res.* **31**, 6748-6757 (2003).
90. Sudarsan, N., Wickiser, J.K., Nakamura, S., Ebert, M.S. & Breaker, R.R. An mRNA structure in bacteria that controls gene expression by binding lysine. *Genes Dev.* **17**, 2688-2697 (2003).
91. Fire, A. et al. Potent and specific genetic interference by double-stranded RNA in *Caenorhabditis elegans*. *Nature* **391**, 806-811 (1998).
92. Timmons, L., Tabara, H., Mello, C.C. & Fire, A.Z. Inducible systemic RNA silencing in *Caenorhabditis elegans*. *Mol. Biol. Cell* **14**, 2972-2983 (2003).
93. Parrish, S. & Fire, A. Distinct roles for RDE-1 and RDE-4 during RNA interference in *Caenorhabditis elegans*. *RNA* **7**, 1397-1402 (2001).
94. Grishok, A. et al. Genes and mechanisms related to RNA interference regulate expression of the small temporal RNAs that control *C. elegans* developmental timing. *Cell* **106**, 23-34 (2001).
95. Tabara, H. et al. The *rde-1* gene, RNA interference, and transposon silencing in *C. elegans*. *Cell* **99**, 123-132 (1999).
96. Montgomery, M.K., Xu, S. & Fire, A. RNA as a target of double-stranded RNA-mediated genetic interference in *Caenorhabditis elegans*. *PNAS* **95**, 15502-15507 (1998).

97. Timmons, L. & Fire, A. Specific interference by ingested dsRNA. *Nature* **395**, 854 (1998).
98. Schwarz, D.S. et al. Designing siRNA that distinguish between genes that differ by a single nucleotide. *PLoS Genet.* **2**, e140 (2006).
99. Cullen, B.R. RNA interference: antiviral defense and genetic tool. *Nat. Immunol.* **3**, 597-599 (2002).
100. Meister, G. & Tuschl, T. Mechanisms of gene silencing by double-stranded RNA. *Nature* **431**, 343-349 (2004).
101. Lum, L. et al. Identification of Hedgehog Pathway Components by RNAi in *Drosophila* Cultured Cells. *Science* **299**, 2039-2045 (2003).
102. Karhadkar, S.S. et al. Hedgehog signaling in prostate regeneration, neoplasia and metastasis. *Nature* **431**, 707-712 (2004).
103. Novina, C.D. et al. siRNA-directed inhibition of HIV-1 infection. *Nat. Med.* **8**, 681-686 (2002).
104. Loweth, C.J., Caldwell, W.B., Peng, X., Alivisatos, A.P. & Schultz, P.G. DNA-based assembly of gold nanocrystals. *Angew. Chem. Int. Ed.* **38**, 1808-1812 (1999).
105. Seeman, N.C. DNA nanotechnology: novel DNA constructions. *Annu. Rev. Biophys. Biomol. Struct.* **27**, 225-248 (1998).
106. Seeman, N.C. Biochemistry and structural DNA nanotechnology: An evolving symbiotic relationship. *Biochemistry* **42**, 7259-7269 (2003).
107. Chen, J. & Seeman, N.C. Synthesis from DNA of a molecule with the connectivity of a cube. *Nature* **350**, 631-633 (1991).

108. Mao, C., Sun, W. & Seeman, N.C. Assembly of Borromean rings from DNA. *Nature* **386**, 137-138 (1997).
109. Seeman, N.C. et al. Synthetic DNA knots and catenanes. *New J. Chem.* **17**, 739-755 (1993).
110. Zhang, Y. & Seeman, N.C. Construction of a DNA-Truncated Octahedron. *J. Am. Chem. Soc.* **116**, 1661-1669 (1994).
111. LaBean, T.H. et al. Construction, Analysis, Ligation, and Self-Assembly of DNA Triple Crossover Complexes. *J. Am. Chem. Soc.* **122**, 1848-1860 (2000).
112. Shih, W.M., Quispe, J.D. & Joyce, G.F. A 1.7-kilobase single-stranded DNA that folds into a nanoscale octahedron. *Nature* **427**, 618-621 (2004).
113. Henry, A.A. & Romesberg, F.E. Beyond A, C, G and T: augmenting nature's alphabet. *Curr. Opin. Chem. Biol.* **7**, 727-733 (2003).
114. Henry, A.A., Yu, C. & Romesberg, F.E. Determinants of Unnatural Nucleobase Stability and Polymerase Recognition. *J. Am. Chem. Soc.* **125**, 9638-9646 (2003).
115. Fa, M., Radeghieri, A., Henry, A.A. & Romesberg, F.E. Expanding the Substrate Repertoire of a DNA Polymerase by Directed Evolution. *J. Am. Chem. Soc.* **126**, 1748-1754 (2004).
116. Yu, C., Henry, A.A., Romesberg, F.E. & Schultz, P.G. Polymerase recognition of unnatural base pairs. *Angew. Chem. Int. Ed.* **41**, 3841-3844 (2002).
117. Mirkin, C.A., Letsinger, R.L., Mucic, R.C. & Storhoff, J.J. A DNA-based method for rationally assembling nanoparticles into macroscopic materials. *Nature* **382**, 607-609 (1996).

118. Mucic, R.C., Storhoff, J.J., Mirkin, C.A. & Letsinger, R.L. DNA-Directed Synthesis of Binary Nanoparticle Network Materials. *J. Am. Chem. Soc.* **120**, 12674-12675 (1998).
119. Storhoff, J.J. et al. What Controls the Optical Properties of DNA-Linked Gold Nanoparticle Assemblies? *J. Am. Chem. Soc.* **122**, 4640-4650 (2000).
120. Park, S.-J. et al. The electrical properties of gold nanoparticle assemblies linked by DNA. *Angew. Chem. Int. Ed.* **39**, 3845-3848 (2000).
121. Jin, R., Wu, G., Li, Z., Mirkin, C.A. & Schatz, G.C. What controls the melting properties of DNA-linked gold nanoparticle assemblies? *J. Am. Chem. Soc.* **125**, 1643-1654. (2003).
122. Rosi, N.L. et al. Oligonucleotide-Modified Gold Nanoparticles for Intracellular Gene Regulation. *Science* **312**, 1027-1030 (2006).
123. Zheng, M. et al. DNA-assisted dispersion and separation of carbon nanotubes. *Nat. Mat.* **2**, 338-342 (2003).
124. Zheng, M. et al. Structure-Based Carbon Nanotube Sorting by Sequence-Dependent DNA Assembly. *Science* **302**, 1545-1548 (2003).
125. Strano, M.S. et al. Understanding the Nature of the DNA-Assisted Separation of Single-Walled Carbon Nanotubes Using Fluorescence and Raman Spectroscopy. *Nano Lett.* **4**, 543-550 (2004).
126. Kanan, M.W., Rozenman, M.M., Sakurai, K., Snyder, T.M. & Liu, D.R. Reaction discovery enabled by DNA-templated synthesis and in vitro selection. *Nature* **431**, 545-549 (2004).

127. Li, X. & Liu, D.R. DNA-templated organic synthesis: Nature's strategy for controlling chemical reactivity applied to synthetic molecules. *Angew. Chem. Int. Ed.* **43**, 4848-4870 (2004).
128. Gartner, Z.J. & Liu, D.R. The Generality of DNA-Templated Synthesis as a Basis for Evolving Non-Natural Small Molecules. *J. Am. Chem. Soc.* **123**, 6961-6963 (2001).
129. Li, X., Gartner, Z.J., Tse, B.N. & Liu, D.R. Translation of DNA into synthetic N-acyloxazolidines. *J. Am. Chem. Soc.* **126**, 5090-5092 (2004).
130. Gartner, Z.J. et al. DNA-Templated Organic Synthesis and Selection of a Library of Macrocycles. *Science* **305**, 1601-1605 (2004).
131. Perez, J.M., Simeone, F.J., Saeki, Y., Josephson, L. & Weissleder, R. Viral-induced self-assembly of magnetic nanoparticles allows the detection of viral particles in biological media. *J. Am. Chem. Soc.* **125**, 10192-10193 (2003).
132. Perez, J.M., Josephson, L., O'Loughlin, T., Hoegemann, D. & Weissleder, R. Magnetic relaxation switches capable of sensing molecular interactions. *Nat. Biotechnol.* **20**, 816-820 (2002).
133. Perez, J.M., Josephson, L. & Weissleder, R. Use of magnetic nanoparticles as nanosensors to probe for molecular interactions. *ChemBioChem* **5**, 261-264 (2004).
134. Perez, J.M., Simeone, F.J., Tsourkas, A., Josephson, L. & Weissleder, R. Peroxidase substrate nanosensors for MR imaging. *Nano Lett.* **4**, 119-122 (2004).
135. Grimm, J., Perez, J.M., Josephson, L. & Weissleder, R. Novel Nanosensors for Rapid Analysis of Telomerase Activity. *Cancer Res.* **64**, 639-643 (2004).

136. Paunesku, T. et al. Biology of TiO₂-oligonucleotide nanocomposites. *Nat. Mat.* **2**, 343-346 (2003).
137. McClure, M.O. et al. HIV infection of primate lymphocytes and conservation of the CD4 receptor. *Nature* **330**, 487-489 (1987).
138. Alkhatib, G., Broder, C.C. & Berger, E.A. Cell type-specific fusion cofactors determine human immunodeficiency virus type 1 tropism for T-cell lines versus primary macrophages. *J. Virol.* **70**, 5487-5494 (1996).
139. Alkhatib, G. et al. CC CKR5: a RANTES, MIP-1alpha, MIP-1beta receptor as a fusion cofactor for macrophage-tropic HIV-1. *Science* **272**, 1955-1958 (1996).
140. Choe, H. et al. The beta-chemokine receptors CCR3 and CCR5 facilitate infection by primary HIV-1 isolates. *Cell* **85**, 1135-1148 (1996).
141. Li, C.J., Friedman, D.J., Wang, C., Meteleev, V. & Pardee, A.B. Induction of apoptosis in uninfected lymphocytes by HIV-1 Tat protein. *Science* **268**, 429-431 (1995).
142. Huang, L., Bosch, I., Hofmann, W., Sodroski, J. & Pardee, A.B. Tat protein induces human immunodeficiency virus type 1 (HIV-1) coreceptors and promotes infection with both macrophage-tropic and T-lymphotropic HIV-1 strains. *J. Virol.* **72**, 8952-8960 (1998).
143. Bennasser, Y., Le, S.-Y., Benkirane, M. & Jeang, K.-T. Evidence that HIV-1 encodes an siRNA and a suppressor of RNA silencing. *Immunity* **22**, 607-619 (2005).

144. Dragnea, B., Chen, C., Kwak, E.-S., Stein, B. & Kao, C.C. Gold nanoparticles as spectroscopic enhancers for in vitro studies on single viruses. *J. Am. Chem. Soc.* **125**, 6374-6375 (2003).
145. Zinkernagel, R.M. On natural and artificial vaccinations. *Annu. Rev. Immunol.* **21**, 515-546 (2003).
146. Zinkernagel, R.M. et al. On immunological memory. *Annu. Rev. Immunol.* **14**, 333-367 (1996).
147. Kaech, S.M., Wherry, E.J. & Ahmed, R. Effector and memory T-cell differentiation: implications for vaccine development. *Nat. Rev. Immunol.* **2**, 251-262 (2002).
148. Esser, M.T. et al. Memory T cells and vaccines. *Vaccine* **21**, 419-430 (2003).
149. Zinkernagel, R.M. Restriction of H-2 gene complex of transfer of cell-mediated immunity to *Listeria monocytogenes*. *Nature* **251**, 230-233 (1974).
150. Zinkernagel, R.M. & Doherty, P.C. Restriction of in vitro T cell-mediated cytotoxicity in lymphocytic choriomeningitis within a syngeneic or semiallogeneic system. *Nature* **248**, 701-702 (1974).
151. Szabo, S.J. et al. A novel transcription factor, T-bet, directs Th1 lineage commitment. *Cell* **100**, 655-669 (2000).
152. Szabo, S.J., Sullivan, B.M., Peng, S.L. & Glimcher, L.H. Molecular mechanisms regulating Th1 immune responses. *Annu. Rev. Immunol.* **21**, 713-758 (2003).
153. Szabo, S.J. et al. Distinct effects of T-bet in TH1 lineage commitment and IFN- γ production in CD4 and CD8 T cells. *Science* **295**, 338-342 (2002).

154. Barber, D.L., Wherry, E.J. & Ahmed, R. Cutting edge: rapid in vivo killing by memory CD8 T cells. *J. Immunol.* **171**, 27-31 (2003).
155. Mazzola, L. Commercializing nanotechnology. *Nat. Biotechnol.* **21**, 1137-1143 (2003).
156. Takayama, S., Ostuni, E., LeDuc, P. & Whitesides, G.M. Laminar flows: subcellular positioning of small molecules. *Nature* **411**, 1018 (2001).
157. Vo-Dinh, T. Nanobiosensors: Probing the sanctuary of individual living cells. *J. Cell. Biochem.*, 154-161 (2002).
158. Bao, G. Mechanics of biomolecules. *Journal of the Mechanics and Physics of Solids* **50**, 2237-2274 (2002).
159. Misevic, G.N. Atomic force microscopy measurements. Measurements of binding strength between a single pair of molecules in physiological solutions. *Mol. Biotechnol.* **18**, 149-153 (2001).
160. Byfield, M.P. & Abuknesha, R.A. Biochemical aspects of biosensors. *Biosens. Bioelectron.* **9**, 373-399 (1994).
161. Byrne, M.E., Park, K. & Peppas, N.A. Molecular imprinting within hydrogels. *Adv. Drug Del. Rev.* **54**, 149-161 (2002).
162. Wolfbeis, O.S. Fiber-optic chemical sensors and biosensors. *Anal. Chem.* **74**, 2663-2677 (2002).
163. Bakker, E. & Telting-Diaz, M. Electrochemical Sensors. *Anal. Chem.* **74**, 2781-2800 (2002).
164. Schoening, M.J. & Poghossian, A. Recent advances in biologically sensitive field-effect transistors (BioFETs). *Analyst* **127**, 1137-1151 (2002).

165. Benes, E., Groeschl, M., Burger, W. & Schmid, M. Sensors based on piezoelectric resonators. *Sensors and Actuators, A: Physical* **A48**, 1-21 (1995).
166. Gao, X. & Nie, S. Molecular profiling of single cells and tissue specimens with quantum dots. *Trends Biotechnol.* **21**, 371-373 (2003).
167. Kim, J. et al. Cell lysis on a microfluidic CD (compact disc). *Lab on a Chip* **4**, 516-522 (2004).
168. Hong, J.W., Studer, V., Hang, G., Anderson, W.F. & Quake, S.R. A nanoliter-scale nucleic acid processor with parallel architecture. *Nat. Biotechnol.* **22**, 435-439 (2004).
169. Ottesen, E.A., Hong, J.W., Quake, S.R. & Leadbetter, J.R. Microfluidic Digital PCR Enables Multigene Analysis of Individual Environmental Bacteria. *Science* **314**, 1464-1467 (2006).
170. Wang, H. & Branton, D. Nanopores with a spark for single-molecule detection. *Nat. Biotechnol.* **19**, 622-623 (2001).
171. Kasianowicz, J.J., Brandin, E., Branton, D. & Deamer, D.W. Characterization of individual polynucleotide molecules using a membrane channel. *PNAS* **93**, 13770-13773. (1996).
172. Howorka, S., Cheley, S. & Bayley, H. Sequence-specific detection of individual DNA strands using engineered nanopores. *Nat. Biotechnol.* **19**, 636-639 (2001).
173. Austin, R. Nanopores: The art of sucking spaghetti. *Nat. Mat.* **2**, 567-568 (2003).
174. Li, J., Gershow, M., Stein, D., Brandin, E. & Golovchenko, J.A. DNA molecules and configurations in a solid-state nanopore microscope. *Nat. Mat.* **2**, 611-615 (2003).

175. Li, J. et al. Ion-beam sculpting at nanometre length scales. *Nature* **412**, 166-169 (2001).
176. Aylott, J.W. Optical nanosensors--an enabling technology for intracellular measurements. *Analyst* **128**, 309-312 (2003).
177. Park, E.J., Brasuel, M., Behrend, C., Philbert, M.A. & Kopelman, R. Ratiometric optical PEBBLE nanosensors for real-time magnesium ion concentrations inside viable cells. *Anal. Chem.* **75**, 3784-3791 (2003).
178. Clark, H.A. et al. Subcellular optochemical nanobiosensors: probes encapsulated by biologically localized embedding (PEBBLEs). *Sens. Actuators, B* **B51**, 12-16 (1998).
179. Sellergren, B. Noncovalent molecular imprinting: antibody-like molecular recognition in polymeric network materials. *Trends. Anal. Chem.* **16**, 310-320 (1997).
180. Wulff, G. Molecular imprinting in crosslinked materials with the aid of molecular templates - a way towards artificial antibodies. *Angew. Chem. Int. Ed.* **34**, 1812-1832 (1995).
181. Byrne, M.E. & Salián, V. Molecular imprinting within hydrogels II: progress and analysis of the field. Invited Review. *International Journal of Pharmaceutics*, Submitted (2008).
182. Hilt, J.Z. & Byrne, M.E. Configurational biomimesis in drug delivery: molecular imprinting of biologically significant molecules. *Adv. Drug Del. Rev.* **56**, 1599-1620 (2004).

183. Gil, E.S. & Hudson, S.M. Stimuli-responsive polymers and their bioconjugates. *Prog. Polym. Sci.* **29**, 1173 (2004).
184. Drotleff, S. et al. Biomimetic polymers in pharmaceutical and biomedical sciences. *Eur. J. Pharm. Biopharm.* **58**, 385-407 (2004).
185. Dong, C.-M., Faucher, K.M. & Chaikof, E.L. Synthesis and properties of biomimetic poly(L-glutamate)-b-poly(2-acryloyloxyethyl lactoside)-b-poly(L-glutamate) triblock copolymers. *J. Polym. Sci., Part A: Polym. Chem.* **42**, 5754-5765 (2004).

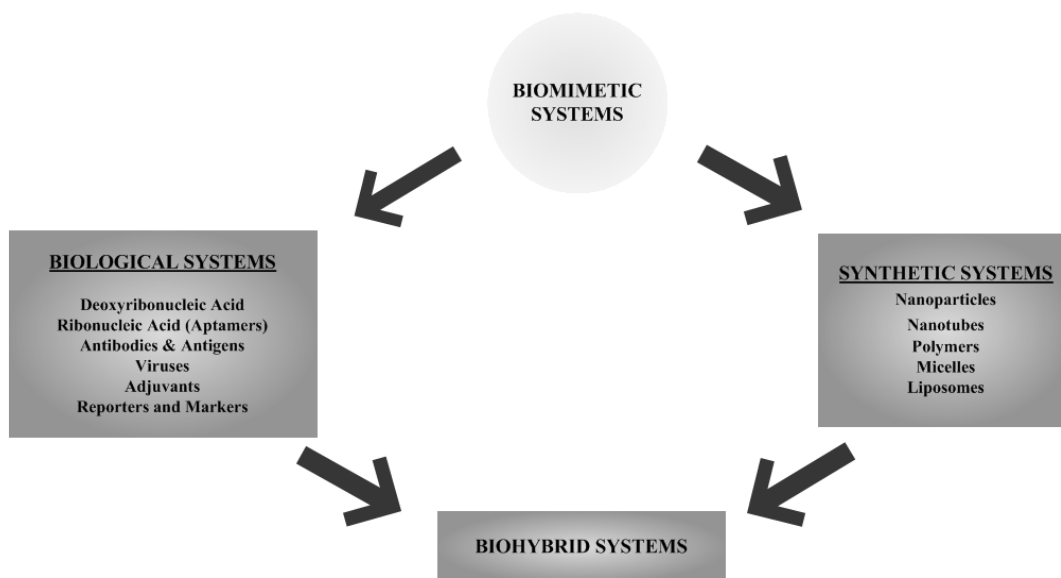


Figure 2.1 Classification of Biomimetic Systems. Biohybrid systems, at the intersection of artificial and biological systems, are used for uncovering biological mechanisms and for identifying therapeutic strategies.

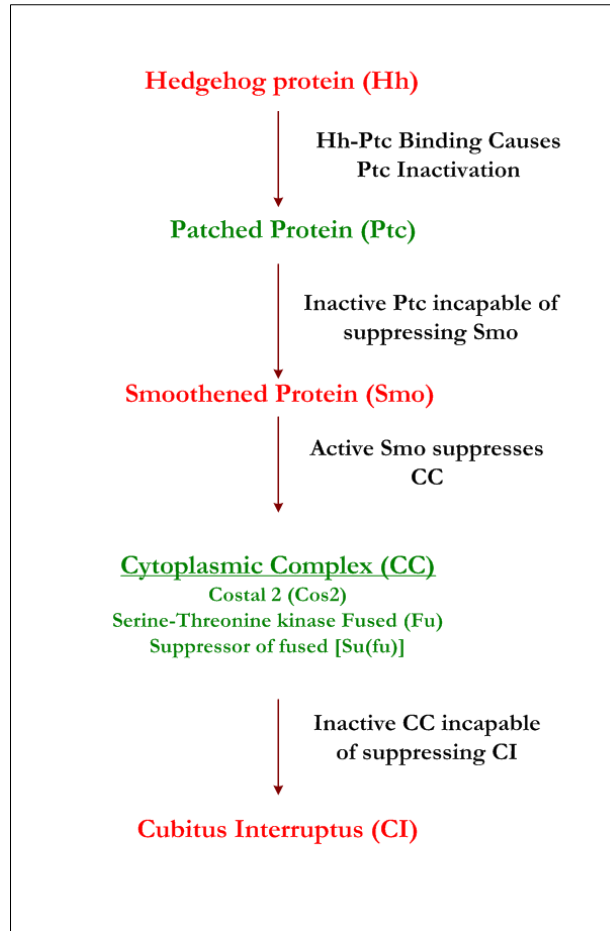


Figure 2.2 Molecular Interactions in the Hedgehog signalling pathway.

Responsible for early embryonic development in *Drosophila* and humans, the Hedgehog pathway is implicated in cancers. The pathway is regulated by a series of suppressive actions. Activated species are shown in red and suppressed species are shown in green.

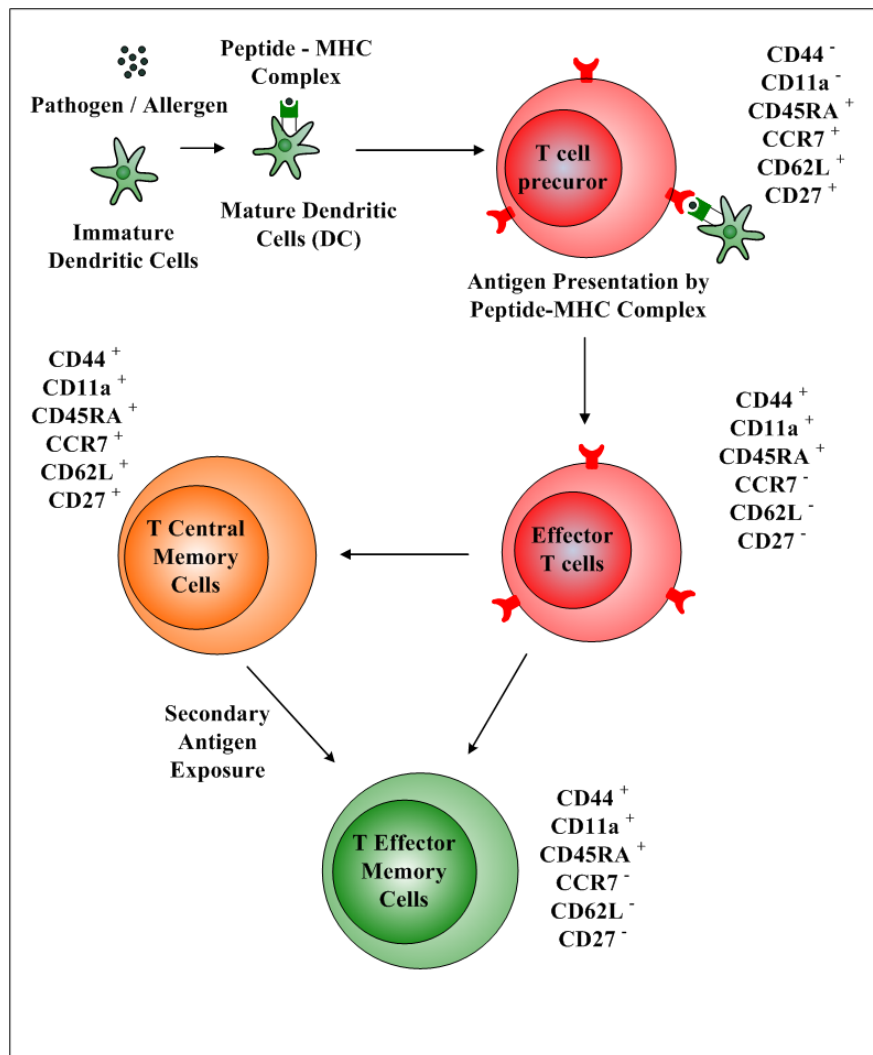


Figure 2.3 T cell differentiation and memory T cell formation. Antigen presentation by dendritic cells primes the naïve T cell. After effector action has cleared infection, about 10% of T cells differentiate into memory T cells. On secondary exposure, these cells show rapid response kinetics and provide adaptive immunity.

3.0 MOLECULAR IMPRINTED POLYMERS IN DRUG DELIVERY

While there has been an explosion in the number of papers in recent years discussing polymer networks prepared using biological template molecules and functional monomers with an enhanced chemical repertoire, relatively little effort has been directed towards understanding and optimizing the molecular mechanisms underpinning template binding and recognition in weakly crosslinked networks. Such a concerted effort would spur the design of more robust molecular imprinted polymer systems, with tailored recognition of biological template molecules, in aqueous or physiological media. In this chapter, we build the theoretical framework for the synthesis, characterization and evaluation of imprinted networks.

3.1 Introduction to Recognitive Polymers

Recognitive hydrogels are insoluble, crosslinked polymers which respond to chemical and physical stimuli, and have tremendous potential in drug delivery, sensing, diagnostics, and separation processes¹. Their outstanding property is that they possess macromolecular memory, i.e. they can easily be “conditioned” or taught to recognize small molecules with great discriminatory ability. Recognitive polymers have been used in separation processes such as chromatography since the early 70s, but only recently have more imaginative lines of research resulted in their applicability to recognizing molecules of physiological relevance.

A polymer consists of linear chains of repeating units, known as monomers, which are linked together by covalent bonds². Functional monomers possess diverse chemical functionalities and are unsaturated, i.e. they have double bonds, which get opened up during the polymerization process. Figure 3.1 is a schematic of a polymer network made up of linear polymer chains connected by crosslinking monomers and with pendant functionalities. This allows them to be added sequentially to the growing chain. These linear chains are also linked to each other in lateral directions, or crosslinked, by a homobifunctional or heterobifunctional monomer known as the crosslinking monomer. Crosslinks (otherwise known as tie-points or junction points) can be covalent bonds, permanent entanglements, ionic interactions, or microcrystalline regions incorporating various chains. The crosslinking density, i.e. the mole fraction of crosslinking monomer in the polymer structure, is an important parameter in the design of polymer networks. Along with the nature of polymer-solute interactions, it determines the swelling behavior of the polymer in a solvent. During the polymerization or gelling process, growth of chains in the linear direction is

accompanied by the three dimensional propagation of the macromolecular structure, due to the crosslinking of the chains at junctions. There comes a critical point during a polymerization reaction, known as the sol-gel transition point, at which the polymer structure is no longer soluble in solvent. The polymer no longer collapses in the presence of solvent, and the degree of swelling is decided by the “tightness” or crosslinking density of the structure.

In the last few years, there has been considerable intent in developing recognitive polymers for biomolecules in aqueous environments. However, such efforts have been limited to highly crosslinked networks, which possess robust macromolecular memory, due to their inherent rigidity. Attempts to develop loosely crosslinked recognitive networks have been unsuccessful. Hydrogels are a class of weakly crosslinked homo- or hetero-co-polymers capable of absorbing significant amounts of water. They have generated much interest as potential drug delivery devices due to their ability to control the diffusion behavior of molecules in or through them; and the ability to amplify the microscopic events occurring at the molecular level into macroscopic phenomena^{3, 4}. Furthermore, they have an inherent property of biocompatibility i.e. they are tolerated by natural tissues without invoking strong immune responses⁵.

3.2 Macromolecular Memory: A Host-Guest Templating Phenomenon

A recognitive polymer is unique in that its synthesis scheme equips it with macromolecular memory, i.e. molecular binding sites with a tailored affinity for a template molecule of choice. This novel synthesis scheme is termed molecular

imprinting, and involves polymerization in the presence of the template, which directs the growth and formation of the polymer structure.

The mechanism of molecular imprinting could be interpreted in terms of host-guest chemistry. The functional monomer (host molecule) is chosen such that it participates in non-covalent interactions with the template molecule (guest molecule). These non-covalent interactions are typically electrostatic forces, Van der Waals forces of attraction, hydrogen bonding or hydrophobic effects, and in a given system, two or more of these forces might influence binding⁶.

Differences in environmental and compositional parameters can change the polymer structure and alter binding parameters. Figure 3.2 exemplifies the imprinting scheme used for creating macromolecular memory in a polymer network. The formation of a molecular binding complex between the host molecule (the functional monomer) and the guest molecule (template) is the critical step towards forming binding sites for the template in the polymerized structure. This occurs in the pre-polymerization mixture, i.e. the homogeneous mixture of functional monomer, crosslinking monomer, template, and the initiator molecule. The functional monomer and the initiator form the molecular binding complex in order to reduce the Gibbs free energy of the solution. It is important to note that the enthalpy of binding pays the entropic penalty of organizing these free molecules in solution. Next, the polymerization process is triggered by exciting the initiator molecule to form highly reactive free radicals. These react with the free functional and crosslinking monomers in solution and start forming the backbone of the macromolecular structure. The molecular binding complexes are incorporated into the polymer backbone *via* the unsaturated bonds of the functional monomer molecule in the binding complex.

Thus, the template molecules act as sites of nucleation and organize the polymer chains around them. In effect, the propagating polymer chains are constrained into conformations which correspond to the three dimensional topology of the template molecule. The binding site as such is composed of functional groups oriented precisely in the polymer structure so that they can form non-covalent bonds with the template molecule. It is incorrect to interpret the rigidity of the network in static terms. A macromolecular structure with binding sites is not static. On the other hand, by rigidity we mean that the polymer chains are constantly in dynamic motion, except that the conformations adopted are dictated by the template molecule.

Once the polymer network is formed, the unreacted monomers and template molecule are washed out from the network with a thermodynamically compatible solvent. The polymer structure now consists of microscopic template-specific cavities or “memory sites” wherein the chemical functional groups are precisely oriented such that they can recognize and bind the template molecule, while the backbone of the polymer network provides the necessary rigidity to maintain the size, overall shape and relative positioning of the functional groups. When such a washed network is placed in a solution of the template molecule, the concentration gradient will provide the inward driving force for the diffusion and specific binding of the template molecule in the memory sites. It is important to note that non-specific binding does occur due to entanglement in the macromolecular chains.

An intense study of the current literature informs us that molecular imprinting has proved more successful in higher crosslinked networks rather than hydrogels, probably due to the fact that the rigidity provided by the polymer backbone and low swelling characteristics maintain the integrity of the memory sites. The reader is

directed to insightful reviews on the conventional applications of molecular imprinting reviews^{7,8}, as well as bio-focused and drug delivery reviews^{6,9,10}.

3.3 Molecular Recognition *via* Non-Covalent Interactions

The main non-covalent interactions responsible for template recognition in molecularly imprinted networks are hydrogen bonding, hydrophobic interactions, London dispersion forces, metal-ion coordination bonds, ion pairing interactions, and π - π or cation- π interactions. The ion pairing interactions could be inter-ionic attraction or repulsion, dipole-dipole, or ion-dipole interactions. Moreover, electronic properties of the template and surrounding polymer matrix might influence template recognition and binding since favorable interactions might offset binding to the memory site. Typically, recognition and binding of the template molecule is a combinatorial effect of these interaction modes, with inter-ionic interactions and hydrogel bonding being the dominant modes.

In general, solvent properties such as the dielectric constant, dipole moment, polarizability, and hydrogen bonding capability, dictate the type and contribution of the non-covalent interactions in the imprinting process. Typically, hydrogen bonding between functional groups and salt bridges formed by ion pairing interactions are the most important interactions determining the stability of the molecular binding complex in polar aprotic solvents such as acetonitrile, acetone, benzene, chloroform and dichloromethane. Polar protic solvents such as water favor interactions such as metal-ion coordination of the template molecule and π - π stacking between aromatic rings. Hydrophobic interactions are favored in highly polar solvents due to thermodynamic considerations.

3.4 Thermodynamic Evaluation of the Imprinting Process

The molecular binding complex formed during imprinting can be evaluated using a number of template binding parameters. The significant parameters in determining the quality and strength of these interactions are the selectivity, the loading capacity, and the equilibrium dissociation constant between the template molecule and imprinted network.

Selectivity, or the separation factor of the network, is the ratio of the partition coefficients of the imprinted polymer with the template molecule, and one of similar structure, size or functionality, and is a measure of the discriminatory ability of the imprinted network. It should be noted that selectivity studies have generally been performed with highly crosslinked systems, since the rigidity of the network maintains the integrity of the memory sites, which can discriminate minute differences in structure. A loosely crosslinked system, on the other hand, is inherently flexible, and can allow the binding of two molecules of comparable structures to the memory sites. Loading capacity is the molar amount of template molecule that is rebound per unit volume of the network. The equilibrium dissociation constant¹¹, which is defined similar to the conventional theories of enzyme-substrate or receptor-ligand binding, provides a quantitative measure of the strength of binding between the template molecule and imprinted network.

The binding interaction can be represented as:



Where, M refers to the memory site, T refers to the template molecule, and M-T refers to the molecular binding complex. The dissociation constant is the ratio of the off and on rate constants and has the units of concentration (i.e. molarity). Lower the value of dissociation constant, tighter the binding, and vice versa.

$$K_D = \frac{k_{\text{off}}}{k_{\text{on}}} = \frac{[M][T]}{[M-T]} \quad 3.2$$

A deeper understanding of the molecular mechanisms underlying template binding and the optimization of the above parameters is fundamental to the rational design of robust intelligent drug delivery devices. Biological dissociation constants can be as low as 10^{-15} M (interaction of biotin and streptavidin) and 10^{-14} M (inhibition of trypsin and chymotrypsin by their inhibitors)¹⁰. Such low dissociation constants may never be reached using artificial imprinted networks, as they lack the precise architecture and configuration of protein binding sites. It should be noted, however, that reaching the realm of biological dissociation constants would be disadvantageous in the design of drug delivery devices, since tight binding of the template molecules (in this case, the drugs or small molecule inhibitors) would preclude their release from the devices.

It is well known that the number and quality of high affinity memory sites depend on the strength and extent of interactions between the functional monomer and the template molecule. Hence, the preservation of the structure and configuration of the molecular binding complex during the polymerization step is crucial for the success of the imprinting procedure. Template complexation, which is under thermodynamic control and is a combinatorial effect of various interactions, is governed by the change in Gibbs free energy of formation of each one of these

interactions. In general, the Gibbs free energy of binding, which dictates the formation of the molecular binding complex¹²⁻¹⁴, is given by:

$$\Delta G_{\text{bind}} = \Delta G_{\text{t+r}} + \Delta G_{\text{r}} + \Delta G_{\text{h}} + \Delta G_{\text{vib}} + \Delta G_{\text{conf}} + \Delta G_{\text{vanWalls}} + \sum \Delta G_{\text{polar}} \quad 3.3$$

Where, the Gibbs free energy of binding ΔG_{bind} , is the sum of translational and rotational free energies $\Delta G_{\text{t+r}}$, the free energy change resulting in restriction of rotors on complexation ΔG_{r} , the free energy change due to the hydrophobic effect ΔG_{h} , the free energy change due to residual soft vibrational modes ΔG_{vib} , the free energy change due to unfavorable conformational changes ΔG_{conf} , the free energy change due to unfavorable van der Waals interactions $\Delta G_{\text{vanWalls}}$, and the sum of free energy of all polar interactions $\sum \Delta G_{\text{polar}}$.

Equation 3.3 can be simplified for template-functional monomer complexation, since the free energy change due to unfavorable conformational changes ΔG_{conf} and the free energy change due to unfavorable van der Waals interactions $\Delta G_{\text{vanWalls}}$ are negligible in solution. In fact, loosely crosslinked imprinted networks also do not have significantly large conformational changes due to their dynamic nature. Furthermore, hydrophobic interactions only occur in extremely polar solvents, while most imprinting studies are carried out in polar aprotic or polar protic solvents. If we make a further assumption that the same solvent is used in the polymerization, washing, and rebinding (i.e. template recognition) steps, then equation 3.3 reduces to,

$$\Delta G_{\text{bind}} = \Delta G_{\text{t+r}} + \Delta G_{\text{r}} + \Delta G_{\text{vib}} + \sum \Delta G_{\text{polar}} \quad 3.4$$

An evaluation of the energetic contribution of the individual free energy terms in equation 3.4 to binding is essential to detailing the molecular recognition events and optimizing the binding parameters. Moreover, one can diagnose the degree of

heterogeneity in affinity of the memory sites. The non-covalent imprinting approach results in the synthesis of networks with high and low affinity memory sites, as well as non-specific binding with the polymer around the memory sites. Even though the template organizes the functional groups around it, the polymerization process is a random process, and hence the memory sites formed are heterogeneous in shape, distribution of functionalities, and hence binding affinities.

In general, functionally diverse pre-polymerization mixtures promote multiple non-covalent interactions with the template molecule, and result in efficient template complexation due to the reduction in the entropically unfavorable translational and rotational free energies ΔG_{tr} ¹⁵. The extent and strength of polar interactions between template and functional monomer described by $\sum \Delta G_{polar}$ will determine the loading capacity and selectivity of the imprinted network. Large and sterically constrained templates and functional monomers have lesser degrees of freedom and form imprinted networks of higher performance due to smaller values of ΔG_r . The free energy of residual soft vibrational modes ΔG_{vib} is a strong function of temperature and can be controlled by polymerization at low temperatures.

Advances in the study of heteropolymers have gained much input from corresponding studies in predicting conformations from protein structure¹⁶⁻²¹. In analogy to a binding site in an enzyme or receptor, where different amino acids contribute to molecular recognition, one functional monomer does not provide optimal interactions between the polymer chains and the template. Depending on the chemistry of the template molecule, the use of chemically diverse functional monomer will have preferred and more energetically favorable interactions with different parts of the template²². Imprinting organizes the incorporation of monomers within the growing polymer chains in a low energy state conformation that favors

multiple point complexation with the template. The imprinting potential is also dramatically lowered if there are strong non-covalent interactions or reactivity between the functional monomers. Hence, increasing the potential for template binding complexes to reach their global free energy minima will lead to increased memorization of the chain conformation and enhance template binding parameters in both highly and weakly crosslinked polymers.

3.5 Analogies between Natural and Synthetic Polymers

Many parallels may be drawn between imprinted networks and proteins. Proteins are linear polymers of amino acids that adopt complex three dimensional tertiary structures and organize critical amino acids, which participate in binding and catalytic events, into precise binding sites for the incoming ligand. While the functional binding site is much smaller in length scale compared to the overall protein, the rest of the architecture is not supererogatory, and is instrumental in maintaining its integrity. Proteins achieve far superior binding complexes than imprinted polymers, perhaps due to their highly structured and robust organization.

On the other hand, proteins remain functional only in physiological or *in-vitro* microenvironments where pH and temperature are tightly controlled, and are susceptible to denaturation or cleavage by proteolytic agents. Imprinted networks remain structurally robust at wide ranges of temperature and pH, and are unaffected by most solvents, additives and other reagents²³⁻²⁵.

Furthermore, proteins are generally composed of the canonical twenty amino acids, and are hence functionally restricted. Many applications require a more diverse set of chemical functionalities, and monomers with these functionalities are readily

synthesized *via* organic synthetic methods. Ease of synthesis, stability in fickle environments and chemical versatility enhance the potential of imprinted networks over natural building blocks such as proteins.

However, there are also problems which are peculiar to imprinted networks. When a population of a protein receptor or binding molecule is examined, uniform affinity is observed towards the cognate ligand. This is because protein synthesis, one of the most critical processes governing life, is tightly regulated in the cell. So every protein molecule in a population is synthesized by the stepwise addition of amino acids in the correct order, leading to homogeneity in the structure and configuration of the binding site. On the other hand, imprinted networks have a wide distribution of affinity in their memory sites due to the polymerization technique, which involves the random assembly and linking of a heterogeneous population of linear chains.

3.6 Design or Operational Parameters of an Imprinted Network

The main challenge facing the field of molecular imprinting is that it is still impossible to suggest a reliable and reproducible protocol for the synthesis of a network with the required properties for a specific type of application. The realization of drug delivery and other medical applications of imprinted networks demand a strict control of network structure, in order to obtain reproducible and consistent properties without hysteresis. A keener understanding of how certain design parameters can alter network structure will aid in the development of more reliable and robust recognition devices. These include environmental parameters such as pressure and temperature, and compositional variables such as solvent weight percentage, monomer-template ratio, length of crosslinking monomer, crosslinking density, initiator weight

percentage and the iniferter weight percentage. In this section, we will discuss the effects of these parameters on template binding parameters. Figure 3.3 reviews the key trends of these parameters on template rebinding properties of the network. There are very few investigations in the literature on how such parameters can be used to optimize and enhance the imprinted polymer binding parameters. The reader is directed to two commanding references in the literature^{26, 27}, which present some of these trends along with the theoretical arguments.

3.6.1 Pressure

The pressure effects on molecular binding events are usually considerably smaller than the effects of temperature and solvent. The response of an intermolecular binding event in solution to pressure depends on the change in free volume (ΔV°) upon association according to equation 3.5, which is derived from the basic definitions of the thermodynamics potentials,

$$\left[\frac{\partial RT \ln K}{\partial P} \right]_T = -\Delta V^\circ \quad 3.5$$

Where, K is the association constant of the complex, R is the gas constant, T is the absolute temperature, P is the pressure, and ΔV° is the difference in volume occupied by the products and the reactants. If the binding event leads to a net decrease in volume, it follows that the association constant increases with increasing pressure. It has been observed that weak solution complexes respond to pressure in this way although ΔV° is usually smaller.

The influence of pressure on the propagation rate coefficients of free-radical polymerization are given in equation 3.6²⁸.

$$\frac{\partial \ln k_p}{\partial P} = \frac{\Delta V'}{RT} \quad 3.6$$

Where, k_p is the propagation constant of the complex, and $\Delta V'$ is the activation volume.

Recent investigations indicate that polymerization reaction kinetics, the template binding parameters and the polymer morphology are strongly affected by high operational pressures^{29, 30}. Imprinted polymers of ametryn synthesized at 1000 bars using 2-propanol as solvent showed a higher capacity factor (3.2) as compared to networks synthesized at 1 bar (2.3). However, the mechanisms by which high pressures exert their effects during free radical polymerization are complex.

High pressure applied during free radical polymerization commonly results in increased temperatures, which causes an explosion in the number of free radical collisions. This is reflected in enhanced rates of polymerization as well as higher molecular weights of the propagating chains.

An isotactic polymer is one which has a more ordered arrangement of functional groups. It has been observed that high pressures increase the isotacticity of the resulting polymer, and this might be translated into memory sites of better structural integrity³¹. Furthermore, it has been proposed that the molecular binding complex is stabilized by high pressure, which in turn results in an increase in affinity, capacity and selectivity³⁰.

The effects of pressure are also closely related to the variation of the boiling point of the porogen with temperature. It is important to note that the solvent, which would remain a liquid at ambient pressures, would volatilize at higher pressures due to the exothermicity of the polymerization reaction. If chloroform is used as the porogen, it should be noted an increase in pressure by 10 bars would result in an

increase in boiling temperature from 61 to 184 °C. The temperature developed during the exothermic polymerization reaction at ambient pressure (66°C) is above the boiling temperature for chloroform. In contrast, the temperature developed at 10 bar (127 °C) is comfortably below the chloroform boiling temperature at this pressure. The boiling solvent leaves behind a more rigid network, which is more compact due to lesser macroporous zones, and is more capable of maintaining the memory sites. Furthermore, the $\Delta V'$ term in equation 3.6 is greatly affected when the solvent viscosity is enhanced at higher pressures.

3.6.2 Temperature

The polymerization reaction is exothermic, and hence the temperature increases as chain propagation occurs. The progress of the reaction can be monitored by measuring the instantaneous polymerization reaction rate or the instantaneous double bond conversion. The enthalpy of polymerization, being an extensive thermodynamic quantity, is a function of the number of moles of double bonds reacted.

Higher operational temperatures result in a larger number of free radicals, higher double bond conversions and higher molecular weights of polymer chains. The higher temperatures are responsible for enhanced mobilities of the chains of large molecular weight, which maximizes double bond conversions. Typically, this trend is followed in acrylated and methacrylated networks. Controlling the temperature by the continuous removal of heat becomes especially critical when the solvent boiling point is exceeded as the reaction progresses, leading to entrainment of solvent molecules.

It has been observed that pre-polymerization mixtures polymerized at lower temperatures form imprinted networks with lower dissociation constants and higher enantioselectivities compared to those synthesized at elevated temperatures³²⁻³⁴. Imprinted polymers of L-phenylalanine anilide prepared photochemically at 0°C with acetonitrile and chloroform as solvents showed higher separation factors (2.275 and 2.5) as compared to polymers synthesized thermally at 60°C (1.57 and 2.01)³⁵. Free radical polymerization carried out at 5°C yielded imprinted networks with higher binding and selectivity for 9-ethyladenine, than polymers that were synthesized thermally at 60 °C³⁶.

The inverse effect of temperature on template binding parameters can be interpreted in three ways. According to the laws of mass action and Le Chatelier's principle, the formation of the molecular binding complex would release energy, and hence lower temperatures will drive the formation of the molecular binding complex. The formation of a large number of these complexes in solution is then translated into a larger number of memory sites in the imprinted network, which have higher capacities and enantioselectivities

The inverse binding trends are also due to the fact that non-covalent interactions are responsible for binding in the pre-polymerization solution. In particular, most imprinted networks rely on hydrogen bonding to create memory sites. It is well known that hydrogen bonding vanishes at higher temperatures, due to higher translational, vibrational and kinetic energies of the participating molecules³⁷. Hence, polymerization at lower temperatures yields imprinted networks with improved template binding parameters. However, it should be noted that at very low temperatures, the change in free energies due to unfavorable conformations (ΔG_{conf}) and van der Waal's interactions ($\Delta G_{\text{vanWalls}}$) will no longer remain negligible.

Furthermore, the polymerization reaction rate is decreased when the synthesis is carried out at lower temperatures. The macromolecular structure is formed at a more controlled rate, and this is translated into the formation of binding sites of higher fidelity¹⁵.

Clearly, an imprinted network polymerized at lower temperatures has weaker mechanical and morphological properties and lower double bond conversions than those polymerized at higher temperatures. Hence, an optimum should be determined between the polymer characteristics and maximizing the functional monomer-template molecule interactions. The caveat is that this optimum is empirical and has to be determined for every system under study. Imprinted polymers of 3-L-Phenylalanylaminopyridine prepared photochemically at 10, 40 and 60°C with chloroform as solvents performed best at 40°C, and not 10°C³⁸. This shows that template binding parameters are governed by a balance between two effects- polymer characteristics and the stability of the molecular binding complex.

3.6.3 Solvent Weight Percentage

The solvent weight percentage in the pre-polymerization mixture is a crucial factor determining template binding. The solvent dictates the overall morphology of the imprinted network and hence the integrity of the memory sites, as well as the modes of the non-covalent interactions involved in the recognition process. Typically, solvent is used in the synthesis of highly crosslinked networks in order to increase the porosity, i.e. the void fraction, and the internal surface area of the network. This enhances the mass transport of the template molecule during rebinding and release³⁹. It is important to note that a highly porous structure is more permeable to template

diffusion, but has diminished mechanical properties and memory sites of lesser fidelity.

A similarity in polarity between the polymer chains and the solvent is responsible for the degree of chain solvation. Hence, even a loosely crosslinked network could remain a collapsed state when placed in a solvent of opposite polarity. During polymerization, the solvent does not become incorporated into the polymer backbone and the propagating polymer chains have to form around the solvent molecules. This results in a network with a higher degree of porosity and mesh size, i.e. the average linear distance between two crosslinking points in the network⁴⁰⁻⁴². Depending on the weight percentage of solvent in the formulation, which directs the space available for template transport, the network could be macroporous, microporous, or nanoporous and Figure 3.4 is a pictorial depiction typifying these differences. A novel critical point drying based sample preparation technique has been employed to prepare imprinted networks for bovine hemoglobin, so that the memory sites could be visualized by transmission electron microscopy⁴³. Magnifications and resolutions were obtained in length scales which were less than 10 nm. The imaged memory sites, ranging from 5 to 50 nm in size, correlated with the hydrodynamic radii of individual bovine hemoglobin molecules and their oligomers due to protein-protein aggregation. Interestingly, there were lighter areas of lesser electron density, which correspond to the nanoporous region as well as washed memory sites. Two-photon confocal microscopy has been used to detail the structure of imprinted networks for a FITC labeled albumin and bovine hemoglobin⁴⁴. There was clearly no collapse in network structure on the denaturation of the imprinted protein template by a denaturation solvent, and the amount of removed template was easily quantified due to the reduction in fluorescence. These studies offer evidence as to the size of the

imprinted cavities, as well as the existence of microporous regions in the imprinted network.

The solvent also makes thermodynamic contributions towards the functional monomer-template molecule complexation by directing the non-covalent modes of interaction, as described in section 3.3. The energetic contributions correspond to maximizing the $\sum\Delta G_{\text{polar}}$ and ΔG_{h} terms in equation 3.4. Furthermore, solvation of polymer chains reduces unfavorable conformations (ΔG_{conf}) in the network.

The predilection of solvents to interact and react with their solutes are represented by the three solvatochromic scales (π^* , α and β)⁴⁵⁻⁵⁰. These scales can be used to predict solvent enhancement or disruption of the non-covalent interactions between functional monomer and template molecule. The π^* scale is an index of solvent polarizability, which measures the ability of the solvent to stabilize a charge or a dipole by virtue of its dielectric effect. Typical values have been shown to be proportional to the dipole moments. The α scale of acidity is an index of hydrogen donor capability, i.e. the ability of the solvent to donate a proton in a solvent-to-solute hydrogen bond. The β scale of basicity provides a measure of the solvent's ability to accept a proton in a solute-to-solvent hydrogen bond.

Hence, the solvent can positively influence the template affinity, capacity, and selectivity of a given system^{51, 52}. However, this does not mean that rebinding can only take place in the presence of a solvent. If one of the backbone monomers is in large excess in the pre-polymerization mixture, it has been demonstrated that imprinted networks possess higher affinities and capacities than non-imprinted networks, in the absence of a solvent^{15, 53-56}. In this case, the monomer in excess is not a typical solvent, as it gets incorporated into the polymer backbone during the polymerization reaction.

3.6.4 Monomer-Template Ratio

The monomer-template (M/T) ratio is the ratio of the number of moles of functional monomer to the number of moles of template molecule in the pre-polymerization mixture. Optimizing the M/T ratio is crucial to the success of imprinting.

The effect of the M/T ratio is complex, and many different mechanisms contribute to its influence on binding. Polymers formed in the polymerization of N-vinylimidazole along poly(methacrylic acid) as template in water demonstrate enhanced rates of polymerization on the addition of the template poly(methacrylic acid)⁵⁷. The enhanced rate is due to the suppression of the termination step through loss of mobility of the free radicals on association with the template, as well as the reduction of electrostatic repulsions between the propagating free radicals and monomers due to association with the template⁵⁸. The suppression of the termination step yields polymer chains of up to 70 times higher molecular weight than those of polymers produced in the absence of the template. Longer template chains appear to promote higher rates of retardation of termination, as the number of associated free radicals is maximized⁵⁹.

Equation 3.1 suggests that the equilibrium can be driven towards the formation of the pre-polymerization complex by increasing either the concentration of functional monomer (M) or template molecule (T), or both. In general, an excess of functional monomer is needed to drive this interaction to the complexed state. Therefore, M/T ratios are usually much higher than unity and are not commonly in stoichiometric amounts based on the functionality of the template. This optimum is purely empirical

for each system and exists between two limiting cases. It is important to note that all M/T studies should follow a careful analysis of the choice of functional monomer⁶⁰. Analytical techniques, such as FTIR⁶¹⁻⁶³, Raman⁶⁴, NMR⁶⁵⁻⁶⁹, and UV⁷⁰⁻⁷³ spectroscopy, are used to diagnose the formation of the molecular binding complex and the stoichiometry of interactions. Computer simulations⁷⁴⁻⁷⁶ and combinatorial screening⁷⁷⁻⁸² are also powerful tools to evaluate functional monomer-template interactions.

At very large M/T ratio, the memorized configuration of monomer within the polymer chains is very small compared to the randomly incorporated monomer and there is no difference between the nonimprinted and imprinted gels, i.e. hardly any macromolecular memory is created in the network. The reason is that a large number of functional monomer molecules do not interact with the template molecule for the required imprinting effect.

At very small M/T ratios, the template molecule is at far higher concentrations than monomer. An argument can be made on the basis of Le Chatelier's principle that the concentration of the template molecule could be increased to very high concentrations without having any change on the composition of monomers in the final polymer, as the template molecule is not covalently incorporated into the final polymer, and is removed at the end of the imprinting process. Furthermore, once all the functional monomer molecules are complexed, any further addition of template should have no effect on memory site formation.

However, very few studies have shown the creation of macromolecular memory at low M/T ratios. The template molecules do not organize an optimum number of functional groups during the polymerization reaction, resulting in non-specific recognition and binding. It has been shown that higher M/T ratios have

produced higher populations of template-functional monomer complexes resulting in higher binding affinities^{32, 83-85}. M/T ratios of 3 and 4 was shown to be optimum in the range 1-16, for imprinting norfloxacin with single functional monomer systems⁸⁶.

Our group has recently demonstrated an inverse trend of the rate of polymerization reaction with template concentration, in pre-polymerization mixtures of diverse functional groups¹⁵. These studies support the hypothesis that the template molecule organizes the functional groups and controls the rate of polymerization for a successful imprinting effect. For highly crosslinked networks using a single functional monomer, there was no effect of changing M/T ratio on the polymerization reaction rate²⁶. It is possible that the highly crosslinked structures have memory sites of more robust integrity, and hence varying the M/T ratio does not have much of an observable effect.

3.6.5 Crosslinking Monomer Length and Density

The degree of flexibility of the polymer network chains is heavily influenced by the amount of crosslinking and type of crosslinking molecule within the polymer network. Decreasing the crosslinking monomer length has shown to decrease the mesh size⁸⁷. Highly crosslinked networks have a tighter mesh structure than loosely crosslinked networks, swell to a lesser extent, and are less permeable to mass transport⁸⁸. Highly crosslinked imprinted networks have higher affinities, binding capacities, and selectivity compared to less crosslinked polymers^{26, 89}. As an example, imprinted polymers of D-glucose were synthesized with 30, 67 and 80% mole percentage of three crosslinking monomers, which differed in their linear dimensions^{90, 91}. Except for the 30% crosslinked networks, there is an inverse relation

of binding capacity and crosslinker length. These trends are correlated to the inherent rigidity of these networks, which have the propensity to maintain the integrity of their memory sites. There is also a direct relationship between crosslinking density and diffusion coefficients of template molecules through the networks, indicating that there are greater transport resistances in a highly crosslinked structure.

When a dry network is immersed in a thermodynamically compatible solvent, the polymer chains get solvated, and the solvent penetrates into the polymer network. The volumetric expansion and extent of macromolecular rearrangement of the network depend on the nature and molar amounts of crosslinking monomers within the network. It is essential to realize that the extent and kinetics of swelling have the propensity to disrupt the memorized conformations of the polymer chains and hence interfere with the integrity of the memory sites.

Structural characterization of networks is usually performed by determining parameters such as the mesh size or the correlation length (ξ), equilibrium volume swelling ratio (Q), equilibrium swollen and relaxed specific volumes, polymer volume fraction in the swollen state ($v_{2,s}$), and the average molecular weight between crosslinks (\overline{M}_c)⁴. The two theories used to determine these parameters are the Flory-Rehner equilibrium swelling theory and the rubber elasticity theory.

The mesh size of a crosslinked polymer network is defined as the linear distance between two adjacent crosslinks, and it is representative of the space available within the macromolecular network for molecular diffusion^{53, 92}. Figure 3.5 is a schematic of the mesh size. The mesh size (ξ) can be controlled by altering the nature of the crosslinking monomer (i.e. the crosslinker length and degree of branching), crosslinking density (i.e., the percentage of crosslinking in the pre-polymerization mixture), and valency (i.e. a crosslinking monomer might be

heterobifunctional or homobifunctional). Mesh sizes are determined using the rubber elasticity theory⁹³⁻⁹⁵.

The equilibrium volume swelling ratio (Q) is a measure of the swelling capacity, i.e. the amount of solvent absorbed and retained by the gel at equilibrium. It is defined as is the ratio of the swollen volume of the gel in the swollen and dry states. The polymer volume fraction in the swollen state ($v_{2,s}$) is a measure of the open nature of the network and the free-volume available for mass transport. It is a reciprocal of the equilibrium volume swelling ratio. These parameters are evaluated by penetrant uptake and buoyancy studies⁵³.

The average molecular weight between crosslinks (\overline{M}_c) is a measure of the extent of crosslinking, whether covalent or non-covalent crosslinking. Due to the random nature of the polymerization process itself, only average values of \overline{M}_c can be calculated. \overline{M}_c is determined either using the Flory-Rehner equilibrium swelling theory or by the rubber elasticity theory⁹³⁻⁹⁵.

According to the Flory-Rehner theory, a polymer network placed in solvent swells until the thermodynamically driven mixing force, responsible for swelling of the network, is counterbalanced by the elastic, retractive force of the crosslinked structure. Equation 3.7 indicates that both forces are equal at equilibrium.

$$\Delta G_{Total} = \Delta G_{mixing} + \Delta G_{elastic} \quad 3.7$$

Where, ΔG_{mixing} , the Flory-Huggins free energy of mixing, is a measure of the thermodynamic compatibility of the polymer network and the penetrating solvent, and describes the physical mixing of the chains and the solvent. $\Delta G_{elastic}$ is the change in free energy due to the elastic forces developed inside the gel.

The Flory-Huggins free energy of mixing ΔG_{mixing} is determined by equation 3.8.

$$\Delta G_{mixing} = kT(n_1 \ln \nu_1 + n_2 \ln \nu_{2,s} + \chi n_1) \quad 3.8$$

Where, k is the Boltzmann constant, T is the absolute temperature, n_1 is the number of moles of the penetrating solvent, n_2 is the number of molecules of the polymer, ν_1 is the volume fraction of the solvent, $\nu_{2,s}$ is the polymer volume fraction in the swollen state, and χ is the Flory polymer-solvent interaction parameter. A network swells when χ is negative and collapses when χ is positive. A change in solvent or pH of the solvent would alter the Flory interaction parameter thus altering the swelling behavior and mesh size.

For a cross-linked system, the number of molecules of the polymer n_2 is zero, and hence, equation 3.8 reduces to equation 3.9.

$$\Delta G_{mixing} = kT(n_1 \ln \nu_1 + \chi n_1) \quad 3.9$$

The deformation process occurs without an appreciable change in internal energy, and so the enthalpy of mixing vanishes. Hence, $\Delta G_{elastic}$ can be represented by equation 3.10.

$$\Delta G_{elastic} = -T \Delta S_{elastic} \quad 3.10$$

Where, $\Delta S_{elastic}$ is the change in entropy from the deformation process. If we assume that swelling is isotropic, i.e. the deformation is equal along all three axes, the elastic free energy is given by 3.11.

$$\Delta G_{elastic} = \left(\frac{kT\nu_e}{2}\right)(3\alpha_s^2 - 3 - \ln \alpha_s^3) \quad 3.11$$

Where, ν_e is the effective number of chains in the network and α_s is the linear deformation, which is given by equation 3.12.

$$\alpha_s^3 = \frac{1}{\nu_{2,s}} = \frac{(V_0 + \frac{n_1 V_1}{N})}{V_0} \quad 3.12$$

Where, N is the Avogadro number, V_1 is the molar volume of the penetrating solvent and V_0 is volume of the relaxed network.

The change in chemical potential of the solvent can be obtained by differentiating equation 3.7 with respect to the number of moles of penetrating solvent at constant temperature and pressure, and applying the chain rule to elastic free energy expression.

$$\Delta\mu = N \left(\frac{\partial \Delta G_{mixing}}{\partial n_1} \right)_{T,P} + N \left(\frac{\partial \Delta G_{elastic}}{\partial \alpha_s} \right)_{T,P} \left(\frac{\partial \alpha_s}{\partial n_1} \right)_{T,P} \quad 3.13$$

Differentiating equations 3.9, 3.11, and 3.12 with respect to the number of moles of penetrating solvent, and substituting it in equation 3.13, yields the following equation.

$$\Delta\mu = RT \left[\ln(1 - \nu_{2,s}) + \nu_{2,s} + \chi \nu_{2,s}^2 + V_1 \left(\frac{\nu_e}{V_0} \right) \left(\nu_{2,s}^{1/3} - \frac{\nu_{2,s}}{2} \right) \right] \quad 3.14$$

At equilibrium, the chemical potential of the solvent inside and outside the gel is the same. Eliminating the effective chain density, (ν_e/V_0) and rearranging the expression yields equation 3.15, which is the Flory-Rehner expression for the average molecular weight between crosslinks ($\overline{M_c}$) of a neutral polymer synthesized without solvent.

$$\frac{1}{\overline{M}_c} = \frac{2}{\overline{M}_n} - \frac{\left(\frac{\bar{v}}{V_1}\right) \left[\ln(1 - \nu_{2,s}) + \nu_2 + \chi \nu_{2,s}^2 \right]}{\left(\nu_{2,s}^{1/3} - \frac{\nu_{2,s}}{2} \right)} \quad 3.15$$

Where, \bar{v} is the specific volume of the swollen polymer and \overline{M}_n is the number average molecular weight of the polymer chains synthesized in the absence of crosslinking agent.

For a polymer prepared in the presence of solvent, equation 3.15 needs to be modified to incorporate the changes in elastic chemical potential due to the presence of water. There must now be a parameter which accounts for the volume fraction density of the chains immediately after polymerization, when the network has neither swelled nor collapsed in the solvent. This parameter is the polymer volume fraction in the relaxed state ($\nu_{2,r}$). It makes sense that $\nu_{2,r}$ is greater than $\nu_{2,s}$. Equation 3.16 is an expression for the average molecular weight between crosslinks (\overline{M}_c) of a neutral polymer synthesized in the presence of solvent.

$$\frac{1}{\overline{M}_c} = \frac{2}{\overline{M}_n} - \frac{\left(\frac{\bar{v}}{V_1}\right) \left[\ln(1 - \nu_{2,s}) + \nu_2 + \chi \nu_{2,s}^2 \right]}{(\nu_{2,r}) \left[\left(\frac{\nu_{2,s}}{\nu_{2,r}}\right)^{1/3} - \left(\frac{\nu_{2,s}}{2\nu_{2,r}}\right) \right]} \quad 3.16$$

If the imprinted network has pendant acidic or basic groups, an ionic contribution is added to the expression of chemical potential. Depending on whether the ionic concentration in the gel is much higher or comparable than that in the surrounding solvent, and if the polymer chain distribution is Gaussian or non-Gaussian, the equations will get altered⁹⁶⁻⁹⁸.

Equation 3.17 is valid for an anionic polymer with ionic concentration comparable to that in the surrounding solvent, with Gaussian chain distribution, and synthesized in the absence of a solvent.

$$\frac{V_1}{4I} \left(\frac{f' \nu_{2,s}}{\bar{\nu}} \right)^2 \left[\frac{K_a}{10^{-pH} + K_a} \right]^2 = \left[\ln(1 - \nu_{2,s}) + \nu_2 + \chi \nu_{2,s}^2 \right] + \left(\frac{V_1}{\bar{\nu} M_c} \right) \left(1 - \frac{2\bar{M}_c}{M_n} \right) \left(\nu_{2,s}^{1/3} - \frac{\nu_{2,s}}{2} \right) \quad 3.17$$

Where, f' is number of moles of ionizable groups in the gel, K_a is the acid dissociation constant of the ionizable groups in the gel, and I is the ionic strength of the solution.

Equation 3.18 is valid for an anionic polymer with ionic concentration comparable to that in the surrounding solvent, with Gaussian chain distribution, and synthesized in the presence of a solvent.

$$\frac{V_1}{4I} \left(\frac{f' \nu_{2,s}}{\bar{\nu}} \right)^2 \left[\frac{K_a}{10^{-pH} + K_a} \right]^2 = \left[\ln(1 - \nu_{2,s}) + \nu_2 + \chi \nu_{2,s}^2 \right] + \left\{ \left(\frac{V_1}{\bar{\nu} M_c} \right) \left(1 - \frac{2\bar{M}_c}{M_n} \right) (\nu_{2,r}) \left[\left(\frac{\nu_{2,s}}{\nu_{2,r}} \right)^{1/3} - \frac{1}{2} \left(\frac{\nu_{2,s}}{\nu_{2,r}} \right) \right] \right\} \quad 3.18$$

The valency of the crosslinking monomer is critical in determining the final structure of the network. A crosslinking monomer should have at least two double bonds in order to link two linear polymer chains, and is frequently trifunctional or tetrafunctional. Branching, cycling and physical entanglements are commonly found in polymers when chains propagate in many directions or loop back onto

themselves⁹⁹⁻¹⁰¹. In concentrated solutions such as melts, long linear flexible polymers form temporary networks of entangled chains. The molecular weight between entanglements is a measure of the network mesh size and increases with crosslinking density and solvent weight percentage. Interpenetrating networks are formed in between two or more miscible polymers of different chemistry. It is important to note that entanglements between identical chains lie further apart in a mixture than in a pure system due to the random nature of entanglement.

3.6.6 Initiator Weight Percentages and the Use of Controlled/Living Polymerization

An increase in initiator concentration leads to a high concentration of free radicals, and leads to increased rates of polymerization reaction and increased double bond conversions. This yields polymers of more rigidity and homogeneity, and with greater affinity and capacity for their templates, due to the maintenance of their memorized conformations. The homogeneity of the polymer network is evaluated by the polydispersity of the network and the kinetic chain length.

Polydispersity is a measure of the distribution of molecular weights of the polymer chains over the entire population. The polydispersity index (PDI) is given by equation 3.19.

$$PDI = \frac{\overline{M}_w}{\overline{M}_n} \quad 3.19$$

Where, \overline{M}_w is the weighted average molecular weight of the polymer chains in the population. The PDI has a value always greater than 1, but as the polymer chains approach uniform chain length, the PDI approaches unity.

The kinetic chain length of a polymer is defined as the number of monomer units that make up one dynamically growing polymer chain. The average kinetic chain length is the average number of monomer molecules for each chain initiated. Clearly, the PDI is also a measure of distribution of the kinetic chain length. Increasing the double bond conversion decreases the kinetic chain length thus affecting the structural properties of crosslinked polymer system.

Networks with increased tailorability can be synthesized if parameters such as the kinetic chain length and mesh sizes can be controlled. An intense study of the current literature reveals that a variety of controlled polymerizations strategies have been devised. There include dithiocarbamate-mediated radical polymerization^{102, 103}, atom transfer radical polymerization (ATRP)¹⁰⁴⁻¹¹¹, metal catalyzed living radical polymerization (MCLRP)¹¹², nitroxide mediated radical polymerization (NMP)¹¹³⁻¹¹⁸, and reversible additional fragmentation transfer polymerization (RAFT)¹¹⁹⁻¹²¹. The surface-initiated controlled radical polymerization was also developed using these techniques.

Iniferters^{102, 122, 123}, i.e. initiator-chain transfer molecules, have the potential to significantly enhance binding parameters of imprinted networks, as they control the rates of polymerization, and yield networks with a narrow distribution of kinetic chain length^{26, 124}. An amphiphilic initiator, (4-cyano-4-diethyl dithio carbamyl) pentanoic acid, has been used as an iniferter for the free-radical polymerizations of methacrylic acid in methanol¹⁰³. The polydispersity index was invariant (1.21) with molecular weight and double bond conversions were high (80%). Polydispersity indices of 1.3-2.1 and number-average molecular weights of 64 000-319 000 were obtained when the graft polymerization of N-isopropylacrylamide was carried out using an iniferter N,N-diethyldithiocarbamide acetic acid¹²⁵. The initial polymerization rate of

acrylates, carried out with the iniferter tetraethylthiuram disulfide (TED), exhibited an inverse relationship with the concentration of TED, with the order of dependence ranging from -0.96 to -1¹²⁶. Higher TED concentrations reduce the chain length of the growing acrylic radicals and enhance the mobility of the system, which raise the termination kinetics and further suppresses the polymerization kinetics along with the rate reduction already present as a result of inhibition due to chain transfer to TED.

3.7 List of References

1. Peppas, N.A., Hilt, J.Z., Khademhosseini, A. & Langer, R. Hydrogels in Biology and Medicine: From Molecular Principles to Bionanotechnology. *Adv. Mater.* **18**, 1345-1360 (2006).
2. Sperling, L.H. Introduction to Physical Polymer Science, Edn. 4th. (Wiley-Interscience, 2005).
3. Peppas, N.A. Hydrogels in Medicine and Pharmacy. (CRC Press, Boca Raton, FL, 1987).
4. Peppas, N.A., Bures, P., Leobandung, W. & Ichikawa, H. Hydrogels in pharmaceutical formulations. *Eur. J. Pharm. Biopharm.* **50**, 27-46 (2000).
5. Pack, D.W., Hoffman, A.S., Pun, S. & Stayton, P.S. Design and development of polymers for gene delivery. *Nat. Rev. Drug Discov.* **4**, 581-593 (2005).
6. Byrne, M.E., Park, K. & Peppas, N.A. Molecular imprinting within hydrogels. *Adv. Drug Del. Rev.* **54**, 149-161 (2002).
7. Wulff, G. Molecular imprinting in crosslinked materials with the aid of molecular templates - a way towards artificial antibodies. *Angew. Chem. Int. Ed.* **34**, 1812-1832 (1995).

8. Sellergren, B. Noncovalent molecular imprinting: antibody-like molecular recognition in polymeric network materials. *Trends. Anal. Chem.* **16**, 310-320 (1997).
9. Alvarez-Lorenzo, C. & Concheiro, A. Molecularly imprinted polymers for drug delivery. *Journal of Chromatography, B: Analytical Technologies in the Biomedical and Life Sciences* **804**, 231-245 (2004).
10. Hilt, J.Z. & Byrne, M.E. Configurational biomimesis in drug delivery: molecular imprinting of biologically significant molecules. *Adv. Drug Del. Rev.* **56**, 1599-1620 (2004).
11. Cornish-Bowden, A. Fundamentals of Enzyme Kinetics. (*Portland Press Limited*, 1995).
12. Nicholls, I.A. Thermodynamic considerations for the design of molecularly imprinted polymers with ligand recognition sites. *Chem. Lett.*, 1035-1036 (1995).
13. Nicholls, I.A. Towards the rational design of molecularly imprinted polymers. *J. Mol. Recognit.* **11**, 79-82 (1998).
14. Nicholls, I.A. et al. Can we rationally design molecularly imprinted polymers? *Anal. Chim. Acta* **435**, 9-18 (2001).
15. Venkatesh, S., Sizemore, S.P. & Byrne, M.E. Biomimetic hydrogels for enhanced loading and extended release of ocular therapeutics. *Biomat.* **28**, 717-724 (2007).
16. Bryngelson, J.D. & Wolynes, P.G. A simple statistical field theory of heteropolymer collapse with application to protein folding. *Biopolymers* **30**, 177-188 (1990).

17. Bryngelson, J.D. & Wolynes, P.G. Spin glasses and the statistical mechanics of protein folding. *PNAS* **84**, 7524-7528 (1987).
18. Bryngelson, J.D., Onuchic, J.N., Socci, N.D. & Wolynes, P.G. Funnel, pathways, and the energy landscape of protein folding: a synthesis. *Proteins* **21**, 167-195 (1995).
19. Pande, V.S., Grosberg, A.Y. & Tanaka, T. Heteropolymer freezing and design: towards physical models of protein folding. *Rev. Mod. Phys.* **72**, 259-314 (2000).
20. Pande, V.S., Grosberg, A.Y. & Tanaka, T. Statistical mechanics of simple models of protein folding and design. *Biophys. J.* **73**, 3192-3210 (1997).
21. Pande, V.S., Grosberg, A.Y. & Tanaka, T. Thermodynamic procedure to synthesize heteropolymers that can renature to recognize a given target molecule. *PNAS* **91**, 12976-12979 (1994).
22. Demchenko, A.P. Recognition between flexible protein molecules: induced and assisted folding. *J. Mol. Recognit.* **14**, 42-61 (2001).
23. Kriz, D., Ramstroem, O., Svensson, A. & Mosbach, K. A Biomimetic Sensor Based on a Molecularly Imprinted Polymer as a Recognition Element Combined with Fiber-Optic Detection. *Anal. Chem.* **67**, 2142-2144 (1995).
24. Fischer, L., Mueller, R., Ekberg, B. & Mosbach, K. Direct enantioseparation of β -adrenergic blockers using a chiral stationary phase prepared by molecular imprinting. *J. Am. Chem. Soc.* **113**, 9358-9360 (1991).
25. Mulchandani, A., Kaneva, I. & Chen, W. Biosensor for Direct Determination of Organophosphate Nerve Agents Using Recombinant *Escherichia coli* with Surface-Expressed Organophosphorus Hydrolase. 2. Fiber-Optic Microbial Biosensor. *Anal. Chem.* **70**, 5042-5046 (1998).

26. Vaughan, A.D., Sizemore, S.P. & Byrne, M.E. Enhancing molecularly imprinted polymer binding properties via controlled/living radical polymerization and reaction analysis. *Polymer* **48**, 74-81 (2007).
27. Byrne, M.E. & Salián, V. Molecular imprinting within hydrogels II: progress and analysis of the field. Invited Review. *International Journal of Pharmaceutics*, Submitted (2008).
28. Beuermann, S. & Buback, M. Rate coefficients of free-radical polymerization deduced from pulsed laser experiments. *Prog. Polym. Sci.* **27**, 191 (2002).
29. Piletsky, S.A. et al. Polymer Cookery. 2. Influence of Polymerization Pressure and Polymer Swelling on the Performance of Molecularly Imprinted Polymers. *Macromolecules* **37**, 5018-5022 (2004).
30. Sellergren, B., Dauwe, C. & Schneider, T. Pressure-Induced Binding Sites in Molecularly Imprinted Network Polymers. *Macromolecules* **30**, 2454-2459 (1997).
31. Asai, H. & Imoto, T. High-pressure copolymerization of styrene with methyl methacrylate in various solvents. *J. Polym. Sci. [B]*. **2**, 558-555 (1964).
32. Rampey, A.M. et al. Characterization of the Imprint Effect and the Influence of Imprinting Conditions on Affinity, Capacity, and Heterogeneity in Molecularly Imprinted Polymers Using the Freundlich Isotherm-Affinity Distribution Analysis. *Anal. Chem.* **76**, 1123-1133 (2004).
33. Piletsky, S.A. et al. Polymer Cookery: Influence of Polymerization Time and Different Initiation Conditions on Performance of Molecularly Imprinted Polymers. *Macromolecules* **38**, 1410-1414 (2005).

34. Piletsky, S.A. et al. Polymer Cookery: Influence of Polymerization Conditions on the Performance of Molecularly Imprinted Polymers. *Macromolecules* **35**, 7499-7504 (2002).
35. O'Shannessy, D.J., Ekberg, B. & Mosbach, K. Molecular imprinting of amino acid derivatives at low temperature (0 DegC) using photolytic homolysis of azobisnitriles. *Anal. Biochem.* **177**, 144-149 (1989).
36. Spivak, D., Gilmore, M.A. & Shea, K.J. Evaluation of Binding and Origins of Specificity of 9-Ethyladenine Imprinted Polymers. *J. Am. Chem. Soc.* **119**, 4388-4393 (1997).
37. Pauling, L. The Nature of the Chemical Bond and the Structure of Molecules and Crystals. (*Cornell University Press*, 1960).
38. Lu, Y., Li, C., Wang, X., Sun, P. & Xing, X. Influence of polymerization temperature on the molecular recognition of imprinted polymers. *J. Chromatogr. B* **804**, 53-59 (2004).
39. Spizzirri, U.G. & Peppas, N.A. Structural Analysis and Diffusional Behavior of Molecularly Imprinted Polymer Networks for Cholesterol Recognition. *Chem. Mater.* **17**, 6719-6727 (2005).
40. Watkins, A.W. & Anseth, K.S. Investigation of Molecular Transport and Distributions in Poly(ethylene glycol) Hydrogels with Confocal Laser Scanning Microscopy. *Macromolecules* **38**, 1326-1334 (2005).
41. Saha, B. & Streat, M. Adsorption of Trace Heavy Metals: Application of Surface Complexation Theory to a Macroporous Polymer and a Weakly Acidic Ion-Exchange Resin. *Ind. Eng. Chem. Res.* **44**, 8671-8681 (2005).

42. Figuly, G.D. et al. Preparation and Characterization of Novel Poly(alkylamine)-Based Hydrogels Designed for Use as Bile Acid Sequestrants. *Macromolecules* **30**, 6174-6184 (1997).
43. Hawkins, D.M., Ellis, E.A., Stevenson, D., Holzenburg, A. & Reddy, S.M. Novel critical point drying (CPD) based preparation and transmission electron microscopy (TEM) imaging of protein specific molecularly imprinted polymers (HydroMIPs). *J. Mat. Sci.* **42**, 9465-9468 (2007).
44. Hawkins, D.M. et al. Quantification and Confocal Imaging of Protein Specific Molecularly Imprinted Polymers. *Biomacromolecules* **7**, 2560-2564 (2006).
45. Kamlet, M.J., Abboud, J.L. & Taft, R.W. The solvatochromic comparison method. 6. The π^* scale of solvent polarities. *J. Am. Chem. Soc.* **99**, 6027-6038 (1977).
46. Kamlet, M.J., Hall, T.N., Boykin, J. & Taft, R.W. Linear solvation energy relationships. 6. Additions to and correlations with the π^* scale of solvent polarities. *J. Org. Chem.* **44**, 2599-2604 (1979).
47. Kamlet, M.J. & Taft, R.W. Linear solvation energy relationships. Part 3. Some reinterpretations of solvent effects based on correlations with solvent π^* and alpha values. *J. Chem. Soc. Perk. Trans. 2*, 349-356 (1979).
48. Kamlet, M.J., Dickinson, C., Gramstad, T. & Taft, R.W. Linear solvation energy relationships. 16. Dipole/dipole contributions to formation constants of some "hydrogen bonded complexes". *J. Org. Chem.* **47**, 4971-4975 (1982).
49. Taft, R.W., Gramstad, T. & Kamlet, M.J. Linear solvation energy relationships. 14. Additions to and correlations with the beta scale of hydrogen bond acceptor basicities. *J. Org. Chem.* **47**, 4557-4563 (1982).

50. Kamlet, M.J., Abboud, J.L.M., Abraham, M.H. & Taft, R.W. Linear solvation energy relationships. 23. A comprehensive collection of the solvatochromic parameters, π^* , α , and β , and some methods for simplifying the generalized solvatochromic equation. *J. Org. Chem.* **48**, 2877-2887 (1983).
51. Piletsky, S.A., Andersson, H.S. & Nicholls, I.A. Combined Hydrophobic and Electrostatic Interaction-Based Recognition in Molecularly Imprinted Polymers. *Macromolecules* **32**, 633-636 (1999).
52. Gorbachuk, V.V., Mironov, N.A., Solomonov, B.N. & Habicher, W.D. Biomimetic Cooperative Interactions of Dried Cross-Linked Poly(N-6-aminohexylacrylamide) with Binary Mixtures of Solvent Vapors. *Biomacromolecules* **5**, 1615-1623 (2004).
53. Venkatesh, S., Saha, J., Pass, S. & Byrne, M.E. Transport and structural analysis of molecular imprinted hydrogels for controlled drug delivery. *Eur. J. Pharm. Biopharm.* doi:10.1016/j.ejpb.2008.01.036 (2008).
54. Ali, M. et al. Zero-order therapeutic release from imprinted hydrogel contact lenses within in vitro physiological ocular tear flow. *J. Controlled Release* **124**, 154-162 (2007).
55. Alvarez-Lorenzo, C. et al. Soft contact lenses capable of sustained delivery of timolol. *J. Pharm. Sci.* **91**, 2182-2192 (2002).
56. Hiratani, H., Fujiwara, A., Tamiya, Y., Mizutani, Y. & Alvarez-Lorenzo, C. Ocular release of timolol from molecularly imprinted soft contact lenses. *Biomat.* **26**, 1293-1298 (2005).
57. Van de Grampel, H.T., Tan, Y.Y. & Challa, G. Template polymerization of N-vinylimidazole along poly(methacrylic acid) in water. 1. Influence of template concentration. *Macromolecules* **23**, 5209-5216 (1990).

58. Van de Grampel, H.T., Tan, Y.Y. & Challa, G. Template polymerization of N-vinylimidazole along poly(methacrylic acid) in water. 2. Kinetics of the template polymerization. *Macromolecules* **24**, 3767-3772 (1991).
59. Van de Grampel, H.T., Tan, Y.Y. & Challa, G. Template polymerization of N-vinylimidazole along poly(methacrylic acid) in water. 3. Molecular weights of the formed polymers. *Macromolecules* **24**, 3773-3778 (1991).
60. Karim, K. et al. How to find effective functional monomers for effective molecularly imprinted polymers? *Adv. Drug Del. Rev.* **57**, 1795-1808 (2005).
61. Molinelli, A. et al. Analyzing the Mechanisms of Selectivity in Biomimetic Self-Assemblies via IR and NMR Spectroscopy of Prepolymerization Solutions and Molecular Dynamics Simulations. *Anal. Chem.* **77**, 5196-5204 (2005).
62. Katz, A. & Davis, M.E. Investigations into the Mechanisms of Molecular Recognition with Imprinted Polymers. *Macromolecules* **32**, 4113-4121 (1999).
63. Duffy, D.J. et al. Binding Efficiency and Transport Properties of Molecularly Imprinted Polymer Thin Films. *J. Am. Chem. Soc.* **124**, 8290-8296 (2002).
64. McStay, D., Al-Obaidi, A.H., Hoskins, R. & Quinn, P.J. Raman spectroscopy of molecular imprinted polymers. *Journal of Optics A: Pure and applied optics* **7**, S340-S345 (2005).
65. O'Mahony, J., Molinelli, A., Nolan, K., Smyth, M.R. & Mizaikoff, B. Towards the rational development of molecularly imprinted polymers: ¹H NMR studies on hydrophobicity and ion-pair interactions as driving forces for selectivity. *Biosens. Bioelectron.* **20**, 1884-1893 (2005).
66. Svenson, J., Karlsson Jesper, G. & Nicholls Ian, A. ¹H nuclear magnetic resonance study of the molecular imprinting of (-)-nicotine: template self-

- association, a molecular basis for cooperative ligand binding. *J. Chromatogr. A* **1024**, 39-44 (2004).
67. Karlsson, J.G., Karlsson, B., Andersson, L.I. & Nicholls, I.A. The roles of template complexation and ligand binding conditions on recognition in bupivacaine molecularly imprinted polymers. *Analyst* **129**, 456-462 (2004).
68. Jie, Z. & Xiwen, H. Study of the nature of recognition in molecularly imprinted polymer selective for 2-aminopyridine. *Anal. Chim. Acta* **381**, 85-91 (1999).
69. Idziak, I., Benrebouh, A. & Deschamps, F. Simple NMR experiments as a means to predict the performance of an anti-17 α -ethynylestradiol molecularly imprinted polymer. *Anal. Chim. Acta* **435**, 137-140 (2001).
70. Svenson, J., Andersson, H.S., Piletsky, S.A. & Nicholls, I.A. Spectroscopic studies of the molecular imprinting self-assembly process. *J. Mol. Recognit.* **11**, 83-86 (1998).
71. Andersson, H.S. & Nicholls, I.A. Spectroscopic evaluation of molecular imprinting polymerization systems. *Bioorg. Chem.* **25**, 203-211 (1997).
72. Striegler, S. & Tewes, E. Investigation of sugar-binding sites in ternary ligand-copper(II)-carbohydrate complexes. *Eur. J. Inorg. Chem.*, 487-495 (2002).
73. Guo, H. & He, X. Study of the binding characteristics of molecular imprinted polymer selective for cefalexin in aqueous media. *Fresenius J. Anal. Chem.* **368**, 461-465 (2000).
74. Chianella, I. et al. Rational design of a polymer specific for microcystin-LR using a computational approach. *Anal. Chem.* **74**, 1288-1293 (2002).

75. Subrahmanyam, S. et al. 'Bite-and-Switch' approach using computationally designed molecularly imprinted polymers for sensing of creatinine¹. *Biosens. Bioelectron.* **16**, 631-637 (2001).
76. Piletsky, S.A. et al. Recognition of ephedrine enantiomers by molecularly imprinted polymers designed using a computational approach. *Analyst* **126**, 1826-1830 (2001).
77. Takeuchi, T., Fukuma, D., Matsui, J. & Mukawa, T. Combinatorial molecular imprinting for formation of atrazine decomposing polymers. *Chem. Lett.*, 530-531 (2001).
78. Takeuchi, T., Fukuma, D. & Matsui, J. Combinatorial Molecular Imprinting: An Approach to Synthetic Polymer Receptors. *Anal. Chem.* **71**, 285-290 (1999).
79. Lanza, F. & Sellergren, B. Method for Synthesis and Screening of Large Groups of Molecularly Imprinted Polymers. *Anal. Chem.* **71**, 2092-2096 (1999).
80. Lanza, F. et al. Development of a semiautomated procedure for the synthesis and evaluation of molecularly imprinted polymers applied to the search for functional monomers for phenytoin and nifedipine. *Anal. Chim. Acta* **435**, 91-106 (2001).
81. Lanza, F. & Sellergren, B. Molecularly imprinted polymers via high-throughput and combinatorial techniques. *Macromol. Rapid Commun.* **25**, 59-68 (2004).
82. Lanza, F., Dirion, B. & Sellergren, B. Combinatorial approaches to molecular imprinting. (*Marcel Dekker*, 2005).

83. Kim, H. & Spivak, D.A. New Insight into Modeling Non-Covalently Imprinted Polymers. *J. Am. Chem. Soc.* **125**, 11269-11275 (2003).
84. Piletsky, S.A., Piletskaya, E.V., Sergeyeva, T.A., Panasyuk, T.L. & El'skaya, A.V. Molecularly imprinted self-assembled films with specificity to cholesterol. *Sensors and Actuators B: Chemical* **60**, 216-220 (1999).
85. Sergeyeva, T.A. et al. Selective recognition of atrazine by molecularly imprinted polymer membranes. Development of conductometric sensor for herbicides detection. *Analytica Chimica Acta* **392**, 105-111 (1999).
86. Alvarez-Lorenzo, C., Yanez, F., Barreiro-Iglesias, R. & Concheiro, A. Imprinted soft contact lenses as norfloxacin delivery systems. *J. Controlled Release* **113**, 236-244 (2006).
87. Flory, P.J. Principles of Polymer Chemistry, Edn. 1st. (*Cornell University Press*, 1953).
88. Lovestead, T.M., Berchtold, K.A. & Bowman, C.N. An Investigation of Chain Length Dependent Termination and Reaction Diffusion Controlled Termination during the Free Radical Photopolymerization of Multivinyl Monomers. *Macromolecules* **38**, 6374-6381 (2005).
89. Noss, K.R., Vaughan, A.D. & Byrne, M.E. Tailored binding and transport parameters of molecularly imprinted films via macromolecular structure: the rational design of recognitive polymers. *J. Appl. Polym. Sci.* **107**, 3435-3441 (2008).
90. Byrne, M.E., Hilt, J.Z. & Peppas, N.A. Recognitive biomimetic networks with moiety imprinting for intelligent drug delivery. *J. Biomed. Mater. Res. A* **84A**, 137-147 (2007).

91. Hilt, J.Z., Byrne, M.E. & Peppas, N.A. Microfabrication of Intelligent Biomimetic Networks for Recognition of D-Glucose. *Chem. Mater.* **18**, 5869-5875 (2006).
92. Brazel, C.S. & Peppas, N.A. Synthesis and Characterization of Thermo- and Chemomechanically Responsive Poly(N-isopropylacrylamide-co-methacrylic acid) Hydrogels. *Macromolecules* **28**, 8016-8020 (1995).
93. Flory, P.J. Principles of Polymer Chemistry. (*Cornell University Press*, 1953).
94. Flory, P.J. & Rehner, J., Jr. Statistical mechanics of cross-linked polymer networks. II. Swelling. *J. Chem. Phys.* **11**, 521-526 (1943).
95. Flory, P.J. & Rehner, J., Jr. Statistical mechanics of cross-linked polymer networks. I. Rubberlike elasticity. *J. Chem. Phys.* **11**, 512-520 (1943).
96. Brannon-Peppas, L. & Peppas, N.A. Solute and penetrant diffusion in swellable polymers. IX. The mechanisms of drug release from pH-sensitive swelling-controlled systems. *J. Controlled Release* **8**, 267-274 (1989).
97. Brannon-Peppas, L. & Peppas, N.A. Equilibrium swelling behavior of dilute ionic hydrogels in electrolytic solutions. *J. Controlled Release* **16**, 319-329 (1991).
98. Brannon-Peppas, L. & Peppas, N.A. Equilibrium swelling behavior of pH-sensitive hydrogels. *Chem. Eng. Sci.* **46**, 715-722 (1991).
99. Tsenoglou, C. Rubber elasticity of cross-linked networks with trapped entanglements and dangling chains. *Macromolecules* **22**, 284-289 (1989).
100. Tsenoglou, C. Network architecture and modulus of miscible heteropolymer blends. *J. Polym. Sci., Part B: Polym. Phys.* **26**, 2329-2339 (1988).
101. Tsenoglou, C. Rubber elasticity modulus of interpenetrating heteropolymer networks. *Polym. Mater. Sci. Eng.* **56**, 11-14 (1987).

102. Otsu, T. & Yoshida, M. Role of initiator-transfer agent-terminator (iniferter) in radical polymerizations: polymer design by organic disulfides as iniferters. *Die Makromolekulare Chemie, Rapid Communications* **3**, 127-132 (1982).
103. Ishizu, K., Katsuhara, H. & Itoya, K. Controlled radical polymerization of methacrylic acid initiated by diethyldithio-carbamate-mediated iniferter. *J. Polym. Sci., Part A: Polym. Chem.* **43**, 230-233 (2005).
104. Gan, L.-H., Ravi, P., Mao, B.W. & Tam, K.-C. Controlled/living polymerization of 2-(diethylamino)ethyl methacrylate and its block copolymer with tert-butyl methacrylate by atom transfer radical polymerization. *J. Polym. Sci., Part A: Polym. Chem.* **41**, 2688-2695 (2003).
105. Xia, J. & Matyjaszewski, K. Controlled/"Living" Radical Polymerization. Homogeneous Reverse Atom Transfer Radical Polymerization Using AIBN as the Initiator. *Macromolecules* **30**, 7692-7696 (1997).
106. Matyjaszewski, K., Davis, K., Patten, T.E. & Wei, M. Observation and analysis of a slow termination process in the atom transfer radical polymerization of styrene. *Tetrahedron* **53**, 15321-15329 (1997).
107. Matyjaszewski, K. & Gaynor, S.G. Preparation of Hyperbranched Polyacrylates by Atom Transfer Radical Polymerization. 3. Effect of Reaction Conditions on the Self-Condensing Vinyl Polymerization of 2-((2-Bromopropionyl)oxy)ethyl Acrylate. *Macromolecules* **30**, 7042-7049 (1997).
108. Matyjaszewski, K. Mechanistic and synthetic aspects of atom transfer radical polymerization. *J. Macromol. Sci., Pure Appl. Chem.* **A34**, 1785-1801 (1997).
109. Wang, J.-L., Grimaud, T. & Matyjaszewski, K. Kinetic Study of the Homogeneous Atom Transfer Radical Polymerization of Methyl Methacrylate. *Macromolecules* **30**, 6507-6512 (1997).

110. Matyjaszewski, K. & Kajiwara, A. EPR Study of Atom Transfer Radical Polymerization (ATRP) of Styrene. *Macromolecules* **31**, 548-550 (1998).
111. Luo, R. & Sen, A. Electron-Transfer-Induced Iron-Based Atom Transfer Radical Polymerization of Styrene Derivatives and Copolymerization of Styrene and Methyl Methacrylate. *Macromolecules* **41**, 4514-4518 (2008).
112. Leduc, M.R., Hayes, W. & Frechet, J.M.J. Controlling surfaces and interfaces with functional polymers: preparation and functionalization of dendritic-linear block copolymers via metal catalyzed "living" free radical polymerization. *J. Polym. Sci., Part A: Polym. Chem.* **36**, 1-10 (1998).
113. Georges, M.K., Kee, R.A., Veregin, R.P.N., Hamer, G.K. & Kazmaier, P.M. Nitroxide mediated free radical polymerization process. Autopolymerization. *J. Phys. Org. Chem.* **8**, 301-305 (1995).
114. Veregin, R.P.N., Odell, P.G., Michalak, L.M. & Georges, M.K. Mechanism of Rate Enhancement Using Organic Acids in Nitroxide-Mediated Living Free-Radical Polymerizations. *Macromolecules* **29**, 4161-4163 (1996).
115. Veregin, R.P.N., Kazmaier, P.M., Odell, P.G. & Georges, M.K. The role of thermal initiation in nitroxide mediated living free radical polymerizations. *Chem. Lett.*, 467-468 (1997).
116. Kazmaier, P.M., Daimon, K., Georges, M.K., Hamer, G.K. & Veregin, R.P.N. Nitroxide-Mediated "Living" Free Radical Polymerization: A Rapid Polymerization of (Chloromethyl)styrene for the Preparation of Random, Block, and Segmental Arborescent Polymers. *Macromolecules* **30**, 2228-2231 (1997).

117. MacLeod, P.J., Veregin, R.P.N., Odell, P.G. & Georges, M.K. Stable Free Radical Polymerization of Styrene: Controlling the Process with Low Levels of Nitroxide. *Macromolecules* **30**, 2207-2208 (1997).
118. Debuigne, A., Chan-Seng, D., Li, L., Hamer, G.K. & Georges, M.K. Synthesis and Evaluation of Sterically Hindered 1,1-Diadamantyl Nitroxide as a Low-Temperature Mediator for the Stable Free Radical Polymerization Process. *Macromolecules* **40**, 6224-6232 (2007).
119. Vasilieva, Y.A. et al. Controlled/living polymerization of methacrylamide in aqueous media via the RAFT process. *J. Polym. Sci., Part A: Polym. Chem.* **43**, 3141-3152 (2005).
120. Donovan, M.S., Sumerlin, B.S., Lowe, A.B. & McCormick, C.L. Controlled/"Living" Polymerization of Sulfobetaine Monomers Directly in Aqueous Media via RAFT. *Macromolecules* **35**, 8663-8666 (2002).
121. Convertine Anthony, J., Ayres, N., Scales Charles, W., Lowe Andrew, B. & McCormick Charles, L. Facile, controlled, room-temperature RAFT polymerization of N-isopropylacrylamide. *Biomacromolecules* **5**, 1177-1180 (2004).
122. Otsu, T. Iniferter concept and living radical polymerization. *J. Polym. Sci., Part A: Polym. Chem.* **38**, 2121-2136 (2000).
123. Otsu, T. & Matsumoto, A. Controlled synthesis of polymers using the iniferter technique: developments in living radical polymerization. *Adv. Polym. Sci.* **136**, 75-137 (1998).
124. Matyjaszewski, K. A commentary on "role of initiator-transfer agent-terminator (iniferter) in radical polymerizations: polymer design by organic

- disulfides as iniferters" by T. Otsu, M. Yoshida (*Macromol. Rapid Commun.* 1982, 3, 127-132). *Macromol. Rapid Commun.* **26**, 135-142 (2005).
125. Tsuji, S. & Kawaguchi, H. Effect of Graft Chain Length and Structure Design on Temperature-Sensitive Hairy Particles. *Macromolecules* **39**, 4338-4344 (2006).
126. Kilambi, H., Reddy, S.K. & Bowman, C.N. Kinetic and Mechanistic Studies of Photopolymerizations of Acrylates in the Presence of Iniferters. *Macromolecules* **40**, 6131-6135 (2007).

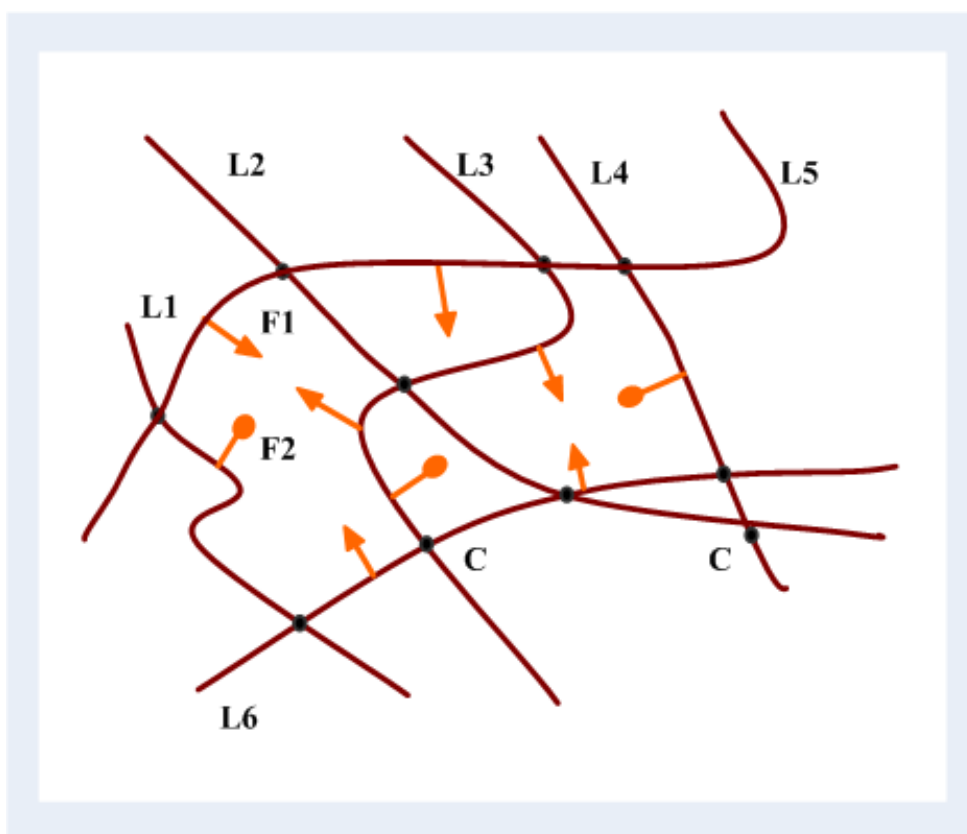


Figure 3.1 General schematic of a polymer network. The linear chains (L1-L6) are a heterogeneous population, consisting of sequences of functional monomers. The crosslinking monomer (C) is usually much smaller in molecular weight than the linear chains and is as a volumeless point. Diverse pendant functionalities (F1 and F2) can be used for template binding and recognition.

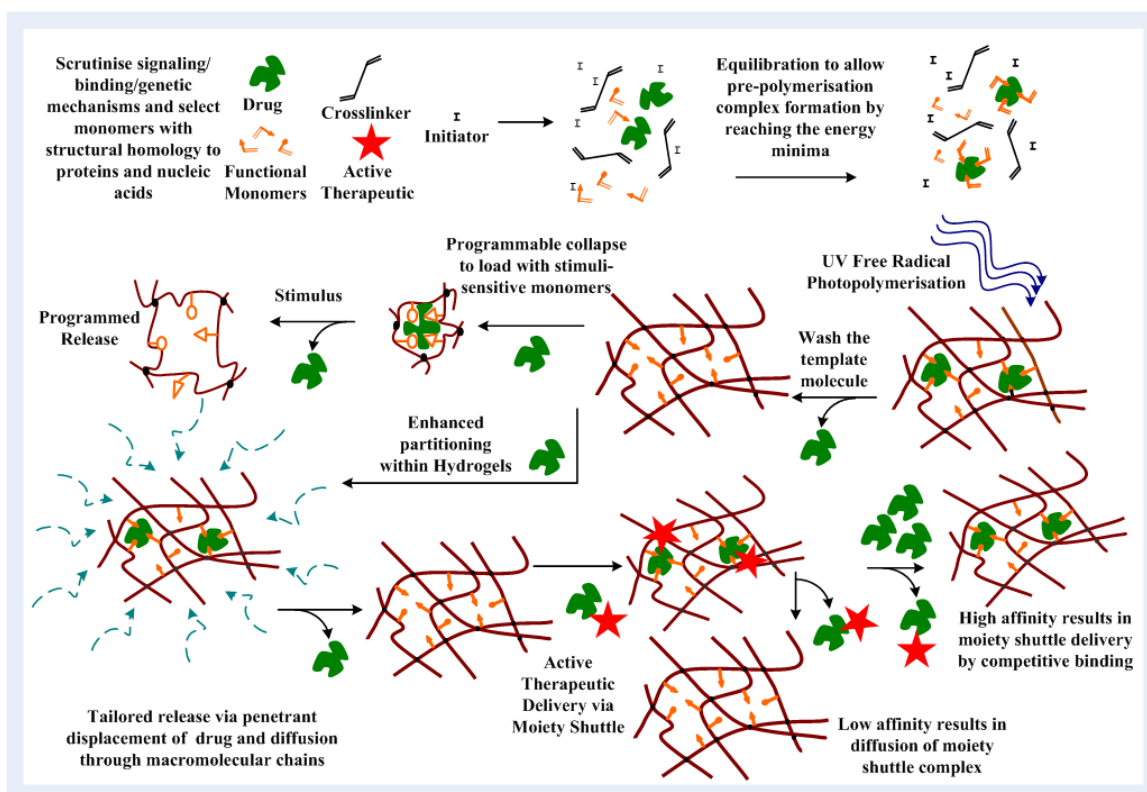


Figure 3.2 General schematic of the configurational biomimetic imprinting synthesis scheme. Upon gleaning fundamental binding principles from Nature, one incorporates diverse chemical functionalities at the molecular level in the network, and maximizes the non-covalent interactions with the drug. The drug acts as a template and organizes the growing polymer chains during the formation of the network, and hence “imprints” or creates macromolecular memory in the memory



Figure 3.3 Design Parameters of a Hydrogel. The macromolecular structure of imprinted polymer networks, and hence in effect the template binding parameters, can be controlled by tuning various environmental and compositional parameters.

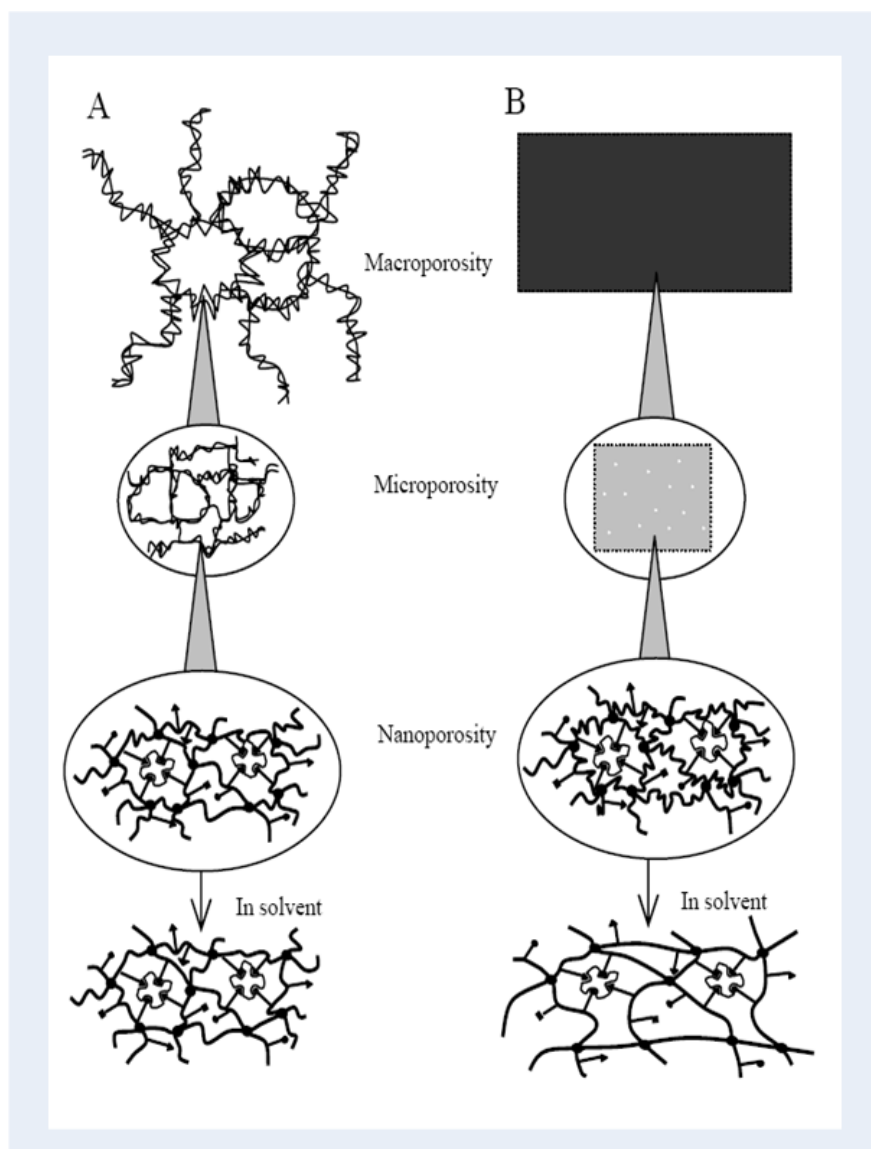


Figure 3.4 Porosity Within Imprinted Hydrogels. A. For templated gels prepared in solvent the polymer will contain significant macro- and microporosity. Template transport will be primarily related to the porosity and tortuosity within the polymer, as in conventional hydrogels. **B.** For imprinted gels prepared without solvent, the polymer will not typically exhibit macro and micro-porosity, and it is the mesh size which influences template transport.

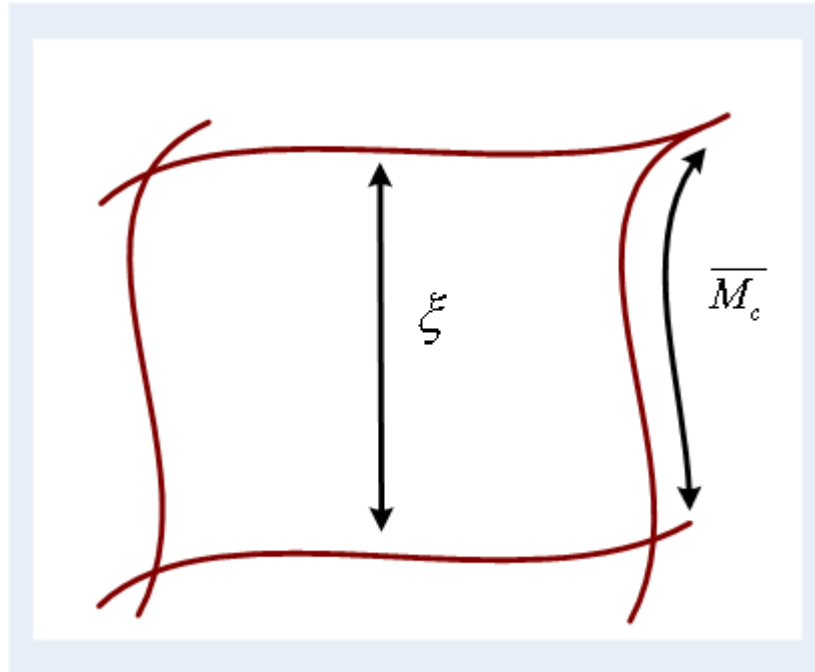


Figure 3.5 General Schematic of Mesh Size. The average mesh size (ξ) of the polymer represents the space available within the macromolecule for mass transport. The average molecular weight between crosslinks (\overline{M}_c) is a measure of the extent of crosslinking, whether covalent or non-covalent crosslinking.

4.0 ENHANCED LOADING AND REACTION ANALYSIS ON BIOMIMETIC RECOGNITIVE CONTACT LENSES

In this chapter, we studied molecular imprinted networks with a particular emphasis on enhancing the therapeutic loading potential and extending the release kinetics *via* rational design. We designed such systems using the logic of configurational biomimetic imprinting, a variant of the conventional molecular imprinting technique, which builds in macromolecular memory in the network. By incorporating a natural receptor-based rational design strategy in the synthesis of novel recognitive weakly crosslinked networks, we demonstrated the potential of biomimetic polymers to load significant amounts of ocular medication such as H₁-antihistamines. The most biomimetic imprinted network, poly (AA-co-AM-co-NVP-co-HEMA-co-PEG200DMA), i.e. the network synthesized from the pre-polymerization mixture of maximum diversity in chemical functionalities, demonstrated a dramatic increase in loading and slower release kinetics than the networks synthesized from a less diverse mixture of functional monomers. The imprinting effect was reflected in a reduced propagation of polymer chains. The transport and structural characteristics of these networks will be presented in chapter 5. The results presented in the following chapter have been published as a research article¹, which was the first study in the literature lending evidence to the hypothesis that maximizing functional monomer-template molecule interactions in the pre-polymerization complex, would result in enhanced loading during rebinding and extended release profiles.

4.1 Scientific Rationale

Biomimetic and biohybrid materials are prime candidates for the creation of enhanced delivery systems with tremendous promise to profoundly impact medicine *via* improved treatment options for disease and better quality of life². Within the field of advanced drug delivery, major emphasis is now being focused toward engineering the architectural design of biomaterials at the molecular level³. In this chapter, we discuss the methods to synthesize, characterize and optimize soft therapeutic contact lenses to tackle the unmet need for non-invasive, controlled release of ocular drugs. To achieve this end, we developed a biomimetic approach to design imprinted networks for the amelioration of seasonal allergic rhinoconjunctivitis. Our original objective was to investigate the potential of these networks to load therapeutically relevant concentrations of a H₁-antihistamine drug. We chose ketotifen fumarate as our model drug since it is an FDA-approved potent fast-acting molecule which targets histamine H₁-receptors and down regulates the pharmacological effects of histamine. An intense study of the crystal structures of ligand-receptor complexes revealed critical amino acids in the binding pockets and we chose FDA-approved monomers bearing side chains of similar functionalities, in order to mimic the complex non-covalent binding patterns found in Nature. We designed networks of varying compositions of functional monomers and determined their loading potential *via* equilibrium rebinding studies.

In this chapter, we also discuss an unprecedented observation in such systems- that enriching the functional diversity of monomers in the pre-polymerization mixture resulted in enhanced loading over networks prepared with less diverse functional monomers. Furthermore, we determined double bond conversions and rates of

polymerization *via* reaction analysis for varying template and functional monomer compositions, with the hypothesis that the imprinting effect would be reflected in the propagation of polymer chains during polymerization. The objective of these studies was to determine the design parameters for template recognition and binding and to determine observable trends on varying these parameters. This would increase the tailorability of the platform towards further optimization.

4.2 Historical Background and Current Trends in Ocular Drug Delivery

There are many topical ocular drug delivery systems which are in clinical trials or on the market for disorders such as macular degeneration, viral diseases such as chronic cytomegalovirus retinitis, glaucoma, allergic rhinoconjunctivitis, dry eye syndrome, and retinal degenerations. However, topical strategies have been in use since ancient civilizations. Eye drops such as *belladonna* were used for dilating the pupils of female patients and thespians⁴. Physicians in ancient Rome espoused the notion of a dissolved therapeutic in an aqueous constituent, and used honey soaked linen as an ophthalmic dressing in the treatment of disease⁵.

The first patent in the field from Otto Wichterle in 1965⁶ stated that “bacteriostatic, bacteriocidal or otherwise medicinally active substances such as antibiotics may be dissolved in the aqueous constituent of hydrogels to provide medication over an extended period *via* diffusion”. Since then, delivering ocular drugs *via* contact lenses has been considered an effective alternative to topical application *via* eye drops⁷. This notion stems from the observation that drug molecules loaded in a lens have a much longer residence time in the tear film, compared to the residence time of two minutes in the case of eye drops. This longer residence time enhances

drug permeation through the cornea and minimizes non-productive drug absorption into the blood stream through the conjunctiva or nasolacrimal duct⁸. Furthermore, it is believed that contact lenses can also provide controlled drug release profiles, due to the diffusion of the drug molecules through the polymer network.

Topically applied drugs in the forms of solutions, suspensions, and ointments account for 90% of ophthalmological formulations on the market today⁹. The caveat of topical delivery is that bioavailability tends to be low, i.e. only about 5% is productively absorbed¹⁰ due to various factors and ocular protective mechanisms. These include lachrymation and tear turnover, nasolachrymal drainage, spillage from the eye, metabolic degradation, and non-corneal absorption, poor impermeability of hydrophobic and large hydrophilic drugs through the cornea etc. Topical solutions and suspensions are administered at very high concentrations of drug multiple times a day, leading to increased toxicity, burning, itching sensations, and gritty feelings, etc. experienced by the patient. Typically, there is also the problem of compliance as patients using topical eye drops receive large variances in medication from application to application due to insufficient dosages, skipping dosages, and/or over-administering dosages which can lead to ocular damage and side effects. While ointments can lead to slightly increased bioavailabilities over drops, they are difficult to apply, uncomfortable to use, and severely reduce vision. Efficient ocular delivery rests on two important factors- (i) enhancing drug bioavailability by improving retention of drug on the ocular surface thereby limiting loss by lachrymation, tear turnover, and drainage, and (ii) increasing drug transport through ocular barriers¹¹ such as the cornea, a transparent, dome-shaped window covering the front of the eye; the sclera, tough, opaque, white of the eye; and the conjunctiva - a mucous membrane of the eye with a highly vascularized stroma that covers the visible part of the sclera.

Soft contact lenses are made of hydrogels, which are hydrophilic polymers with dramatic implications in drug delivery¹²⁻¹⁶. Delivering ocular medications *via* contact lenses has pharmaceutical implications in that it can solve problems such as low bioavailability, irritation to ocular tissue, and ocular and systemic side effects due to high dosages. However, drug release *via* contact lenses has not become a commercial reality due to the inability of conventional contact lenses to load and release a significant concentration of drug to have a therapeutically relevant effect¹⁷. This can be directly attributed to lack of functionality at the molecular level, which would enhance carrier-target interactions, and maximize loading of the drug within the polymer network. Thus, there is a clear need to examine a target molecule and synthesize carriers with chemical functionality specific to it, using bottom-up synthetic strategies. Rationally designed biomaterials to increase drug partitioning or loading is paramount to the development and commercial sustainability of lenses for ophthalmic drug delivery.

The traditional ophthalmic systems like aqueous solutions, suspensions and ointments are associated with transient over dosage followed by interim periods of no dosage, which leads to decrease in bioavailability, and greater risks of ocular tissue irritation. A number of erodible and nonerodible inserts have been devised, which overcome these disadvantages by providing a more sustained release profile and more effective concentrations of drug in the target tissues. The earliest insert in the market was Ocusert® (Alza, USA) which consisted of a small wafer of drug reservoir enclosed by two ethylene-vinyl acetate copolymer membranes that was placed in the corner of the eye and provided extended release of a therapeutic agent for approximately 7 days at the rate of 40 µg/hr¹⁸. The insert delivered the drug pilocarpine, for treating glaucoma, and reduced intraocular pressure of the eye by

increasing fluid drainage. Another popular insert by the same company was an osmotically controlled insert for epinephrine¹⁹. Lacrisert (Merck, USA) is a cellulose based polymer insert used to treat dry eye syndrome²⁰. An ocular insert delivering oxytetracycline provided a sustained release for 14 days *in vitro* and 7 days *in vivo* in humans^{21, 22}. All these inserts had improved release profiles, but rapidly gained notoriety because elderly patients had difficulties using them. Occasionally the insert was expelled from the conjunctiva or the membrane would rupture, resulting in burst kinetics of drug, which was highly toxic. More recently, encouraging results have been obtained with polymeric inserts composed of poly(2-hydroxyethyl methacrylate) loaded with pilocarpine. *In vitro* release studies confirmed a 24-hour release period²³.

Intravitreal injections require repeated injections and have potential side effects such as hemorrhage, retinal detachment, cataract along with low patient compliance. Intravitreal injections of ganciclovir, an antiviral drug used for treating chronic cytomegalovirus retinitis, requires frequent injections for maintaining therapeutic levels, since this drug prevents viral replication but does not lower viral titers. This results in cataracts and retinal detachment²⁴.

Non-biodegradable implants such as Vitrasert and Retisert (Bausch & Lomb, USA) provide strict control of drug release and sustained release profiles, but require intraocular surgery and often have the same incidence of side effects. Vitrasert is a polymeric implant loaded with ganciclovir, which has been used to control the progression of CMV retinitis in AIDS patients for a mean period of six months²⁵, but increased rate of retinal detachments have rendered it unsafe for use. Retisert is a non-biodegradable intravitreal implant that delivers fluocinolone acetonide, a synthetic corticosteroid, which is used for the treatment of intraocular inflammation. It has been approved for the treatment of chronic uveitis, which is a set of intraocular

inflammatory disorders affecting the uveal tract of the eye. It delivers drug at an initial rate of 0.6 µg/day over the first month and attains a steady-state rate of 0.3–0.4 µg/day over approximately 30 months²⁶⁻²⁸. Posurdex (Allergan, USA) is a polymeric biodegradable implants currently in clinical trials. This implant provides sustained delivery of dexamethasone, a corticosteroid known for its anti-inflammatory and anti-angiogenic properties, directly to the targeted disease site. The implant has potential to treat patients with macular edema, an ocular disorder which is normally associated with diabetic retinopathy, retinal vascular occlusions and uveitis.

Increasing the drug reservoir within contact lenses has included nanoparticulate²⁹ and liposomal laden lenses, ion exchange hydrogels³⁰, and molecular imprinting methods³¹, but the duration of release has been limited to most drug being delivered during *in-vitro* and *in-vivo*³² experiments in under 1 day. Recently researchers have demonstrated that the molecular imprinting effect leads to a slower *in-vitro* release rate, with 50% of drug being released in 3 days³³. Nanoparticulate laden lenses have shown promise within *in-vitro* studies and demonstrate 55% of drug released in 3 days. However, these successes suffer from concerns such as inadequate drug loading for long release times; and for lens dispersed nanoparticles, decreased mechanical stability induced by grain boundaries, reduced optical clarity, and longer production schemes. Therefore, a tremendous need exists to increase drug loading to ensure a sufficient supply of drug to maintain longer release durations of therapeutically relevant concentrations.

Controlling and tailoring the release of drugs *via* novel contact lenses can solve these problems with increased drug bioavailability, less irritation to eye tissue, and reduced eye and systemic side effects. This new class of cognitive intelligent biomaterials is designed by incorporating motifs with structural and molecular

homology to biological receptor docking sites and has a strong potential to work with a wide spectrum of drugs and impact the administration of a number of ocular therapies. The US prescription ophthalmic drug market, in which 90% is controlled by the eye drop and ointment sector, is approximately \$ 4.5 billion and growing at a 10% average annual growth rate since 2002.

4.3 The Mammalian Inflammation Pathway

The mammalian inflammation pathway is illustrated in Figure 4.2. In higher vertebrates, Langerhans cells pinocytose allergens of significant pathology, and start migrating towards the secondary lymphoid organs, while expressing MHC-peptide complexes on their surfaces^{34, 35}. These produce cytokine microenvironments, and launch naïve T cells on a complex program of differentiation. Depending on which interleukin sits on their receptor, these differentiate into T_H1 or T_H2 cells^{36, 37}, the latter which bear as stimulants of B cells to produce antibodies such as IgE from IL-4 and CD40 interactions. IgE crosslinking with allergens on the Fc^εRI receptors of mast cells, results in degranulation and secretion of inflammatory mediators such as histamine³⁸. Histamine acts at H₁, H₂, H₃ and H₄-receptors, and induces the nitric oxide signaling pathway in the vascular endothelium, causing vasodilation, erythema, and oedema³⁹. Antihistamines such as ketotifen fumarate (a potent fast acting and highly selective histamine H₁-receptors⁴⁰) downregulate the pharmacological effects of histamine.

4.4 Materials and Methods: Synthesis and Reaction Analysis of Therapeutic Contact Lenses

This section describes materials and methods used for the synthesis of five recognitive networks for ketotifen fumarate created by the configurational biomimetic imprinting method. Imprinted network compositions consisted of 5 mole% crosslinking monomer and 95 mole% functional monomer (92 mole% backbone monomer, HEMA, and 3 mole% functional monomers acrylic acid, acrylamide, and n-vinyl 2-pyrrolidone). The monomer to template (M/T) ratio for all networks was held constant at 185. Equilibrium rebinding studies yielded template binding parameters and reaction analysis was carried out for molecular characterization of the polymerization reaction.

4.4.1 Materials

The functional monomers Acrylic acid (AA), Acrylamide (AM), 2-hydroxyethylmethacrylate (HEMA), N-vinyl 2-pyrrolidinone (NVP), azobisisobutyronitrile (AIBN) and ketotifen fumarate were purchased from Sigma-Aldrich (Milwaukee, WI). Polyethylene glycol (200) dimethacrylate (PEG200DMA) was purchased from Polysciences, Inc (Warrington, PA). Lysozyme was purchased from MP Biomedicals. All chemicals were used as received. Polymer and copolymer networks were made using various mixtures of above monomers (e.g. poly(AA-co-HEMA-co-PEG200DMA), poly(AM-co-HEMA-co-PEG200DMA), poly(NVP-co-

HEMA-co-PEG200DMA), poly(AA-co-AM-co-HEMA-co-PEG200DMA), and poly(AA-co-AM-co-NVP-co-HEMA-co-PEG200DMA)).

4.4.2 Methods: Synthesis of a Typical Imprinted Network

Hydrogels of differing compositions of functional monomers and template molecule were synthesized in a temperature and moisture controlled environment using free-radical UV photopolymerization. Copolymer networks were made using various combinations of the functional monomers (e.g., poly (AA-co-HEMA-co-PEG200DMA), poly(AM-co-HEMA-co-PEG200DMA), poly(NVP-co-HEMA-co-PEG200DMA), poly(AA-co-AM-co-HEMA-co-PEG200DMA), and poly(AA-co-AM-co-NVP-co-HEMA-co-PEG200DMA). Control gels were prepared without the template molecule, keeping similar compositions and following the same mechanical operations. After many trial-and-error experiments, we observed that a M/T ratio of 185 was optimal for enhanced loading in all copolymer networks. Typically, each pre-polymerization mixture consisted of monomers, template molecule and initiator. The exact compositions of each optimized pre-polymerization mixture are attached as Appendix A. As an example, the poly (AA-co-AM-co-NVP-co-HEMA-co-PEG200DMA) mixture consisted of 6291 μ L HEMA (51.772 mmol), 40 mg AM (562.7 μ mol), 38.5 μ L AA (562.7 μ mol), 41.35 μ L NVP (562.7 μ mol), 906.3 μ L PEG200DMA (2.813 mmol), 120 mg ketotifen fumarate (282.2 μ mol), and 35 mg AIBN (213.4 μ mol). Each pre-polymerization mixture was prepared under strict environmental control as light and dust particles can inhibit the rate of polymerization. The monomers, crosslinking monomer and template molecule were sequential added and sonicated for several minutes, until the solution was found to be

stably homogeneous on standing for at least ten minutes. This was essential in order to dissolve the solid template molecule and functional monomer (AM) completely. The pre-polymerization mixtures were then allowed to equilibrate in darkness in order to facilitate non-covalent complexation at the molecular level. After adding the initiator, the pre-polymerization mixtures were then transferred to a MBRAUN Labmaster 130 1500/1000 glovebox, which is a highly controlled environment, where they were sparged continuously with nitrogen until oxygen levels were less than 0.1 ppm. Oxygen retards free radical polymerizations, thus in order to maximize the rates of monomer propagation and to ensure good reproducibility of polymerizations, removal of the dissolved oxygen from monomer solutions immediately prior to polymerization is advisable, either by sparging with an inert gas or ultrasonication.

The pre-polymerization mixtures were pipetted into glass moulds (6'' X 6'') separated by a Teflon frame of varying thicknesses (400 and 700 μm). Before pipetting the solutions, the glass plates were coated with chlorotrimethylsilane and dried by blowing air in order to reduce polymer adhesion to the glass surface. The smaller thickness of the spacer is comparable to the thickness of conventional contact lenses. Thicknesses of teflon spacers were measured by Vernier calipers. The pre-polymerization mixtures were now ready for polymerization. The polymerization reaction was allowed to run for ten minutes with light intensity, measured using a radiometer (International Light IL1400A), equal to 40 mW/cm^2 (Dymax UV flood light) at a constant temperature of 36 $^{\circ}\text{C}$.

The polymerized gels were removed from the nitrogen atmosphere, submerged into a deionized water bath (Millipore, 18.2 $\text{m}\Omega\cdot\text{cm}$, pH 6), and allowed to soften for about 40 minutes before they were carefully peeled from the glass surface. Care was taken to ensure that the softening period was never more than 40 minutes, as the

polymer slab would start rupturing due to the advancing water front. Circular discs of 13.5 mm diameter and 400 μm or 700 μm were cut with cork borer. Polymer discs were then washed with deionized water until ketotifen fumarate, unreacted functional monomers, and AIBN could no longer be detected by spectroscopic monitoring (Biotek UV-vis Spectrophotometer). Recognitive and control gels were then dried at room temperature for 24 hours, followed by vacuum drying ($T=30\text{ }^{\circ}\text{C}$, 28 in. Hg vacuum), until no change in dry weight was observed (i.e., less than 0.1 weight percent difference).

4.4.3 Methods: Equilibrium Rebinding Studies

Equilibrium binding studies were conducted to examine the enhanced loading potential of the hydrogels. A stock solution of 2 mg/mL of ketotifen fumarate was prepared and diluted to five concentrations (0.1 mg/mL, 0.20 mg/mL, 0.3 mg/mL, 0.4 mg/mL, and 0.5 mg/mL) in 50mL conical vials. Initial absorbances of each solution, which corresponded to the initial concentrations by Beer's law, were measured in the Biotek UV-vis Spectrophotometer. The wavelength of maximum absorption for ketotifen fumarate was 268 nm. After the initial absorbance, a washed and dried polymer disk was inserted in each vial and allowed to equilibrate over an average of 70-80 hours. Gentle agitation was performed on a Stovall Belly Button Orbital Shaker. After equilibrium was reached, the polymer disk was removed from the conical vial, and the solutions were vortexed for 10 seconds to provide homogeneity. 200 μL aliquots were pipetted into 96-well plates (Corning Costar UV-transparent microplates and their absorbances, which corresponded to the equilibrium concentrations, were determined in the Biotek UV-vis Spectrophotometer. After

sample readings were recorded, the tested aliquots were returned back to the samples. All experiments were performed in triplicate, averaged, and corrected for the relevant controls. The bound concentrations were then calculated by mass balance (i.e. by subtracting the equilibrium concentrations from the bound concentrations).

The ketotifen fumarate partition coefficient K was calculated at equilibrium as:

$$K = \frac{C_m}{C_e} = \frac{V_{sol} (C_i - C_e)}{V_{2,s} C_e} \quad 4.1$$

Where, C_m is the concentration of solute within the imprinted network, C_e is the concentration of ketotifen in solution after equilibrium has been reached, C_i is the initial concentration of ketotifen in solution (0.4 mg/mL), and V_{sol} and $V_{2,s}$ are the volumes of the solution and the swollen network, respectively.

4.4.4 Methods: Polymerization Reaction Analysis

Polymerization reaction analysis was carried out *via* UV free radical polymerization in a Q-100 modulated differential photocalorimeter (DPC) (TA Instruments, New Castle, DE) at a constant light intensity of 40 mW/cm². The DPC was calibrated prior to use by performing a baseline, temperature, and cell constant calibration. Pre-polymerization solutions (10 μ L) were weighed in aluminium hermetic pans and placing it in sample cell of the DPC. Samples sizes were always limited to such small volumes in order to prevent entraining of polymer. The sample was purged with nitrogen at a flow rate of 40 ml/min at 20°C, in order to prevent oxidative inhibition. They were then allowed to equilibrate at 35°C for 15 minutes, before opening the shutter of the UV light source (Novecure 2100, Exfo, Mississauga,

Canada with a Hg arc light bulb) for 12 minutes at isothermal conditions. It had already been determined while synthesizing the polymer disks, that the polymerization reaction was completed within 3-4 minutes.

The DPC records the heat of reaction from the sample relative to a reference pan. The rates of polymerization, in the units of fractional double bond conversion per second, are calculated using average molecular weight and theoretical enthalpy of acrylate and methacrylate double bonds. Integration of the rate of polymerization curve versus time yields the experimental heat of reaction. The experimental heat of reaction and the theoretical heat of reaction yield the conversion, which can be plotted as a function of time or reaction rate. The presence of template is accounted for in the calculations, as it is only involved in non-covalent complexation and does not participate in the polymerization reaction.

In such calculations, it is generally assumed that each functional monomer has equal reactivity. The theoretical enthalpy of methacrylate double bonds is equal to 13.1 kcal mole⁻¹ and the theoretical enthalpy of acrylate double bonds is equal to 20.6 kcal mole⁻¹. The theoretical enthalpy derived for a comonomer mixture is a weighted mean of the enthalpies of individual monomers.

4.5 Results and Discussion

In this particular section, we describe our observations on enhanced template binding parameters for the poly(AA-co-HEMA-co-PEG200DMA), poly(AM-co-HEMA-co-PEG200DMA), poly(NVP-co-HEMA-co-PEG200DMA), poly(AA-co-AM-co-HEMA-co-PEG200DMA), poly(AA-co-AM-co-NVP-co-HEMA-co-PEG200DMA)) networks. We also discuss the reaction analysis of these imprinted

networks with a particular emphasis on observed trends in double bond conversions and rates of polymerization for varying template and functional monomer compositions. It is important to note that the monomer to template ratio was optimized to achieve desired amount of partitioning.

4.5.1 Enhanced Loading of Imprinted Networks Formed from Pre-polymerization Mixtures of Diverse Functionalities

We hypothesized, based on an analysis of structural biology, that multiplicity and type of functional chemistry in a pre-polymerization complex, would prove critical in maximizing loading. This would provide a higher probability of ligand docking or memory sites at the molecular level, with relevant multiple chemical functionality for optimal non-covalent interactions. Monomers were then selected based on the fact that residues such as aspartic acid, lysine, arginine and tyrosine form the docking site in the H₁-receptor, and by matching the side chain chemistry, and this is depicted in Figure 4.3. The one-to-one correspondence between the amino acids in the binding receptor and the functional monomer selected is shown in Figure 4.4. The guiding hypothesis is that if antihistamines have a greater affinity for the H₁-receptor, a hydrogel with similar chemical functionality would bind the antihistamine tightly, increase loading, and show delayed kinetics of release. This strategy is outlined in Figure 4.5.

Dynamic and equilibrium binding isotherms of the copolymer networks are attached in section A.1 and A.2 of appendix A. Figure 4.6 shows 2 times improvement in the loading of ketotifen by the poly(AA-co-AM-co-HEMA-co-PEG200DMA) networks over control networks. As hypothesized, the most

biomimetic formulation that included four functional monomers demonstrated the potential of maximal enhanced loading. Figure 4.7 shows a significant (6 times) increase in loading was observed over the control network and 3 times increased loading over the networks containing two or three functional monomers. This observation suggests that supplying the necessary functionality enhances loading by mimicking the complex hydrogen bonding patterns found in Nature. The next-generation biomaterials may involve non-natural amino acid-monomer conjugates to further the loading potential.

The partition coefficients for the imprinted networks, determined from equilibrium partitioning experiments, were 2 or more times greater than the control networks. Also, the partition coefficient of the (poly(AA-co-AM-co-NVP-co-HEMA-co-PEG200DMA)) network was measured as 45.05 as compared to 5.65, 7.13, and 5.31 for the single monomer networks poly (AA-co-HEMA-PEG200DMA), poly (AM-co-HEMA-PEG200DMA), and poly (NVP-co-HEMA-PEG200DMA), which is at least 8 times improvement in loading. These observations indicate that the imprinting technique results in structural plasticity of polymer chains, and is responsible for creating macromolecular memory due to the organization of multiple functionalities in the macromolecular architecture. Structural plasticity occurs in nature and an analogous situation is found in nervous systems. During a learning experience, reversible structural changes to synaptic morphology (such as remodeling of cytoskeletal and adhesion molecules, and AMPA receptor trafficking during long term potentiation and long term depression) result in modifications to synaptic transmission, and these changes are then stabilized for the creation of memory⁴¹⁻⁴³. The imprinting process also involves structural changes, with the stabilization and constraining of polymer chain conformations by the template molecule, leading to the

creation of memory sites. The octanol and water phase concentrations were calculated and checked by mass balance. The \log_{10} octanol-water partition coefficient of ketotifen is -0.3, and it has an aqueous solubility of 3.4 mg/mL at pH 7 ± 0.2 and 25°C . This indicates that the enhanced loading of the therapeutic is not due to hydrophobic interactions between the functional monomers and therapeutic, but rather due to the memory created by template-mediated constraints during polymerization.

4.5.2 Imprinting Effects on Polymerization Kinetics

We used differential scanning photocalorimetry to investigate the influence of the template molecule (ketotifen) on CBIP and are the first to provide evidence that the formation of polymer chains with enhanced loading, due to the imprinting effect in hydrogels, is inversely related to the propagation of polymer chains. The reaction signatures and conversion profiles of all copolymer networks are attached in section A.4 of Appendix A. Figure 4.8 demonstrates that the rate of polymerization for a given conversion decreased for increasing mole percentage of template molecule in pre-polymerization monomer solution.

It is hypothesized that the template molecules places physical restrictions on free radical and propagating chain diffusional motion, and hence constrains certain monomer configurations, due to pre-polymerization assembly. This effectively lowers the rate of polymerization, thus aiding the creation of molecular memory, or binding pockets, within the polymer chains. A parallel theme in Nature is seen in crystallization, wherein a slower rate of cooling affords the formation of better crystals. These results are in contrast to acrylate monomer-monomer pre-organization *via* hydrogen bonding⁴⁴ or radical-initiated template polymerizations in dilute

template systems⁴⁵ where rate enhancement occurs due to propagation due to hydrogen bonding between monomers or non-covalent interactions along the template, where the monomer double bonds are positioned in very close vicinity to each other (e.g. double bonds of monomers lined up using another polymer as a pattern⁴⁵).

In addition, Figure 4.9 depicts that for fixed ketotifen concentration, the rate of polymerization for a given conversion was lower for multiple functional monomer pre-polymerization mixtures than the single monomer mixtures. The CBIP process with multiple monomers results in the formation of improved template binding pockets with enhanced loading properties and decreased dissociation kinetics (i.e., delayed release) due to complex non-covalent bonding patterns and organization, which is reflected in slower rates of polymerization.

4.6 List of References

1. Venkatesh, S., Sizemore, S.P. & Byrne, M.E. Biomimetic hydrogels for enhanced loading and extended release of ocular therapeutics. *Biomat.* **28**, 717-724 (2007).
2. Venkatesh, S., Byrne, M.E., Peppas, N.A. & Hilt, J.Z. Applications of biomimetic systems in drug delivery. *Exp. Opin. Drug Del.* **2**, 1085-1096 (2005).
3. Tu, R.S. & Tirrell, M. Bottom-up design of biomimetic assemblies. *Adv. Drug Del. Rev.* **56**, 1537-1563 (2004).

4. del Amo, E.M. & Urtti, A. Current and future ophthalmic drug delivery systems: A shift to the posterior segment. *Drug Discovery Today* **13**, 135 (2008).
5. Arrington, G.E. A History of Ophthalmology. (*MD Publications*, 1959).
6. Wichterle, O. Cross-linked Hydrophilic Polymers and Articles made therefrom. USA (1965)
7. Wichterle, O. & Lim, D. Hydrophilic gels for biological use. *Nature* **185**, 117-118 (1960).
8. Sahoo, S.K., Dilnawaz, F. & Krishnakumar, S. Nanotechnology in ocular drug delivery. *Drug Discovery Today* **13**, 144 (2008).
9. Saettone, M.F. Progress and Problems in Ophthalmic Drug Delivery. *Pharmatech*, 1-6 (2002).
10. Schoenwald, R.D. Ocular Pharmacokinetics. (*Lipincott-Raven Publishers*, 1997).
11. Ali, M. & Byrne, M.E. Challenges and solutions in topical ocular drug-delivery systems. *Expert Review of Clinical Pharmacology* **1**, 145-161 (2008).
12. Peppas, N.A., Wood, K.M. & Blanchette, J.O. Hydrogels for oral delivery of therapeutic proteins. *Exp. Opin. Biological Therapy* **4**, 881-887 (2004).
13. Byrne, M.E., Park, K. & Peppas, N.A. Molecular imprinting within hydrogels. *Adv. Drug Del. Rev.* **54**, 149-161 (2002).
14. Peppas, N.A. Hydrogels in Medicine and Pharmacy. (*CRC Press, Boca Raton, FL.*, 1987).
15. Peppas, N.A., Hilt, J.Z., Khademhosseini, A. & Langer, R. Hydrogels in Biology and Medicine: From Molecular Principles to Bionanotechnology. *Adv. Mater.* **18**, 1345-1360 (2006).

16. Langer, R. & Tirrell, D.A. Designing materials for biology and medicine. *Nature* **428**, 487-492 (2004).
17. Karlgard, C.C.S., Wong, N.S., Jones, L.W. & Moresoli, C. In vitro uptake and release studies of ocular pharmaceutical agents by silicon-containing and p-HEMA hydrogel contact lens materials. *Int. J. Pharm.* **257**, 141-151 (2003).
18. Armaly, M.F. & Rao, K.R. The effect of pilocarpine Ocusert with different release rates on ocular pressure. *Invest. Ophthalmol.* **12**, 491-496 (1973).
19. Gale, R.M., Ben-Dor, M. & Keller, N. Ocular therapeutic system for dispensing a medication formulation. USA (1980)
20. Prause, J.U. Treatment of keratoconjunctivitis sicca with Lacrisert. *Scand. J. Rheumatol. Suppl.* **61**, 261-263 (1986).
21. Di Colo, G. & Zambito, Y. A study of release mechanisms of different ophthalmic drugs from erodible ocular inserts based on poly(ethylene oxide). *Eur. J. Pharm. Biopharm.* **54**, 193-199 (2002).
22. Chetoni, P. et al. Silicone rubber/hydrogel composite ophthalmic inserts. Preparation and preliminary in vitro/in vivo evaluation. *Eur. J. Pharm. Biopharm.* **46**, 125-132 (1998).
23. Hsiue, G.H., Guu, J.A. & Cheng, C.C. Poly(2-hydroxyethyl methacrylate) film as a drug delivery system for pilocarpine. *Biomater.* **22**, 1763-1769 (2001).
24. Henderly, D.E., Freeman, W.R., Causey, D.M. & Rao, N.A. Cytomegalovirus retinitis and response to therapy with ganciclovir. *Ophthalmology* **94**, 425-434 (1987).
25. Dhillon, B., Kamal, A. & Leen, C. Intravitreal sustained-release ganciclovir implantation to control cytomegalovirus retinitis in AIDS. *Int. J. STD AIDS* **9**, 227-230 (1998).

26. Jaffe Glenn, J. et al. Fluocinolone acetonide implant (Retisert) for noninfectious posterior uveitis: thirty-four-week results of a multicenter randomized clinical study. *Ophthalmology* **113**, 1020-1027 (2006).
27. Mohammad, D.A., Sweet, B.V. & Elner, S.G. Retisert: is the new advance in treatment of uveitis a good one? *Ann. Pharmacother.* **41**, 449-455 (2007).
28. Hsu, J. Drug delivery methods for posterior segment disease. *Curr. Opin. Ophthalmol.* **18**, 235-239 (2007).
29. Gulsen, D. & Chauhan, A. Dispersion of microemulsion drops in HEMA hydrogel: a potential ophthalmic drug delivery vehicle. *Int. J. Pharm.* **292**, 95-117 (2005).
30. Uchida, R., Sato, T., Tanigawa, H. & Uno, K. Azulene incorporation and release by hydrogel containing methacrylamide propyltrimethylammonium chloride, and its application to soft contact lens. *J. Controlled Release* **92**, 259-264 (2003).
31. Hiratani, H. & Alvarez-Lorenzo, C. The nature of backbone monomers determines the performance of imprinted soft contact lenses as timolol drug delivery systems. *Biomater.* **25**, 1105-1113 (2003).
32. Hiratani, H., Fujiwara, A., Tamiya, Y., Mizutani, Y. & Alvarez-Lorenzo, C. Ocular release of timolol from molecularly imprinted soft contact lenses. *Biomater.* **26**, 1293-1298 (2005).
33. Hiratani, H., Mizutani, Y. & Alvarez-Lorenzo, C. Controlling drug release from imprinted hydrogels by modifying the characteristics of the imprinted cavities. *Macromol. Biosci.* **5**, 728-733 (2005).
34. Holt, P.G., Macaubas, C., Stumbles, P.A. & Sly, P.D. The role of allergy in the development of asthma. *Nature* **402**, B12-17 (1999).

35. Oettgen, H.C. & Geha, R.S. IgE regulation and roles in asthma pathogenesis. *J. Allergy Clin. Immunol.* **107**, 429-440 (2001).
36. Mosmann, T.R. & Coffman, R.L. Heterogeneity of cytokine secretion patterns and functions of helper T cells. *Adv. Immunol.* **46**, 111-147 (1989).
37. Mosmann, T.R. & Coffman, R.L. TH1 and TH2 cells: different patterns of lymphokine secretion lead to different functional properties. *Annu. Rev. Immunol.* **7**, 145-173 (1989).
38. Reischl, I.G., Coward, W.R. & Church, M.K. Molecular consequences of human mast cell activation following immunoglobulin E-high-affinity immunoglobulin E receptor (IgE-FcεRI) interaction. *Biochem. Pharmacol.* **58**, 1841-1850 (1999).
39. Bryce, P.J. et al. The H1 histamine receptor regulates allergic lung responses. *J. Clin. Invest.* **116**, 1624-1632 (2006).
40. Bielory, L. Role of antihistamines in ocular allergy. *Am. J. Med.* **113**, 34S-37S (2002).
41. Brown, T.H. et al. Learning and memory: basic mechanisms. *From Molecules to Networks*, 499-574 (2004).
42. Lamprecht, R. & LeDoux, J. Structural plasticity and memory. *Nat. Rev. Neurosci.* **5**, 45-54 (2004).
43. Tronson, N.C. & Taylor, J.R. Molecular mechanisms of memory reconsolidation. *Nat. Rev. Neurosci.* **8**, 262-275 (2007).
44. Jansen, J.F.G.A., Dias, A.A., Dorsch, M. & Coussens, B. Fast Monomers: Factors Affecting the Inherent Reactivity of Acrylate Monomers in Photoinitiated Acrylate Polymerization. *Macromolecules* **36**, 3861-3873 (2003).

45. Tan, Y.Y. & Alberda van Ekenstein, G.O.R. A generalized kinetic model for radical-initiated template polymerizations in dilute template systems. *Macromolecules* **24**, 1641-1647 (1991).

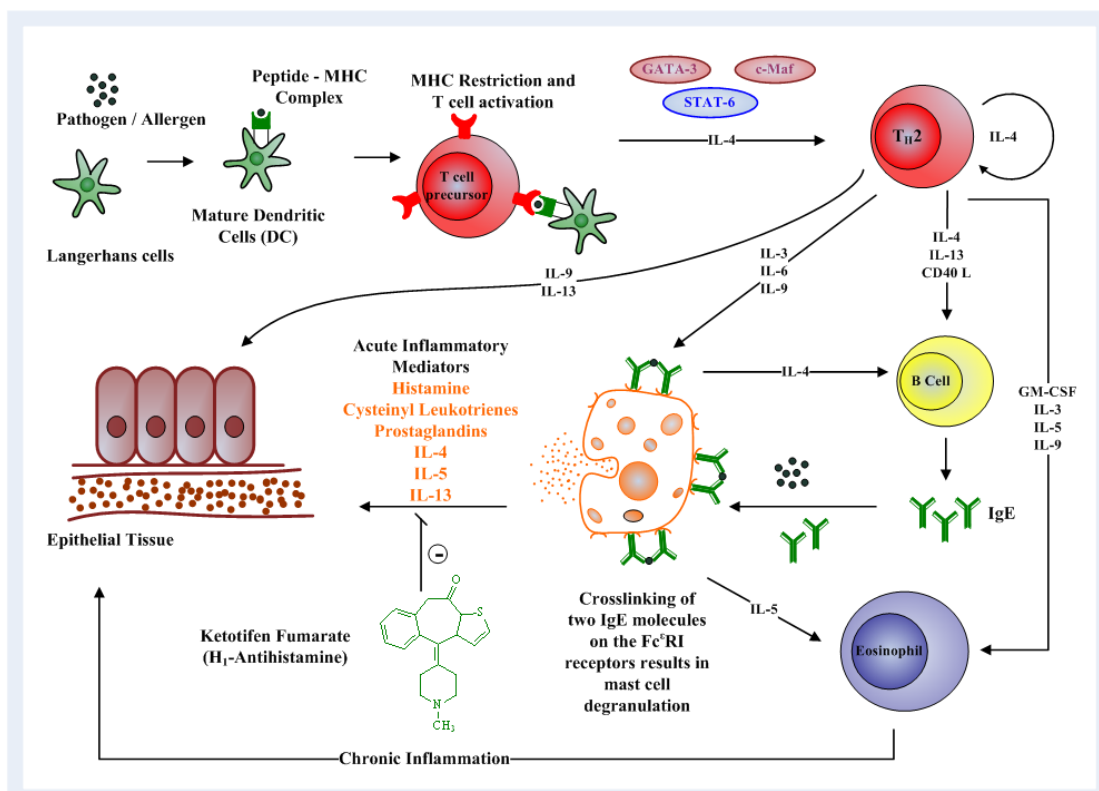


Figure 4.1 Mammalian Allergy Pathway and Biomimetic Synthesis of Recognitive Contact Lenses. Pharmacological down regulation of histamine *via* antihistamines. In higher vertebrates, Langerhans cells pinocytose allergens of significant pathology, express MHC-peptide complexes on their surfaces, and launch naïve T cells on a complex program of differentiation into T_H1 or T_H2 cells. The latter stimulate B cells to produce IgE, which causes degranulation of mast cells and secretion of inflammatory mediators such as histamine.

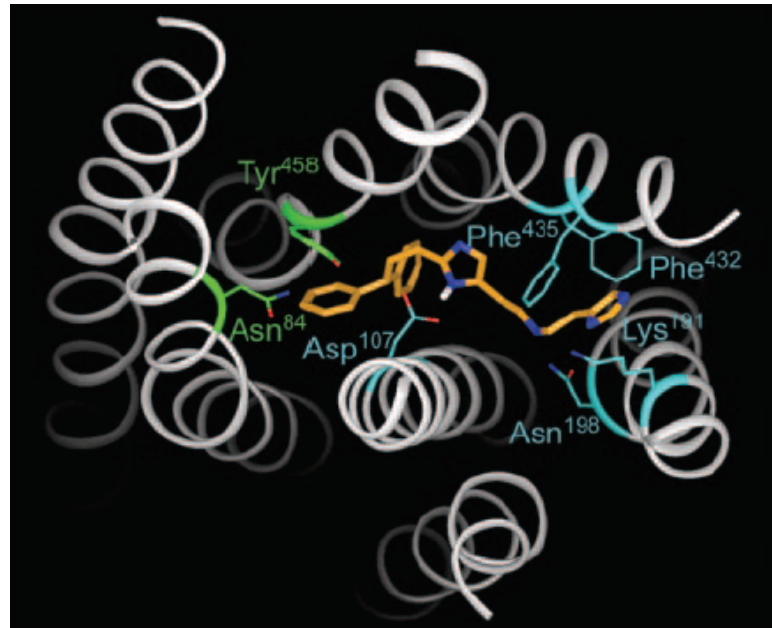


Figure 4.2 Representation of the crystal structure of the H1 receptor. The receptor consists of lysine, aspartic acid, asparagine, and tyrosine. Permission for picture given by Elsevier publishing.

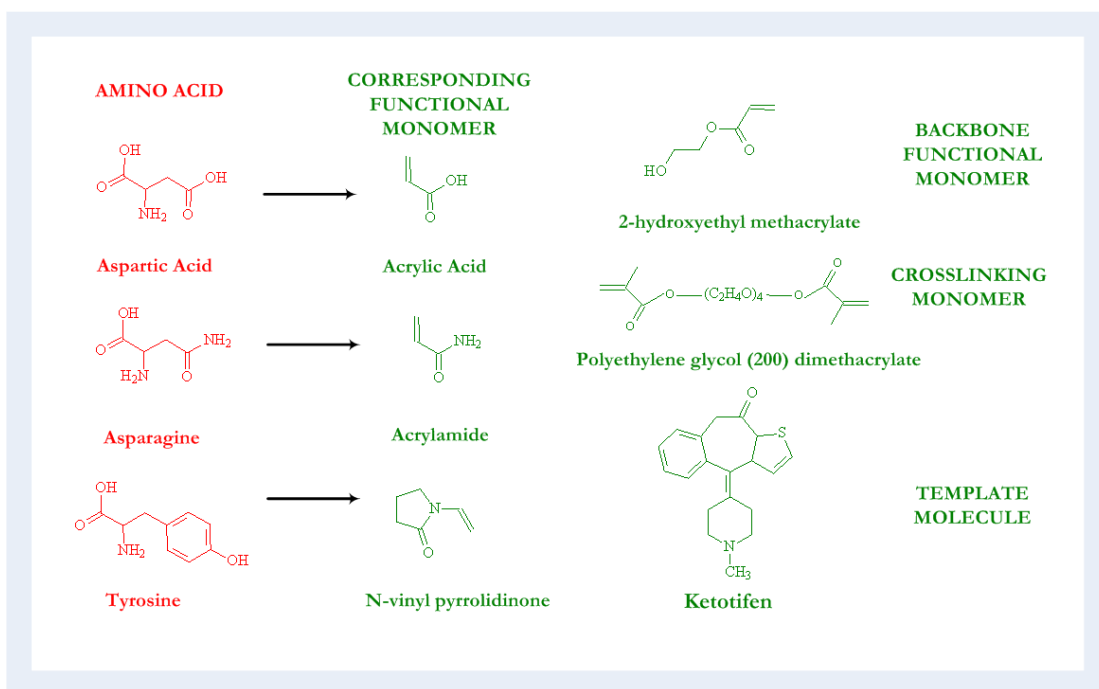


Figure 4.3 One-To-One Correspondence of Amino Acids and Functional Monomers in Memory Sites. Also listed are the crosslinking monomer, backbone monomer, and template molecule.

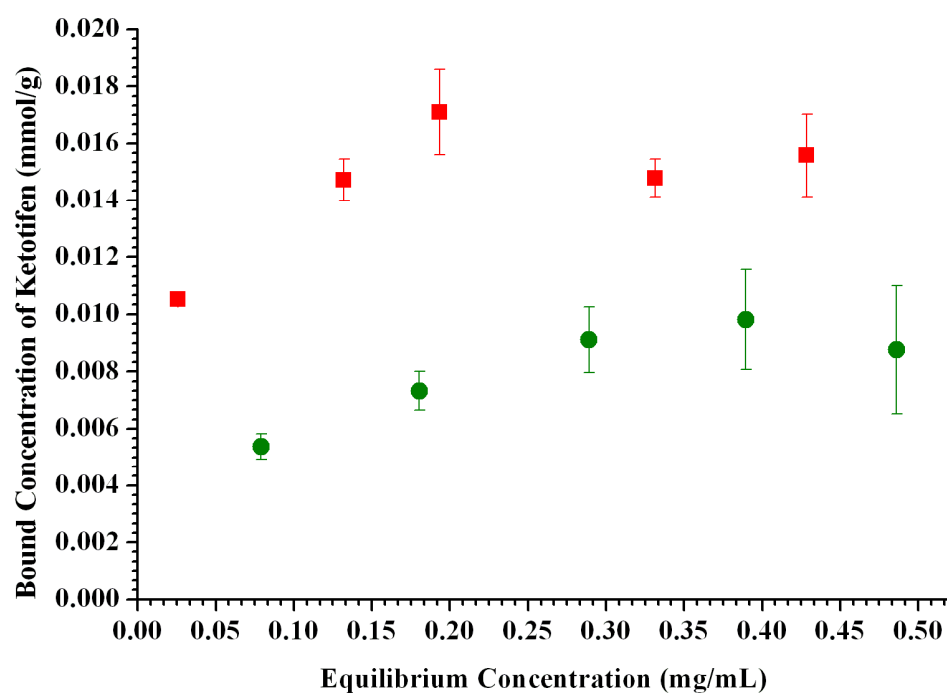


Figure 4.4 Ketotifen Equilibrium Binding Isotherm in Water for Poly(AM-co-AA-co-HEMA-co- PEG200DMA) Networks. N=3, and T=25°C. Recognitive network (■) and Control network (●).

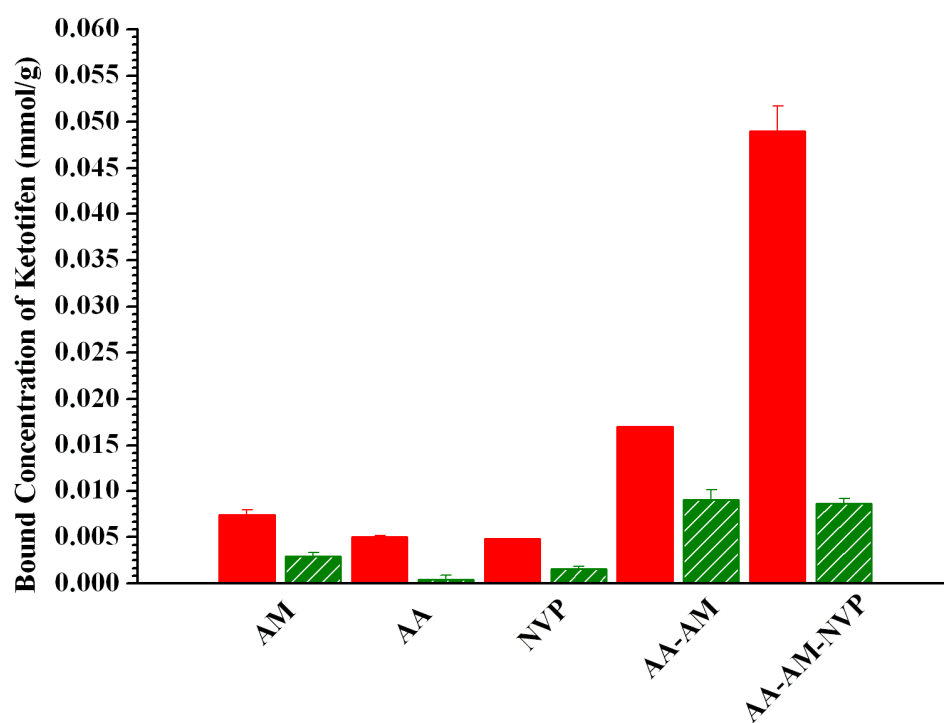


Figure 4.5 Comparison of Enhanced Loading of Ketotifen in Functionally Diverse Poly(n-co-HEMA-co-PEG200DMA) Networks. Functional monomer (n) is AA, AM, NVP, AM-AA, or AM-AA-NVP. Recognitive network (■) and Control network (hatched ■).

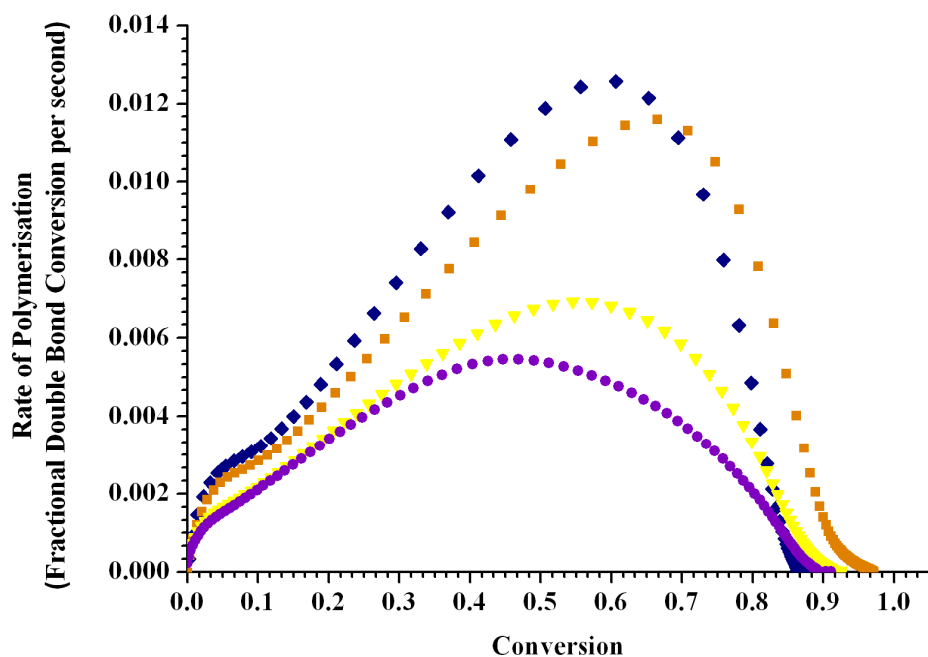


Figure 4.6 Polymerization Reaction Rate versus Conversion for Poly(AM-co-HEMA-co-PEG200DMA) Networks. Recognitive networks of varying ketotifen concentration in the initial polymer solutions- (♦) represents the control network; (■) represents 0.1 mole %; (▼) represents 0.5 mole %; (●) represents 1.0 mole %.

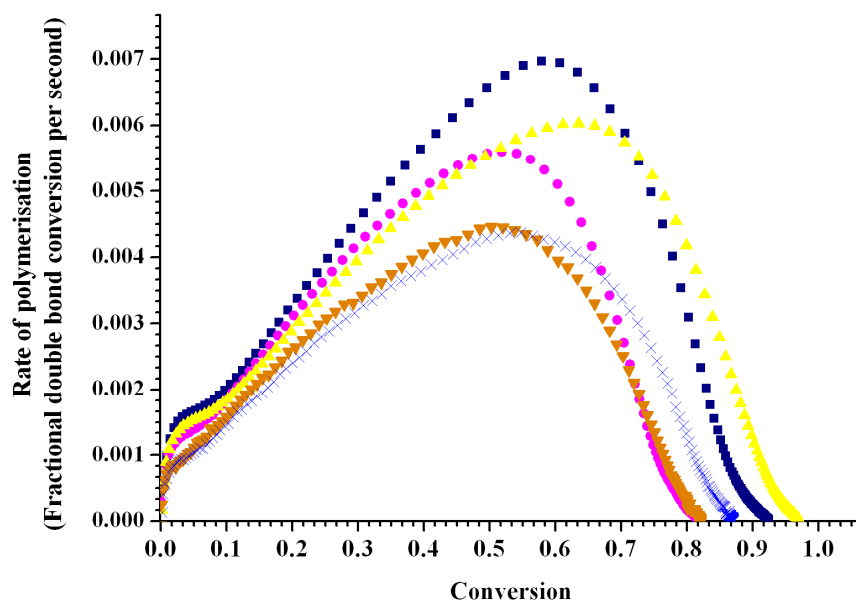


Figure 4.7 Polymerization Reaction Rate versus Conversion for Varying Comonomer Percentages in Poly(n-HEMA-co-PEG200DMA) Networks. N=3, and T=25°C. Recognitive networks of constant ketotifen concentration (0.5 mole %) and monomer/template ratio (181) in the initial polymer solutions (■) represents 3 mole % AM; (●) represents 3 mole % AA, (▲) represents 3 mole % NVP ; (▼) represents 1.5 mole % AA and AM, and (X) represents 1.0 mole % each of AM, AA and NVP. Error bars indicate standard deviation.

5.0 TRANSPORT AND STRUCTURAL ANALYSIS OF MOLECULAR IMPRINTED NETWORKS FOR CONTROLLED DELIVERY OF OCULAR THERAPEUTICS

In this chapter, we analyzed the transport and structural characteristics of polymer networks imprinted for an ocular H₁-antihistamine, with a particular emphasis on extending the therapeutic release rate. One dimensional permeation studies showed that the imprinted network with maximum incorporated chemical functionality had the lowest permeability and diffusion coefficients, which was at least an order of magnitude lower than all other networks studied. A startling observation was that all imprinted networks had significantly lower diffusion coefficients than non-imprinted networks, in spite of comparable mesh sizes and equilibrium polymer volume fractions in the swollen state. We also proposed the “tumbling hypothesis” to place our observations into a theoretical framework, wherein a molecule tumbling through an imprinted network with multiple, organized functionalities and an appropriate mesh size, experiences heightened interactions with memory sites and shows delayed transport kinetics. Our results add thrust to a growing suspicion- that the structural plasticity of polymer chains, i.e. the organization of functional groups into memory sites, may be responsible for enhanced loading and extended release. All results presented in the following chapter have been published as two research articles^{1,2}.

5.1 Scientific Rationale

Configurational biomimetic imprinting provides a rational design strategy for the development of controlled release drug delivery systems. Our objective was to extend the release rate of the drug in a fully swollen hydrogel, by providing a diverse spectrum of chemical functionalities at the level of the memory site. We reasoned that the drug's heightened interaction with the memory pockets would slow down its diffusional transport within the network as well its release from the network despite comparable free volume within the polymer chains for drug transport. Once macromolecular memory for the drug was created within the network, we observed delayed kinetics of release from the imprinted network. This type of network formation – with a proper optimization of drug affinity relating to number and strength of functional monomer interactions, crosslinking structure, and mobility of polymer chains – has a strong potential to influence a number of hydrogel carriers and add to the variables one can alter to tune the release profile.

Furthermore, we performed penetrant uptake in order to support our hypothesis that the imprinting effect, and not porosity of the macromolecular network, is responsible for enhanced loading and extended release. One dimensional permeation studies and dynamic release studies under infinite sink conditions were performed in order to assess transport parameters such as diffusion constants and permeability constants, using well-known mathematical models. Mechanical analysis was also carried out in order to compare the storage and loss moduli and damping factors of the imprinted networks with conventional contact lenses.

5.2 Analysis of Diffusion and Controlled Release in Imprinted Networks

In physicochemical systems, drug release is controlled by processes such as diffusion, osmosis, dissolution etc. Dosage forms may either consist of drugs contained within a polymeric membrane or immobilized within a polymer network. Drug molecules are typically dissolved or dispersed homogeneously throughout the network and exhibit a release which is controlled either by the transport properties of the drug through the polymer or by the dissolution of the polymer, or both.

When a dry polymer network is immersed in a thermodynamically compatible solvent, the solvent movement into the macromolecular structure leads to considerable volume expansion and rearrangement depending on the extent of crosslinking within the network. The solvent penetrates the polymer and dissolves the drug molecules, which then diffuse out of the network along their concentration gradient.

Generally, the network transitions in a moving front from an unperturbed, glassy state to a solvated, rubbery state with an increase in macromolecular mobility due to chain extension, and this leads to additional free-volume for transport. The glassy to rubbery transition is known as the glass transition temperature. In glassy networks, which are below the glass transition temperature, a solvent front normally develops that moves into the network at a characteristic rate, causing swelling just behind the front. Drugs dissolved or dispersed in the network are released from the rubbery, swollen part behind the advancing front, and hence it becomes clear that the swelling kinetics dictate the release profile.

The swelling behaviors of glassy and rubbery networks are markedly different from each other primarily due to the relaxation of polymer chains, i.e. the polymer's

mean or characteristic time of response to stress. While rubbery networks have nearly instantaneous response to applied stresses, glassy networks show time-dependent responses. Thus, the rate at which a network swells is dependent upon the relative rates of polymer-chain relaxation and solvent penetration into the network.

The relative contribution of diffusion and relaxation processes can be evaluated with the Deborah number (De)³, which is given by equation 5.1.

$$De = \frac{\lambda}{\theta} \quad 5.1$$

Where, λ is the characteristic relaxation time and θ is the characteristic diffusion time, which in itself is given by equation 5.2.

$$\theta = \frac{L^2}{D} \quad 5.2$$

Where, L is the characteristic length, and D is the diffusion coefficient.

When $De \ll 1$, relaxation is much faster than diffusion. This occurs in rubbery networks, at temperatures well above the glass transition temperature, wherein the macromolecular chains have high mobilities. The diffusion coefficient is a strong function of concentration and position. This limiting case is known as Fickian diffusion.

When $De \gg 1$, relaxation is rate limiting for swelling. This occurs in glassy networks, at temperatures well below the glass transition temperatures. The diffusion coefficient is constant, i.e. it is independent of concentration and position. This limiting case is known as non-Fickian transport.

When $De \approx 1$, the relaxation and diffusion rates are comparable. Transport regime is known as anomalous transport, and is normally observed when a network passes from the diffusion-controlled regime to the relaxation-controlled regime, or vice versa.

In a Fickian model of release kinetics, the release rate of a drug from the delivery device is proportional to the concentration gradient between the drug source and the surroundings. In practical terms, this means that as the finite drug source is depleted, the rate of drug release decreases until there is no more drug in the gel, whereupon the rate is zero. A zero-order release rate is preferable because it would deliver medication at a constant rate for an extended time, irrespective of the concentration of loaded drug in the network. Recently, a finite drug source has been used to achieve an extended zero-order release in a physiomimetic device², and a number of strategies have been attempted in hydrogel drug delivery systems such as bioerodible and biodegradable systems with solvent penetration fronts moving with similar velocities as the outer eroding front⁴, hydrogels with rate controlling-barriers such as higher crosslinked outer edges⁵, and non-uniform drug distribution⁶.

In non-Fickian transport, the sharp, advancing solvent front moves with a constant velocity between the outer permeable rubbery region and the inner glassy region. There is a linear gain of polymer weight with time. Drug release is rapid and is dictated by the rate of water sorption. Typically, drug transport can be controlled by swelling-controlled systems (i.e., drug-loaded dry state with water uptake, gel swelling, and drug release) or swellable systems such as a swollen gel that undergoes a reversible volume transition based on a stimulus (e.g., pH, temperature, ionic strength, biomolecular binding event etc.). Swellable hydrogels can be engineered to be sensitive to environmental conditions due to the presence of specific chemical/biological species along their backbone polymer chains (Figure 5.1b).

In an effort to understand the mechanisms behind release kinetics, various mathematical models of solvent penetration and solute release have been developed⁷⁻⁹. Typically, in both modeling and experimental work, infinite sink conditions are

assumed and accumulation of drug in the solution surrounding the hydrogel is considered to be negligible. Typically, an empirical power law given by equation 5.3 is used to determine the order of release^{10, 11}.

$$\frac{M_t}{M_\infty} = kt^n \quad 5.3$$

Where, M_t/M_∞ is the fractional drug released over the entire period, and the parameters k and n are constants related to diffusion coefficients and the specific transport mechanism respectively, and $(n-1)$ is the order of release. The equation can be linearized by plotting the log of fractional release versus the log of time, where the slope corresponds to the order of release. It is evident that when n has a value of one, the drug release is independent of concentration and time, corresponding to zero order release. Here, for planar systems, $n = 0.5$ describes Fickian behavior indicating diffusion controlled drug release, $n = 1.0$ describes zero-order or case II transport, and anomalous diffusion is characterized by intermediate values of n . Equation 5.3 is valid only for the first 60% of the total amount of drug released, regardless of the geometry of the polymer.

Bioerodible and biodegradable hydrogel systems demonstrate zero-order release when the penetration front moves with a velocity similar to the outer eroding front⁴. Other methods that have led to zero-order release within monolithic systems include hydrogels with non-uniform drug distribution⁶ or rate controlling-barriers on the surface such as higher crosslinked outer edges⁵. Multi-layers/geometries exploiting drug restrictive diffusion within non-monolithic devices have also been used.

A relatively new method is to exploit molecular imprinting methods which can create macromolecular memory for the drug within the network and delay the

transport of drug from the matrix *via* interaction of the drug with numerous functional groups organized within the network (Figure 5.1c). The drug's heightened interaction with the memory pockets slows its release from the hydrogel despite comparable free volume within the polymer chains for drug transport. With a proper optimization of template molecule-functional monomer interactions, crosslinking density, and other design parameters, the macromolecular structure can be controlled to obtain tailored release profiles. As drug delivery materials decrease in length scales towards nanoparticles and thin films, further control of transport at decreasing thicknesses is paramount for the success of such systems. The additional rational design of hydrogel structures has significant potential in limited volume applications.

5.3 Diffusion Models

The study of the diffusion of small molecules is essential to understand how drugs are transported in extracellular fluids, how they diffuse to cell surface receptors, their mechanism of internalization into the cell and intracellular pharmacokinetic distribution. Furthermore, diffusion is the mechanism underlying the dissolution of pharmacological dosage forms such as tablets. In order to accurately design drug delivery systems and predict their efficacies, mathematical expressions to calculate diffusion coefficients of solutes have been developed in the literature. The four major theories of solute diffusion¹²⁻²¹ are Eyring's jump theory, the free volume theory, the hydrodynamic theory, and the obstruction theory. Solute molecule transport in polymer networks occurs in the solvent-filled domains between the macromolecular chains. The mean free path length and residence time of the solute diffusing through the network is dependent on various factors which can affect either mesh size or the

strength and quality of non-covalent interactions experienced by the solute molecule as it traverses through the network. These factors include the polymer chain mobility, the relative size of solute and mesh size of the network, and the electronic interactions between the solute and pendant functional groups. Clearly, the solute diffusion is impaired in highly crosslinked networks, where mesh sizes are small, or when the hydrodynamic radius of the solute is comparable to the mesh size of the network. In particular, the polymer chains have the propensity to strongly influence solute diffusion characteristics. Loosely crosslinked networks have highly mobile polymer chains, which can act as physical obstructions to the solute and increase the hydrodynamic drag on the solute particles.

Most models in the literature assume that solute molecules are spherical in shape, and hence their sizes can be expressed in terms of hydrodynamic radii. These models also utilize polymer solution scaling relationships to describe mesh sizes. The average mesh size is a function of the polymer physical properties, its affinity for the solvent, and the concentration of polymer in the solution. Here, we present a few scaling concepts for a deeper understanding of some of the solute diffusion models.

The polymer chain radius r_f is given by equation 5.24.

$$r_f = \sqrt{\frac{M_m \bar{v}}{l\pi N_A}} + r_w \quad 5.24$$

Where, l is the length of the monomer unit, M_m is the molecular weight of the monomer, \bar{v} is the specific volume of the polymer, r_w is the radius of a water molecule and N_A is Avogadro's number.

The hydrodynamic radius of a molecule, r_s is given by equation 5.25.

$$r_s = \frac{k_b T}{f \pi \eta D_o} \quad 5.25$$

Where, k_b is Boltzmann's constant, T is temperature, η is solvent viscosity, D_o is the diffusivity at infinite dilution, and f is the frictional drag coefficient. This is usually 4 for solutes whose size approach that of the solvent and 6 for solutes greater in size than the solvent.

Hydrodynamic descriptions of solute transport within polymer solutions are based on the Stokes–Einstein treatment^{22, 23}. The movement of the solute in the network is resisted by frictional drag caused by the solvent molecules. The polymer chains are the centers of hydrodynamic resistance and enhance the drag on the solute by slowing down the fluid near the polymer chains. Hydrodynamic models hinge upon the accurate determination of f .

Obstruction theories of solute diffusion assume that the impenetrable polymer chains increase the mean free path length for diffusive transport. The polymer chains act as a sieve, allowing passage of a solute molecule only if it can pass between the polymer chains. Various obstruction theories have been generated. In one approach, it was assumed that solute diffusion in the polymer solution occurs as a random walk, i.e. as a series of random unit steps²⁴. The polymer solution is considered as a random network of straight, long chains of negligible width. The unit step is the root mean square average mesh diameter. In another approach, researchers have developed an obstruction model based on the idea that the polymer solution can be viewed as being composed of a number of cylindrical cells^{25, 26}. Each cylindrical cell consists of an infinite polymer rod centered in a cylinder of solvent of a given radius. The global diffusivity of the solute is calculated by summing up the number of cells having a given radius multiplied by the average diffusivity within that cell. The distribution of

the cell radii is calculated using an expression for the distribution of spherical spaces within a random network of straight fibers.

Free volume theories have also been proposed to explain solute diffusion²⁷. The solute diffuses by jumping into voids formed in the solvent space by the redistribution of the free volume within the solvent. These redistributions can occur without any energy change. The voids are pictured as being formed the random thermal motion of the solvent molecules. The solute can diffuse through the gel only if it finds a succession of free volumes larger than it.

5.4 Methods

In this particular section, we describe the experimental methods used for the transport and structural characterization of five recognitive networks for ketotifen fumarate created by the CBIP method. Polymer and copolymer networks were made using various mixtures of above monomers (e.g. poly(AA-co-HEMA-co-PEG200DMA), poly(AM-co-HEMA-co-PEG200DMA), poly(NVP-co-HEMA-co-PEG200DMA), poly(AA-co-AM-co-HEMA-co-PEG200DMA), Poly(AA-co-AM-co-NVP-co-HEMA-co-PEG200DMA)). These networks were synthesized using the same techniques described in section 4.4.2 in chapter 4.

5.4.1 Methods: Kinetic Release Profiles of Ketotifen Fumarate from Loaded Networks

After equilibrium rebinding studies were conducted on the imprinted networks, kinetic release studies were conducted in deionized water, artificial lachrymal fluid (6.78 g/L NaCl, 2.18 g/L NaHCO₃, 1.38 g/L KCl, 0.084 g/L CaCl₂·2 H₂O, pH 8)²⁸, and lysozyme (1 mg/ml) in artificial lachrymal fluid. Preliminary experiments were conducted to determine the amount of fluid needed to approximate infinite sink analysis by comparing release rates for a fixed amount of fluid versus release rates when refreshing the fluid at specific various time intervals. The imprinted networks were placed in 30 ml of solution which was continuously agitated with a Servodyne mixer (Cole Palmer Instrument Co.) at 120 rpm at 25°C. Aliquots were withdrawn at pre-determined time intervals and their absorbances were measured *via* a Biotek Synergy UV/Vis at 276 nm until saturation (i.e. the change in concentration within the solution was not more than 1%). These aliquots were always replaced after analysis.

The fractional release profiles were constructed by taking the cumulative amount of ketotifen released, M_t divided by the final cumulative amount of ketotifen released at saturation, M_∞ . The fractional release ratio, M_t/M_∞ was plotted against time for each imprinted network.

5.4.2 Methods: Diffusion Analysis of Ketotifen from Kinetic Release Profiles

The diffusion coefficient of template was calculated from Fick's law, which describes one-dimensional planar solute release from a polymer network. For

geometries with aspect ratios (exposed surface length/thickness) greater than 10, edge effects can be ignored and the problem approached as a one-dimensional process²⁹.

Figure 5.2 outlines the theoretical concentration profiles within the gel as drug is released for the infinite and physiological release cases. Before we place the gel in solution, the concentration of drug in bulk fluid is zero. After placing the gel in solution, a thin film layer forms between the gel and the bulk fluid, with drug concentration decreasing at positions further from the gel. The thickness of the film is time and mixing dependent. For the physiological flow model, we assume that the concentrations at the boundaries of this film match the adjacent gel and bulk fluid concentrations. Diffusional transport decreases as the bulk concentration increases to the gel surface concentration and the driving force diminishes. For the infinite sink model, the boundary layer is infinitesimally thin, and the diffusion continues until there is little to no drug left in the gel.

The following partial differential equation, initial conditions, and boundary conditions can adequately describe one-dimensional planar solute release from a hydrogel. A special case of this problem with $C_s = 0$ exists with boundary conditions for only one face of a slab predicting fractional release for different proteins over the entire time course of release.

$$\frac{\partial C}{\partial t} = D \frac{\partial^2 C}{\partial x^2} \quad 5.4$$

$$t = 0 \quad C(x, t) = C_0 \quad 5.5$$

$$t > 0 \quad x = 0 \quad \frac{\partial C}{\partial x} = 0 \quad 5.6$$

$$t > 0 \quad x = \pm L \quad C = C_s \quad 5.7$$

Where, C_0 represents the initial drug concentration (assumed to be uniform in the homogeneous gel), x represents the distance from the center of the sample to the

surface, C_s represents the surface concentration, C is the concentration of the drug within the gel, D represents a diffusion coefficient independent of position and concentration, t is time, and $2L$ is the thickness of the gel.

Using integral transform techniques, the solution of the PDE is given by equation

$$\frac{C - C_0}{C_s - C_0} = 1 - \frac{4}{\pi} \sum_{n=0}^{\infty} \frac{(-1)^n}{2n+1} e^{-\frac{(2n+1)^2 \pi^2 D t}{4L^2}} \cos \frac{(2n+1)\pi x}{2L} \quad 5.8$$

If M_t is the total cumulative mass of therapeutic released at time t , and M_∞ is the total cumulative mass of therapeutic released at infinite time, M_t/M_∞ represents the fractional release of therapeutic with respect to the value at infinite time,

$$\frac{M_t}{M_\infty} = 1 - \sum_{n=0}^{\infty} \frac{8}{(2n+1)^2 \pi^2} e^{-\frac{(2n+1)^2 \pi^2 D t}{4L^2}} \quad 5.9$$

The above expression is cumbersome to estimate a value of the diffusion coefficient, and hence, a solution is obtained in terms of error functions.

$$\frac{M_t}{M_\infty} = 4 \left[\frac{Dt}{L^2} \right]^{\frac{1}{2}} \left[\frac{1}{\pi^{\frac{1}{2}}} + 2 \sum_{n=1}^{\infty} (-1)^n \operatorname{ierfc} \left(\frac{nL}{2\sqrt{Dt}} \right) \right] \quad 5.10$$

The integral complementary error function vanishes for short times (as $t \rightarrow 0$), and an expression is obtained for short times of diffusion.

$$\frac{M_t}{M_\infty} = 4 \left[\frac{Dt}{\pi L^2} \right]^{\frac{1}{2}} \quad 5.11$$

5.4.3 Methods: One-Dimensional Diffusion Analysis

The diffusion studies for the imprinted networks employed a Side-Bi-Side Cell Diffusion Apparatus, (PermeGear, Hellertown, PA). After the washing procedure, the

thickness of the swollen networks was measured with an electronic micrometer. The networks were then placed between the diffusion cells. An aliquot of 3.4 mL of 1 mM ketotifen aqueous solution was placed on one side of the hydrogel while another 3.4 mL aliquot of DI water was placed in the other side of the cell. At various times, 0.2 mL aliquots were taken from both the donor and receptor cell and were measured *via* a Synergy UV-Vis spectrophotometer (BioTek Instruments, Winooski, Vermont) to determine the concentration within each side of the cell. Data was collected and equation 5.12 was used to calculate the permeability.

$$\ln \left[1 - \frac{2C_t}{C_d} \right] = -\frac{2A}{V} Pt \quad 5.12$$

Where C_t is the concentration in the receptor cell, C_d is the concentration of the donor cell, A is the area of diffusion, V is the volume of each half cell, t is time, and P is the permeability. Diffusion was calculated from the following two equations.

$$D = \frac{P\delta}{K_d} \quad 5.13$$

$$K = \frac{C_m}{C_s} = \frac{V_s(C_i - C_o)}{V_m C_o} \quad 5.14$$

Where, D is the diffusion coefficient, P is the permeability, δ is the hydrogel thickness, K is the partition coefficient, C_m is the concentration of the solute in the hydrogel at equilibrium, C_s is the concentration of the solute in solution at equilibrium, C_i is the initial concentration of the solute in solution, and C_o is the concentration of the solute in solution after equilibrium. The volumes of the solution and the hydrogel are V_s and V_m , respectively.

5.4.4 Methods: Determination of Structural Parameters.

After polymerization, the imprinted networks were taken for dry, swollen, and relaxed specific volume determination experiments. For the dry specific volume determination, the networks were placed in the vacuum oven at a temperature and pressure of 30°C 28 inches of Hg vacuum until the weight change was less than 0.1 wt%. Once dry, the networks were then taken out and the dry mass was measured on a Sartorius scale. Afterward, a density determination kit was installed on the Sartorius scale. The mass of the gel was then measured in heptane, a non-solvent (density of 0.684 g/mL at a temperature of 25°C). Once measurements were taken, Archimedes bouyancy principle was used to calculate the density of the dry polymer,

$$\rho_x = \frac{W_a \cdot \rho_h}{W_a - W_h} \quad 5.15$$

Where, ρ_x is the density of the sample, W_a is the mass of the sample in air, ρ_h is the density of heptane, and W_h is the weight of the sample in heptane. The specific volume of the polymer was calculated as the reciprocal of density. The experiment was repeated for both the relaxed and swollen gel. The relaxed gel specific volume was calculated directly after the polymerization reaction without any additional solvent being introduced into the gel. The swollen gel specific volume was calculated after the gel reached swelling equilibrium with the solvent for each system. The equilibrium volume swelling ratio Q is calculated with the swollen volume V_s and the specific volume of the dry polymer V_{dry} .

$$Q = \frac{1}{v_{2,s}} = \frac{V_s}{V_{dry}} \quad 5.16$$

Where, $v_{2,s}$ is the polymer volume fraction in the swollen state, which is the ratio of the polymer dry volume V_{dry} to the polymer swollen volume V_s .

Stress-strain experiments were performed on poly(AA-co-HEMA-co-PEG200DMA), poly(AM-co-HEMA-co-PEG200DMA), poly(NVP-co-HEMA-co-PEG200DMA), poly(AA-co-AM-co-HEMA-co-PEG200DMA), poly(AA-co-AM-co-NVP-co-HEMA-co-PEG200DMA)) in the equilibrium swollen state. Samples of each polymer system were loaded onto the two parallel arms of a RSA III Dynamic Mechanical Analyzer (DMA), (TA Instruments, New Castle, DE) and subjected to a tensile load until breaking point. Each experiment was conducted in controlled force mode with a force ramp from 0.001 to 0.3 N.

Polymer gel mesh size was calculated *via* data collected from the static experiments *via* a DMA and by using the theory of rubber elasticity. The following equation³⁰⁻³² describes the tension of a swollen, un-stretched polymer sample, τ .

$$\tau = \left(\frac{RTv_e}{Vv_{2,s}^{2/3}} \right) \left(\alpha - \frac{1}{\alpha^2} \right) \quad 5.17$$

Where, R is the universal gas constant, T is the temperature, v_e is the effective number of moles of chains in a real network, V is the volume of the swollen polymer, and α is the deformation of a network structure by elongation which is equivalent to the stretched length over initial length ($\alpha = L/L_0$).

Equation 5.18^{30, 33} takes into account the polymer swollen until equilibrium with the solvent, but not prepared in solvent.

$$\tau = RT \left(\frac{1}{\bar{v}M_c} \right) \left(1 - \frac{2\bar{M}_c}{M_n} \right) \left(\alpha - \frac{1}{\alpha^2} \right) v_{2,s}^{1/3} \quad 5.18$$

Where, \bar{v} is the specific volume of the polymer, M_n is the number average molecular weight, and \bar{M}_c is the average molecular weight between crosslinks. We confirmed that the average molecular weight between crosslinks is much smaller than the

number average molecular weight (i.e., $\overline{M}_c \ll M_n$) and so equation 5.18 gets reduced to 5.19.

$$\tau = RT \left(\frac{1}{\overline{v} M_c} \right) \left(\alpha - \frac{1}{\alpha^2} \right) v_{2,s}^{1/3} \quad 5.19$$

Strain values obtained from the tensile studies were converted into the elongation function $\left(\alpha - \frac{1}{\alpha^2} \right)$ and the curves obtained had excellent correlation coefficients (>0.99). The slopes were used to calculate \overline{M}_c .

A structural parameter that is often used in describing the size of the network pores is the correlation length, ξ , which is defined as the linear distance between two adjacent crosslinks, and can be calculated using Equation 5.20:

$$\xi = \alpha \sqrt{\overline{r}_o^2} \quad 5.20$$

Where, $\sqrt{\overline{r}_o^2}$ is the root-mean-square, unperturbed, end-to-end distance of the polymer chains between two neighboring crosslinks. For isotropically swollen networks, the elongation ratio, α , is related to the swollen polymer volume fraction, using Equation 5.21:

$$\alpha = v_{2,s}^{-1/3} \quad 5.21$$

The unperturbed end-to-end distance of the polymer chain between two adjacent crosslinks can be calculated using equation 5.19,

$$\sqrt{\overline{r}_o^2} = l(C_n N)^{1/2} \quad 5.22$$

Where, C_n is the Flory characteristic ratio (obtained from the molar average of the C_n from the homopolymers), l is the length of the bond along the polymer backbone (which is equal to 1.54 Å for vinyl polymers), and N is the number of links/chain. The Flory characteristic ratio was taken as 6.2 (an arithmetic mean of syndiotactic and

isotactic poly(HEMA) networks) for these calculations³⁴. The number of links per chain is equal to 2 times the average molecular weight between crosslinks divided by the molecular weight of the repeating units from which the polymer chain is composed. Combining equations yields the correlation distance between two adjacent crosslinks in a swollen hydrogel:

$$\xi = v_{2,s}^{-1/3} \left(\frac{2C_n \bar{M}_c}{M_r} \right)^{1/2} l \quad 5.23$$

Where, M_r is the effective molecular weight of the repeating unit (determined by a weighted average of the copolymer composition). It is important to note the equilibrium volume swelling ratio, Q , is the swollen volume of the gel divided by the dry volume of the gel or the reciprocal of the polymer volume fraction in the swollen state. The carbon-carbon bond length of the polymer backbone, which is equal to 1.54 Å is represented by length, l .

5.4.5 Methods: Mechanical Analysis of Imprinted Networks

The mechanical properties of the imprinted networks such as elastic and viscous moduli were tested *via* dynamic mechanical analysis (Seiko Exstar 6000 DMS-6100). Specifically the storage and loss moduli were calculated in swollen and dry lenses and compared to literature values of conventional lenses. Polymer strips 5 inches long and several millimeters wide were cut out directly from the freshly synthesized sheets. The rheological behavior of the networks when dry and fully swollen were measured in triplicate at 37°C, applying initial tension of 1 mN and angular frequencies of 0-100 Hz, with corrected offset load. The inverse problem was also investigated, i.e. the temperature dependence of the elastic and viscous moduli of

the imprinted networks (G' and G'' respectively) and of damping factor values were recorded at an angular frequency of 5 Hz, by subjecting the networks to a temperature sweep of 20-160°C.

5.4.6 Methods: Penetrant Uptake Studies

Kinetic penetrant uptake studies of the poly(AA-co-HEMA-co-PEG200DMA), poly(AM-co-HEMA-co-PEG200DMA), poly(NVP-co-HEMA-co-PEG200DMA), poly(AA-co-AM-co-HEMA-co-PEG200DMA), Poly(AA-co-AM-co-NVP-co-HEMA-co-PEG200DMA)) networks were performed by measuring the initial gel dry weight to determine the dry mass of polymer. The gel was then placed in a 0.5 mg/mL ketotifen solution (i.e., gel was loading in addition to swelling). The gel was taken out of solution and patted dry with Kimwipes®, and the gel weight measured. After the weight was measured, the gel was placed back in solution to continue swelling. The measurement was repeated once every 5 minutes for the first hour, once every 10 minutes for the second hour, and then every 30 minutes until the gel reached a constant mass which indicated equilibrium.

5.5 Results and Discussions

In this particular section, we report our observations on the transport and structural characteristics for the poly(AA-co-HEMA-co-PEG200DMA), poly(AM-co-HEMA-co-PEG200DMA), poly(NVP-co-HEMA-co-PEG200DMA), poly(AA-co-AM-co-HEMA-co-PEG200DMA), poly(AA-co-AM-co-NVP-co-HEMA-co-PEG200DMA)) networks.

5.5.1 Extended Release of a Therapeutic Dosage of Ketotifen from Imprinted Networks

Dynamic release profiles, performed in artificial lachrymal solution to mimic ocular physiological conditions, demonstrated extended release of a viable therapeutic concentration of ketotifen. Release conditions were performed under infinite sink conditions in order to maintain a maximum concentration driving force. We confirmed that release rates can be tailored *via* type and amount of functionality. As presented in Figure 5.3, the most structurally biomimetic network, poly(AA-co-AM-co-NVP-co-HEMA-PEG200DMA), exhibited an extended release profile for a duration of 5 days (80% of drug was released in approximately 4 days).

The slower release of drug compared to control networks proves that providing the relevant functionality to the mimicked docking site with CBIP affords a higher affinity of the drug for the network. The other systems, which showed extended release over a day, could be used as once-a-day contact lenses, thus precluding the need for administration of topical medication every two hours. Cumulative mass released in Figure 5.4 highlight that we are able to deliver a therapeutically relevant mass of ketotifen in comparison to contemporary topical ketotifen dosages (Figure 5.5).

5.5.2 Effect of Adsorbed Protein on Kinetic Release

To investigate the effect of protein on dynamic release, we chose lysozyme as a model protein since it is the largest protein component in tear fluid³⁵. It is well known that ionic contact lenses bind lysozyme *via* surface adsorption and matrix

penetration³⁶. Figure 5.6 highlights the poly(AM-co-HEMA-co-PEG200DMA) network release profile in artificial lachrymal solution with lysozyme, which leads to a factor of 5 increase in the duration of release. These studies demonstrate that the time of release may be delayed even further in an *in vivo* environment, due to ocular constituents and finite tear turnover rates, leading to wide applicability of contact lens ocular delivery.

Within a Fickian diffusion process, the fractional mass released depends linearly on $t^{0.5}/L$ at short times or fractional release less than 0.67 with a slope directly proportional to the diffusion coefficient. Poly (AA-co-AM-co-NVP-co-HEMA-PEG200DMA) networks exhibited a ketotifen fumarate diffusion coefficient of 5.57×10^{-10} cm²/sec, which was a factor of 9, 7.2, and 13.8 less than poly (AA-co-HEMA-PEG200DMA), poly (AM-co-HEMA-PEG200DMA), and poly (AA-co-AM-co-HEMA-PEG200DMA) networks, respectively. These results show that therapeutic release can be tailored *via* the memory within the polymer chains, which is tailored through the arrangement, type, and amount of functionality. This is significant considering all networks exhibited equilibrium volume swelling ratios that were in close agreement with one another suggesting similar structures available for free volume transport. Also, the monomers PEG200DMA and HEMA make up 97% of the feed monomers in each gel, and reaction analysis indicated that most of the double bonds within the systems reacted.

5.5.3 Dynamic Penetrant Studies of Imprinted Networks

In order to verify that the imprinting process, and not increased porosity or internal surface area of the gel, is responsible for the enhanced loading properties, we

conducted dynamic penetrant studies in deionized water and 0.5 mg/ml concentrated ketotifen solution and determined equilibrium weight swelling ratios. Figure 5.7 is a representative example of the penetrant uptake for poly(AM-co-AA-co-HEMA-co-PEG(200)DMA) with a crosslinking percentage of 5% in deionized water. Recognitive and control networks, for each formulation, had statistically similar swelling ratios. The water content at equilibrium was about 40-45% of the swollen networks. This indicates that the comfort of wearing and oxygen permeability of these networks is in agreement with conventional lenses synthesized from these monomers, as there is a direct correlation between water volume fraction and oxygen permeability. This also suggests that similar macromolecular architectures are available for free volume transport. The networks in this work contain less than 1% monomers of ionic nature and are therefore considered neutral networks. Swelling studies at different pH values revealed no differences in swollen polymer volume fractions.

5.5.4 Structural Analysis of Imprinted Networks

A critical experimental parameter in the structural analysis of polymer networks, the swollen polymer volume fraction can be correlated with molecular parameters such as mesh size, average molecular weight between crosslinks and correlation length. The experimentally determined parameters of all copolymer networks are attached in section A.3 and A.5 of Appendix A. Figures A.20 and A.21 depict the tensile characteristics of the non-imprinted and imprinted poly(AA-co-AM-co-HEMA-co-PEG200DMA) networks, and are representative of the tensile behavior of all copolymer networks. Tables A.5 to A.8 present the measured slopes of

these tensile curves, which were used for the mesh size calculations according to the theory of rubber elasticity. There were no observable trends in the mesh sizes obtained from the tensile behavior of the networks. Figure 5.8 shows that comparable values were obtained for imprinted and non-imprinted networks, in the ranges of 21-31 Å. The Flory characteristic ratio was taken as 6.2 (an arithmetic mean of syndiotactic and isotactic poly(HEMA) networks) for these calculations³⁴. The hydrodynamic radius of ketotifen fumarate is 4.2 Å, making it amenable to diffusion through the network. The equilibrium polymer volume fraction in the swollen state was determined to be 0.634 ± 0.025 for the imprinted networks and was 0.645 ± 0.02 for the control networks (Figure 5.9, Table I). These experimental results suggest that the structural plasticity due to imprinting, i.e. organization of multiple chemical functionalities is responsible for enhanced partitioning.

Furthermore, the polymer volume fraction in the swollen state for the poly(AA-co-AM-co-NVP-co-HEMA-co-PEG200DMA) network was observed to be lesser than the other networks, which could mean a more open network available for free volume transport. In spite of this, the drug does not diffuse through faster, but is delayed compared to all the other systems due to the tumbling from one memory site to the next.

5.5.5 Experimental Determination of Diffusion Coefficients

Permeation studies conducted on the imprinted networks yielded a permeability coefficient of 7.98×10^{-7} cm/s for the (poly(AA-co-AM-co-NVP-co-HEMA-co-PEG200DMA)) network as compared to 4.34×10^{-6} cm/s, 3.5×10^{-6} cm/s and 6.06×10^{-6} cm/s (Table I) for the single monomer networks, poly (AA-co-

HEMA-PEG200DMA), poly (AM-co-HEMA-PEG200DMA), and poly (NVP-co-HEMA-PEG200DMA). Figure 5.10 presents the diffusion coefficients of all gel formulations studied. The diffusion coefficient of the poly(AA-co-AM-co-NVP-co-HEMA-co-PEG200DMA)) network was 7.08×10^{-10} cm²/s which was lesser by factors of 15, 76, 49 and 113 than the other imprinted networks (Table I). We conclude that the multiplicity and organization of functionality is responsible in binding events and a delay in transport. The imprinted networks had lower permeability and diffusion coefficients than the non-imprinted networks, in spite of comparable mesh sizes and equilibrium polymer volume fractions in the swollen state, demonstrating that imprinting does delay transport. It is expected that the phenomenon of enhanced loading and extended release would be significantly reduced upon increasing the mesh size, which would affect the organization of functional groups interacting with the template.

5.5.6 The “Tumbling Hypothesis” of Solute Diffusion

We propose that as a molecule makes its random walk through a network imprinted by it, it tumbles from one memory site to the next, where it is held by the complex hydrogen bonding patterns, thus increasing its mean residence time in the network (Figure 5.11). There are greater and more productive binding events in a recognitive network composed of multiple functional monomers than in non-imprinted control networks and networks composed of single functional monomers. A control network is not constrained to polymerize around the template during polymerization and hence possesses no macromolecular memory. Networks composed of single functional monomers do not have multiple contact points with the

drug to bind to it for a longer duration. These molecular binding events are translated into extended release and lower diffusion coefficients.

The “tumbling hypothesis” is supported by earlier thermodynamic theories of imprinting processes. The free energy of functional monomer-template complex formation in the pre-polymerization complex and the stability of the complex, are a function of the extent of favorable non-covalent interactions and determine the fidelity of memory sites^{37, 38}. Functionally diverse systems are capable of multiple contact points with the template molecule, and result in efficient template complexation due to the reduction in the entropically unfavorable translational and rotational free energies. The poly(AA-co-AM-co-NVP-co-HEMA-co-PEG200DMA)) network can form multiple favorable non-covalent interactions with the template molecule, as it tumbles through the network. The functional monomer-template binding is not tight enough to preclude the unbinding event.

5.6 List of References

1. Venkatesh, S., Saha, J., Pass, S. & Byrne, M.E. Transport and structural analysis of molecular imprinted hydrogels for controlled drug delivery. *Eur. J. Pharm. Biopharm.* doi:10.1016/j.ejpb.2008.01.036 (2008).
2. Ali, M. et al. Zero-order therapeutic release from imprinted hydrogel contact lenses within in vitro physiological ocular tear flow. *J. Controlled Release* **124**, 154-162 (2007).
3. Gehrke, S.H. & Lee, P.I. Hydrogels for drug delivery systems, Vol. 41. (*Marcel Dekker, Inc.*, 1990).

4. Tahara, K., Yamamoto, K. & Nishihata, T. Overall mechanism behind matrix sustained-release tablets prepared with hydroxypropyl methyl cellulose 2910. *J. Controlled Release* **35**, 59-66 (1995).
5. Lee, E.S., Kim, S.W., Kim, S.H., Cardinal, J.R. & Jacobs, H. Drug release from hydrogel devices with rate-controlling barriers. *J. Membr. Sci.* **7**, 293-303 (1980).
6. Lee, P.I. Novel approach to zero-order drug delivery via immobilized nonuniform drug distribution in glassy hydrogels. *J. Pharm. Sci.* **73**, 1344-1347 (1984).
7. Crank, J. *The Mathematics of Diffusion*, Edn. 2. (Oxford University Press, 1975).
8. Lin, C.C. & Metters, A.T. Hydrogels in controlled release formulations: network design and mathematical modeling. *Adv. Drug Del. Rev.* **58**, 1379-1408 (2006).
9. Brazel, C.S. & Peppas, N.A. Modeling of drug release from swellable polymers. *Eur. J. Pharm. Biopharm.* **49**, 47-58 (2000).
10. Ritger, P.L. & Peppas, N.A. A simple equation for description of solute release. II. Fickian and anomalous release from swellable devices. *J. Controlled Release* **5**, 37-42 (1987).
11. Ritger, P.L. & Peppas, N.A. A simple equation for description of solute release. I. Fickian and non-Fickian release from non-swellable devices in the form of slabs, spheres, cylinders or disks. *J. Controlled Release* **5**, 23-36 (1987).

12. Glasstone, S., Laidler, K.J. & Eyring, H. The Theory of Rate Processes. The Kinetics of Chemical Reactions, Viscosity, Diffusion and Electrochemical Phenomena. (*McGraw Hill*, 1941).
13. Johnson, F.H., Eyring, H. & Stover, B.J. The Theory of Rate Processes in Biology and Medicine. (*John Wiley & Sons, Inc.*, 1974).
14. Matsuyama, H., Teramoto, M. & Urano, H. Analysis of solute diffusion in poly(vinyl alcohol) hydrogel membrane. *J. Membr. Sci.* **126**, 151-160 (1997).
15. Amsden, B. Solute Diffusion within Hydrogels. Mechanisms and Models. *Macromolecules* **31**, 8382-8395 (1998).
16. Amsden, B. Solute diffusion in hydrogels. An examination of the retardation effect. *Polym. Gels Networks* **6**, 13-43 (1998).
17. Amsden, B. An Obstruction-Scaling Model for Diffusion in Homogeneous Hydrogels. *Macromolecules* **32**, 874-879 (1999).
18. Amsden, B. Diffusion in Polyelectrolyte Hydrogels: Application of an Obstruction-Scaling Model to Solute Diffusion in Calcium Alginate. *Macromolecules* **34**, 1430-1435 (2001).
19. Cohen, M.H. & Turnbull, D. Molecular transport in liquids and glasses. *J. Chem. Phys.* **31**, 1164-1169 (1959).
20. Cohen, M.H. & Turnbull, D. Composition requirements for glass formation in metallic and ionic systems. *Nature* **189**, 131-132 (1961).
21. Turnbull, D. & Cohen, M.H. Free-volume model of the amorphous:glass transition. *J. Chem. Phys.* **34**, 120-125 (1961).
22. Altenberger, A.R., Tirrell, M. & Dahler, J.S. Hydrodynamic screening and particle dynamics in porous media, semidilute polymer solutions and polymer gels. *J. Chem. Phys.* **84**, 5122-5130 (1986).

23. Cukier, R.I. Diffusion of Brownian spheres in semidilute polymer solutions. *Macromolecules* **17**, 252-255 (1984).
24. Ogston, A.G., Preston, B.N., Wells, J.D. & Snowden, J.M. Transport of compact particles through solutions of chain-polymers. *Proc. R. Soc. London, Ser. A* **333**, 297-316 (1973).
25. Johansson, L., Skantze, U. & Lofroth, J.E. Diffusion and interaction in gels and solutions. 2. Experimental results on the obstruction effect. *Macromolecules* **24**, 6019-6023 (1991).
26. Johansson, L., Elvingson, C. & Lofroth, J.E. Diffusion and interaction in gels and solutions. 3. Theoretical results on the obstruction effect. *Macromolecules* **24**, 6024-6029 (1991).
27. Yasuda, H., Peterlin, A., Colton, C.K., Smith, K.A. & Merrill, E.W. Permeability of solutes through hydrated polymer membranes. III. Theoretical background for the selectivity of dialysis membranes. *Makromolekulare Chemie* **126**, 177-186 (1969).
28. Hagerstrom, H., Paulsson, M. & Edsman, K. Evaluation of mucoadhesion for two polyelectrolyte gels in simulated physiological conditions using a rheological method. *Eur. J. Pharm. Sci.* **9**, 301-309 (2000).
29. Crank, J. *The Mathematics of Diffusion.* (Oxford University Press, 1975).
30. Flory, P.J. *Principles of Polymer Chemistry*, Edn. 1st. (Cornell University Press, 1953).
31. Hariharan, D. & Peppas, N.A. Characterization, dynamic swelling behaviour and solute transport in cationic networks with applications to the development of swelling-controlled release systems. *Polymer* **37**, 149-161 (1996).

32. Nikolaos A. Peppas, E.W.M. Crosslinked poly(vinyl alcohol) hydrogels as swollen elastic networks. *Journal of Applied Polymer Science* **21**, 1763-1770 (1977).
33. Sperling, L.H. Introduction to Physical Polymer Science, Edn. 4th. (*John Wiley & Sons, Inc*, 2005).
34. Yoon, J.H., Shin, J.M., Kang, Y.K. & Jhon, M.S. Conformational analysis of poly(2-hydroxyethyl methacrylate). *J. Polym. Sci., Part A: Polym. Chem.* **29**, 393-398 (1991).
35. Van Haeringen, N.J. Clinical biochemistry of tears. *Surv. Ophthalmol.* **26**, 84-96 (1981).
36. Garrett, Q., Garrett, R.W. & Milthorpe, B.K. Lysozyme sorption in hydrogel contact lenses. *Invest. Ophthalmol. Vis. Sci.* **40**, 897-903 (1999).
37. Nicholls, I.A. et al. Can we rationally design molecularly imprinted polymers? *Anal. Chim. Acta* **435**, 9-18 (2001).
38. Nicholls, I.A. Towards the rational design of molecularly imprinted polymers. *J. Mol. Recognit.* **11**, 79-82 (1998).

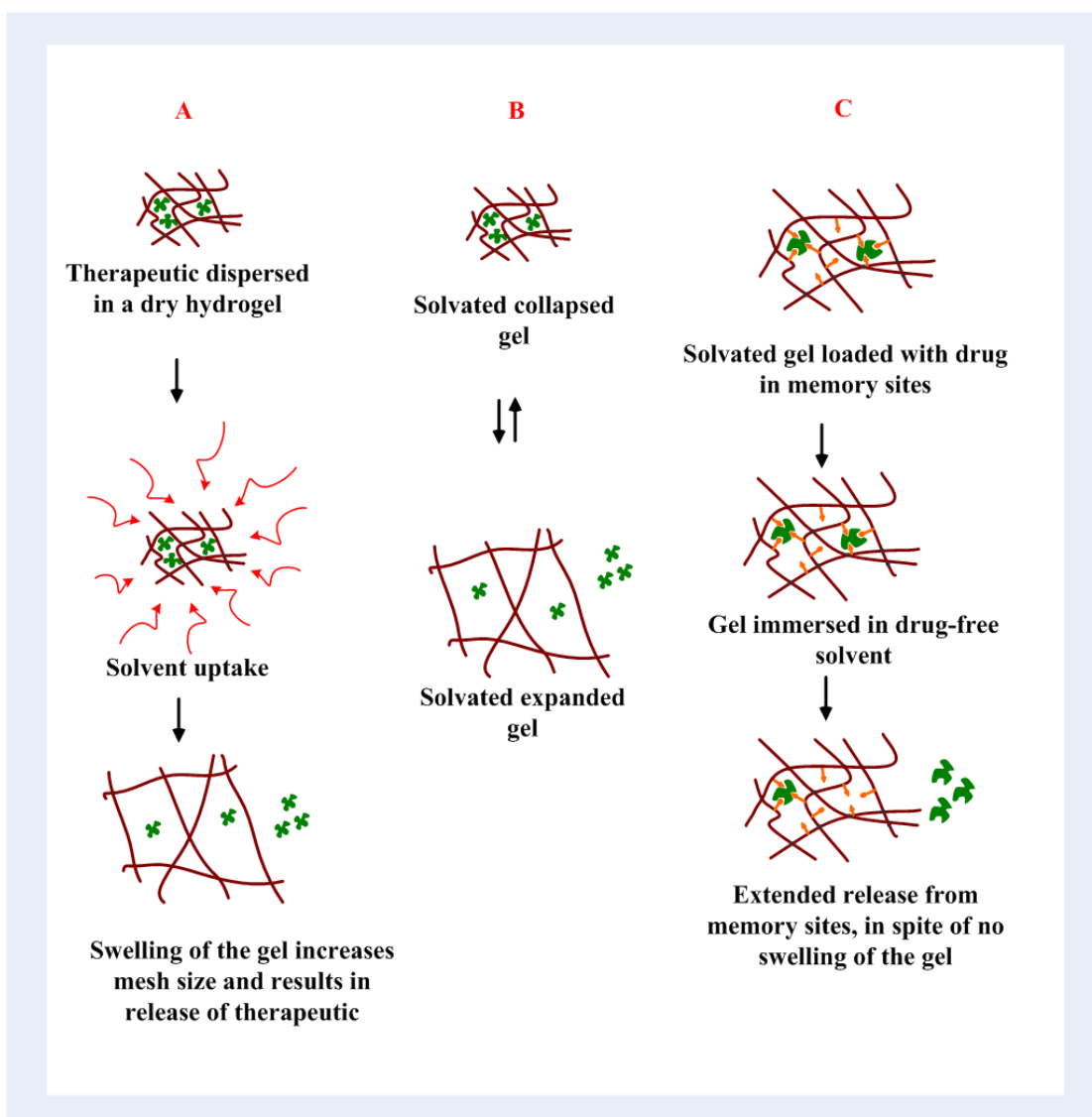


Figure 5.1 Controlled Release Strategies in Hydrogels. (A) Controlled drug release in hydrogels hinges upon their swelling either upon solvent uptake from a dry state or, (B) their thermodynamic compatibility with the solvent. (C) Macromolecular memory obtained by the imprinting of a multifunctional pre-polymerization complex with the drug, is an alternative strategy to release the drug in a controlled fashion when the gels are already solvated and fully swollen.

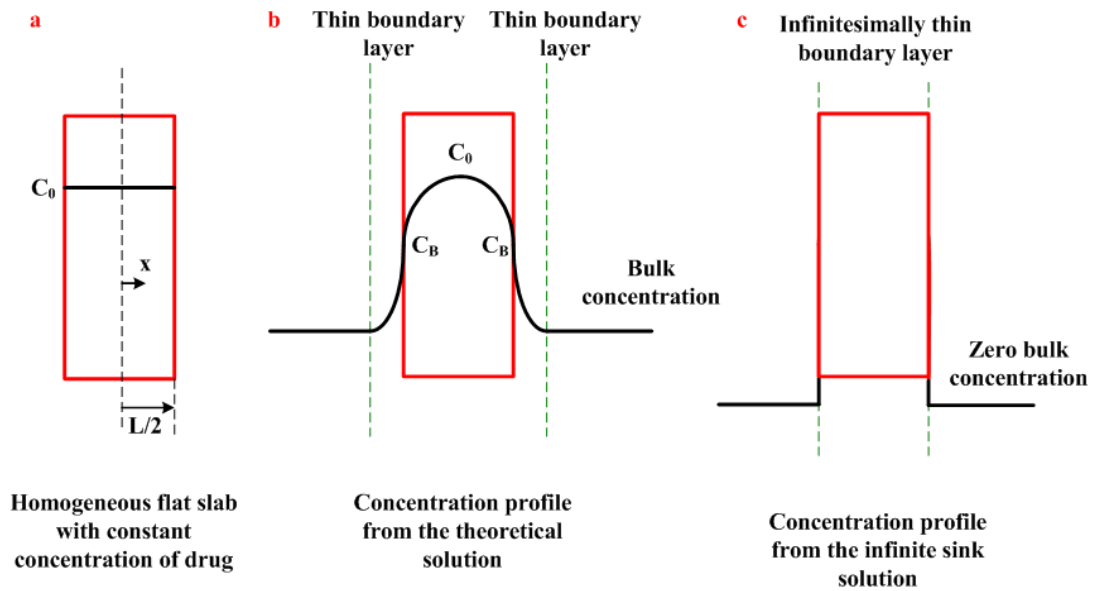


Figure 5.2 Schematic Representation of One-dimensional Planar Diffusive Transport from a Polymer Network. (a) Initial state of gel, with homogeneous drug distribution in the network (b) Physiological flow model, where the concentration at the surface of the network is non-zero, and the bulk concentration increases from zero to a finite amount. (c) Infinite sink model, where we assume that the surface concentration of the network (C_b) is always zero.

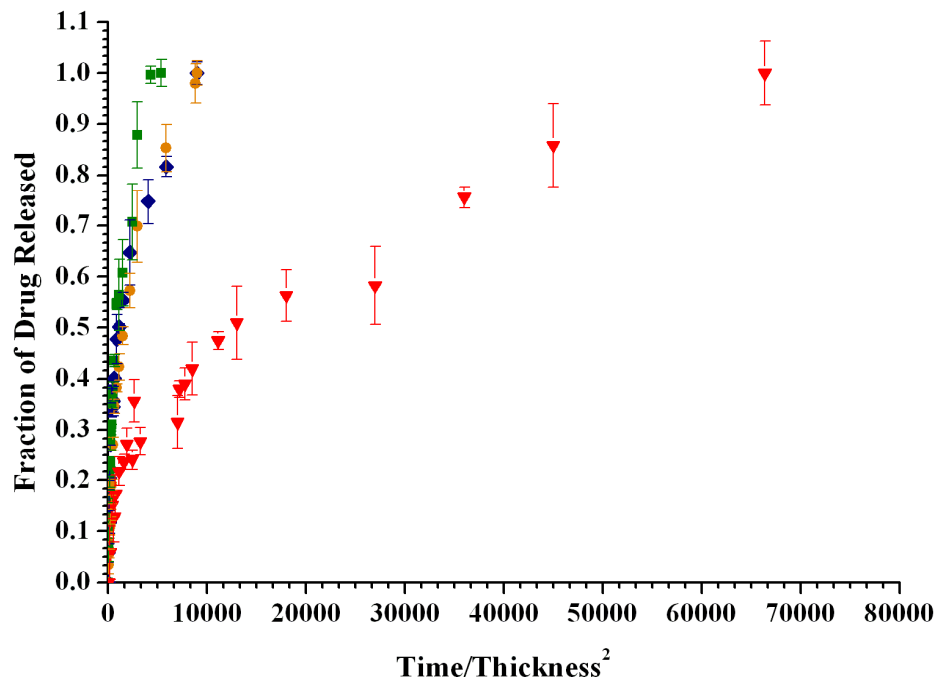


Figure 5.3 Dynamic Extended Release in Biomimetic Networks. Tailored release profiles of therapeutic contact lenses for poly(n-co-HEMA-co-PEG200DMA) networks in artificial lachrymal fluid at 25°C, where n is AM (●), AA (◆), AA-AM(■), and NVP-AA-AM (▼) recognitive networks respectively. Fraction of drug released is the ratio of mass released at an instantaneous time t and that at infinite time. The abscissa is time normalized to the square of thickness, as the thicknesses of the gels differed; 700 μm (●, ◆, ■) and 400 μm (▼).

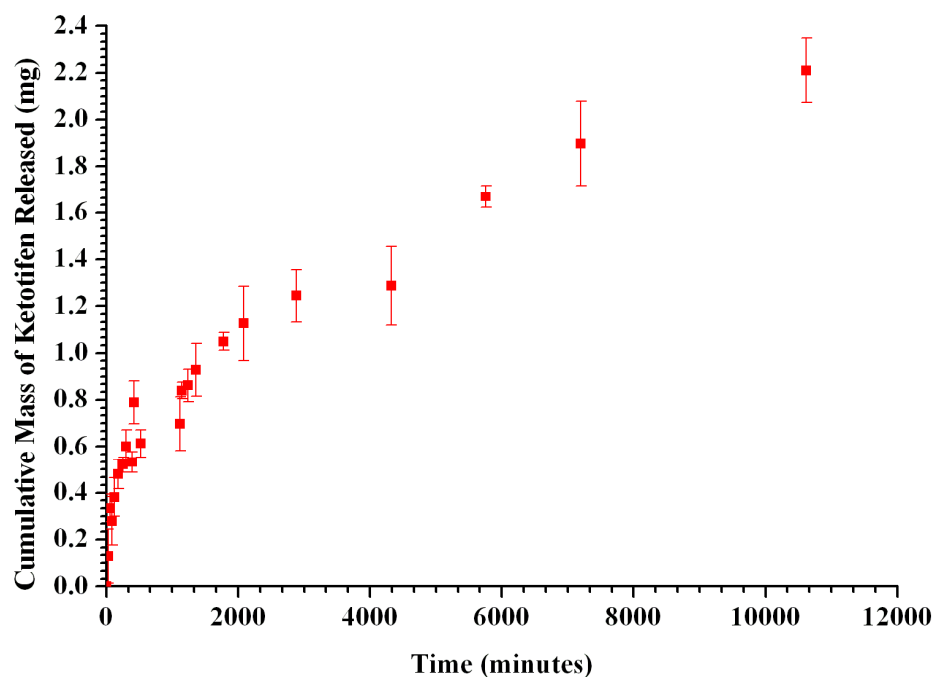


Figure 5.4 Cumulative Mass of Ketotifen Released in Artificial Lachrymal Fluid for Poly(AA-co-AM-co-NVP-co-HEMA-co-PEG200DMA) Networks. Tailored release profiles of therapeutic contact lenses for the most biomimetic recognitive networks (■) at 25°C.

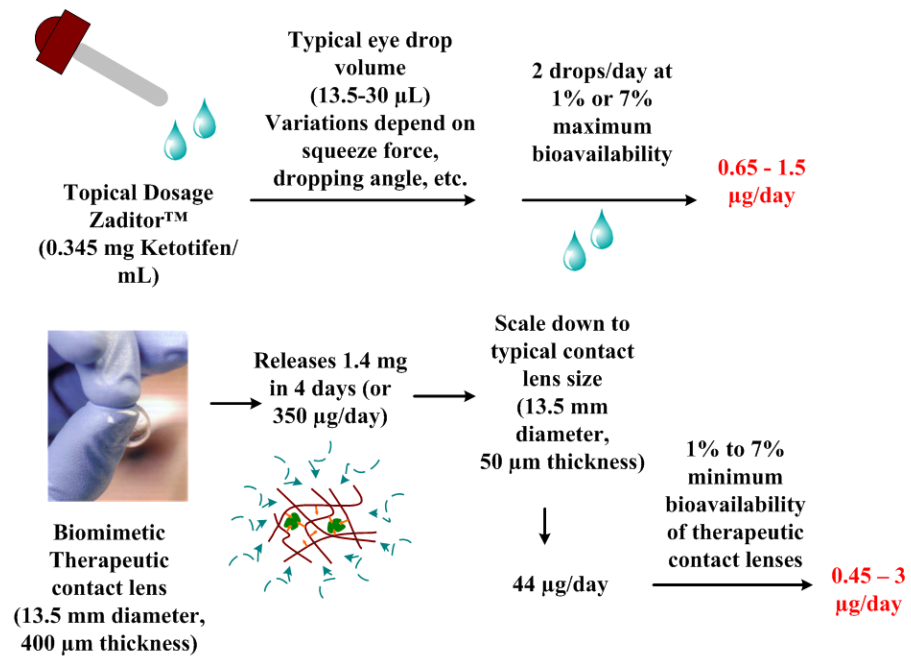


Figure 5.5 Comparison between Ketotifen Delivery by Therapeutic Contact Lenses and Topical Eye Drops.

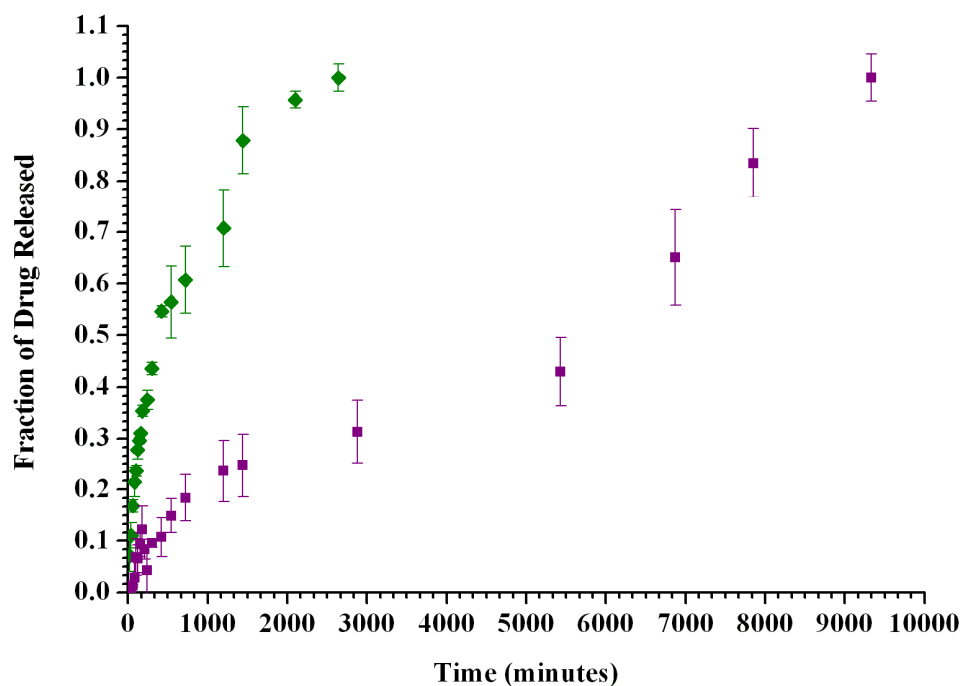


Figure 5.6 Effect of Protein on Dynamic Release of Ketotifen. Introduction of lysozyme (1 mg/ml) to an artificial lachrymal solution (■) versus artificial lachrymal solutions (◆) to observe effects of proteins on release profiles of a poly(AA-AM-co-HEMA-co-PEG200DMA) network . Error bars indicate standard deviation.

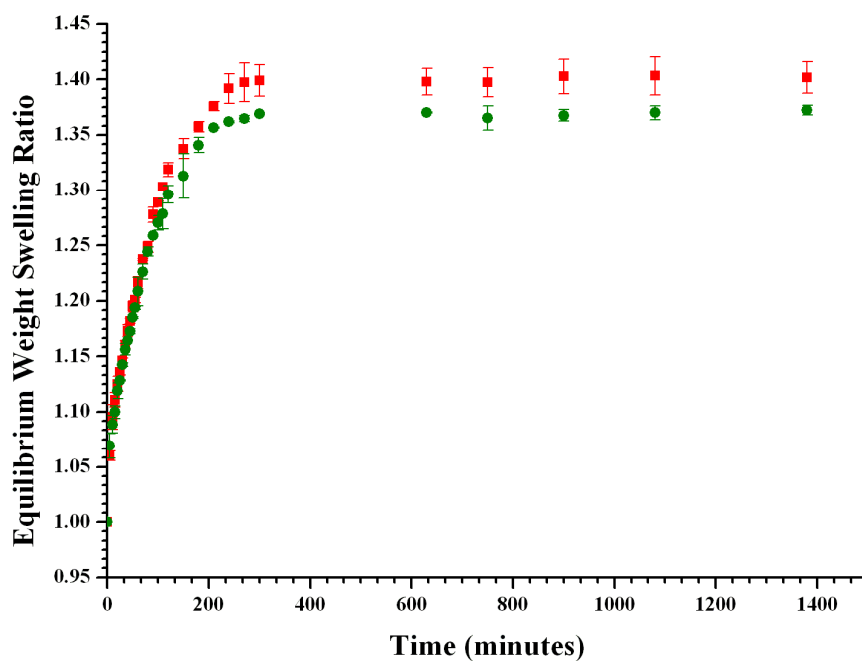


Figure 5.7 Equilibrium Weight Swelling Ratios for Poly(AM-co-AA-co-HEMA-co-PEG(200)DMA) Networks. Networks had a crosslinking percentage of 5% in reverse osmosis water. N=3, and T=25°C. Recognitive network (■) and Control network (●). Percentage denotes percent mole crosslinker per mole total monomers in feed.

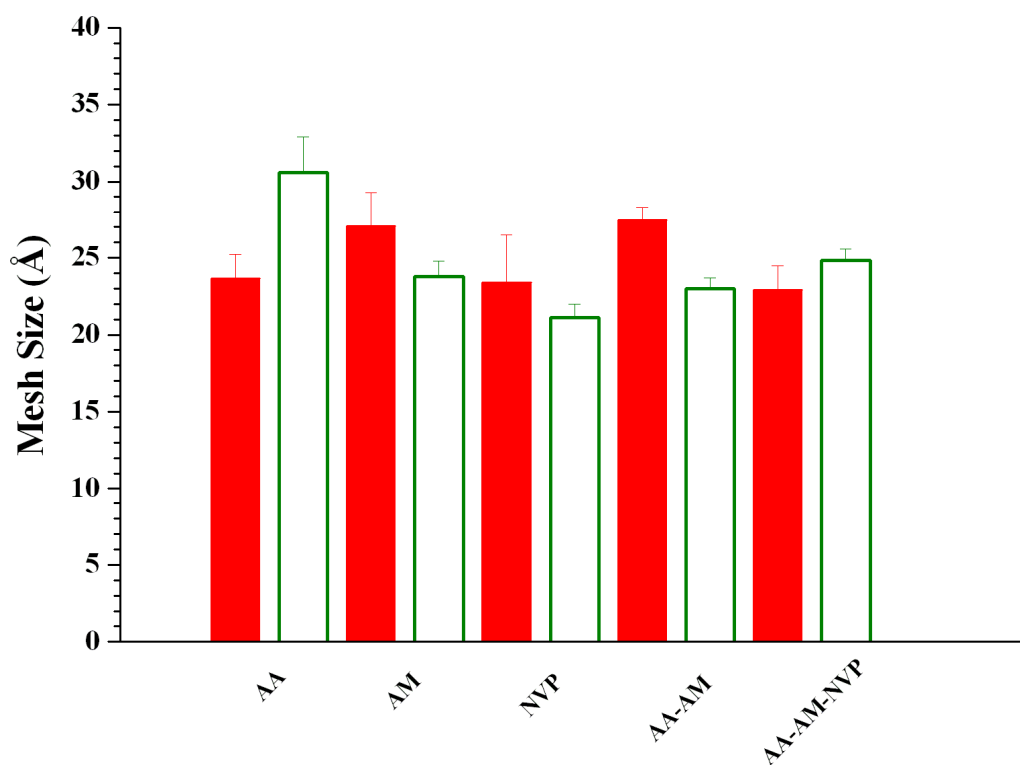


Figure 5.8 Partition coefficients for poly(n-co-HEMA-co-PEG200DMA) networks. Networks had a crosslinking percentage of 5 mole %, $N^{\circ}=3$, and $T=25^{\circ}\text{C}$, where n is AA, AM, NVP, AA-co-AM, and AA-co-AM-co-NVP. Imprinted network (■) and Control network (□).

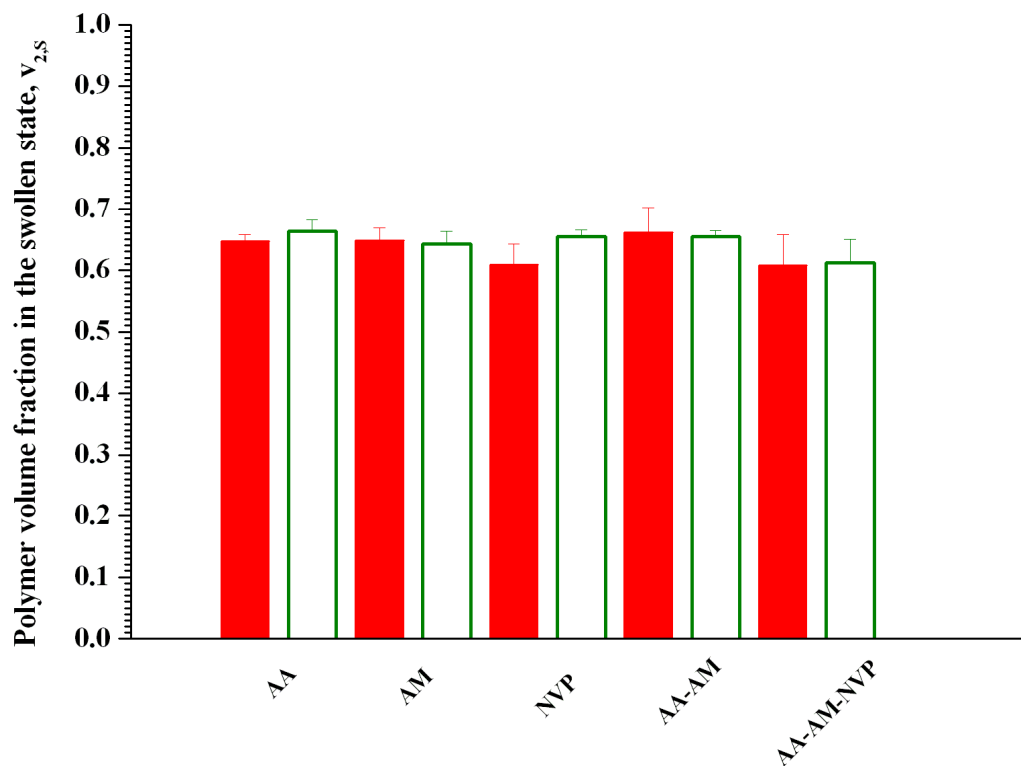


Figure 5.9 Equilibrium polymer volume fractions in the swollen state for poly(**n-co-HEMA-co-PEG200DMA**) networks. Networks had a crosslinking percentage of 5 mole %. $N^{\circ}=3$, and $T=25^{\circ}\text{C}$, where n is AA, AM, NVP, AA-co-AM, and AA-co-AM-co-NVP. Imprinted network (■) and Control network (□).

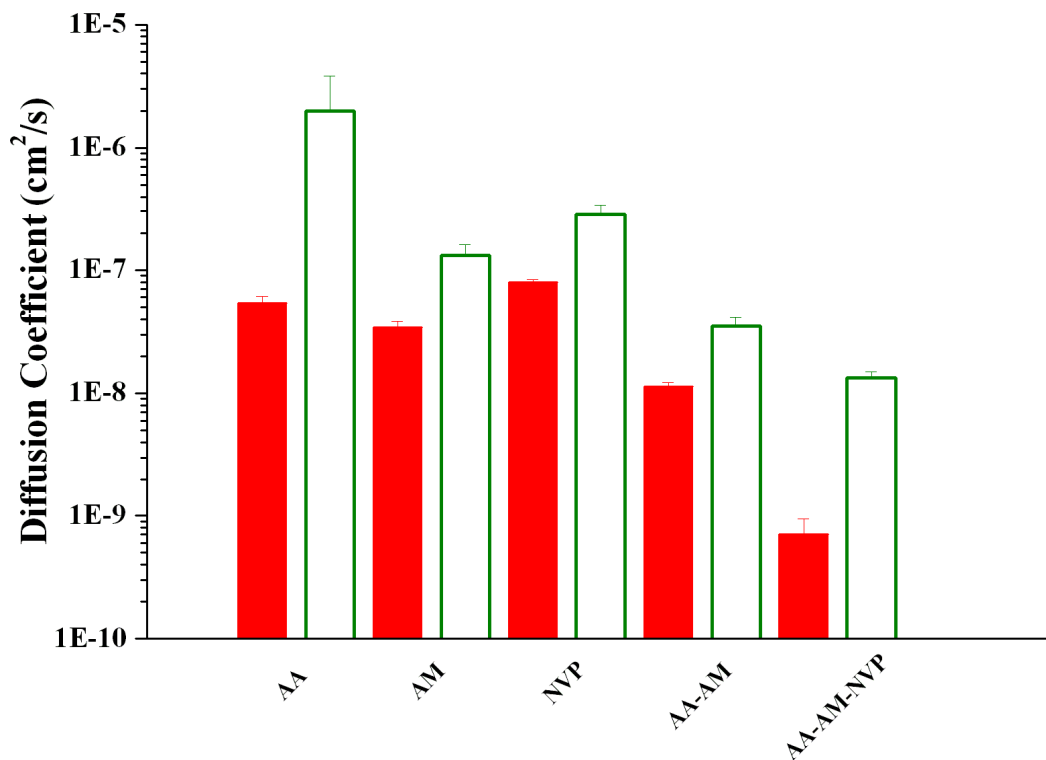


Figure 5.10 Diffusion Coefficients for poly(n-co-HEMA-co-PEG200DMA) networks. Networks had a crosslinking percentage of 5 mole %. $N^{\circ}=3$, and $T=25^{\circ}\text{C}$, where n is AA, AM, NVP, AA-co-AM, and AA-co-AM-co-NVP. Imprinted network (■) and Control network (□).

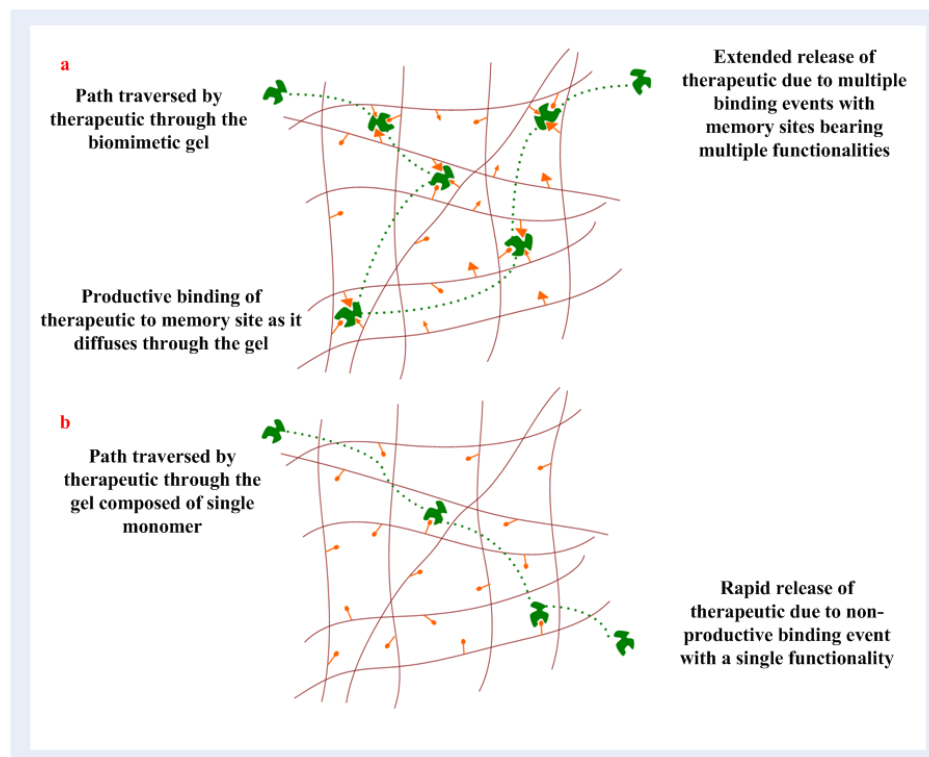


Figure 5.11 The Tumbling Model of Drug Diffusion in Imprinted Networks. (a)

Tumbling of the drug through the gel from one memory site to the next results in slower diffusion coefficients and delayed kinetics of release. This could be imputed to productive binding of the drug at every memory site a drug molecule encounters due to multiple contact points. **(b)** Single monomer gels have single contact points and have less effective binding events with the drug, resulting in rapid release. Dotted lines (.....) indicate the pathway of diffusion through the gel in both cases.

Table 5.1 Transport Coefficients and Swelling Data of poly(n-co-HEMA-co-PEG200DMA) networks

Network Monomers (n)	Network type	Permeability P (x 10⁶ cm/s)	Diffusion coefficient (x 10⁹ cm²/s)	$v_{2,s}$ Equilibrium polymer volume fraction in the swollen state	\overline{M}_c, Average molecular weight between crosslinks, g/mol
AA	Imprinted	4.34 ± 0.51	53.68 ± 7.09	0.647 ± 0.011	1823 ± 244
	Control	9.87 ± 0.27	1988 ± 1860	0.664 ± 0.018	3109 ± 466
AM	Imprinted	3.5 ± 0.2	34.4 ± 4.08	0.648 ± 0.021	2502 ± 392
	Control	5.03 ± 0.12	132.1 ± 28.8	0.643 ± 0.020	1838 ± 153
NVP	Imprinted	6.06 ± 0.24	79.92 ± 4.03	0.608 ± 0.034	1728 ± 452
	Control	6.52 ± 0.15	281.7 ± 58.2	0.654 ± 0.012	1481 ± 121
AA-co-AM	Imprinted	2.92 ± 0.21	11.33 ± 0.88	0.661 ± 0.041	2494 ± 123
	Control	5.11 ± 0.28	35.11 ± 6.44	0.654 ± 0.010	1736 ± 102
AA-co-AM-co-NVP	Imprinted	0.8 ± 0.2	0.708 ± 0.236	0.608 ± 0.049	1647 ± 211
	Control	3.65 ± 0.24	13.31 ± 1.62	0.612 ± 0.038	1948 ± 83

6.0 PROGRAMMABLE, ON-DEMAND RELEASE OF NUCLEIC ACID THERAPEUTICS FROM BIOHYBRID PLATFORMS BY THE APPLICATION OF PHYSICAL AND ENZYMATIC TRIGGERS

In this chapter, we designed novel platforms for drug and gene delivery such as synthetic polymer networks and gold nanoparticles using concepts derived from molecular biology and biochemistry, with a particular emphasis on creating programmable, on-demand switches and devices. We hypothesized that the covalent incorporation of nucleic acid constructs into such platforms could produce novel gene delivery vehicles, capable of responding to specific triggering agents with unprecedented sensitivity and control. We established the potential of synthetic polymer networks as controlled release vehicles of nucleic acid therapeutics *via* enzymatic and physical triggers such as specific and non-specific endonucleases and temperature. In order to evaluate our platform in the physiological landscape, we demonstrated the down regulation of a HIV-1 Tat/Rev gene by the specific release of a deoxyribozyme bearing the catalytic 10-23 motif, from a polymer network. We also developed methods for the functionalization of gold nanoparticles with aptamers capable of binding the antibiotic neomycin, and expect that such platforms would be amenable to a wide variety of triggering and modifying agents for the tailored release of the payload. These novel biomaterials, designed using the fundamental principles of molecular biology, are expected to profoundly impact gene therapy regimes.

6.1 Scientific Rationale

Nucleic acids are attractive targets for research efforts in nanotechnology because they can easily be programmed to bind metals, small organic compounds, nucleic acids, and proteins *via* SELEX^{1, 2}. Nucleic acids are emerging as important drug targets and versatile therapeutic agents because they fold into complex three-dimensional structures capable of performing critical enzymatic activities and regulate the flow of genetic information from DNA to proteins³⁻⁵. However, one of the principal hurdles to be crossed is the targeted and controlled delivery of the nucleic acid payload. While novel drug discovery such as RNA interference is vital for combating the multifactorial and complex disorders, it is equally imperative to develop devices and shuttles that enable precise delivery of therapeutics to the diseased tissue or cells, at controlled release rates.

Off-targeting, toxicity, reduced *in-vivo* potency and interferon responses are some of the pressing concerns for the clinical viability of nucleic acid based therapies. Biohybrid platforms, particularly synthetic polymers engineered from artificial and natural materials and metallic nanoparticles, hold immense potential in the amelioration of such concerns⁶⁻¹⁰. In this chapter, we discuss the methods of synthesis and characterization of novel synthetic polymer networks, and evaluate their potential as vehicles for the controlled release of nucleic acid therapeutics *via* enzymatic and physical triggers such as specific and non-specific endonucleases and temperature. The physiological relevance of the platform was demonstrated by the *in-vitro* down regulation of a HIV Tat/Rev gene by the specific release of an anti-HIV deoxyribozyme. Furthermore, the crosslinking densities of the networks were varied in order to obtain tunable release profiles of DNA. We also discuss how the design of

these novel biomaterials was biomimetic, i.e. guided by the principles of molecular biology.

DNA-functionalized gold nanoparticles have been widely used for nanoscale assembly, as antisense agents for gene regulation, and as probes in contemporary diagnostics applications such as single nucleotide polymorphism scans, due to their efficient uptake by cells and unique optical, mechanical and electrical properties. We investigated the potential of gold nanoparticles to load DNA aptamers for the antibiotic neomycin, in order to create a drug delivery platform sensitive to a variety of triggering agents. The objective of these studies was to create nucleic acid based programmable on-demand switches and modulatory mechanisms, with exquisite control and sensitivity. These novel schemes could spur further inquiry into the development of drug and gene delivery platforms, for the intracellular delivery of multiple drugs from the same platform, and as injectable systems targeted to specific cells using functionalized ligands such as folic acid.

6.2 Stimuli-Sensitive Synthetic Polymers in Drug Delivery

Stimuli-sensitive, tunable, drug delivery devices, such as synthetic polymers, have been shown to control drug release over extended periods of time¹¹. They are the subject of intense scrutiny due to striking properties such as biocompatibility, greater flexibility in their bottom-up design, and well-studied synthetic protocols. In this section, we will classify the contemporary synthetic polymers into three generations, based on their types of stimuli or pattern of response. Artificial materials that demonstrate reproducible and tailorable responses to stimuli are termed “intelligent”, and can be envisioned to respond similarly in the cellular milieu. In the case of a drug

delivery device, this response would be the controlled release of the payload in response to a cellular or extracellular stimulus. The design of biomaterials with heightened sensitivity to changes in the biological environment is critical in the applicability of intelligent platforms for drug and gene delivery.

First generation intelligent networks (Figure 6.1) were synthesised purely from artificial monomers such as methacrylic acid, acrylamide, N-isopropylacrylamide etc. and demonstrated phase or volume transitions on varying pH¹², temperature¹³⁻¹⁵, light¹⁶, magnetic field^{17, 18}, and electric field¹⁹⁻²¹.

Synthetic polymers with ionizable groups such as carboxylic acids and amines with pK_a values between 4 and 10 are the basis of pH-responsive systems. Changes in pH result in changes in the ionization states of the functional groups, which in turn results in swelling of the macromolecular architecture *via* mutual repulsions of the functional groups. A functional biomimetic system, which involved the use of a pH-responsive polymer²² as a membrane-disrupting agent that aided the transport of antibody conjugates from the endosome to the cytoplasm, is a classic study in the literature, which highlights the use of endosomal releasing agents for targeted therapeutics that are internalized through receptor-mediated endocytosis.

Temperature sensitive polymers exhibit volume phase transitions at certain transition temperatures, which are caused by changes in their hydration states. Polymer networks synthesized from N-isopropylacrylamide, N,N-diethylacrylamide, and N- vinylcaprolactam²³⁻²⁸, become insoluble upon raising their temperature above the lower critical solution temperature. In particular, poly(N-isopropylacrylamide) has sweeping implications in drug delivery^{29, 30}. The network has negative thermosensitivity, i.e. it is swollen at temperatures lower than 33°C and collapses when the temperature is raised. Interpenetrating polymer networks synthesized from

poly(acrylamide) and poly(acrylic acid)^{31, 32}, become soluble upon raising their temperature above the upper critical solution temperature. These volume transitions are due to dominant cooperative hydrogen bonding between polymer chains compared to solvation by water.

Polymer networks sensitive to electric fields have shown great potential as programmable switches for drug delivery. Networks assembled *via* intermolecular hydrogen bonding of poly(ethylloxazoline) and poly(acrylic acid) collapse on the application of small amperages of current¹⁹. Such networks assemble at a pH below 5 as the carboxy groups get protonated and are capable of hydrogen bonding with the ethyloxazoline groups. On passing electric current through the solution, hydroxyl ions are produced due to the electrolysis of water, followed by a local increase in pH and collapse of the gel. Stepwise current inputs resulted in pulsatile release of insulin which was encapsulated within the network while it was assembled. Recent studies with polymeric biodegradable microchips³³ containing nanosize drug reservoirs indicate that such systems might be able to deliver pharmaceuticals for long time periods in a controlled manner, by electrically opening the caps of these reservoirs.

Any material experiences a torque when subjected to an electric or magnetic field. While this effect is weak in solutions, complex fluids such as electrorheological fluids, magnetorheological fluids and ferrofluids respond to applied electric or magnetic fields by rapidly changing their apparent viscosity and yield stress. Field sensitive responses have been tuned by swelling a polymer network in a complex fluid^{17, 18}. Furthermore, if a field-sensitive gel is exposed to a non-uniform external field, the field-polymer chain interactions overshadow the interactions between chains. The chains experience a dielectrophoretic or a magnetophoretic force, and

undergo macroscopic volume transitions. Such field-sensitive properties can be exploited in sensing and controlled drug delivery systems.

Light sensitive networks, which display observable volume transitions on ultraviolet or visible light irradiation, have been also synthesized for drug delivery. The incident light is absorbed by the chromophore and then the isomerization of the chromophores in the photoreceptor converts it to a chemical signal. The first efforts in this direction involved the polymerization of chromophores such as chlorophyllin, leucocyanide and cinnamic acid using conventional redox techniques^{16, 34}.

Second generation intelligent networks (Figure 6.2) were conglomerates of artificial materials and biomolecules immobilized within the network³⁵⁻³⁹. These networks consisted of protein molecules such as antibodies, enzymes, and receptors, which were immobilized within the network. The protein causes a local change, which is translated to observable volume transitions of the network.

Antigen sensitive networks were synthesized by immobilizing antigens and their specific immunoglobulins in the backbone, and binding of these protein molecules created effective crosslinking in the network³⁵. On sensing a greater concentration of antigen, the antibodies bound the free antigen competitively, resulting in loss of effective crosslinks and disassembly of the network. Such networks could be used as a treatment option, by encapsulating a therapeutic in them, which would be delivered only during infection with antigen. Following a similar strategy of competitive binding, glucose sensitive networks have been synthesized in which glucose binding protein motifs would bind free glucose and would degrade, resulting in controlled release of insulin which would be encapsulated within such networks.

Third generation networks were self-assembling or crosslinked systems of peptides, proteins and nucleic acid sequences⁴⁰⁻⁴⁴. They utilized the hyperfine switching processes which are the hallmark of protein-protein and protein-ligand interactions. Three-dimensional conformation switches led to observable volume transitions, which are highly temperature and pH-sensitive. Such conformational switches at the molecular level are similar to those found in enzyme catalysis, gene regulation, and signal transduction.

Wang and coworkers³⁷ have prepared copolymers of metal-chelating hydrophilic monomers and coiled-coils. These networks undergo a reversible, temperature-induced collapse owing to the cooperative conformational transition of the coiled-coil protein domain. The backbone consisted of N-(2-hydroxypropyl)-methacrylamide and the metal chelating (N',N'-dicarboxymethylaminopropyl)methacrylamide. Hence, genetic engineering can aid in the design and tailoring of stimuli-sensitive networks with well-defined volume transitions based on pH and temperature changes in the environment.

Daunert and coworkers³⁸ have produced stimuli-responsive hybrid materials consisting of polymer networks and the calcium ion-responsive calmodulin protein, which demonstrates dramatic switches in conformation in its bound and chelated states. The stimuli-responsive network exhibits three specific swelling stages, induced by conformational changes and binding to various ligands. The authors showed gating and transport of biomolecules across a polymer network, demonstrating its potential in microfluidics and drug delivery.

Tirrell and coworkers³⁶ have prepared thermally reversible networks from polymer networks and recombinant proteins. The block copolymer consisted of a leucine zipper and polyelectrolyte domains. The triblock structure had a few

interesting features, including a terminal cysteine residue, intended for disulfide bridging between individual strands and a His-tag at the N-terminal. Coiled-coil formation was observed at low pH, and protonation of the Glu residues at higher pH led to dissociation of heterodimer. The triblock structure underwent bridging and formed complex networks. The fact that the biocompatibility of these gels was high due to the PEG-rich region in the polyelectrolyte domain, and that the switching of these gels can be controlled by crafting custom sequences, lends them great potential in controlled release

Strict control of monomer and polymer structure is of high importance in design of materials with reproducible and consistent properties. Deming has pioneered the use of transition metals as initiators for the ring-opening polymerization of N-carboxyanhydrides. The use of organonickel as initiator effectively suppresses the chain termination and transfer reactions, giving block copolypeptides of highly controlled chain lengths which produce novel polypeptide hydrogels⁴⁵. Variation of copolymer chain length and composition produced various hydrogels, characterized by confocal microscopy and TEM. At the molecular level, familiar conformations of poly peptides were obtained with poly-(L) giving α -helices and poly-(V) giving β -sheets⁴².

Hydrogels that are responsive to biological agents such as enzymes have been the subject of many research efforts in the recent literature. In particular, the focus is on hydrogels whose crosslinks are selectively synthesised or hydrolysed by enzymes, resulting in a sol-to-gel or gel-to-sol transition respectively. These are attractive as they can assemble or disassemble on enzymatic action, and can show different responses depending on the cellular microenvironment⁴⁶⁻⁴⁹. Chemically crosslinked polymer networks that carry pendant enzyme-sensitive moieties have also been

synthesized. Upon enzyme action macroscopic transitions (swelling/collapse) take place while the overall crosslinked structure stays robust due to the chemical crosslinks.

The ability of transglutaminase (TGase), a blood clotting enzyme, to crosslink the side chains of lysine residues with those of glutamine residues has been exploited in a number of synthesis schemes of peptide-based hydrogels. The crosslinking of PEG-Gln with poly(Lys-Phe) was shown to generate hydrogel formation by self assembly, and gelation kinetics in these systems was predicted^{46, 47}. It has been observed that a facile design of the TGase peptide substrate based on enzyme specificity has the potential to reduce the gelation times significantly, and crosslinked gels can be formed from liquid precursors within a few minutes⁴⁸. Furthermore, the discovery that mutant transglutaminases are inactive in the absence of calcium, has led to the exploitation of hydrogels assembly triggered by calcium addition. A temperature-responsive calcium-containing liposome was shown to release its payload when the temperature was raised to body temperature⁵⁰. The released calcium, in combination with a second enzyme, thrombin, activated the TGase precursor factor XIII which triggered crosslinking of a peptide-PEG conjugate.

Affinity-based delivery systems such as the heparin binding delivery system exploit non-covalent interactions between the drug or protein and heparin to provide controlled release. Such delivery systems have been designed to release growth factors such as the basic fibroblast growth factor and nerve growth factor⁵¹⁻⁵⁵. The heparin binding delivery system consists of a scaffold, a bidentate peptide, heparin, and a growth factor which can bind heparin. The peptide has two functional domains- a factor XIIIa substrate, which allows the covalent incorporation into fibrin scaffolds, and a heparin binding domain derived from anti-thrombin III, which allows it to

sequester heparin *via* electrostatic interactions. Heparin-binding growth factors are immobilized within this system based on electrostatic interactions between basic heparin-binding domains on the growth factors and sulfated groups on heparin. Mathematical modeling was performed to determine dissociation constants and optimal molar ratios required for the diffusion-based release of growth factors such as nerve growth factor. The growth factors are protected from proteases by heparin and are released in a controlled fashion over time. Growth factors delivered using the heparin binding delivery system enhance neurite extension *in vitro* compared to fibrin scaffolds without the delivery system. Furthermore, phage display library have been screened against heparin-conjugated chromatography resin to isolate peptides with varying affinities for heparin^{56, 57}. This affinity spectrum of NGF-binding peptides has been shown to modulate the release NGF at different rates.

In addition to the heparin-based affinity strategy, other types of delivery systems have been designed by functionalizing a high affinity version of the growth factor itself into the biomaterial. This approach has been used to enhance the ability of collagen matrices to sequester TGF- β 1^{58, 59}, by designing recombinant fusion proteins of TGF- β 1 that contained collagen-binding domains. The fusion protein binds collagen with much higher affinity than recombinant TGF- β 1, which lacks the collagen-binding domain, and has been shown to promote higher levels of migration and differentiation of bone marrow cells in collagen gels.

6.3. Materials and Methods

In this particular section, we describe the materials and methods used for the synthesis and characterization of novel platforms loaded with nucleic acid

therapeutics. The nucleic acid sequences were custom designed by minimizing secondary structure formation due to intramolecular hydrogen bonding, and were labeled either with radioactive nucleotides or fluorescent probes for biochemical monitoring. The loading of the polymer networks with nucleic acid strands was performed *via* conventional redox polymerization techniques. Enzymatic and temperature triggers were used to release the payload from these platforms. Aptamers specific to the antibiotic neomycin were attached to gold nanoparticles by conventional ligand exchange methods and different point mutants were tested for differential binding of neomycin by affinity chromatography.

6.3.1 Materials

The functional monomers acrylamide and 2-hydroxyethylmethacrylate were purchased from Sigma-Aldrich (Milwaukee, WI). Polyethylene glycol (600) dimethacrylate (PEG200DMA) was purchased from Polysciences, Inc (Warrington, PA). T4 RNA Ligase and DNA Polymerase I (Klenow fragment) were obtained from New England BioLabs. T4 Polynucleotide Kinase (3' phosphatase-free) was purchased from Roche Diagnostics. Restriction enzymes BamHI and EcoRI were purchased from New England BioLabs. SUPERase-In was obtained from Ambion. Custom oligonucleotides with modifications were obtained from Operon Biotechnologies, and the exact sequences are attached as Appendix B. All buffers were prepared according to standard recipes, which are attached in Appendix C. Gold nanoparticles (15nm particle size) were purchased from Ted Pella, Inc. All radiochemicals were purchased from ICN Biochemicals, Inc. Neomycin sulfate was purchased from Sigma. NAP-5 columns were obtained from GE Healthcare.

6.3.2 Methods: *In-vitro* Hybridization.

The anchoring 5' acrydite oligonucleotide (sequence AC-SID-1, section C.1 in Appendix C) and its complementary oligonucleotide (sequence AC-SID-1C, section C.1 in Appendix C) were commercially obtained and resuspended to 1 mM in Tris buffer, 0.5 mM EDTA, pH 8. The complementary oligonucleotide was ³²P-end labeled at its 5'-hydroxy end with [γ -³²P] ATP. Reaction mixtures (10 μ L) consisted of 2 μ L of the 1 mM oligonucleotide, 5 μ L of TE buffer (pH 7.5), 1 μ L of 10X PNK buffer (Appendix B), 2 μ L of [γ -³²P]ATP and 0.7 μ L of 3'phosphatase-free polynucleotide kinase. After incubating the reaction mixtures at 37°C for 30 minutes, the labeled oligonucleotide was purified on a denaturing 12% polyacrylamide gel. The typical protocol followed was to add 10 μ L of 2X Formamide Buffer (Appendix B) to each reaction mixture before loading them onto the lanes of the 12% polyacrylamide gel. On carrying out electrophoresis for 90 minutes at 10 W, the bands were visualized by autoradiography and cut out using a sterile blade. The gel fragments were incubated overnight in 400 μ L of DNA/RNA Extraction Buffer (Appendix B) at room temperature, purified on a NAP-5 column according to the manufacturer's specifications, and concentrated by freeze-drying in a Savant Integrated SpeedVac System.

Annealing of DNA strands to form double helical DNA was tested by the increasing addition (0, 100, 200, 300 and 500 picomoles) of acrylated oligonucleotide to aliquots of complementary oligonucleotide (5000 cpm). Reaction mixtures (11.1 μ L) consisted of 5 μ L of the acrylated oligonucleotide, 5 μ L of the complementary oligonucleotide and 1.1 μ L of 10X Hybridization buffer (Appendix B). A negative

control reaction mixture consisted of 5 μL of RNase-free water, 5 μL of the complementary oligonucleotide and 1.1 μL of 10X Hybridization buffer. The reaction mixtures were heated to 90°C for 3 minutes and directly placed on ice. 2.2 μL of 6X Loading buffer (Appendix B) was added and the samples were analyzed by electrophoresis on a 12% poly(acrylamide-co-bisacrylamide) non-denaturing gel in cold conditions. Formation of the annealed duplexes was quantified using Typhoon phosphoimager and ImageQuant software (Molecular Dynamics). Hybridization conditions were optimized in different buffers such as water and various concentrations of Tris-HCl, pH 7.5.

6.3.3 Methods: *In-vitro* Restriction Enzyme Digestion.

Digestion of the annealed duplex was carried out by incubating the duplex with restriction enzyme BamHI and BamHI buffer at 37°C for 1 hour, as per the manufacturer's instructions. Reaction mixtures (11.1 μL) consisted of 10 μL of the hybridized oligonucleotides, 1.1 μL of 10X NEBuffer 3 (Appendix B), and 0.6 μL of BamHI enzyme. Control experiments were performed in the absence of BamHI at 37°C for 1 hour, or on ice. The digests were analyzed by electrophoresis on non-denaturing gel. Autoradiograms were quantified using Typhoon phosphoimager and ImageQuant software.

6.3.4 Methods: Synthesis and Characterization of Biocompatible Networks Loaded with DNA.

Novel poly(acrylamide-co-N,N' methylenebisacrylamide-co-acrylated DNA), poly(acrylamide-co-polyethylene glycol 200 dimethacrylate-co-acrylated DNA), poly(2-hydroxyethyl methacrylate-co-polyethylene glycol 600 dimethacrylate-co-acrylated DNA) networks of varying crosslinking densities were prepared *via* redox polymerization at 25°C in the loading lanes of a 12% non-denaturing gel. Typically, the non-denaturing gel was prepared using the 12% non-denaturing gel mix, and then 10 µL of the same mixture was added to 10 µL of the annealed duplex. Redox polymerization was carried out in the loading lanes using TEMED and 50% APS. The only difference while synthesizing the poly(acrylamide-co-polyethylene glycol 200 dimethacrylate-co-acrylated DNA) and poly(2-hydroxyethyl methacrylate-co-polyethylene glycol 600 dimethacrylate-co-acrylated DNA) networks was that homogeneous mixtures of desired mole ratios of 2-hydroxyethyl methacrylate and polyethylene glycol 600 dimethacrylate was first prepared, and then added to 10 µL of the annealed duplex. After polymerization, the unreacted annealed duplex and unhybridized ³²P-labeled oligonucleotides (from the earlier hybridization step) were efficiently eluted by electrophoresis. The polymer gels in the loading lanes were cut out and incubated in 10mM Tris-HCl buffer, pH 7.5. The rest of the base gel was dried and imaged as described earlier, in order to quantify the amount of unreacted annealed duplex, and hence the efficiency of the polymerization reaction.

6.3.5 Methods: *In-vitro* Kinetic Release of DNA Strands upon Restriction Enzyme and Temperature Triggers.

Kinetic release studies of ^{32}P -labeled DNA from poly(acrylamide-co-N,N'-methylenebisacrylamide-co-acrylated DNA) networks were conducted by incubating the networks under physiological conditions in the presence of BamHI and BamHI buffer, and by monitoring the release of the digested fragments by Cerenkov counting. Reaction mixtures (80 μL) in which the networks were incubated, consisted of 8 μL of 10X NEBuffer 3 (Appendix B), 70 μL of 10mM Tris-HCl buffer, pH 7.5, and 2 μL of BamHI enzyme. Control experiments were performed, by incubating the networks in the absence of BamHI, and by incubating the gels in the restriction endonuclease EcoRI, which does not recognize the BamHI recognition site. Temperature-responsive release characteristics of melted DNA strands were also investigated between 30°C and 85°C.

6.3.6 Methods: *In-vitro* Kinetic Release of DNA Strands upon Deoxynuclease I Trigger.

Release studies of ^{32}P -labeled DNA from poly(2-hydroxyethyl methacrylate-co-polyethylene glycol 600 dimethacrylate-co-acrylated DNA) networks were conducted by incubating them in the presence of DNase I (which is a non-specific endonuclease) and monitoring the release of the digested fragments by Cerenkov counting. Control experiments were performed by incubating the networks in the absence of DNase I.

The effect of the macromolecular architecture on the diffusion of DNA strands from the poly(2-hydroxyethyl methacrylate-co-polyethylene glycol 600 dimethacrylate-co-acrylated DNA) networks were investigated by synthesizing networks of varying crosslinking densities (0.15%, 0.22% and 0.45%).

6.3.7 Methods: Physiological validation of the platform: Downregulation of HIV-1 Tat/Rev mRNA.

The double stranded helix substrate was redesigned to include the catalytic 10-23 motif of a deoxyribozyme (Dz 5970, Section C.2, Appendix C) that can bind to and cleave HIV-1 TAT/Rev mRNA, along with the BamHI recognition site. While the original anchoring oligonucleotide (AC-SID-1) was unchanged, the complementary sequence (AC-SIC-1C) was modified to include the deoxyribozyme (AC-SID-AH, Section C.2, Appendix C). Annealed duplexes of AC-SID-1 and AC-SID-AH were then polymerized into poly(acrylamide-co-N,N' methylenebisacrylamide-co-acrylated DNA) networks.

The HIV-1 TAT/Rev mRNA was synthesized by run-off transcription of synthetic DNA templates under the control of promoters specific to T7 RNA polymerase. The full-length DNA templates were generated by performing a PCR reaction on the commercially obtained partially complementary sequences (Tat-up and Tat-down, Section C.2, Appendix C). Reaction mixtures (50 μ L) consisted of 2 μ L of the 0.1 mM DNA substrates, 5 μ L of 10X Klenow buffer, 5 μ L of 4 mM deoxyribonucleotide triphosphates, 37.5 μ L of water, and 0.5 μ L of the Klenow fragment of DNA Polymerase I. The PCR program consisted of 8 alternating cycles of 10°C for 30 seconds, and of 37°C for 30 seconds. The reaction was then incubated at

37°C for 8 minutes. The integrity of the DNA templates was tested by electrophoresis on a 2% agarose gel.

The DNA templates were then used for synthesizing the HIV-1 TAT/Rev mRNA. Reaction mixtures (20 µL) consisted of 10 µL of 2X T7 buffer, 5.1 µL of ribonucleotide triphosphates, 2.9 µL of water, 2 µL of DNA templates, 0.5 µL of T7 RNA Polymerase, and 0.5 µL of SUPERase-In at 37°C for 2 hours. The integrity of the transcripts was tested by electrophoresis on a 2% agarose gel.

The transcripts were then radiolabeled using [5'-³²P]pCp and T4 RNA Ligase and purified on a 12% poly(acrylamide-co-bisacrylamide) non-denaturing gel. 3'-end labeled HIV-1 TAT/Rev mRNA was incubated along with the poly(acrylamide-co-N,N'-methylenebisacrylamide-co-acrylated DNA) networks and BamHI under physiological conditions, and the cleaved RNA fragments were analyzed by analyzing aliquots on a denaturing 12% polyacrylamide gel. Autoradiograms were quantified using Typhoon phosphorimager and ImageQuant software.

6.3.8 Methods: Generation of the Neomycin Aptamer Spectrum

Conjugation of the neomycin aptamers to the gold nanoparticles was carried out *via* a linking 5'-thiol modified oligonucleotide (NAN-ANC-SH, Section C.3, Appendix C). The neomycin RNA aptamer was obtained from literature⁶⁰⁻⁶² and modified to its DNA sequence (NEOMYCIN) by replacing all the uridines with thymines. This sequence was extended in the 3' direction (NAN-NEO, Section C.3, Appendix C) so that it would be partially complementary to NAN-ANC-SH. Annealed duplexes of NAN-ANC-SH and NAN-NEO were conjugated to the surface of the gold nanoparticles by ligand exchange methods.

Single and double point mutations in the original aptamer sequence (NEOMYCIN) were used to generate a spectrum of neomycin binding aptamers of differing affinities, and their sequences are given in section C.4 of Appendix C. They were ^{32}P -labeled at their 5' ends and tested for binding efficacy by affinity chromatography using neomycin columns synthesized by conventional techniques. 1 g of freeze-dried Epoxy-activated Sepharose 6B was suspended in 3.5 mL distilled water and washed continuously for a few hours with approximately 500 mL RNase-free water. 1000 μmoles of neomycin sulfate (about 5 times excess ligand) was added to the medium and shaken continuously for 16 hours at 25°C. After washing away the excess ligand with RNase-free water, the remaining ligand groups were blocked by transferring the medium to 1M ethanolamine, pH 8.0 for at least 5 hours at 40°C. The medium was then washed alternately with 0.1 M acetate buffer, pH 4.0 containing 0.5 M NaCl, and followed by a wash with 0.1 M Tris-HCl buffer, pH 8.0 containing 0.5 M NaCl.

The neomycin columns were used to screen the single and double mutants for neomycin binding efficacy. Typically, 200 μL of medium was first equilibrated with about 5 column volumes of 1X neomycin binding buffer (5X composition is given in Appendix B). The ^{32}P -labeled aptamer was first equilibrated with 5X neomycin binding buffer at 37°C for 30 minutes, loaded on the column and allowed to further equilibrate for 30 minutes. The column was then washed with 1X neomycin binding buffer for 10-12 times and then with 6M urea solution. Each wash was allowed to proceed for 5 minutes, followed by spinning of the column at 3000 rpm to collect the wash liquid. The ^{32}P -labeled aptamer in the collected washes were then analyzed by Cerenkov counting.

6.3.9 Methods: Functionalization and characterization of gold nanoparticles

Gold nanoparticles (Au NPs) with an average diameter of 15.6 nm (Ted Pella, Inc.) were obtained suspended in water at a concentration of 330 pm (1.4×10^{11} particles/mL). No preservatives were used to stabilize the gold colloid.

Annealed duplexes of NAN-ANC-SH and NAN-NEO were conjugated to the surface of the gold nanoparticles by ligand exchange methods. The disulfide bonds in the linking oligonucleotide (NAN-ANC-SH) were reduced prior to mixing with the Au colloid. Reaction mixtures (17 μ L) consisted of 100 μ M of annealed duplex, 175 mM phosphate buffer and 1000 mM dithiothreitol at 37°C for 16 hours. The solutions of deprotected DNA were purified through desalting NAP-5 columns, and the amount of DNA from each column was determined by reading the absorbance of the solutions at 260 nm. The freshly deprotected DNA was then added to 1 mL of the Au colloid, 10 μ L of 1% sodium dodecyl sulfate and 10 μ L of 5M NaCl, in order to functionalize the Au NPs. The colloid was buffered with 1X PBS (10 X composition is given in Appendix B) and the NaCl concentration was brought to 0.2 M in a stepwise manner over 5 days. Agarose gel electrophoresis was used as a diagnostic tool for confirming that the gold nanoparticles were functionalized by the annealed duplex.

Surface coverage densities of the DNA were quantified by using oligonucleotides with fluorescent dyes at the 3' end, and were optimized by varying buffer ionic strengths, reaction times and sonication. β -mercaptoethanol (ME) was added (final concentration 12 mM) to fluorophore-labeled oligonucleotide-modified nanoparticles. After incubating for 18 h at room temperature with constant shaking, the solutions containing displaced oligonucleotides were separated from the gold by

centrifugation of the gold nanoparticle aggregates. Care was taken to keep the pH and ionic strength of the sample and calibration standard solutions the same for all measurements. The fluorescence maximums, obtained from the Bio-Tek Fluorescence Spectrophotometer, were converted to molar concentrations of the 3'-fluorophore-labeled, 5' thiol modified oligonucleotide by interpolation from a standard linear calibration curve. Standard curves were prepared with known concentrations of fluorophore-labeled oligonucleotides using identical buffer pH, salt, and mercaptoethanol concentrations. The average number of oligonucleotides per particle was obtained by dividing the molar concentration by the original Au NP concentration. Normalized surface coverage values were then calculated by dividing by the estimated particle surface area.

Substrate non-specific (DNase I) enzymes were used to trigger the release of fluorescent neomycin immobilized onto gold nanoparticles. The neomycin was fluorescently labeled with the dye Tetramethylrhodamine (maximal excitation at 555 nm, maximal emission 580 nm, molecular weight is 1326 Da) in order to monitor release rates.

6.4 Results and Discussions

We reasoned that covalently tethered nucleic acid sequences in synthetic polymer networks would be amenable to the action of their cognate enzymes used in gene cloning and analysis, and release kinetics would be governed by scission rates and the polymer macromolecular structure. Early efforts to chemically crosslink 5'-amino modified DNA sequences via conventional zero length crosslinkers⁶³ in interpenetrating poly(acrylic acid) and poly(allylamine) chains resulted in inefficient

gelation and poor mechanical characteristics of polymer networks. This could be due to heterogeneous concentrations of reactants in reaction mixtures due to difficulties encountered in mixing and poor diffusion of DNA into the macromolecular architecture. Since we hypothesized that redox polymerization would pre-empt some of these problems, we redesigned all our constructs with 5'-acrydite functionality, which would anchor the DNA duplex into the backbone during redox polymerization.

Our first construct involved hybridizing two custom oligonucleotides, a 5'-acrydite sequence, and another sequence bearing partial complementarity, which was radiolabeled prior to hybridization (Figure 6.4). The partial double stranded region was programmed with the recognition site of the restriction endonuclease BamHI. We chose a type II restriction endonuclease as our model enzyme as these enzymes have sequence specific interactions with DNA.

In-vitro hybridization conditions were optimized in various concentrations of Tris buffer and water, and magnesium was determined to be critical for hybridization of the construct (Figure 6.5, lane 4). Hybridization was inefficient in water (Figure 6.5, lane 2) and 20 mM Tris buffer (Figure 6.5, lane 3). About 10% of the complementary oligonucleotide self-annealed. The functional monomers used for polymer synthesis had no effect on hybridization efficiency (data not shown).

The ability of the annealed duplex to serve as a substrate for the restriction enzyme BamHI was confirmed by carrying out digestion in BamHI (Figure 6.6, lane 4). In the absence of BamHI, the annealed duplex remained stable on ice (Figure 6.6, lane 2) and at 37°C (Figure 6.6, lane 3). These control experiments were carried out in BamHI buffer, which did not disrupt the annealed duplex.

During the redox polymerization, unhybridized single stranded DNA (from the earlier hybridization step) and unreacted annealed duplex get entangled in the

macromolecular chains, and interfere with the analysis. We synthesized poly(acrylamide-co-N,N' methylenebisacrylamide-co-acrylated DNA) networks in the loading lanes of non-denaturing gels, in order to facilitate the elution of the unincorporated DNA by electrophoresis. Various control experiments were performed to characterize the process. In order to test if the anchoring of the annealed duplex was due to the acrylated oligonucleotide (AC-SID-1), the ^{32}P -labeled complementary oligonucleotide (AC-SID-1C) was polymerized without the acrylated oligonucleotide and eluted readily from the network during electrophoresis (Figure 6.7, lane 3). On the other hand, the annealed duplex was covalently incorporated into the network (Figure 6.7, lane 4). Quantification *via* phosphoimaging indicated 70% capture, 25% unincorporated annealed duplex, and 5% ^{32}P -labeled oligonucleotide. To conclusively demonstrate that Watson-Crick pairing between the acrylated oligonucleotide and the complementary oligonucleotide, and not physical entanglement, is responsible for the incorporation of DNA, a labeled oligonucleotide of similar size and a non-complementary sequence to the acrylated oligonucleotide was polymerized into the network along with the acrylated oligonucleotide. As annealing did not occur between the two strands, the oligonucleotide eluted from the network during electrophoresis, with the same rate of migration as the complementary oligonucleotide (Figure 6.7, lane 5).

The poly(acrylamide-co-N,N' methylenebisacrylamide-co-acrylated DNA) networks were then incubated with BamHI to evaluate their potential as controlled release vehicles. We observed that the DNA helix was readily cleaved and diffusion of the cleaved fragments through the macromolecular chains resulted in Fickian release profiles (Figure 6.8). Incubating the hydrogels in the absence of BamHI did not result in DNA release from the network. Furthermore, EcoRI, a restriction

endonuclease which does not recognise the BamHI recognition site, did not trigger DNA release. It is particularly important to note that EcoRI has a similar size (molecular weight of 31057 Da) compared to BamHI (molecular weight of 24569), and that these two enzymes are among the most efficient restriction enzymes known. The efficiency of these enzymes is enhanced by programming flanking sequences, which increase the binding affinity of the enzyme to the recognition site. Release profiles of delayed kinetics can be envisioned by using restriction enzymes of lesser native efficiency, or by using such enzymes without their flanking sequences. The star activity of these enzymes was curtailed by tightly controlling pH, using low concentrations of glycerol, and avoiding the use of organic solvents or alternate divalent cations.

The annealed duplex anchored in the hydrogel can be melted by raising the temperature to the melting temperature of the double stranded region, resulting in the release of the labeled complementary oligonucleotide. Figure 6.9 highlights the temperature responsive release characteristics which matched the theoretical melting temperature (58°C). We conclude that sequence is an additional parameter to tune the release profiles from this platform, since melting temperature is a direct function of G-C pairs.

We next investigated the clinical viability of the platform *in vitro* by redesigning the DNA construct to encode an RNA-cleaving deoxyribozyme that possessed the catalytic 10-23 motif and specifically cleaved the overlapping sequences of the Tat and Rev exons^{64, 65}. These genes are critical for viral replication and pathogenesis, and their mRNAs are attractive targets for gene therapy⁶⁶ (Figure 6.10). We hypothesized that incubation of a polymer network loaded with deoxyribozyme with BamHI, would result in the release of the deoxyribozyme, and

down regulate the HIV-1 TAT/Rev mRNA by trans-esterification (Figure 6.11). Incubation of the HIV-1 TAT/Rev mRNA along with the deoxyribozyme-loaded network and BamHI resulted in specific cleavage (Figure 6.12, lane 3). BamHI action on a network lacking the deoxyribozyme construct had no effect on the HIV-1 Tat/Rev RNA (Figure 6.12, lane 2). We conclude that our platform could be used for siRNA and ribozyme mediated therapy.

We reasoned that macromolecular structure could affect the DNA diffusional rates and synthesized poly(2-hydroxyethyl methacrylate-co-polyethylene glycol 600 dimethacrylate-co-acrylated DNA) networks of varying crosslinking densities. These biocompatible networks were triggered to release DNA by the non-specific endonuclease DNase I. Figure 6.13 highlights the release characteristics of biocompatible gels of varying crosslinking densities on treatment with DNase I, and we conclude that crosslinking density, which can be correlated with molecular parameters such as mesh size, can be used to tailor release rates.

Delivery remains a huge obstacle to the development of RNAi-based therapeutics. Conventional thinking leans towards the delivery of double stranded RNAs from which siRNAs are derived by the action of Dicer, or the direct delivery of the artificial siRNAs⁶⁷. The caveat of inserting foreign vector sequences into chromosomes is that if the process is not tightly untargeted, it might result in insertional activation or inactivation of critical genes. A variety of strategies to express interfering RNAs with the use of plasmid and viral vector-based cassettes have been developed. Intravenous administration of siRNAs requires siRNAs to be resistant to nucleases via modification^{68, 69}, and conjugated with a ligand such as folic acid, galactosamine or transferrin, to enhance specificity. Certain tissues of the body such as the respiratory, urogenital and ocular tissues can take up siRNAs after topical

application or direct injection of naked siRNAs alone or in complexes with cationic lipids used for in vitro transfection, but most tissues are refractory to the direct uptake of siRNAs. Recently, gold nanoparticles, in the size range of 2-30 nm, have generated much excitement due to their amenability to be taken up by the cell, without causing negative reactions, although the exact mechanism of uptake remains unclear.

The functionalization of gold nanoparticles by oligonucleotides received much attention and has been well characterized in the last decade^{9, 70-77}. We believed that gold nanoparticles conjugated with nucleic acid aptamers, selected for various therapeutics via SELEX^{1, 2, 60, 61, 78-83}, would serve as excellent moiety shuttles for therapeutics. Furthermore, we rationalized that if we could functionalize the nanoparticles with aptamers bearing different affinities towards the same ligand, we could achieve unprecedented, graded control of release rates. Such systems have immense potential, as the nanoparticles can be injected into the bloodstream, can be targeted to specific cells using ligands, and can be passivated to immune surveillance and opsonization using polyethylene glycol. The size of the nanoparticles can be finely controlled to facilitate uptake by cells and the loading density of therapeutic. Recently, 2nm gold particles have been functionalized with high grafting density (~70 molecules of paclitaxel per nanoparticle).

By covalently incorporating specific, multiple RNA sequences onto gold nanoparticles (Figure 6.14), control of multiple therapeutic release can be achieved by (i) incorporating different aptamer-drug complexes of different drug affinities; (ii) altering the stability of the RNA molecules leading to programmable RNA degradation and subsequent drug release; (iii) specific scission profiles of nucleic acid sequences by exonucleases or endonucleases; and (iv) changing the temperature resulting in the loss of RNA tertiary structure leading to release of drug due to loss of

affinity with the drug. The RNA molecules that bind molecules suggested in this work are relatively small and have been shown to fall under the immunological radar.

We chose neomycin as the model antibiotic and evaluated the binding efficacies of the neomycin binding aptamer and certain point mutants, the sequences of which have been attached in section C.4 of Appendix C. Neomycin, paromomycin, and tobramycin are the oldest known class of broad-spectrum antibacterial agents with potent activity against Gram-positive and Gram-negative microorganisms, as well as mycobacteria. The aminoglycoside antibiotics bind various sites and motifs of RNA, and in so doing inhibit critical RNA-mediated functions. Neomycin B has also been shown to inhibit the function of various important ribozymes such as the group I ribozyme, hammerhead ribozyme and human hepatitis delta virus ribozymes. The positively charged amine groups compete with Mg^{2+} ions sites to bind various sites in RNA.

We tested the binding efficacy of the wild type neomycin DNA aptamer via affinity chromatography. Binding between neomycin and its cognate aptamer was robust when the column was washed with neomycin binding buffer, but dissociation of the complex, triggered by urea washes, resulted in release of the aptamer from the column (Figure 6.15). Furthermore, comparison of binding between two mutants (G7T-T17A and T17C) demonstrated significant differences in the binding patterns towards neomycin (Figure 6.16). We conclude that the substitution of the G-T pair with a T-A pair weakens the neomycin aptamer secondary structure, and hence reduces its affinity to neomycin. On the other hand, substitution of thymine with cytosine results in a G-C pair instead of a G-T pair, which tightens the neomycin aptamer structure and might increase its affinity to neomycin. Our studies are

supported by the solution structure of the neomycin binding aptamer and neomycin⁶²,

84

The neomycin aptamers were conjugated to the gold nanoparticles via the linking sequence NAN-ANC-SH. For the first time in the literature, agarose gel electrophoresis was used as a diagnostic tool to confirm the functionalization of gold nanoparticles with DNA (data not shown). While gold nanoparticles colloids are neutral and fail to migrate in the electric field, the DNA conjugated to the nanoparticles migrate and carry the gold nanoparticles with them. Homogeneous bands are obtained, since saturated concentrations of oligonucleotides are used to functionalize the gold nanoparticles.

Future directions of this work include the conjugation of multiple neomycin binding mutant aptamers with differing affinity to neomycin on the gold nanoparticles, and the controlled release of fluorescent neomycin from these mutants. We are also currently conjugating gold nanoparticles with aptamers for different therapeutics, in order to achieve intracellular delivery of multiple drugs from the same platform.

6.5 List of References

1. Ellington, A.D. & Szostak, J.W. In vitro selection of RNA molecules that bind specific ligands. *Nature* **346**, 818-822 (1990).
2. Tuerk, C. & Gold, L. Systematic evolution of ligands by exponential enrichment: RNA ligands to bacteriophage T4 DNA polymerase. *Science* **249**, 505-510 (1990).

3. Fedor, M.J. & Williamson, J.R. The catalytic diversity of RNAs. *Nat. Rev. Mol. Cell Biol.* **6**, 399-412 (2005).
4. Kim, D.H. & Rossi, J.J. Strategies for silencing human disease using RNA interference. *Nat. Rev. Genet.* **8**, 173-184 (2007).
5. Serganov, A. & Patel, D.J. Ribozymes, riboswitches and beyond: regulation of gene expression without proteins. *Nat. Rev. Genet.* **8**, 776-790 (2007).
6. Langer, R. & Peppas, N.A. Advances in biomaterials, drug delivery, and bionanotechnology. *AIChE J.* **49**, 2990-3006 (2003).
7. Venkatesh, S., Byrne, M.E., Peppas, N.A. & Hilt, J.Z. Applications of biomimetic systems in drug delivery. *Exp. Opin. Drug Del.* **2**, 1085-1096 (2005).
8. Pack, D.W., Hoffman, A.S., Pun, S. & Stayton, P.S. Design and development of polymers for gene delivery. *Nat. Rev. Drug Discov.* **4**, 581-593 (2005).
9. Rosi, N.L. et al. Oligonucleotide-Modified Gold Nanoparticles for Intracellular Gene Regulation. *Science* **312**, 1027-1030 (2006).
10. Liu, Y. & Franzen, S. Factors Determining the Efficacy of Nuclear Delivery of Antisense Oligonucleotides by Gold Nanoparticles. *Bioconjugate Chem.* **19**, 1009-1016 (2008).
11. Byrne, M.E., Park, K. & Peppas, N.A. Molecular imprinting within hydrogels. *Adv. Drug Del. Rev.* **54**, 149-161 (2002).
12. Tanaka, T. et al. Phase transitions in ionic gels. *Phys. Rev. Lett.* **45**, 1636-1639 (1980).
13. Chen, G. & Hoffman, A.S. Graft copolymers that exhibit temperature-induced phase transitions over a wide range of pH. *Nature* **373**, 49-52 (1995).

14. Yoshida, R. et al. Comb-type grafted hydrogels with rapid de-swelling response to temperature changes. *Nature* **374**, 240-242 (1995).
15. Stayton, P.S. et al. Control of protein-ligand recognition using a stimuli-responsive polymer. *Nature* **378**, 472-474 (1995).
16. Suzuki, A. & Tanaka, T. Phase transition in polymer gels induced by visible light. *Nature* **346**, 345-347 (1990).
17. Zrinyi, M., Szabo, D., Filipcsei, G. & Feher, J. Electrical and magnetic field-sensitive smart polymer gels. *Polym. Gels Networks*, 309-355 (2002).
18. Szabo, D., Szeghy, G. & Zrinyi, M. Shape Transition of Magnetic Field Sensitive Polymer Gels. *Macromolecules* **31**, 6541-6548 (1998).
19. Kwon, I.C., Bae, Y.H. & Kim, S.W. Electrically erodible polymer gel for controlled release of drugs. *Nature* **354**, 291-293 (1991).
20. Osada, Y., Okuzaki, H. & Hori, H. A polymer gel with electrically driven motility. *Nature* **355**, 242-244 (1992).
21. Tanaka, T., Nishio, I., Sun, S.T. & Ueno-Nishio, S. Collapse of gels in an electric field. *Science* **218**, 467-469 (1982).
22. Lackey, C.A., Press, O.W., Hoffman, A.S. & Stayton, P.S. A Biomimetic pH-Responsive Polymer Directs Endosomal Release and Intracellular Delivery of an Endocytosed Antibody Complex. *Bioconjugate Chem.* **13**, 996-1001 (2002).
23. Shibayama, M., Suetoh, Y. & Nomura, S. Structure Relaxation of Hydrophobically Aggregated Poly(N-isopropylacrylamide) in Water. *Macromolecules* **29**, 6966-6968 (1996).

24. Shibayama, M., Mizutani, S.-y. & Nomura, S. Thermal Properties of Copolymer Gels Containing N-Isopropylacrylamide. *Macromolecules* **29**, 2019-2024 (1996).
25. Idziak, I., Avoce, D., Lessard, D., Gravel, D. & Zhu, X.X. Thermosensitivity of Aqueous Solutions of Poly(N,N-diethylacrylamide). *Macromolecules* **32**, 1260-1263 (1999).
26. Makhaeva, E.E., Tenhu, H. & Khokhlov, A.R. Behavior of poly(N-vinylcaprolactam) macromolecules in the presence of organic compounds in aqueous solution. *Polymer* **41**, 9139-9145 (2000).
27. Lozinsky, V.I. et al. Synthesis of N-vinylcaprolactam polymers in water-containing media. *Polymer* **41**, 6507-6518 (2000).
28. Mikheeva, L.M. et al. Microcalorimetric study of thermal cooperative transitions in poly(N-vinylcaprolactam) hydrogels. *Macromolecules* **30**, 2693-2699 (1997).
29. Serres, A., Baudys, M. & Kim, S.W. Temperature and pH-sensitive polymers for human calcitonin delivery. *Pharm. Res.* **13**, 196-201 (1996).
30. Ramkissoon-Ganorkar, C., Liu, F., Baudys, M. & Kim, S.W. Effect of molecular weight and polydispersity on kinetics of dissolution and release from pH/temperature-sensitive polymers. *J. Biomater. Sci. Polym. Ed.* **10**, 1149-1161 (1999).
31. Aoki, T. et al. Temperature-Responsive Interpenetrating Polymer Networks Constructed with Poly(acrylic acid) and Poly(N,N-dimethylacrylamide). *Macromolecules* **27**, 947-952 (1994).

32. Shibamura, T. et al. Thermosensitive Phase-Separation Behavior of Poly(acrylic acid)-graft-poly(N,N-dimethylacrylamide) Aqueous Solution. *Macromolecules* **33**, 444-450 (2000).
33. Grayson, A.C.R. et al. Multi-pulse drug delivery from a resorbable polymeric microchip device. *Nat Mater* **2**, 767-772 (2003).
34. Mamada, A., Tanaka, T., Kungwachakun, D. & Isie, M. Photoinduced Phase Transition of Gels. *Macromolecules* **23**, 1517-1519 (1990).
35. Miyata, T., Asami, N. & Urugami, T. A reversibly antigen-responsive hydrogel. *Nature* **399**, 766-769 (1999).
36. Petka, W.A., Hardin, J.L., McGrath, K.P., Wirtz, D. & Tirrell, D.A. Reversible hydrogels from self-assembling artificial proteins. *Science* **281**, 389-392 (1998).
37. Wang, C., Stewart, R.J. & Kopecek, J. Hybrid hydrogels assembled from synthetic polymers and coiled-coil protein domains. *Nature* **397**, 417-420 (1999).
38. Ehrick, J.D. et al. Genetically engineered protein in hydrogels tailors stimulus-responsive characteristics. *Nat. Mat.* **4**, 298-302 (2005).
39. Obaidat, A.A. & Park, K. Characterization of glucose dependent gel-sol phase transition of the polymeric glucose-concanavalin A hydrogel system. *Pharm. Res.* **13**, 989-995 (1996).
40. Schneider, J.P. et al. Responsive Hydrogels from the Intramolecular Folding and Self-Assembly of a Designed Peptide. *J. Am. Chem. Soc.* **124**, 15030-15037 (2002).
41. Collier, J.H. et al. Thermally and photochemically triggered self-assembly of peptide hydrogels. *J. Am. Chem. Soc.* **123**, 9463-9464 (2001).

42. Nowak, A.P. et al. Rapidly recovering hydrogel scaffolds from self-assembling diblock copolypeptide amphiphiles. *Nature* **417**, 424-428 (2002).
43. Nagahara, S. & Matsuda, T. Hydrogel formation via hybridization of oligodeoxyribonucleotides derivatized in water-soluble vinyl polymers. *Polym. Gels Networks* **4**, 111-127 (1996).
44. Um, S.H. et al. Enzyme-catalysed assembly of DNA hydrogel. *Nat. Mat.* **5**, 797-801 (2006).
45. Deming, T.J. Facile synthesis of block copolypeptides of defined architecture. *Nature* **390**, 386-389 (1997).
46. Sperinde, J.J. & Griffith, L.G. Control and Prediction of Gelation Kinetics in Enzymatically Cross-Linked Poly(ethylene glycol) Hydrogels. *Macromolecules* **33**, 5476-5480 (2000).
47. Sperinde, J.J. & Griffith, L.G. Synthesis and Characterization of Enzymically-Crosslinked Poly(ethylene glycol) Hydrogels. *Macromolecules* **30**, 5255-5264 (1997).
48. Hu, B.-H. & Messersmith, P.B. Rational Design of Transglutaminase Substrate Peptides for Rapid Enzymatic Formation of Hydrogels. *J. Am. Chem. Soc.* **125**, 14298-14299 (2003).
49. Collier, J.H. & Messersmith, P.B. Enzymatic modification of self-assembled peptide structures with tissue transglutaminase. *Bioconjugate Chem.* **14**, 748-755 (2003).
50. Sanborn, T.J., Messersmith, P.B. & Barron, A.E. In situ crosslinking of a biomimetic peptide-PEG hydrogel via thermally triggered activation of factor XIII. *Biomater.* **23**, 2703-2710 (2002).

51. Sakiyama-Elbert, S.E. & Hubbell, J.A. Controlled release of nerve growth factor from a heparin-containing fibrin-based cell ingrowth matrix. *J. Controlled Release* **69**, 149-158 (2000).
52. Wood, M.D. & Sakiyama-Elbert, S.E. Release rate controls biological activity of nerve growth factor released from fibrin matrices containing affinity-based delivery systems. *J. Biomed. Mater. Res.* **84**, 300-312 (2008).
53. Willerth, S.M. & Sakiyama-Elbert, S.E. Approaches to neural tissue engineering using scaffolds for drug delivery. *Adv. Drug Del. Rev.* **59**, 325-338 (2007).
54. Taylor, S.J. & Sakiyama-Elbert, S.E. Effect of controlled delivery of neurotrophin-3 from fibrin on spinal cord injury in a long term model. *J. Controlled Release* **116**, 204-210 (2006).
55. Sakiyama-Elbert, S.E. & Hubbell, J.A. Development of fibrin derivatives for controlled release of heparin-binding growth factors. *J. Controlled Release* **65**, 389-402 (2000).
56. Maxwell, D.J., Hicks, B.C., Parsons, S. & Sakiyama-Elbert, S.E. Development of rationally designed affinity-based drug delivery systems. *Acta Biomater.* **1**, 101-113 (2005).
57. Willerth, S.M. et al. Rationally designed peptides for controlled release of nerve growth factor from fibrin matrices. *J. Biomed. Mater. Res. A* **80A**, 13-23 (2006).
58. Andrades, J.A. et al. Production of a recombinant human basic fibroblast growth factor with a collagen binding domain. *Protoplasma* **218**, 95-103 (2001).

59. Andrades, J.A. et al. A recombinant human TGF-beta1 fusion protein with collagen-binding domain promotes migration, growth, and differentiation of bone marrow mesenchymal cells. *Exp. Cell Res.* **250**, 485-498 (1999).
60. Famulok, M. & Huettenhofer, A. In Vitro Selection Analysis of Neomycin Binding RNAs with a Mutagenized Pool of Variants of the 16S rRNA Decoding Region. *Biochemistry* **35**, 4265-4270 (1996).
61. Wallis, M.G., von Ahsen, U., Schroeder, R. & Famulok, M. A novel RNA motif for neomycin recognition. *Chem. Biol.* **2**, 543-552 (1995).
62. Jiang, L. et al. Saccharide-RNA recognition in a complex formed between neomycin B and an RNA aptamer. *Structure* **7**, 817-827 (1999).
63. Grabarek, Z. & Gergely, J. Zero-length crosslinking procedure with the use of active esters. *Anal. Biochem.* **185**, 131-135 (1990).
64. Unwalla, H. & Banerjea, A.C. Novel mono- and di-DNA-enzymes targeted to cleave TAT or TAT-REV RNA inhibit HIV-1 gene expression. *Antiviral Res.* **51**, 127-139 (2001).
65. Unwalla, H. & Banerjea, A.C. Inhibition of HIV-1 gene expression by novel macrophage-tropic DNA enzymes targeted to cleave HIV-1 TAT/Rev RNA. *Biochem. J.* **357**, 147-155 (2001).
66. Stevenson, M. Dissecting HIV-1 through RNA interference. *Nat. Rev. Immunol.* **3**, 851-858 (2003).
67. Stevenson, M. Therapeutic potential of RNA interference. *New Engl. J. Med.* **351**, 1772-1777 (2004).
68. Morrissey, D.V. et al. Potent and persistent in vivo anti-HBV activity of chemically modified siRNAs. *Nat. Biotechnol.* **23**, 1002-1007 (2005).

69. Bumcrot, D., Manoharan, M., Koteliansky, V. & Sah, D.W.Y. RNAi therapeutics: a potential new class of pharmaceutical drugs. *Nat. Chem. Biol.* **2**, 711-719 (2006).
70. Mirkin, C.A., Letsinger, R.L., Mucic, R.C. & Storhoff, J.J. A DNA-based method for rationally assembling nanoparticles into macroscopic materials. *Nature* **382**, 607-609 (1996).
71. Park, S.-J. et al. The electrical properties of gold nanoparticle assemblies linked by DNA. *Angew. Chem. Int. Ed.* **39**, 3845-3848 (2000).
72. Storhoff, J.J. et al. What Controls the Optical Properties of DNA-Linked Gold Nanoparticle Assemblies? *J. Am. Chem. Soc.* **122**, 4640-4650 (2000).
73. Demers, L.M. et al. A Fluorescence-Based Method for Determining the Surface Coverage and Hybridization Efficiency of Thiol-Capped Oligonucleotides Bound to Gold Thin Films and Nanoparticles. *Anal. Chem.* **72**, 5535-5541 (2000).
74. Jin, R., Wu, G., Li, Z., Mirkin, C.A. & Schatz, G.C. What controls the melting properties of DNA-linked gold nanoparticle assemblies? *J. Am. Chem. Soc.* **125**, 1643-1654. (2003).
75. Thaxton, C.S., Hill, H.D., Georganopoulou, D.G., Stoeva, S.I. & Mirkin, C.A. A Bio-Bar-Code Assay Based upon Dithiothreitol-Induced Oligonucleotide Release. *Anal. Chem.* **77**, 8174-8178 (2005).
76. Hurst, S.J., Lytton-Jean, A.K.R. & Mirkin, C.A. Maximizing DNA Loading on a Range of Gold Nanoparticle Sizes. *Anal. Chem.* **78**, 8313-8318 (2006).
77. Kim, E.-Y. et al. A real-time PCR-based method for determining the surface coverage of thiol-capped oligonucleotides bound onto gold nanoparticles. *Nucleic Acids Res.* **34**, e54/51-e54/57 (2006).

78. Gold, L., Polisky, B., Uhlenbeck, O. & Yarus, M. Diversity of oligonucleotide functions. *Annu. Rev. Biochem.* **64**, 763-797 (1995).
79. Jhaveri, S., Rajendran, M. & Ellington, A.D. In vitro selection of signaling aptamers. *Nat. Biotechnol.* **18**, 1293-1297 (2000).
80. Hermann, T. & Patel, D.J. Adaptive recognition by nucleic acid aptamers. *Science* **287**, 820-825 (2000).
81. Koizumi, M. & Breaker, R.R. Molecular Recognition of cAMP by an RNA Aptamer. *Biochemistry* **39**, 8983-8992 (2000).
82. Wilson, C., Nix, J. & Szostak, J. Functional requirements for specific ligand recognition by a biotin-binding RNA pseudoknot. *Biochemistry* **37**, 14410-14419 (1998).
83. Lorsch, J.R. & Szostak, J.W. In vitro selection of RNA aptamers specific for cyanocobalamin. *Biochemistry* **33**, 973-982 (1994).
84. Jiang, L., Suri, A.K., Fiala, R. & Patel, D.J. Saccharide-RNA recognition in an aminoglycoside antibiotic-RNA aptamer complex. *Chem. Biol.* **4**, 35-50 (1997).

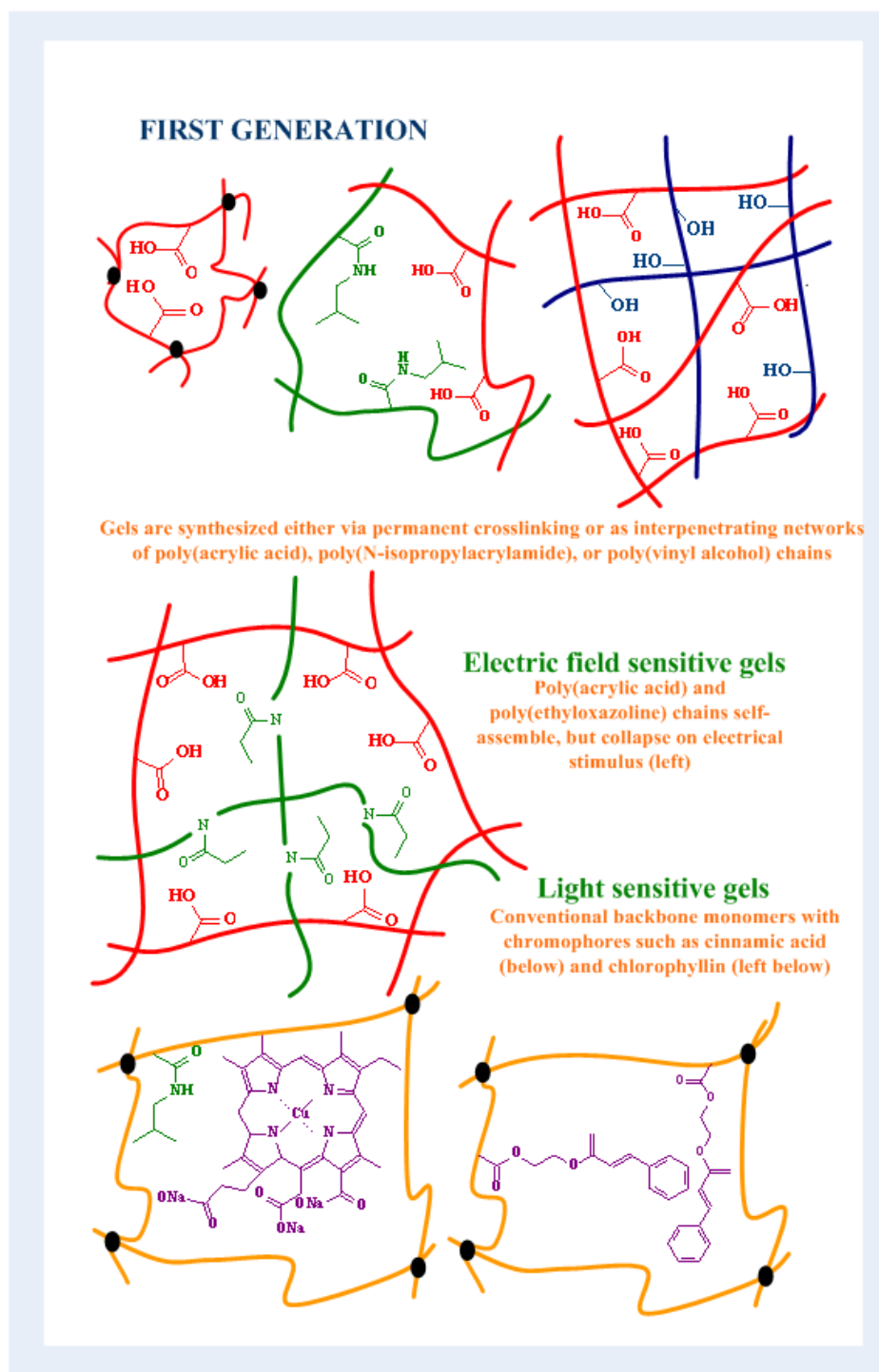


Figure 6.1 First Generation “Intelligent” Networks. These networks consisted of artificial materials which respond to physical and chemical changes in the environment such as pH, temperature, ionic strength, electric field, concentration gradients and light.

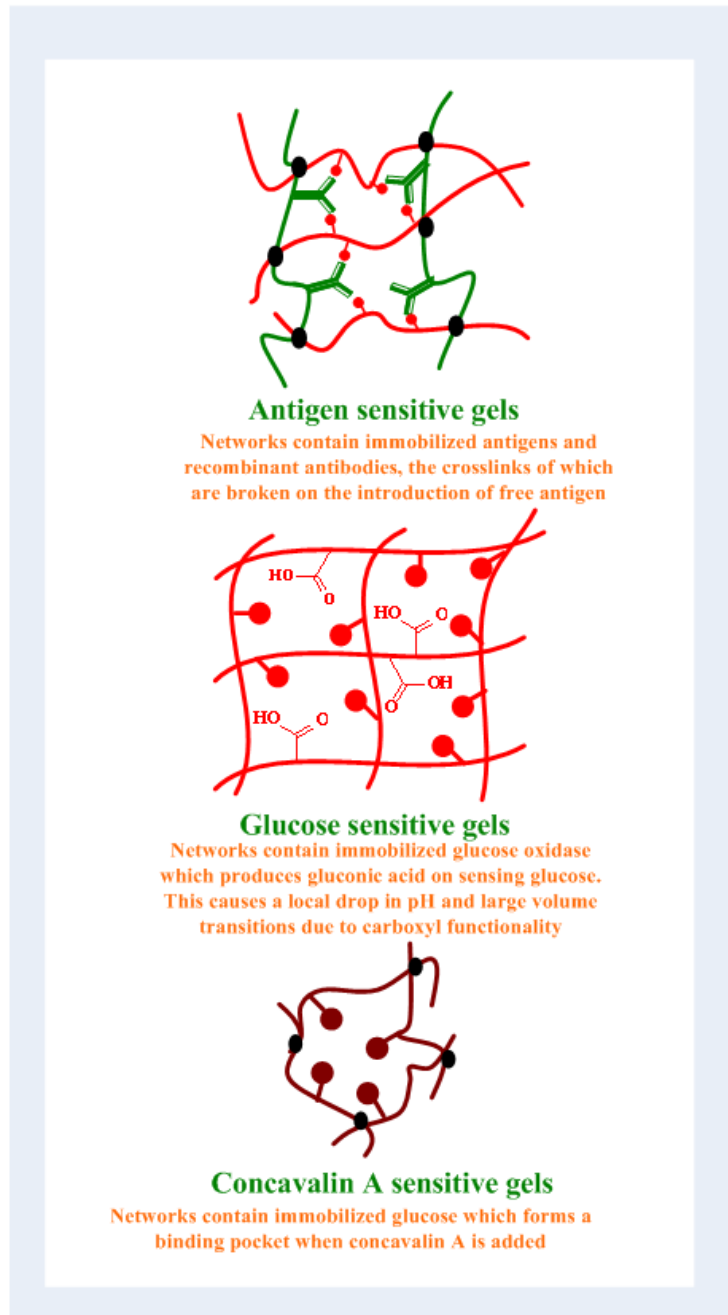


Figure 6.2 Second Generation “Intelligent” Networks. These networks consisted of protein molecules such as antibodies, enzymes, and receptors, which were immobilised within the network. The protein causes a local change, which is translated to observable volume transitions of the network.

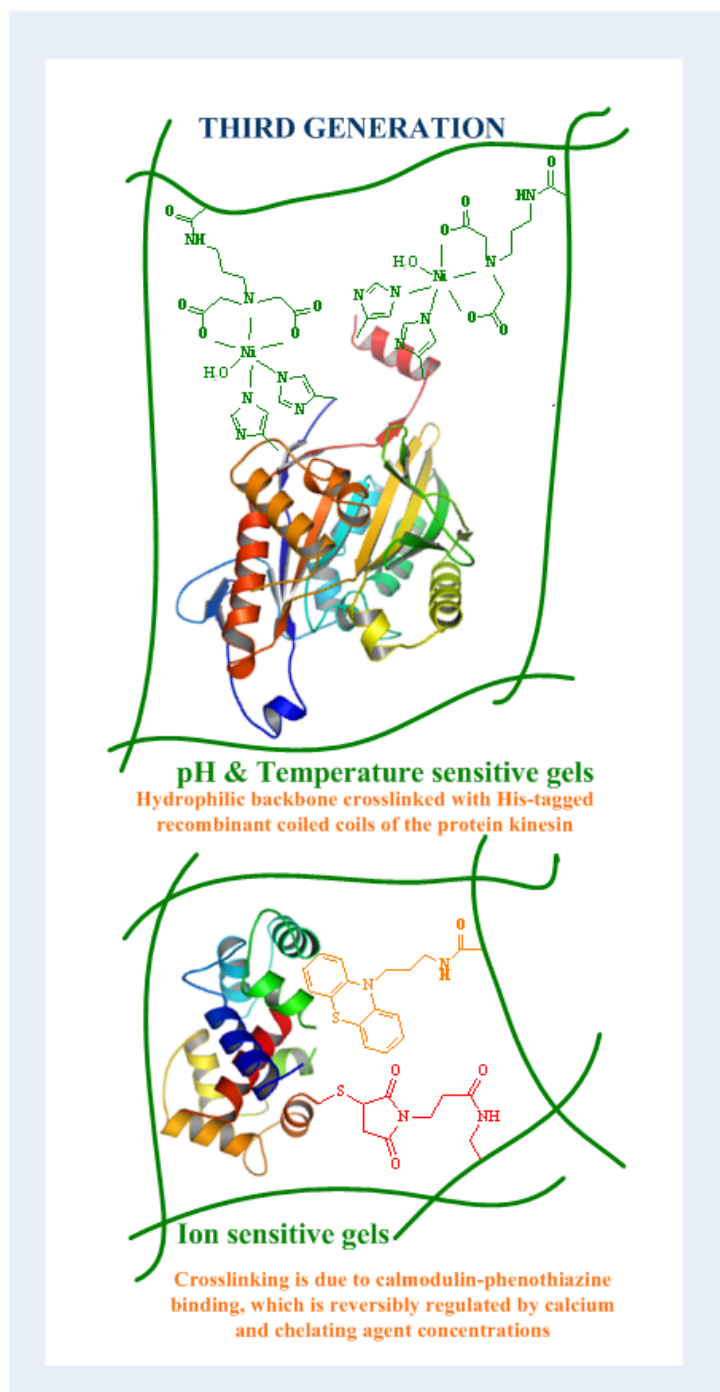


Figure 6.3 Third Generation “Intelligent” Networks. These networks consisted of proteins such as kinesin and calmodulin, which undergo conformational switches and hence demonstrate differential binding to ligands, due to the switching of ions and chelating agents

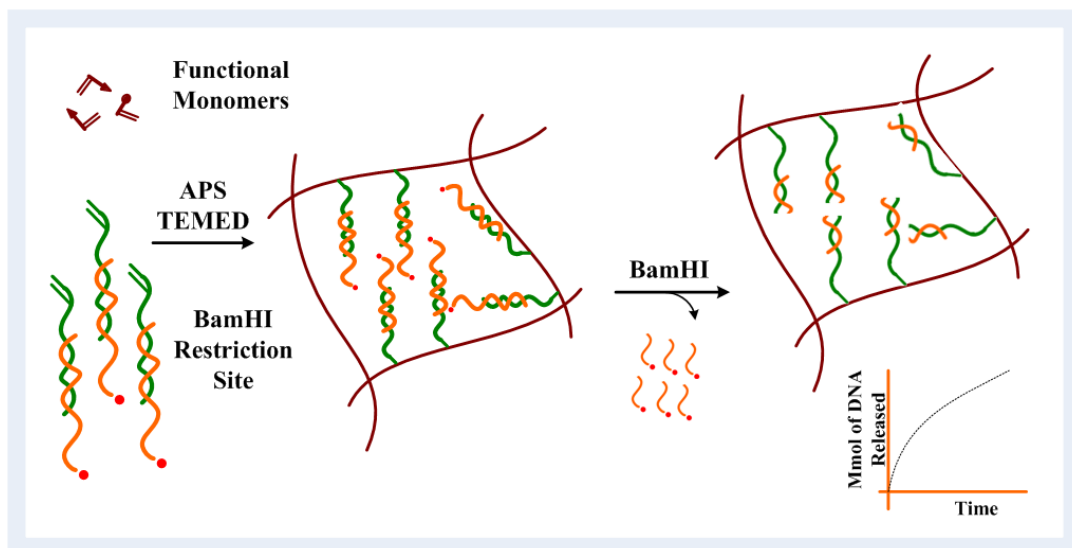


Figure 6.4 Controlled Release of Nucleic Acids from Synthetic Polymers via Enzymatic Triggers. APS and TEMED catalyzed polymerization yields a polymer network containing a DNA double helix. Restriction enzyme BamHI specifically cleaves the sequence and releases a short strand of DNA.

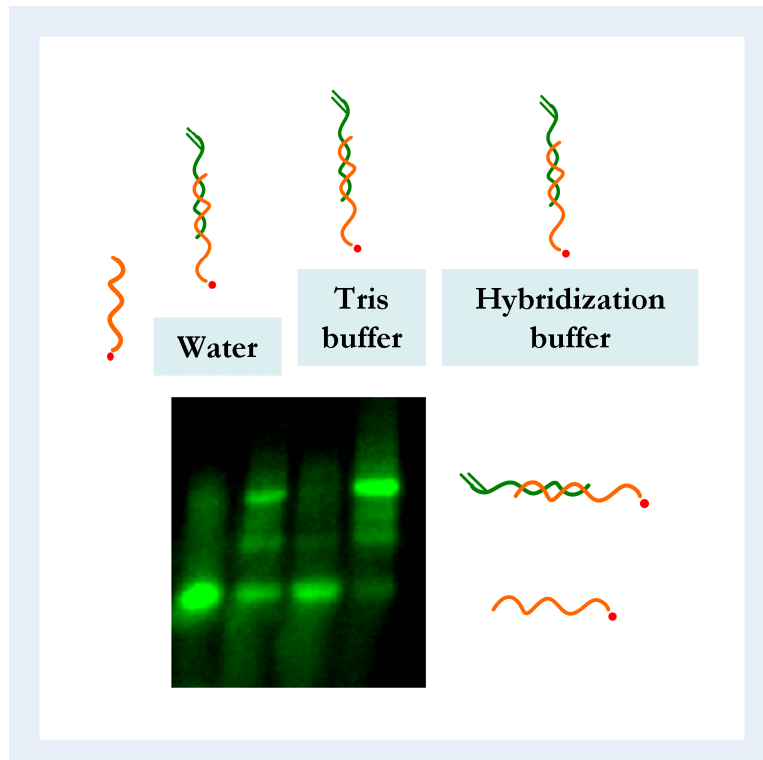


Figure 6.5 Optimization of DNA hybridization conditions. Mg^{2+} ions are critical for efficient hybridization of the acrydite oligonucleotide (green) and ^{32}P -labeled complementary oligonucleotide (lane 4). ^{32}P -labeled complementary oligonucleotide is used as control. Hybridization is inefficient in water and Tris buffer (lanes 2 and 3 respectively).

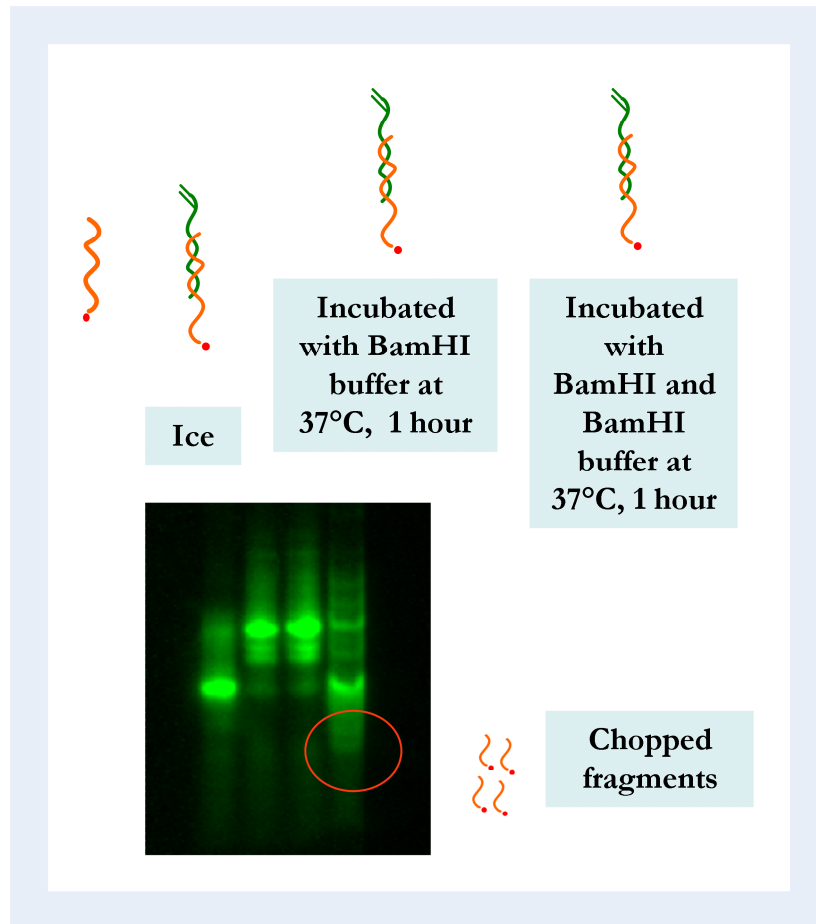


Figure 6.6 *In-vitro* restriction enzyme digestion. BamHI cleaves the annealed duplex (lane 4). The duplex is stable in the absence of BamHI (lane 3) and on ice (lane 2). ^{32}P -labeled complementary oligonucleotide is used as control.

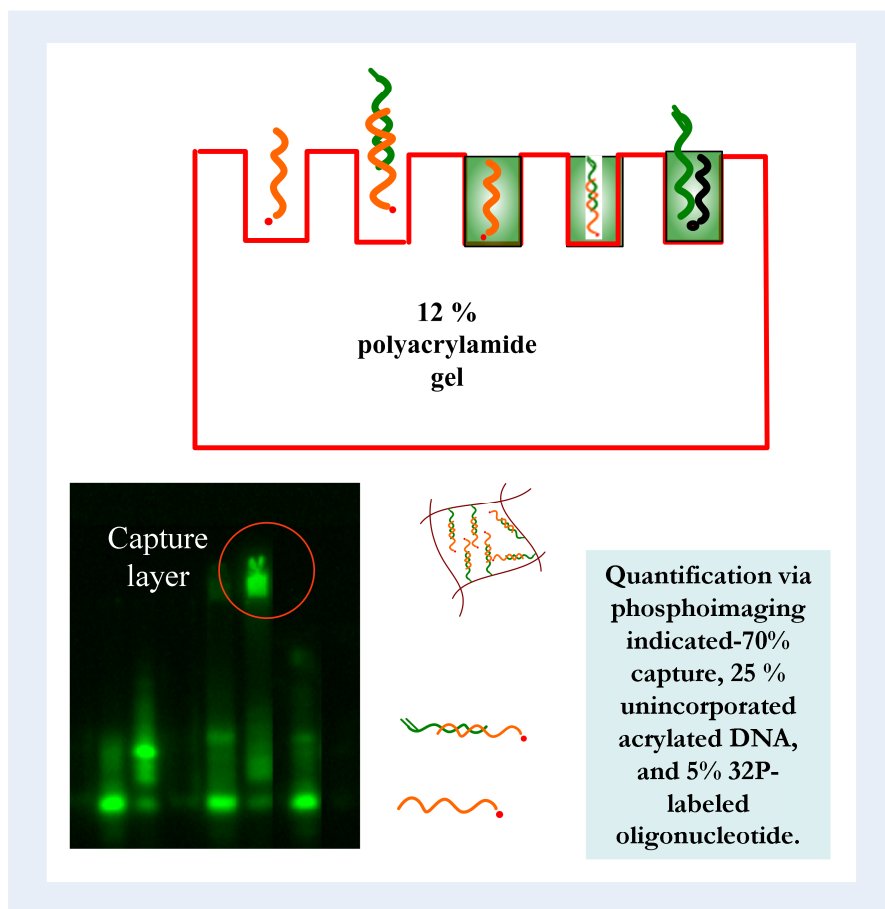


Figure 6.7 Covalent immobilization of acrylated annealed duplex. Annealed duplex is incorporated into the polymer network due to the presence of acrylated oligonucleotide (lane 4). ^{32}P -labeled AC-SID-1C is readily eluted during electrophoresis due to the absence of acrylated oligonucleotide (lane 3). Addition of non-complementary sequence to acrylated oligonucleotide, followed by elution, also results in non-incorporation of DNA into the gel (lane 5). ^{32}P -labeled AC-SID-1C and annealed duplex (lanes 1 and 2, respectively), are controls.

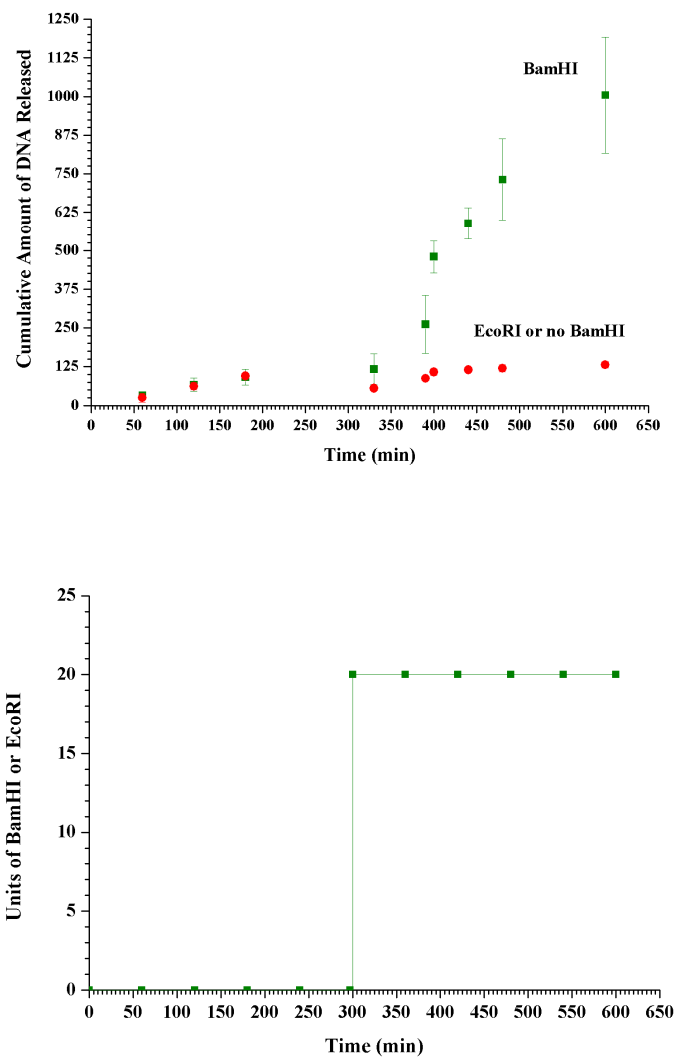


Figure 6.8 Tailored Release of DNA by Enzymatic Trigger. Tailored release of DNA by incubating the gels in BamHI at physiological conditions (■) as compared to incubating in buffer only with no enzyme(●).

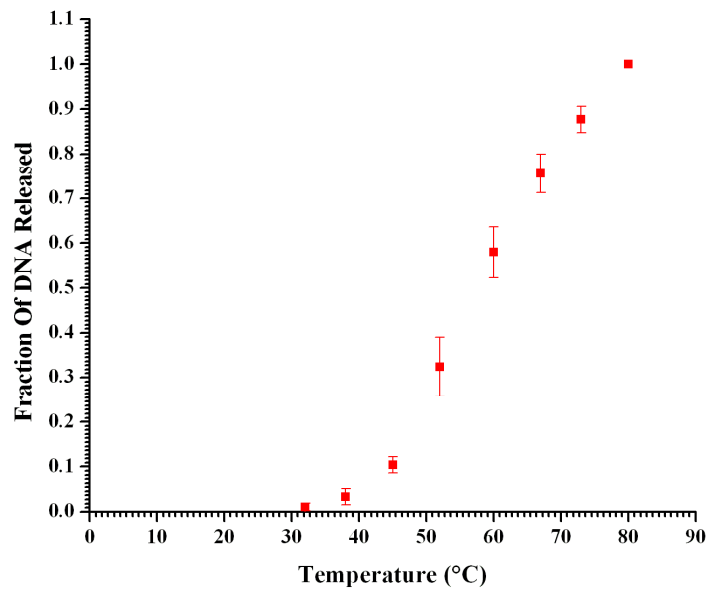


Figure 6.9 Tailored release of DNA by temperature ramp. Sigmoidal temperature dependent release of DNA (■). $N=5 \pm S.D.$

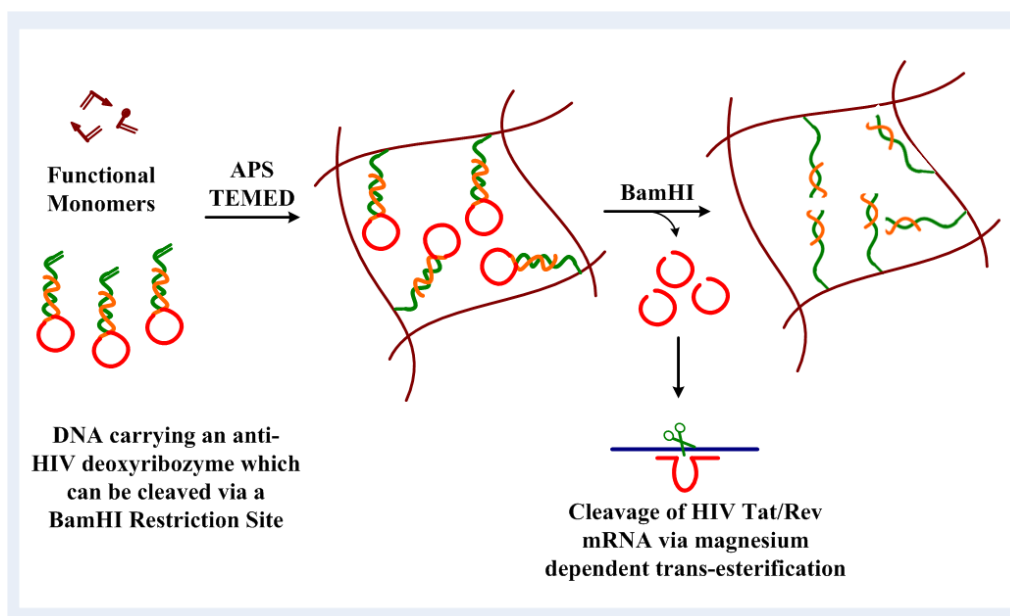


Figure 6.10 Clinical viability of platform triggered by enzymes. Down regulation of a HIV-1 TAT/Rev mRNA by deoxyribozymes loaded into the polymer network.

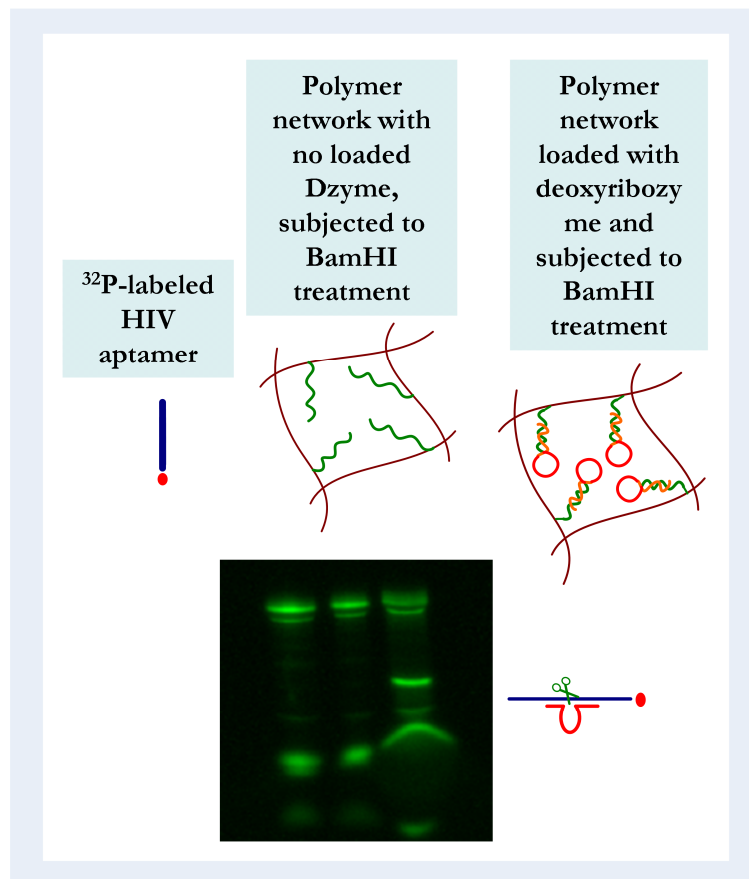


Figure 6.12 Catalytic down regulation of HIV-1 TAT/Rev mRNA by deoxyribozyme released by enzymatic trigger. Incubation of the HIV-1 TAT/Rev mRNA with a polymer network loaded with the deoxyribozymes resulted in its down regulation on the application of BamHI trigger (lane 3) as compared to incubation without deoxyribozyme, where no down regulation occurred (lane 2). HIV-1 TAT/Rev mRNA was used as control (lane 1).

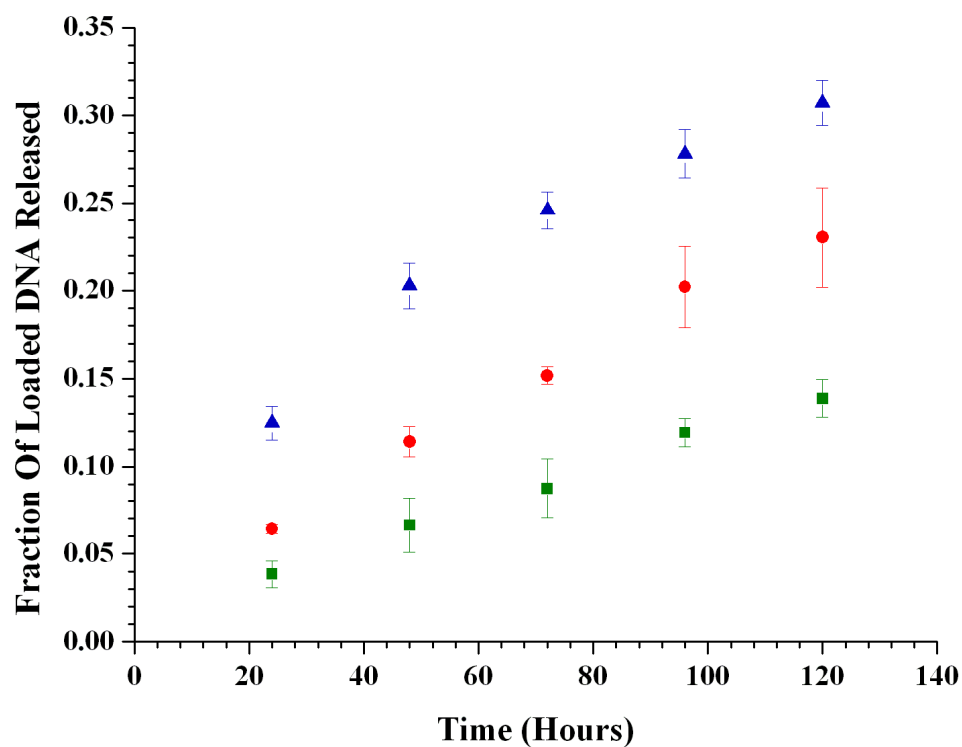


Figure 6.13 Tunable Release Profiles *via* Structural Control. Controlled release of DNA from biocompatible gels *via* DNase I trigger by controlling macromolecular architecture. $N=5 \pm S.D.$ Crosslinking densities were calculated on an acrylated DNA-free basis was 0.15% (\blacktriangle), 0.22 % (\bullet), and 0.45% (\blacksquare).

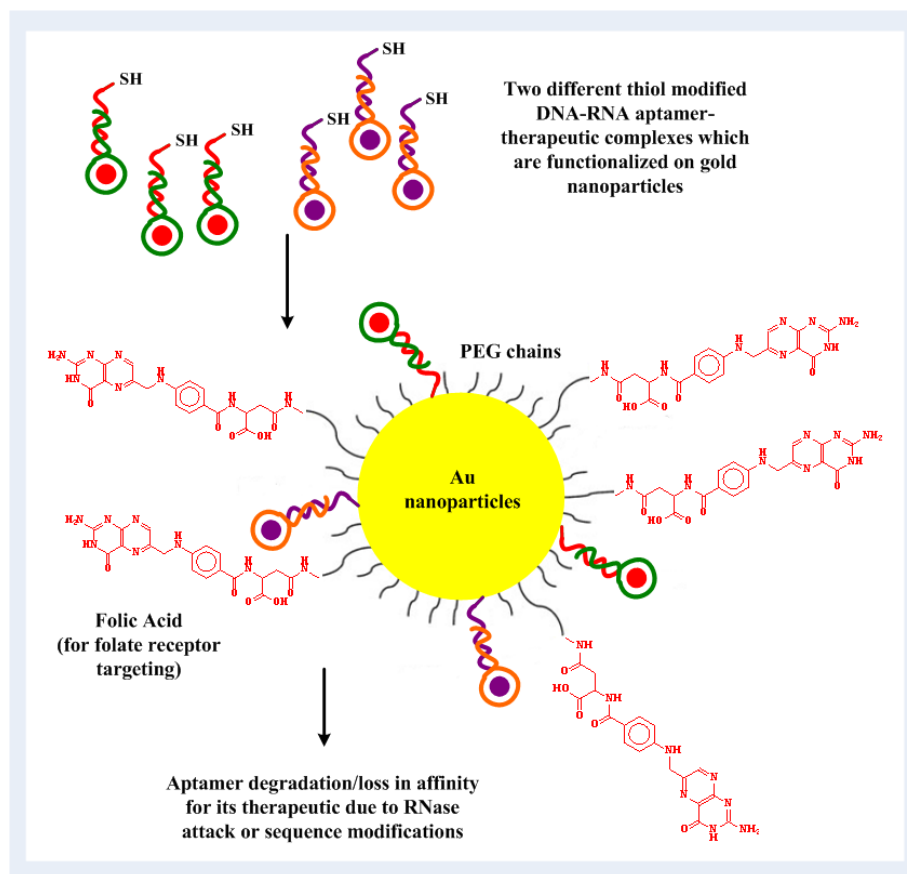


Figure 6.14 Programmable, Multiple Drug Delivery Platform Via Aptamer-Gold Nanoparticle Conjugates. The release rates of multiple therapeutics can be envisioned, by the covalent functionalization of their cognate aptamers on gold nanoparticles. The native degradation rates of the aptamers or differing aptamer-therapeutic affinities would be responsible for different release profiles of the therapeutics.

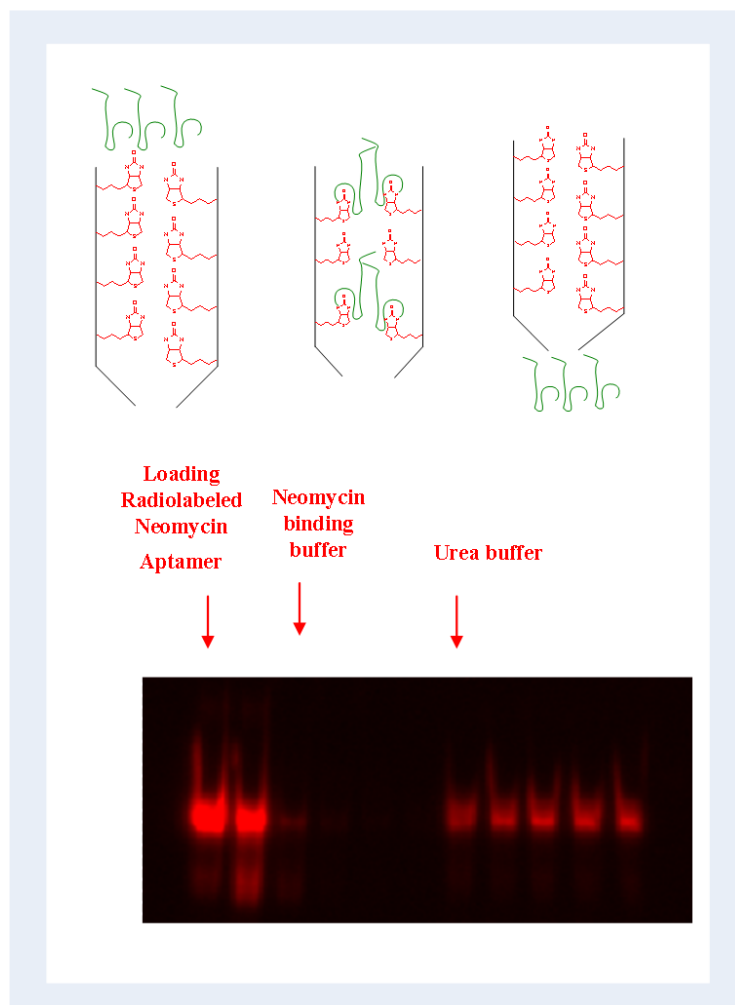


Figure 6.15 Binding efficacy of the wild type neomycin binding aptamer. Binding between neomycin and its cognate aptamer occurs when washes are conducted with the neomycin binding buffer, but dissociation of the complex is triggered by urea washes.

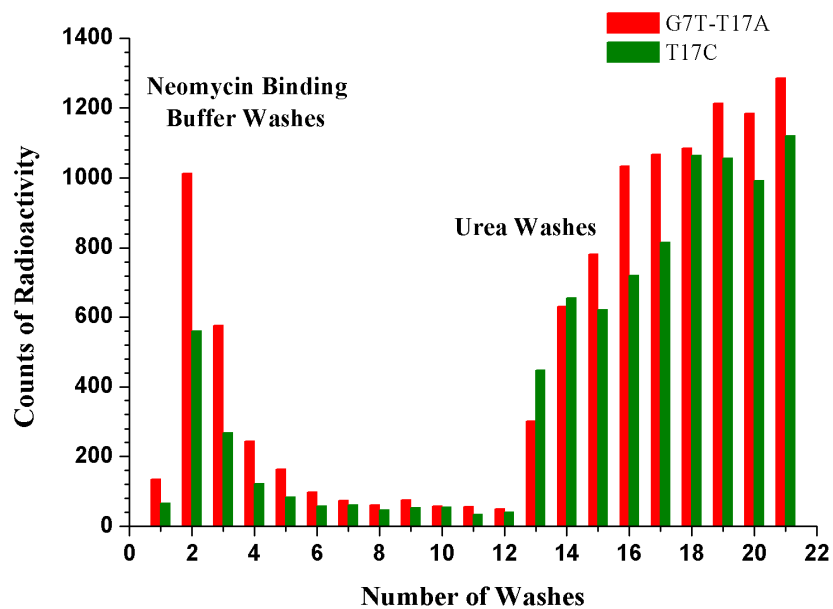


Figure 6.16 Differences in Binding efficacy of two neomycin binding mutant aptamers. Substitution of the G-T pair with a T-A pair weakens the neomycin aptamer secondary structure, and hence reduces its affinity to neomycin. On the other hand, substitution of thymine with cytosine results in a G-C pair instead of a G-T pair, which tightens the neomycin aptamer structure and might increase its affinity to neomycin.

7.0 CONCLUSIONS

Biomimetic and biohybrid materials are prime candidates for the creation of enhanced delivery systems with tremendous promise to profoundly impact medicine via improved treatment options for disease and better quality of life. Within the field of advanced drug delivery, major emphasis is now being focused toward engineering the architectural design of biomaterials at the molecular level. Emerging areas of this technology involve thin film drug release platforms.

In the ocular delivery field, we have developed a biomimetic approach in the design and synthesis of novel therapeutic contact lenses to tackle the unmet need for non-invasive, controlled release of drugs to the eye. This technology, which replaces less efficient/effective and less convenient topical eye drops and ointments, creates a new architecture in polymeric films to enable enhanced drug loading and delayed drug release for treatments including eye comfort, allergy, infection, and inflammation. These lenses can be corrective or non-vision altering (i.e., cosmetic or bandage lenses after cataract removal or Lasik surgery) and can release medication under in-vitro physiological conditions at constant rates for extended periods from 24 hours to 20 days depending on formulation. Patients using topical eye drops typically receive large variances in medication from application to application due to insufficient dosages, skipping dosages, and/or over-administering dosages which can lead to ocular damage and side effects.

Also, topical solutions and suspensions are typically washed completely from the eye in a short period of time (thus requiring multiple daily applications) and contain preservatives and sensitizers which can cause discomfort and adverse reactions. Controlling and tailoring the release of drugs via novel contact lenses can solve these problems with increased drug bioavailability, less irritation to eye tissue, and reduced eye and systemic side effects. This new class of responsive intelligent biomaterials is designed by incorporating motifs with structural and molecular homology to biological receptor docking sites and has a strong potential to work with a wide spectrum of drugs and impact the administration of a number of ocular therapies. The US prescription ophthalmic drug market, in which 90% is controlled by the eye drop and ointment sector, is approximately \$4.5 billion and growing at a 10% average annual growth rate since 2002. By incorporating a natural receptor-based rational design strategy in the synthesis of novel responsive weakly crosslinked networks, we demonstrated the potential of biomimetic polymers to load significant amounts of ocular medication such as H₁-antihistamines. The most biomimetic imprinted network, poly (AA-co-AM-co-NVP-co-HEMA-co-PEG200DMA), i.e. the network synthesized from the pre-polymerization mixture of maximum diversity in chemical functionalities, demonstrated a dramatic increase in loading and slower release kinetics than the networks synthesized from a less diverse mixture of functional monomers. The imprinting effect was reflected in a reduced propagation of polymer chains. One dimensional permeation studies showed that the imprinted network with maximum incorporated chemical functionality had the lowest permeability and diffusion coefficients, which was at least an order of magnitude lower than all other networks studied. A startling observation was that all imprinted networks

had significantly lower diffusion coefficients than non-imprinted networks, in spite of comparable mesh sizes and equilibrium polymer volume fractions in the swollen state. We also proposed the “tumbling hypothesis” to place our observations into a theoretical framework, wherein a molecule tumbling through an imprinted network with multiple, organized functionalities and an appropriate mesh size, experiences heightened interactions with memory sites and shows delayed transport kinetics. Our results add thrust to a growing suspicion- that the structural plasticity of polymer chains, i.e. the organization of functional groups into memory sites, may be responsible for enhanced loading and extended release.

The incorporation of nucleic acid constructs into hydrogels and nanoparticles can produce novel biomaterials with programmable on-demand switches or modulatory mechanisms, with unprecedented control and sensitivity. Custom oligonucleotides, which were partially complementary to each other and had a programmed recognition site for the restriction endonuclease BamHI, were modified with a polymerizable acrylate functionality and ³²P-labeled using T4 polynucleotide kinase. In-vitro hybridization and restriction enzyme digests were optimized in various concentrations of Tris buffer and water, and confirmed using polyacrylamide gel electrophoresis. Magnesium was determined to be critical for hybridization of the construct. About 10% of the complementary oligonucleotide self-annealed. The functional monomers used for hydrogel synthesis had no effect on hybridization efficiency. Digestion of the DNA helices was carried out by incubating the DNA helices with restriction enzyme BamHI and BamHI buffer. Incubation of the DNA double helix (without BamHI) on ice and at 37°C had no effect on the duplex. BamHI buffer did not disrupt the annealed duplex.

Poly(acrylamide-co-N,N' methylene bisacrylamide-co-acrylated DNA) hydrogels were synthesized via redox polymerization and the unincorporated DNA was eluted by electrophoresis. The labeled complementary oligonucleotide, when polymerized into the hydrogel without the anchoring acrylated oligonucleotide, eluted readily from the hydrogel during electrophoresis whereas acrylated DNA duplex was readily incorporated into the network. Quantification of the polymerization process via electrophoresis and phosphoimaging indicated 70% capture of the acrylated DNA, 25 % unincorporated acrylated DNA, and 5% ³²P-labeled oligonucleotide. A labeled oligonucleotide bearing a non-complementary sequence to the acrylated oligonucleotide did not get incorporated as annealing did not occur between the two strands. Release studies of ³²P-labeled loaded DNA were conducted by incubating the DNA-loaded gels under physiological conditions in the presence of BamHI. The release of DNA due to the penetration of restriction enzyme was shown to be highly specific, with no release in the absence of BamHI, and the presence of another endonuclease, EcoRI. Temperature was used to release the ³²P-labeled oligonucleotide as an alternative physical trigger. Temperature responsive release characteristics corresponded to the theoretical melting temperature of the helix (58°C). Poly(2-hydroxyethyl methacrylate-co-polyethylene glycol 600 dimethacrylate-co-acrylated DNA) hydrogels of varying crosslinking densities were triggered to release DNA by the non-specific endonuclease DNase I. Release rate of DNA from biocompatible hydrogels varied inversely with the crosslinking densities, and consequently mesh size.

The physiological significance of this platform was demonstrated by delivering a deoxyribozyme, which bore a catalytic 10-23 motif and was specific to a HIV Tat/Rev

mRNA. The HIV-1 Tat/Rev RNA was synthesized by in vitro transcription and labeled using [5'-³²P]pCp and T4 RNA ligase. Incubation of the deoxyribozyme-loaded hydrogel and the HIV-1 Tat/Rev RNA resulted in down regulation of the gene. BamHI action on a hydrogel lacking the deoxyribozyme construct had no effect on the HIV-1 Tat/Rev RNA.

Here we demonstrate the controlled release of nucleic acid therapeutics loaded into hydrogels and nanoparticles via enzymatic and physical triggers. These novel biomaterials, designed using the principles of molecular biology, are expected to profoundly impact gene therapy regimes. Substrate non-specific (DNase I) enzymes were used to trigger the release of fluorescent neomycin immobilized onto gold nanoparticles. The neomycin molecules were bound by an unstructured thiolated oligonucleotide hybridized to the neomycin aptamer, which was isolated by affinity chromatography. Surface coverage densities of the DNA were quantified by using oligonucleotides with fluorescent dyes at the 3' end, and were optimized by varying buffer ionic strengths, reaction times and sonication.

APPENDIX A

Appendix A consists of the data sets collected from experiments, which were analyzed for generating the results and discussions within the main chapters of this dissertation. Section A.1 consists of the dynamic binding isotherms for the copolymer networks poly(AA-co-HEMA-co-PEG200DMA), poly(AM-co-HEMA-co-PEG200DMA). Section A.2 consists of the equilibrium binding isotherms for the copolymer networks poly(AA-co-HEMA-co-PEG200DMA), poly(AM-co-HEMA-co-PEG200DMA), poly(NVP-co-HEMA-co-PEG200DMA), poly(AA-co-AM-co-HEMA-co-PEG200DMA) and poly(AA-co-AM-co-NVP-co-HEMA-co-PEG200DMA)). Section A.3 consists of the raw experimental data sets which were used for the calculation of network structural parameters. Section A.4 and A.5 present the raw data for the polymerization reaction analysis and structural analysis respectively for all copolymer networks.

A.1 Dynamic Binding Isotherms

In these experiments, a stock solution of 2 mg/mL of ketotifen fumarate was prepared and diluted to five concentrations (0.1 mg/mL, 0.20 mg/mL, 0.3 mg/mL, 0.4 mg/mL, and 0.5 mg/mL) in 50mL conical vials. Initial absorbances of each solution, which corresponded to the initial concentrations by Beer's law, were measured in the Biotek UV-vis Spectrophotometer. Standard charts were prepared each time the studies were conducted in order to account for variables such as the temperature of the room and operator error. The wavelength of maximum absorption for ketotifen fumarate was 268 nm. After the initial absorbance, a washed and dried polymer disk was inserted in each vial. Gentle agitation was performed on a Stovall Belly Button Orbital Shaker. At pre-determined intervals, the polymer disk was removed from the conical vial, and the solutions were vortexed for 10 seconds to provide homogeneity. 200 μ L aliquots were pipetted into 96-well plates (Corning Costar UV-transparent microplates and their absorbances, which corresponded to the equilibrium concentrations, were determined in the Biotek UV-vis Spectrophotometer. These studies were conducted in order to determine the time that it takes for the binding to reach equilibrium.

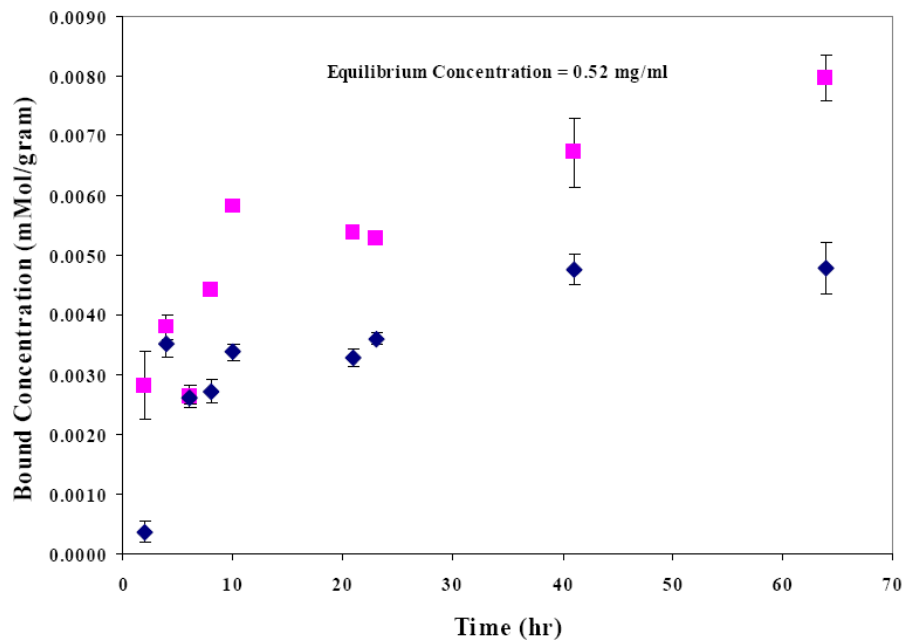


Figure A.1 Ketotifen dynamic binding isotherm in water for poly(AM-co-HEMA-co-poly(ethylene glycol)200 dimethacrylate) networks with a crosslinking percentage of 5%. N=3, and T=25°C. Imprinted network (■) and non-imprinted network (◆). Initial ketotifen concentration was 0.52 mg/mL.

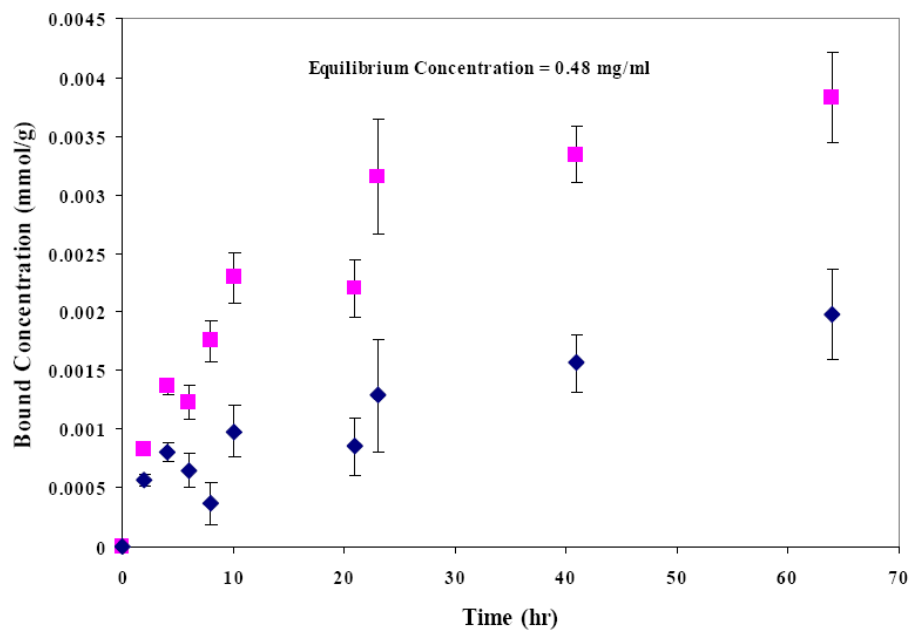


Figure A.2 Ketotifen dynamic binding isotherm in water for poly(AA-co-HEMA-co-poly(ethylene glycol)200 dimethacrylate) networks with a crosslinking percentage of 5%. N=3, and T=25°C. Imprinted network (■) and non-imprinted network (◆). Initial ketotifen concentration was 0.48 mg/mL.

A.2 Equilibrium Binding Isotherms

In these experiments, a stock solution of 2 mg/mL of ketotifen fumarate was prepared and diluted to five concentrations (0.1 mg/mL, 0.20 mg/mL, 0.3 mg/mL, 0.4 mg/mL, and 0.5 mg/mL) in 50mL conical vials. Initial absorbances of each solution, which corresponded to the initial concentrations by Beer's law, were measured in the Biotek UV-vis Spectrophotometer. Standard charts were prepared each time the studies were conducted in order to account for variables such as the temperature of the room and operator error. The wavelength of maximum absorption for ketotifen fumarate was 268 nm. After the initial absorbance, a washed and dried polymer disk was inserted in each vial and allowed to equilibrate over an average of 70-80 hours. Gentle agitation was performed on a Stovall Belly Button Orbital Shaker. After equilibrium was reached, the polymer disk was removed from the conical vial, and the solutions were vortexed for 10 seconds to provide homogeneity. 200 μ L aliquots were pipetted into 96-well plates (Corning Costar UV-transparent microplates and their absorbances, which corresponded to the equilibrium concentrations, were determined in the Biotek UV-vis Spectrophotometer. After sample readings were recorded, the tested aliquots were returned back to the samples. All experiments were performed in triplicate, averaged, and corrected for the relevant controls. The bound concentrations were then calculated by mass balances (i.e. by subtracting the equilibrium concentrations from the initial concentrations). The bound concentration is the capacity of the polymer and is expressed in units of millimoles of drug bound per milligram of dry polymer.

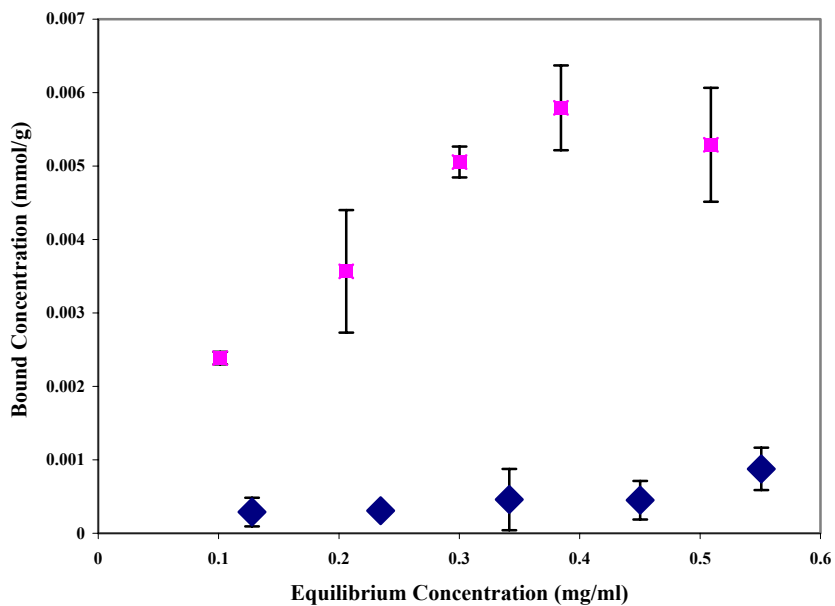


Figure A.3 Ketotifen equilibrium binding isotherm in water for poly(AA-co-HEMA-co-PEG(200)DMA) networks with a crosslinking percentage of 5%. $N=3$, and $T=25^{\circ}\text{C}$. Imprinted network (■) and non-imprinted network (◆). Percentage denotes percent mole crosslinker per mole total monomers in feed. The imprinted network demonstrated approximately a 6 times increase in loading compared to the non-imprinted network.

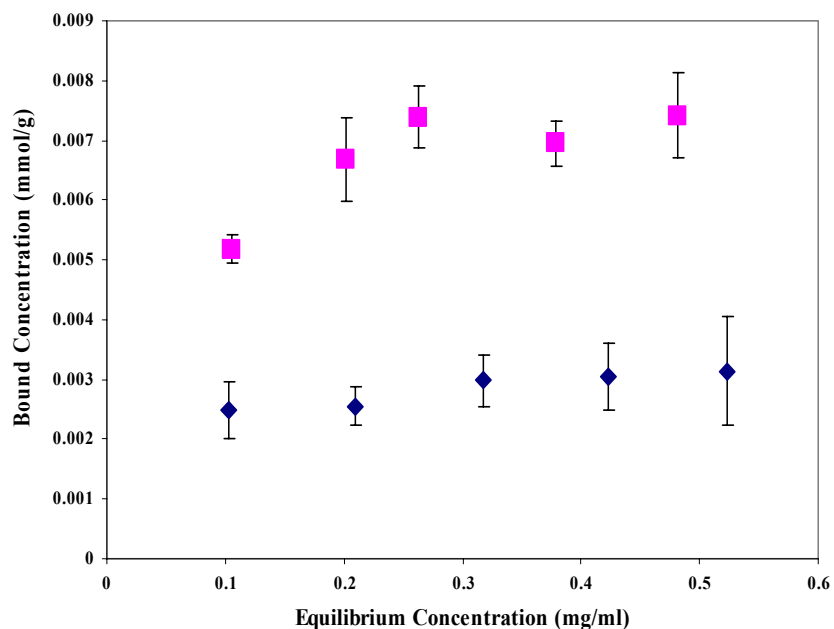


Figure A.4 Ketotifen equilibrium binding isotherm in water for poly(AM-co-HEMA-co-PEG(200)DMA) networks with a crosslinking percentage of 5%. N=3, and T=25°C. Imprinted network (■) and non-imprinted network (◆). Percentage denotes percent mole crosslinker per mole total monomers in feed. The imprinted network demonstrated approximately a 2 times increase in loading compared to the non-imprinted network.

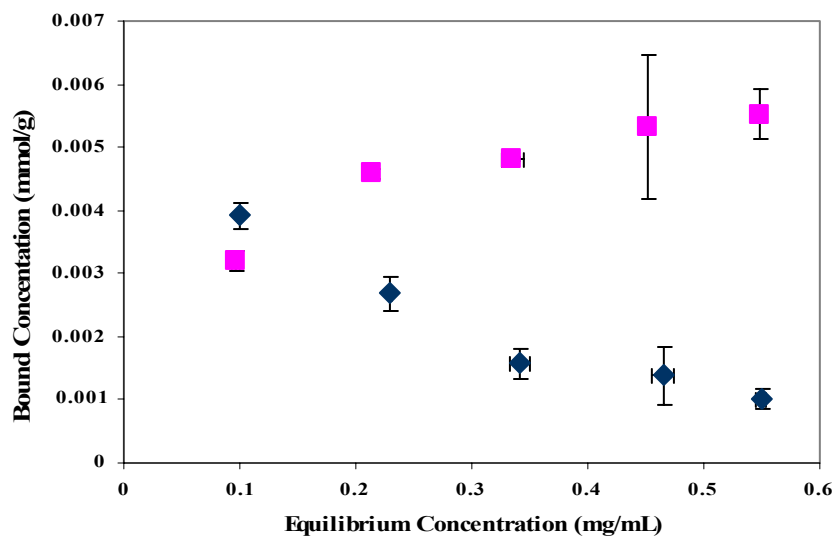


Figure A.5 Ketotifen equilibrium binding isotherm in water for poly(NVP-co-HEMA-co-PEG(200)DMA) networks with a crosslinking percentage of 5%. N=3, and T=25°C. Imprinted network (■) and non-imprinted network (◆). Percentage denotes percent mole crosslinker per mole total monomers in feed. The imprinted network demonstrated approximately a 2 times increase in loading compared to the non-imprinted network.

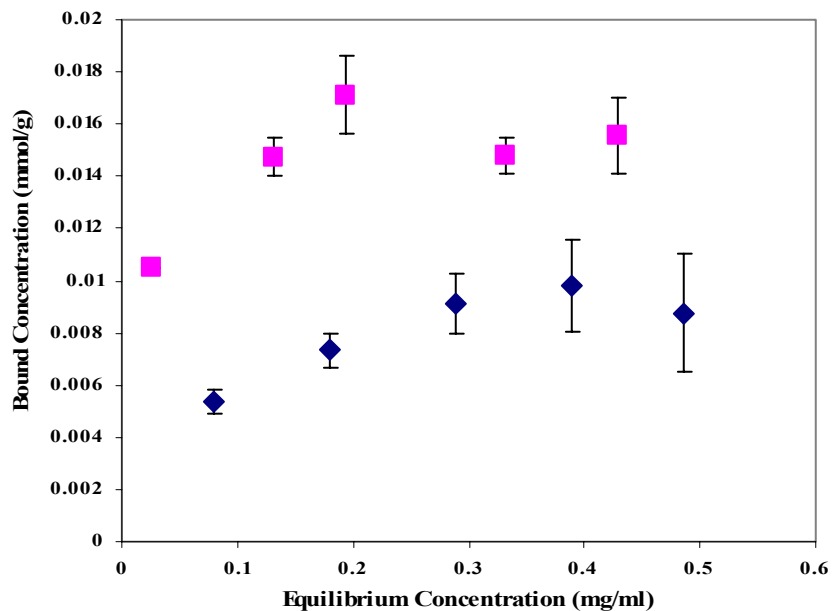


Figure A.6 Ketotifen equilibrium binding isotherm in water for poly(AM-co-AA-co-HEMA-co-PEG(200)DMA) networks with a crosslinking percentage of 5%. N=3, and T=25°C. Imprinted network (■) and non-imprinted network (◆). Percentage denotes percent mole crosslinker per mole total monomers in feed. The imprinted network demonstrated approximately a 2 times increase in loading compared to the non-imprinted network.

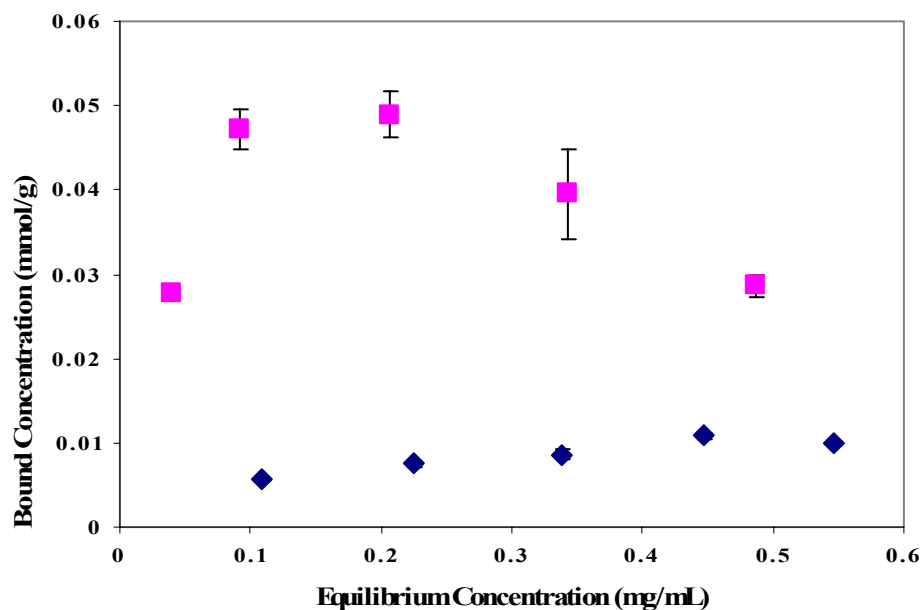


Figure A.7 Ketotifen equilibrium binding isotherm in water for poly(AM-co-AA-co-NVP-co-HEMA-co-PEG(200)DMA) networks with a crosslinking percentage of 5%. N=3, and T=25°C. Imprinted network (■) and non-imprinted network (◆). Percentage denotes percent mole crosslinker per mole total monomers in feed. The imprinted network demonstrated approximately a 6 times increase in loading compared to the non-imprinted network.

A.3 Raw Data for Calculation of Equilibrium Swelling Ratios and Mesh Sizes

The raw data presented in this section were obtained from various swelling and buoyancy studies, which enabled the calculation of various structural parameters such as the volume swelling ratio (Q), the polymer volume fraction in the swollen state ($v_{2,s}$), and the mesh size (ξ) in section 5.4.4 of this dissertation. Tables A.1 to A.4 give the dry and swollen volumes of the imprinted and non-imprinted copolymer networks poly(AA-co-HEMA-co-PEG200DMA), poly(AM-co-HEMA-co-PEG200DMA), poly(NVP-co-HEMA-co-PEG200DMA), poly(AA-co-AM-co-HEMA-co-PEG200DMA) and poly(AA-co-AM-co-NVP-co-HEMA-co-PEG200DMA). Figure A.8 to A.13 are the equilibrium swelling studies of the poly(AA-co-HEMA-co-PEG200DMA), poly(AM-co-HEMA-co-PEG200DMA), poly(AA-co-AM-co-HEMA-co-PEG200DMA) networks in the presence and absence of template molecule in solution. It is important to note that the thicknesses of the samples used for these studies varied from 700 μm for the poly(AA-co-HEMA-co-PEG200DMA), poly(AM-co-HEMA-co-PEG200DMA), poly(NVP-co-HEMA-co-PEG200DMA) networks, to 400 μm for the poly(AA-co-AM-co-HEMA-co-PEG200DMA) and poly(AA-co-AM-co-NVP-co-HEMA-co-PEG200DMA) networks.

**Table A.1 Dry Volumes of Non-imprinted Poly(n-co-HEMA-co-PEG200DMA)
Networks**

Network Monomers (n)	1	2	3	Average Dry Volume (ml)	S.D.
AA	0.0841	0.0878	0.0841	0.0853	0.0021
AM	0.0826	0.0835	0.0865	0.0842	0.0020
NVP	0.0893	0.0889	0.0901	0.0895	0.0006
AA-co-AM	0.0253	0.0260	0.0258	0.0257	0.0003
AA-co-AM-co-NVP	0.0278	0.0276	0.0259	0.0271	0.0010

Table A.2 Dry Volumes of Imprinted Poly(n-co-HEMA-co-PEG200DMA) Networks

Network Monomers (n)	1	2	3	Average Dry Volume (ml)	S.D.
AA	0.0852	0.0832	0.0845	0.0843	0.0010
AM	0.0806	0.0831	0.0815	0.0817	0.0013
NVP	0.0839	0.0754	0.0820	0.0804	0.0045
AA-co-AM	0.0269	0.0249	0.0270	0.0263	0.0012
AA-co-AM-co-NVP	0.0267	0.0244	0.0277	0.0263	0.0017

Table A.3 Swollen Volumes of Non-imprinted Poly(n-co-HEMA-co-PEG200DMA)**Networks**

Network Monomers (n)	1	2	3	Average Swollen Volume (ml)	S.D.
AA	0.1270	0.1299	0.1290	0.1286	0.0015
AM	0.1292	0.1298	0.1340	0.1310	0.0026
NVP	0.1374	0.1344	0.1385	0.1368	0.0021
AA-co-AM	0.0390	0.0393	0.0397	0.0393	0.0004
AA-co-AM-co-NVP	0.0459	0.0451	0.0418	0.0443	0.0022

Table A.4 Swollen Volumes of Imprinted Poly(n-co-HEMA-co-PEG200DMA)**Networks**

Network Monomers (n)	1	2	3	Average Swollen Volume (ml)	S.D.
AA	0.1310	0.1286	0.1316	0.1304	0.0016
AM	0.1222	0.1294	0.1270	0.1262	0.0037
NVP	0.1325	0.1323	0.1318	0.1322	0.0004
AA-co-AM	0.0411	0.0378	0.0404	0.0398	0.0017
AA-co-AM-co-NVP	0.0448	0.0406	0.0444	0.0433	0.0023

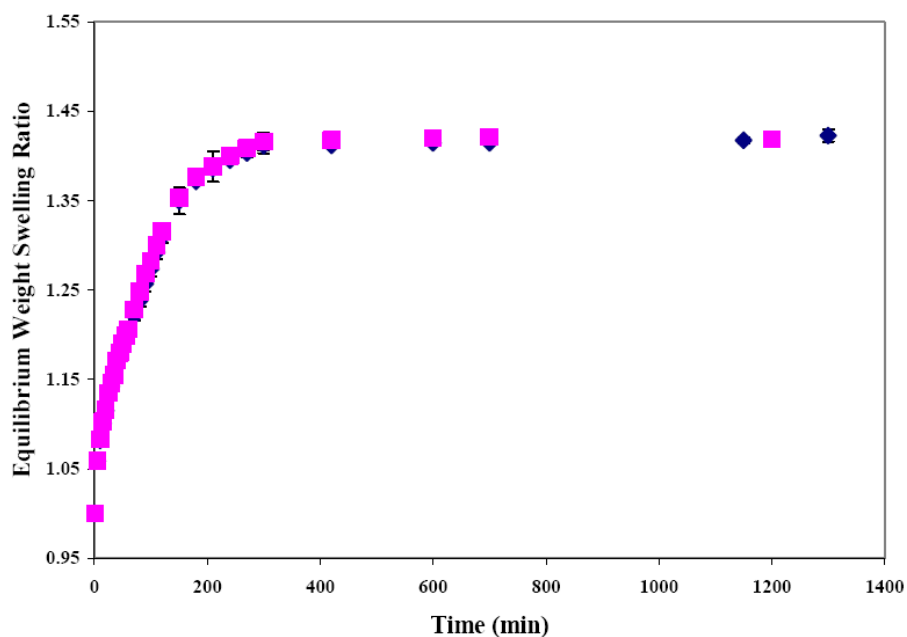


Figure A.8 Equilibrium weight swelling ratio for Poly(AA-co-HEMA-co-poly(ethylene glycol)200 dimethacrylate) networks in water with a crosslinking percentage of 5%. $N=3$, and $T=25^{\circ}\text{C}$. Imprinted network (■) and non-imprinted network (◆). Percentage denotes percent mole crosslinker per mole total monomers in feed.

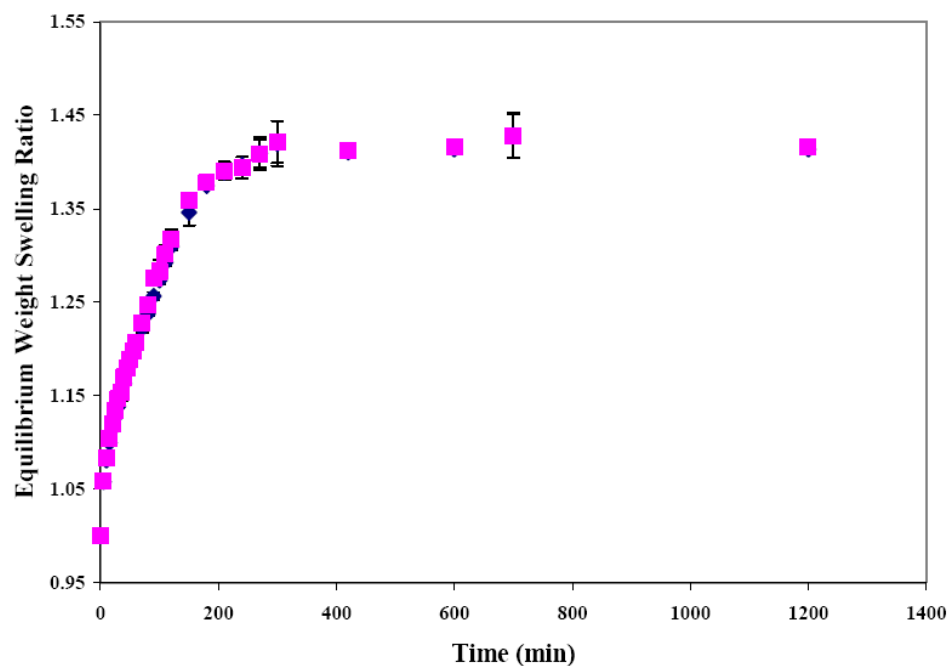


Figure A.9 Equilibrium weight swelling ratio for poly(AA-co-HEMA-co-poly(ethylene glycol)200 dimethacrylate) networks in 0.5 mg/ml ketotifen solution in water with a crosslinking percentage of 5%. N=3, and T=25°C. Imprinted network (■) and non-imprinted network (◆). Percentage denotes percent mole crosslinker per mole total monomers in feed.

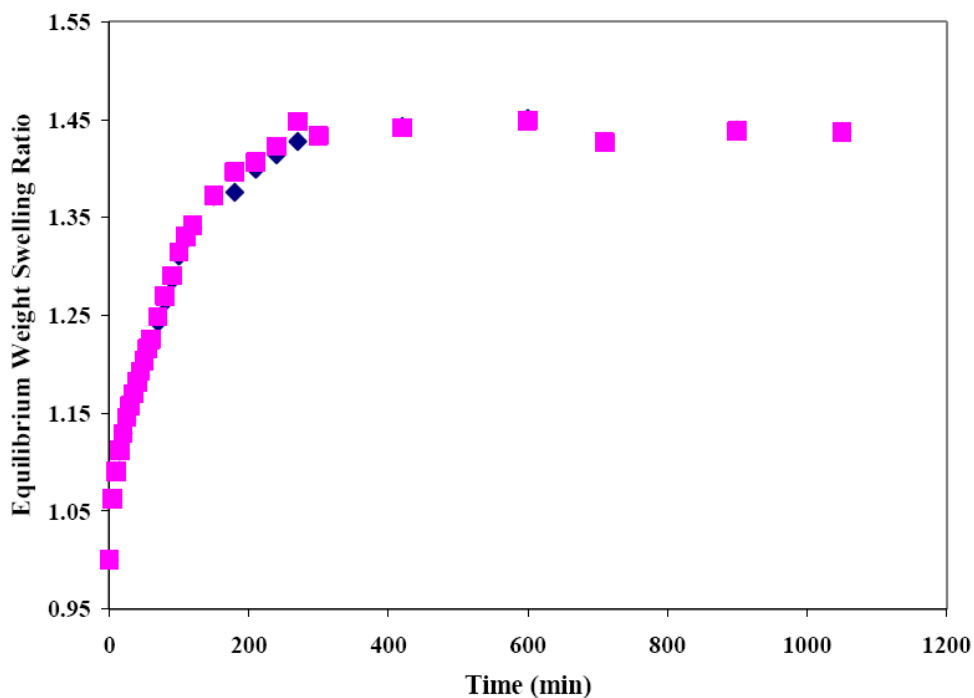


Figure A.10 Equilibrium weight swelling ratio for poly(AM-co-HEMA-co-poly(ethylene glycol)200 dimethacrylate) networks in water with a crosslinking percentage of 5%. $N=3$, and $T=25^{\circ}\text{C}$. Imprinted network (■) and non-imprinted network (◆). Percentage denotes percent mole crosslinker per mole total monomers in feed.

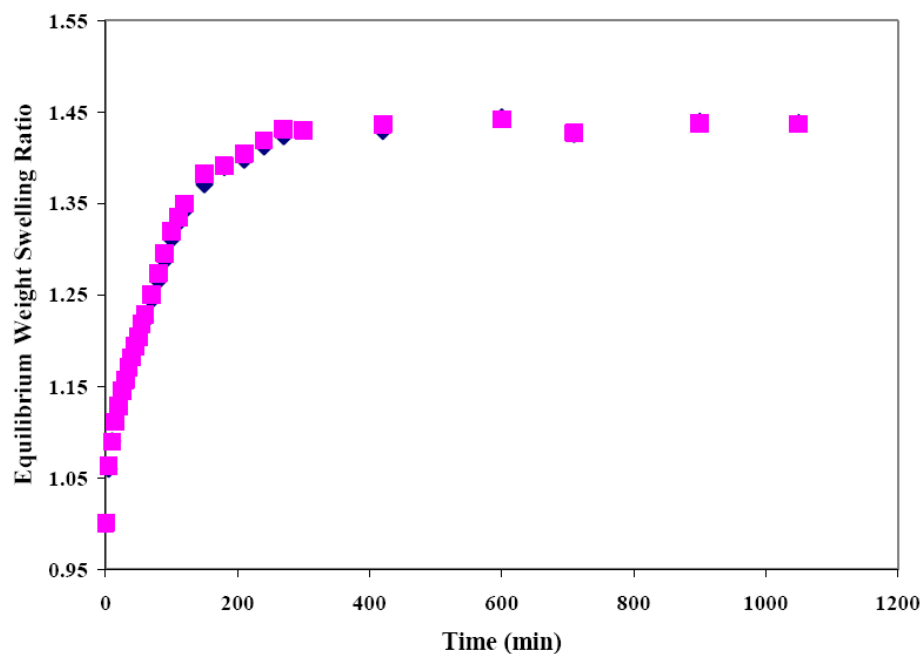


Figure A.11 Equilibrium weight swelling ratio for poly(AM-co-HEMA-co-poly(ethylene glycol)200 dimethacrylate) networks in 0.5 mg/ml ketotifen solution reverse osmosis water with a crosslinking percentage of 5%. $N=3$, and $T=25^{\circ}\text{C}$. Imprinted network (■) and non-imprinted network (◆). Percentage denotes percent mole crosslinker per mole total monomers in feed.

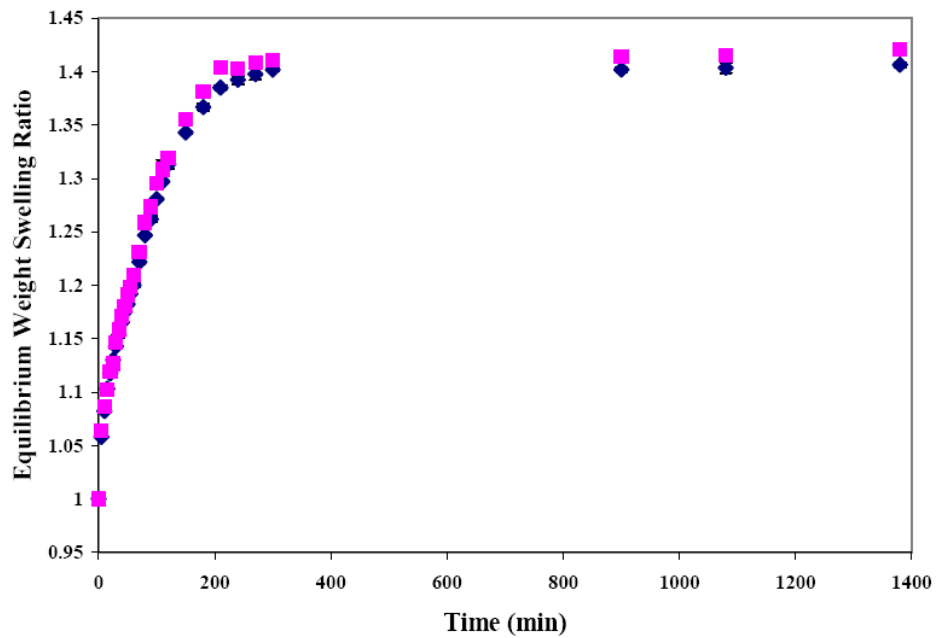


Figure A.12 Equilibrium weight swelling ratio for poly(AA-co-AM-co-HEMA-co-poly(ethylene glycol)200 dimethacrylate) with a crosslinking percentage of 5% in **water**. N=3, and T=25°C. Imprinted network (■) and non-imprinted network (◆). Percentage denotes percent mole crosslinker per mole total monomers in feed.

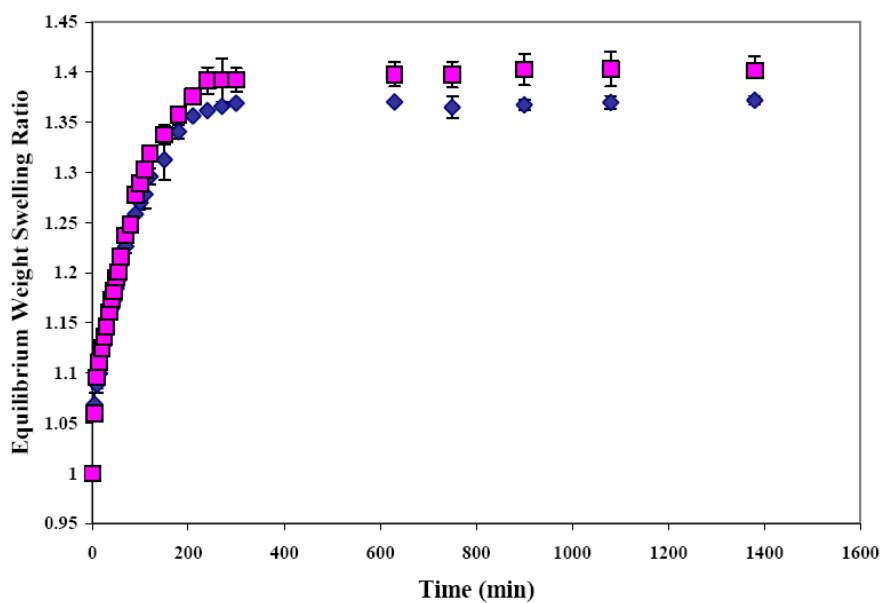


Figure A.13 Equilibrium weight swelling ratio for poly(AA-co-AM-co-HEMA-co-poly(ethylene glycol)200 dimethacrylate) with a crosslinking percentage of 5% in 0.5 mg/ml ketotifen solution in water. N=3, and T=25°C. Imprinted network (■) and non-imprinted network (◆). Percentage denotes percent mole crosslinker per mole total monomers in feed.

A.4 Raw Data for Polymerization Reaction Kinetics

The raw data presented in this section were obtained from differential scanning calorimetric studies, which enabled the characterization of the polymerization reaction in terms of parameters such as the polymerization reaction rate and the double bond conversions in section 4.4.4 of this dissertation. Figures A.14 to A.18 detail the polymerization reaction signatures, i.e. the rates of the polymerization reaction versus time, for the copolymer networks poly(AA-co-HEMA-co-PEG200DMA), poly(AM-co-HEMA-co-PEG200DMA), poly(NVP-co-HEMA-co-PEG200DMA), poly(AA-co-AM-co-HEMA-co-PEG200DMA) and poly(AA-co-AM-co-NVP-co-HEMA-co-PEG200DMA). Figure A.19 details the double bond conversion versus time for all five copolymer networks.

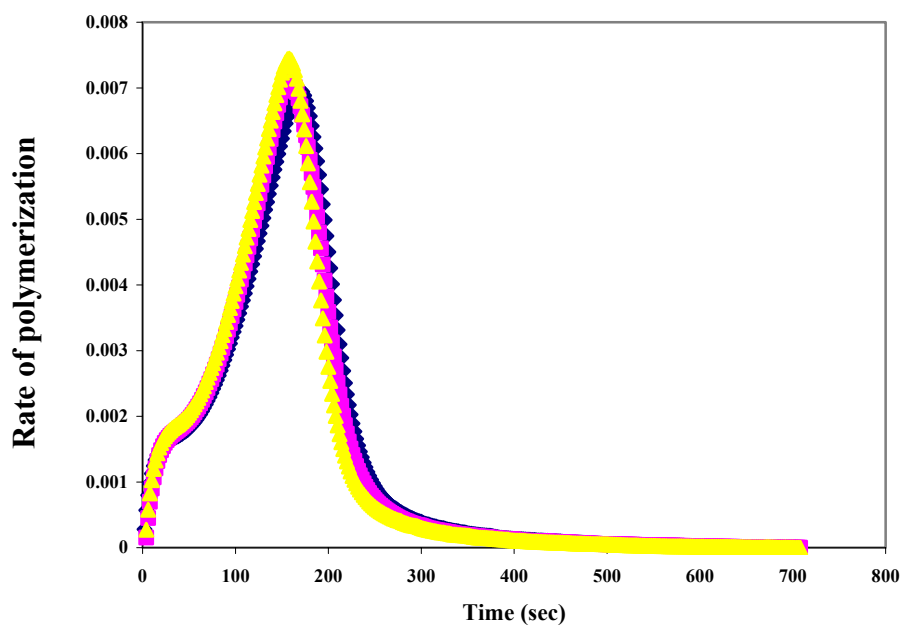


Figure A.14 Polymerization reaction signature for the poly(AM-co-HEMA-co-PEG200DMA) network. It is important to note that there were no significant differences between different runs of the same formulation.

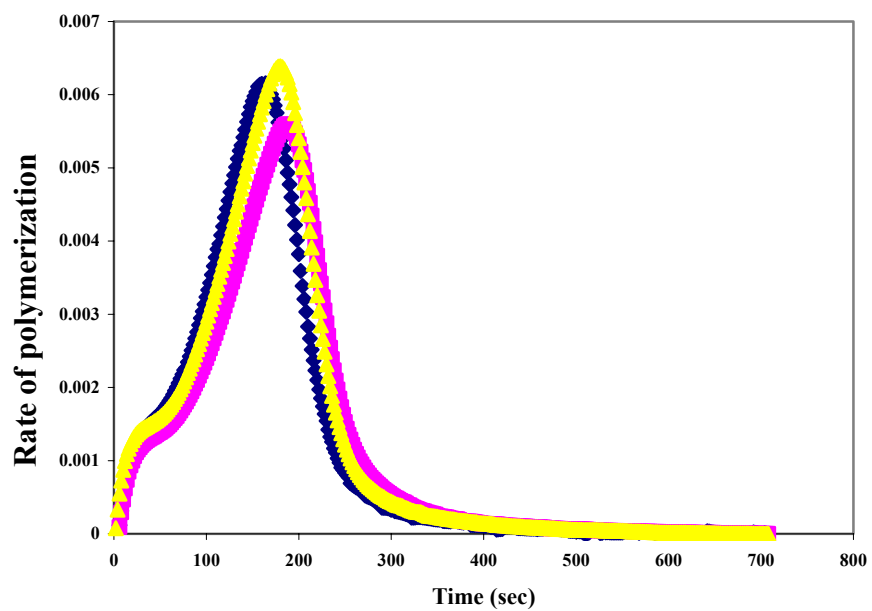


Figure A.15 Polymerization reaction signature for the poly(AA-co-HEMA-co-PEG200DMA) network. It is important to note that there were no significant differences between different runs of the same formulation.

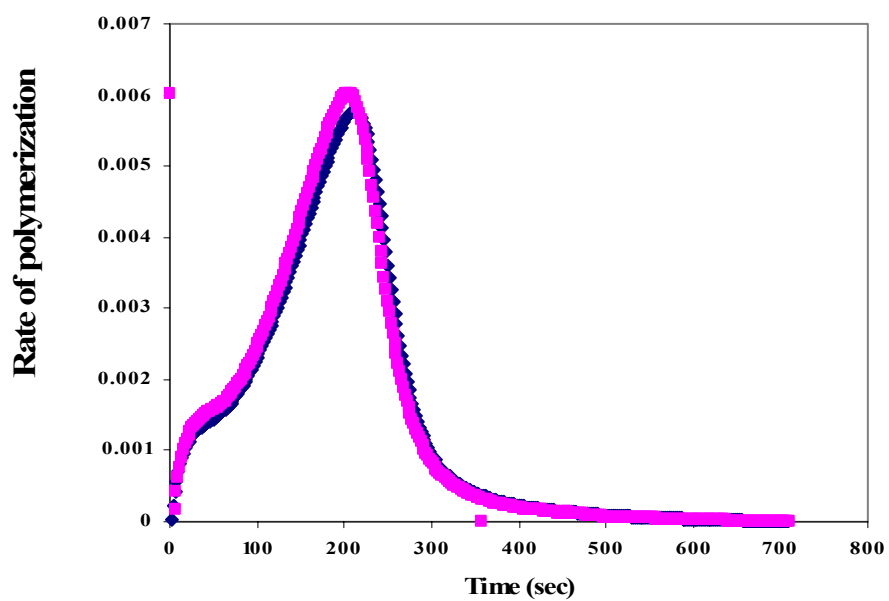


Figure A.16 Polymerization reaction signature for the poly(NVP-co-HEMA-co-PEG200DMA) network. It is important to note that there were no significant differences between different runs of the same formulation.

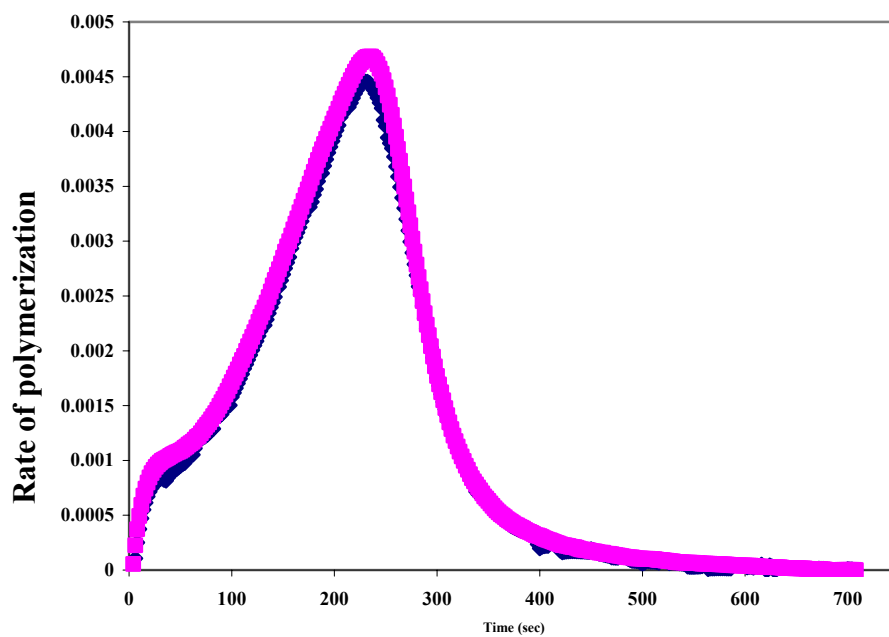


Figure A.17 Polymerization reaction signature for the poly(AA-co-AM-co-HEMA-co-PEG200DMA) network. It is important to note that there were no significant differences between different runs of the same formulation.

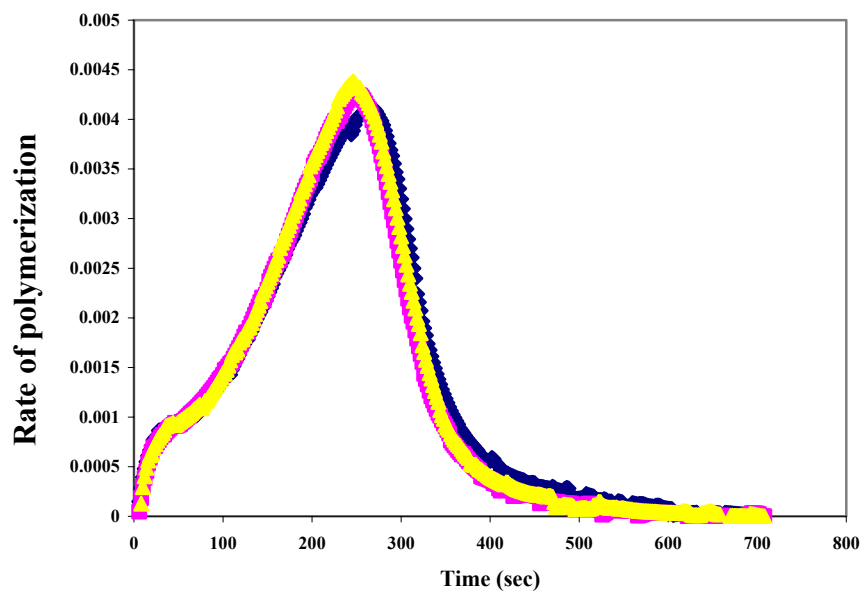


Figure A.18 Polymerization reaction signature for the poly(AA-co-AM-co-NVP-co-HEMA-co-PEG200DMA) network. It is important to note that there were no significant differences between different runs of the same formulation.

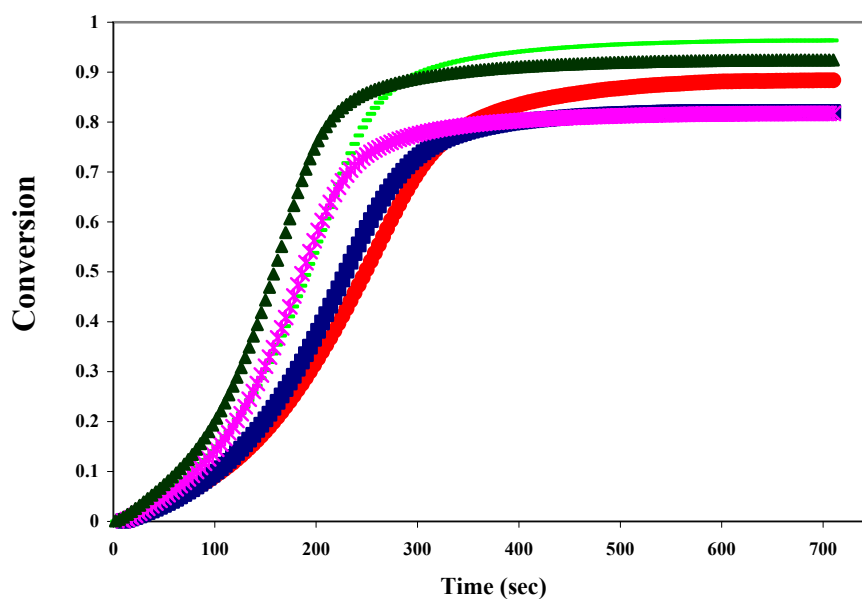


Figure A.19 Double bond conversion versus time for the poly(n-co-HEMA-co-PEG200DMA) network. Here, n is AA (x), AM (▲), NVP (—), AA-co-AM (■), and AA-co-AM-co-NVP (◆). It is important to note that there were no significant differences between different runs of the same formulation.

A.5 Raw Data from Static Experiment for Calculation of Mesh Sizes

The raw data presented in this section were obtained from tensile studies, which enabled the evaluation of structural parameters such as the average molecular weight between crosslinks (\overline{M}_c) and the mesh size (ξ). Figures A.20 and A.21 are representative examples of the tensile behavior of the copolymer imprinted and non-imprinted networks poly(AA-co-AM-co-HEMA-co-PEG200DMA). Figure A.19 details the double bond conversion versus time for all five copolymer networks.

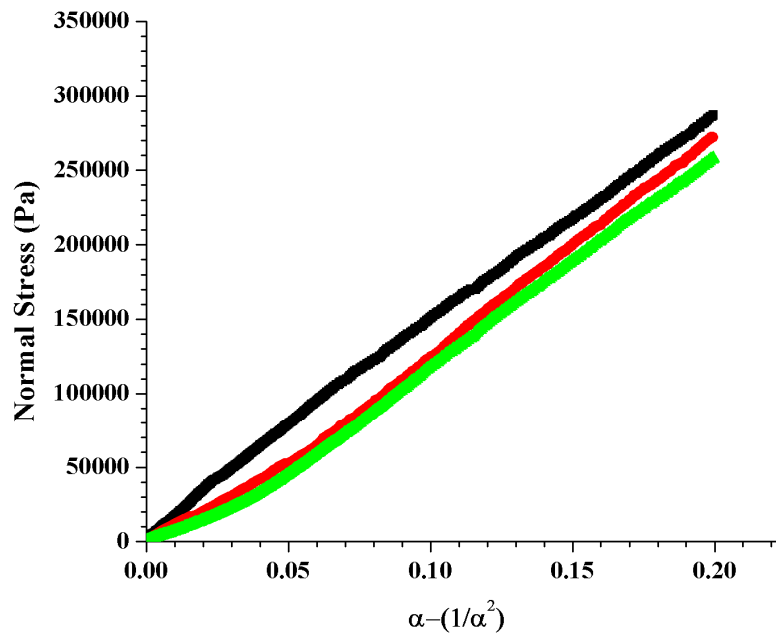


Figure A.20 Tensile behavior of the non-imprinted poly(AA-co-AM-co-HEMA-co-PEG200DMA) network. N=3. The slopes are used to determine the average molecular weight between crosslinks, which is then used to estimate the average mesh size. Here, the abscissa is the elongation function.

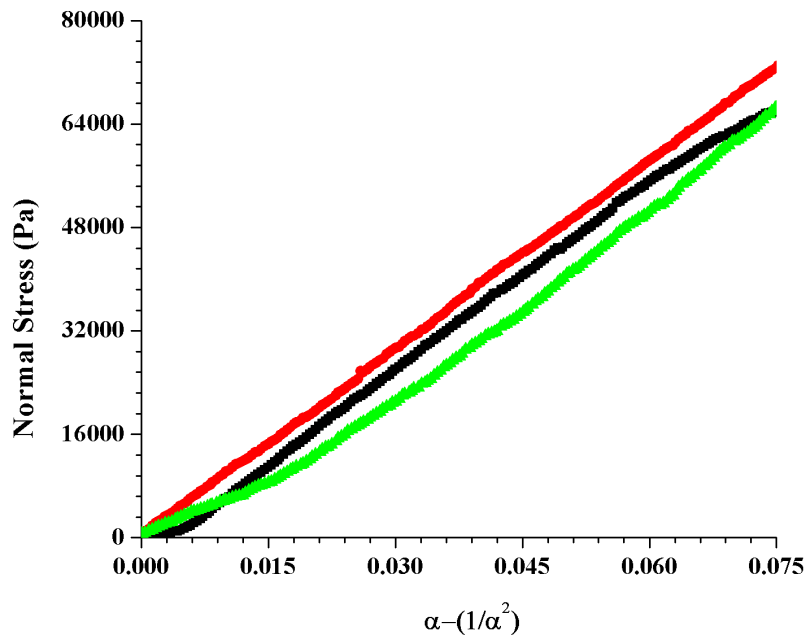


Figure A.21 Tensile behavior of the imprinted poly(AA-co-AM-co-HEMA-co-PEG200DMA) network. N=3. The slopes are used to determine the average molecular weight between crosslinks, which is then used to estimate the average mesh size. Here, the abscissa is the elongation function.

Table A.5 Slopes of the tensile curves of the non-imprinted poly(n-co-HEMA-co-PEG200DMA) networks

Network Monomers (n)	Run 1	Run 2	Run 3	Slope
AA	685134	898941	718558	767544 ± 115013
AM	1166866	1379178	1272146	1272730 ± 106157
NVP	1734709	1489865	1538035	1587536 ± 129711
AA-co-AM	1443515	1315650	1296363	1351843 ± 79974
AA-co-AM-co-NVP	1160205	1234292	1138605	1177701 ± 50186

Table A.6 Slopes of the tensile curves of the imprinted poly(n-co-HEMA-co-PEG200DMA) networks

Network Monomers (n)	Run 1	Run 2	Run 3	Slope
AA	1132053	1275401	1477428	1294961 ± 173516
AM	920028	815461	1108254	947914 ± 148375
NVP	1145086	1195722	1793233	1378013 ± 360481
AA-co-AM	991164	942492	897694	943783 ± 46748
AA-co-AM-co-NVP	1229294	1390940	1587715	1402650 ± 179498

Table A.7 Average molecular weight between crosslinks of the non-imprinted poly(n-co-HEMA-co-PEG200DMA) networks

Network Monomers (n)	Run 1	Run 2	Run 3	\overline{M}_c, average molecular weight between crosslinks, g/mol
AA	3435	2618	3275	3109 ± 466
AM	1995	1688	1830	1838 ± 153
NVP	1350	1572	1523	1481 ± 121
AA-co-AM	1622	1780	1807	1736 ± 102
AA-co-AM-co-NVP	1975	1856	2012	1948 ± 83

Table A.8 Average molecular weight between crosslinks of the imprinted poly(n-co-HEMA-co-PEG200DMA) networks

Network Monomers (n)	Run 1	Run 2	Run 3	\overline{M}_C, average molecular weight between crosslinks, g/mol
AA	2061	1830	1579	1823 ± 244
AM	2538	2863	2107	2502 ± 392
NVP	1997	1912	1275	1728 ± 452
AA-co-AM	2372	2494	2618	2494 ± 123
AA-co-AM-co-NVP	1859	1643	1440	1647 ± 211

Table A.9 Average mesh size calculations of the non-imprinted poly(n-co-HEMA-co-PEG200DMA) networks

Network Monomers (n)	$\nu_{2,S}$, equilibrium polymer volume fraction in the swollen state	M_n , number average molecular weight, g/mol	C_n , Flory characteristic ratio	L (Å)	\bar{v} , specific volume of the polymer	ξ , Mesh Sizes (Å)
AA	0.664 ± 0.018	128.30	6.2	1.54	0.909	30.60 ± 2.31
AM	0.643 ± 0.020	128.49	6.2	1.54	0.909	23.76 ± 1.02
NVP	0.654 ± 0.012	129.54	6.2	1.54	0.909	21.13 ± 0.87
AA-co-AM	0.654 ± 0.010	128.40	6.2	1.54	0.909	22.97 ± 0.69
AA-co-AM-co-NVP	0.612 ± 0.038	128.78	6.2	1.54	0.909	24.83 ± 0.74

**Table A.10 Average mesh size calculation of the imprinted
poly(n-co-HEMA-co-PEG200DMA) networks**

Network Monomers (n)	$\nu_{2,S}$, equilibrium polymer volume fraction in the swollen state	M_n , number average molecular weight, g/mol	C_n , Flory characteristic ratio	L (Å)	$\bar{\nu}$, specific volume of the polymer	ξ , Mesh Sizes (Å)
AA	0.647 ± 0.011	128.30	6.2	1.54	0.909	23.64 ± 1.59
AM	0.648 ± 0.021	128.49	6.2	1.54	0.909	27.66 ± 2.19
NVP	0.608 ± 0.034	129.54	6.2	1.54	0.909	23.37 ± 3.09
AA-co-AM	0.661 ± 0.041	128.40	6.2	1.54	0.909	27.44 ± 0.89
AA-co-AM-co-NVP	0.608 ± 0.049	128.78	6.2	1.54	0.909	22.90 ± 1.60

APPENDIX B

Appendix B consists of the buffer compositions used for all the experiments described in the chapters of this dissertation. Here, “X” refers to the factor of concentration. Hence, a 2X buffer is 2 times concentrated, and would need to be diluted during the experiment. Concentrations of the reagents are expressed in terms of conventional notations. Percentages are generally to be converted to grams of reagent per 100 mL of solution. In certain instances, using a volume-per-volume (v/v) basis is convenient.

<p>2X Formamide Buffer</p> <p>80% formamide (v/v)</p> <p>10 mM EDTA, pH 8.0</p> <p>1 mg/mL xylene cyanol</p> <p>1 mg/mL bromophenol blue</p>	<p>6X LB for Agarose Gel Loading</p> <p>0.25% xylene cyanol</p> <p>0.25% bromophenol blue</p> <p>30 % glycerol in RNase-free water</p>
<p>50% Acrylamide (19:1)</p> <p>(500 mL Total Volume)</p> <p>237.5 g acrylamide</p> <p>12.5 g bisacrylamide</p> <p>Male up to 500 mL with RNase-free water</p>	<p>50% Acrylamide (40:1)</p> <p>(100 mL Total Volume)</p> <p>97.5 g acrylamide</p> <p>2.5 g bisacrylamide</p> <p>Male up to 100 mL with RNase-free water</p>
<p>DNA/RNA Extraction Buffer</p> <p>0.5 M ammonium acetate</p> <p>0.01 M magnesium acetate</p> <p>0.1 mM EDTA</p> <p>0.1% sodium dodecyl sulfate</p>	<p>5X TBE</p> <p>54 g Tris base</p> <p>27.5 g boric acid</p> <p>20 mL 0.5 M EDTA, pH 8.0</p> <p>Make up to 1 L with RNase-free water</p>
<p>6X Loading Buffer</p> <p>(1mL Total Volume)</p> <p>300 μL glycerol</p> <p>200 μL 5X LG</p> <p>20 μL xylene cyanol</p> <p>20 μL bromophenol blue</p> <p>Make up to 1 mL with RNase-free water</p>	<p>10 X Hybridization Buffer</p> <p>100mM Tris-HCl, pH 7.5</p> <p>50 mM MgCl₂</p>
<p>10 X Scission Buffer</p> <p>500mM Tris-HCl, pH 7.5</p> <p>200 mM MgCl₂</p>	<p>10 X PBS</p> <p>137 mM NaCl</p> <p>2.7 mM potassium chloride</p> <p>10 mM disodium hydrogen phosphate</p> <p>2 mM potassium hydrogel phosphate</p>

<p style="text-align: center;">10 X PNK Buffer</p> <p style="text-align: center;">500mM Tris-HCl, pH 7.5</p> <p style="text-align: center;">100 mM MgCl₂</p> <p style="text-align: center;">50 mM dithiothreitol</p>	<p style="text-align: center;">10 X NEBuffer 3</p> <p style="text-align: center;">500 mM Tris-HCl</p> <p style="text-align: center;">1000 mM NaCl</p> <p style="text-align: center;">100 mM MgCl₂</p> <p style="text-align: center;">10 mM Dithiothreitol</p> <p style="text-align: center;">(Supplemented with 100 µg/ml Bovine Serum Albumin)</p> <p style="text-align: center;">pH 7.9 @ 25°C</p>
<p style="text-align: center;">12% Non-Denaturing Gel Mix</p> <p style="text-align: center;">7.2 mL 50% Acrylamide (19:1)</p> <p style="text-align: center;">3 mL 5X TBE</p> <p style="text-align: center;">3 mL 50% glycerol</p> <p style="text-align: center;">18.3 mL water</p> <p style="text-align: center;">60 µL TEMED</p> <p style="text-align: center;">120 µL 50% APS</p>	<p style="text-align: center;">5X Neomycin Binding Buffer</p> <p style="text-align: center;">250 mM Tris-HCl, pH 7.5</p> <p style="text-align: center;">1250 mM NaCl</p> <p style="text-align: center;">25 mM MgCl₂</p>

APPENDIX C

Appendix C consists of the oligonucleotide sequences used in all the experiments described in the chapters of this dissertation.

C.1 Restriction enzyme based DNA release

The anchoring oligo **AC-SID-1** was:

[5' Acry]- ACTGACCAG**AGACGCGGATCCGCGTCG** -3'

The complementary oligo, **AC-SID-1C**, to be released after restriction enzyme digestion was:

5' - CGTAGACCTAGCCT**CGACGCGGATCCGCGTCT** -3'

So the system (with the restriction site in bold) looks like this,

[5' Acry]- ACTGACCAG**AGACGCGGATCCGCGTCG** -3'

3' - **TCTGCGCCTAGGCGCAGCTCCGATCCAGATGC** -5'

After cleavage, you would obtain a shorter fragment which is released. We called that sequence **SID-cut**:

5' - CGTAGACCTAGCCTCGACGCG -3'

C.2 Down regulation of HIV TAT/REV transcript by a deoxyribozyme construct

The original HIV-1 TAT/Rev mRNA was,

5' - UUGUUUCAUGACAAAAGCCUUAGGCAUCUCCUAUGGCAGGAAGAA - 3'

This was modified in order to prevent secondary structure formation.

5' - CUGCAUGACGU AAGCCUUAGGCAUCUCCUAUGGCAGGAAGAA - 3'

The DNA sequence for this is:

5' - CTGCATGACGT AAGCCTTAGGCATCTCCTATGGCAGGAAGAA - 3'

The two DNA strands ordered for synthesizing the above template were:

Tat-up

5' - AATTCCTGCAGTAATACGACTCACTATAGGGGCTGCATGAC - 3'

Tat-down

5' - TTCTTCCTGCCATAGGAGATGCCTAAGGCTTACGTCATGCAGCC - 3'

The original deoxyribozyme, **Dz 5970** had the following sequence:

5' - CCTGCCAGGCTAGCTACAACGAAGGAGAT - 3'

This needed to be delivered via a restriction enzyme cleavable construct as earlier.

So we used our earlier AC-SID-1 as the anchoring strand again.

[5' Acry]- ACTGACCAGAGACGCGGATCCGCGTCC - 3'

3' - TCTGCGCCTAGGCGCAGCTCCGATCCAGATGC - 5'

The only modification is the incorporation of Dz 5970.

3' - TCTGCGCCTAGGCGCAGCTAGAGGAAGCAACATCGATCGGACCGTCC - 5'

This formed a troubled secondary structure so we made one mutation (indicated in brown). There was a bulge in the stem region, but that poses no problem.

3' – TCTGCGCCTAGGCGCA^ACTAGAGGAAGCAACATCGATCGGACCGTCC –5'

We termed this sequence as **AC-SID-AH**, and ordered it from Operon.

5' – CCTGCCAGGCTAGCTACAACGAAGGAGATCA^ACGCGGATCCGCGTCT –3'

We also experimented with a circular construct, removed a GC pair as shown due to secondary structure, and added a BamHI recognition site.

5' – GATCCGCG^{GC}CCTGCCAGGCTAGCTACAACGAAGGAGATCGCG –3'

5' – GATCCGCCCTGCCAGGCTAGCTACAACGAAGGAGATGCG –3'

5' – GATCCGCGTCGCCTGCCAGGCTAGCTACAACGAAGGAGATCGACGCG –3'

C.3 Nucleic acid-nanoparticle constructs

The neomycin aptamer is,

5' – GGACUGGGCGAGAAGUUUAGUCC – 3'

The corresponding DNA aptamer (NEOMYCIN) is,

5' – GGACTGGGCGAGAAGTTTAGTCC – 3'

In reverse,

3' – CCTGATTTGAAGAGCGGGTCAGG – 5'

This has to be extended in the 3' direction, to see if it can be hybridized to the linker oligonucleotide sequence on the gold nanoparticles (AUNP).

5' – (SH) TTTTATGGTTTACAATATT – 3'
3' – CCAAATGTTATAACCTGATTTGAAGAGCGGGTCAGG – 5'

Hence, the two oligonucleotide sequences ordered from Operon were:

NAN-ANC-SH

5' – (SH) TTTTATGGTTTACAATATT – 3'

NAN-NEO

5' – GGACTGGGCGAGAAGTTTAGTCCAATATTGTAAACC – 3'

C.4 Neomycin mutants

NAN-ANC-SH

5' - (SH) TTTTATGGTTTACAATATT -3'

NAN-NEO

5' - GGACTGGGCGAGAAGTTTAGTCCAATATTGTAAACC -3'

The binding worked between the neomycin column and the DNA aptamer (NAN-NEO). We needed to test mutants to see if we could get affinity differences, which could be translated to different release rates. Mutations are shown in bold purple.

NAN-NEO-G7C

5' - GGACTG**C**GCGAGAAGTTTAGTCCAATATTGTAAACC -3'

NAN-NEO-G8C

5' - GGACTGG**C**CGAGAAGTTTAGTCCAATATTGTAAACC -3'

NAN-NEO-T17C

5' - GGACTGGGCGAGAAGT**C**TAGTCCAATATTGTAAACC -3'

NAN-NEO-CCC

5' - GGACTGGGCGAGAAG**CCC**AGTCCAATATTGTAAACC -3'

NAN-NEO-C9A

5' - GGACTGGG**A**GAGAAGTTTAGTCCAATATTGTAAACC -3'

NAN-NEO-A14C

5' - GGACTGGGCGAG**A**CGTTTAGTCCAATATTGTAAACC -3'

NAN-NEO-T17C

5' - GGACTGGGCGAGAAGT**C**TAGTCCAATATTGTAAACC -3'

NAN-NEO-G7T-T17A

5' - GGACTG**T**GCGAGAAGT**A**TAGTCCAATATTGTAAACC -3'

NAN-NEO-G7A

5' - GGACTGAGCGAGAAGTTTAGTCCAATATTGTAAACC -3'

NAN-NEO-A13G

5' - GGACTGGGCGAGGAGTTTAGTCCAATATTGTAAACC -3'

RANDOM

5' - ACTGTCTATTTGAGTCATCTATTTAGCACATTCTTT -3'

APPENDIX D

Appendix D gives an overview of the error analysis used in the dissertation.

D.1 Error Analysis

Average values of multiple experiments were reported with their corresponding standard deviations. When multiplying or dividing quantities, the fractional standard deviations were squared, added, and then the square root of the sum was used to calculate the fractional total deviation. For example, consider $A \pm dA$ and $B \pm dB$, where dA and dB are the corresponding standard deviations. To calculate the multiplication of A and B (i.e., $X = A * B * ... * Z$) equation D.1 was used.

$$\frac{dx}{x} = \sqrt{\left(\frac{dA}{A}\right)^2 + \left(\frac{dB}{B}\right)^2 + \dots + \left(\frac{dZ}{Z}\right)^2} \quad \text{D.1}$$

For addition or subtraction of average values with standard deviations, the propagation of errors was analysed using the methods of sum of squares (equation D.2).

$$dx = \sqrt{(dA)^2 + (dB)^2 + \dots + (dZ)^2} \quad \text{D.2}$$

Sample average values were calculated where appropriate with 95% confidence limits for the mean. For example consider, equation D.3.

$$\bar{Y} \pm \frac{t_{(\alpha/2, n-1)} S}{\sqrt{N}} \quad \text{D.3}$$

where \bar{Y} is the sample mean, $t_{(\alpha/2, n-1)}$ is the upper critical value of the t -distribution with $n-1$ degrees of freedom, s is the standard deviation, and N is the number of observations.

If the quantity x is measured with uncertainty δx , and if $q = x^n$, then, the fractional uncertainty in measuring q is given by equation D.4.

$$\frac{\delta q}{q} = n \frac{\delta x}{|x|} \quad \text{D.4}$$

We will conclude this section by giving a few examples of how the error analysis was conducted, using a few well-known equations.

If $g = \frac{4\pi^2 l}{T^2}$, then the fractional uncertainty for calculating g is given by equation

D.5.

$$\frac{\delta g}{g} = \sqrt{\left(\frac{\delta l}{l}\right)^2 + \left(2\frac{\delta T}{T}\right)^2} \quad \text{D.5}$$

If $r = \left(\frac{125}{32\mu_0^2 N^2}\right)\left(\frac{D^2 V}{d^2 I^2}\right)$, then the fractional uncertainty for calculating r is given

by equation D.6.

$$\frac{\delta r}{r} = \sqrt{\left(2\frac{\delta\mu_0}{\mu_0}\right)^2 + \left(2\frac{\delta N}{N}\right)^2 + \left(2\frac{\delta D}{D}\right)^2 + \left(\frac{1}{3}\frac{\delta V}{V}\right)^2 + \left(2\frac{\delta d}{d}\right)^2 + \left(2\frac{\delta I}{I}\right)^2} \quad \text{D.6}$$